Numerical Simulation of Particle Migration of Concentrated Suspension in Symmetric Bifurcation Channels

Thesis submitted in partial fulfillment of the requirements for the degree of

Doctor of Philosophy

by

S. Yadav

Roll No: 10610712

Department of Chemical Engineering
Indian Institute of Technology Guwahati
Guwahati - 781039, India

July 2016

भारतीय प्रौद्योगिकी संस्थान गुवाहाटी
Indian Institute of Technology Guwahati

Department of Chemical Engineering
Indian Institute of Technology Guwahati
Guwahati -781039

Certificate

It is certified that the work contained in the thesis entitled **"*Numerical Simulation of Particle Migration of Concentrated Suspension in Symmetric Bifurcation channels*",** by **S. Yadav,** for the award of degree of Doctor of Philosophy, has been carried out under my supervision and that this work has not been submitted elsewhere for a degree.

Date:

Dr. Anugrah Singh
Professor
Department of Chemical Engineering
Indian Institute of Technology Guwahati
Guwahati-781039, Assam, India

भारतीय प्रौद्योगिकी संस्थान गुवाहाटी
Indian Institute of Technology Guwahati

Department of Chemical Engineering
Indian Institute of Technology Guwahati
Guwahati -781039

Statement

I do hereby declare that the matter embedded in this thesis and the result of investigations has been carried out by me under the supervision of Dr. Anugrah Singh at the Department of Chemical Engineering, IIT Guwahati. Assam, India.

In keeping with general practice of reporting scientific observations, due acknowledgements have been made wherever the work described and is based on the findings of other investigations.

Date: ***(S. Yadav)***

भारतीय प्रौद्योगिकी संस्थान गुवाहाटी
Indian Institute of Technology Guwahati

Acknowledgements

Working for PhD has been an unforgettable experience for me and it would not have been possible without many people. I would like to express my gratitude to all those who helped me in different ways in completing this research work directly or indirectly.

First and foremost, I would like to express my deep felt gratitude to my thesis supervisor, **Prof. Anugrah Singh** for providing me with an opportunity to work on this interesting area of research under his esteemed guidance. His immense support, encouragement, and endurance, helped me to complete my research work. I really appreciate his energy and hard work for all his students and his willingness to help whenever I had problems. I also remain indebted for his understanding, support and caring during the times when I was really down and depressed due to personal problems. Thank you sir, for all your help, advice and support.

I would like to acknowledge my sincere gratitude to my doctoral committee members **Dr. Subrata K. Majumder, Dr. R. K. Upadhyay** (Department of Chemical Engineering) and **Dr. Amaresh Dalal (**Department of Mechanical Engineering) for their valuable suggestions and constructive criticism during the project work, which helped me make necessary improvements at various stages of my research work.

I would like to also thank **Dr. Katha Anki Reddy (**Department of Chemical Engineering) and **Dr. U.K. Saha (**Department of Mechanical Engineering) for their valuable suggestions to improve my PhD Thesis.

I would like to thank my comprehensive committee members **Dr. Pallab Ghosh, Dr. V.S Moholkar** (Department of Chemical Engineering) and **Dr. Vinayak Kulakarni (**Department of Mechanical Engineering) for their inputs to improve my knowledge in the area of my research.

I also thank all the faculty members of the Department of Chemical Engineering for their kind cooperation during my stay in the department. I am also thankful to all the staff members and scientific officers of the Chemical Engineering Department for their genuine help during my entire research period. I also acknowledge the financial support provided by the IIT Guwahati.

My special thanks to staff Kalyan, Jayanta Mout, Pankaj, Balen, Rukhmoni, Lukumoni, Kaustav Moni, Deepak, Narayana Kalita, Pradeep Sinha, Tahkuria, Mintu, Sunil Kumar,Mehdi, Bhagya and others for their support and encouragement during my stay at IIT Guwahati.

I am also indebted to **Dr. Talib DBOUK** for clearing my doubts in OpenFOAM and always supporting me in my endeavor.

My sincere gratitude to all my research group members M. Mallikarjuna Reddy, Ashish Kumar Thokchom, Bhaskar Jytothi Medhi, Sudarshan, Dr. Ashok Kumar, Imran, Aslam, Dharmendra, Srinivas Ganesh, Niloy and Manjunath for their co-operative assistance in learning the basic concepts and provided me constant encouragement throughout my PhD.

My special thanks to **M. Mallikarjuna Reddy** for his co-operative assistance in coding and CFD Basic concepts, OpenFOAM software and helping me whenever I asked doubts related to my PhD project work and I will not forget his help in my life.

My sincere gratitude to **Ankur Kanaujiya** of Mathematics Department for his co-operation, financial support, sharing positive ideas, helping me in hard times especially in mathematics and OpenFOAM software and providing his personal computer for carrying out my research work and I also thank all the friends who supported me in Mathematics, Design, Computer science and Mechanical Department.

My special thanks to Dr. Subba Rao of Nanotechnology Department, Anmol, Pranav, Paragmoni Kalita, Shelke Gajanan, Bandi, Yedla Santhosh kumar, Mohan, Shrikanth Salve, Mayank Agarwal and Simon Peter for their help and support in my thesis work. I was fortunate enough to get excellent batch mates like Shanthi raju, Chinna, Rajashekar Reddy, Chandra Sekhar, Anand, Anil, Kamal, Manish, Sanjeeb, Sriharsha, Ravi Bolledu, Subbarao, Pitambar, Rajeev Parmar, Rajesh, Laxman, Bhoopal, Mohan, Narsimha, Bharath, Satyanarayana, Ramesh, Raja Shekar, Late Shivaiah, Ramteke, Arvind, Manna, Jitendra, Ravi, Sai, Vijay, Deepak, Swapnendu Panda, Sougata Biswas, Ashish, Bala Subramanyam, Someswaran, Ajith, Rahul Datta, Kundu, Venu Babu, Suresh, Pallab, Anand Bharti, Anisha and Kishant for their friendly support and timely assistance whenever needed. I am thankful to all my departmental friends, seniors and juniors and other departmental friends for their support and good wishes. I am also thankful to many others who have contributed to this work directly or indirectly but somehow I have missed their names either due to lack of space or due to my complete forget fullness.

I wish to express my sincere gratitude my friends, **N. Ganga Reddy, Gujja Sreedar Kumar, Sreekanth, Raju** and **Dr.Mahendar** for their encouragement, motivation and financial support at each and every step that I achieve in my Life.

The last but not the least, I would like to express my deepest sense of gratitude to my parents and family members. Their love, care, sacrifice and encouragement have made it possible for me to come so far. I appreciate the courage, understanding and dedicated support shown by all of them despite many testing times at their end. I will be forever indebted to the courage, understanding and dedicated support shown by my wife **SAMATA** and my uncle **GYANOBA.**

S. Yadav

भारतीय प्रौद्योगिकी संस्थान गुवाहाटी
Indian Institute of Technology Guwahati

Dedicated To

My Family Members

&

My Daughter Sanjana

Without their support this would not have been possible

भारतीय प्रौद्योगिकी संस्थान गुवाहाटी
Indian Institute of Technology Guwahati

ABSTRACT

Suspensions of solid rigid particles in viscous fluids are commonly encountered in many industries, biological processes, natural settings, and in several daily life products such as cosmetics, food stuffs. In many of these applications the goal can be to generate uniform distribution of suspended particle in the finished product. Thus, the knowledge and understanding of their flow behavior is very important and this has motivated numerous theoretical, numerical, and experimental studies. The modeling of concentrated suspensions is a challenging task due to multi body interactions. Experimental characterization of these suspensions is also difficult because several complex phenomena such as wall slip and shear-induced migration can take place during their flow. Shear induced particle migration leads to in-homogeneities in particle concentration and generates segregation in poly-disperse systems. This has been observed in many flows and leads to problems in many industrial processes. Shear-induced particle migration in simple and unidirectional geometries like straight channels and tubes have received wide attention but studies in complex geometries and channels with bifurcations are very few. Suspension flow through such bifurcation channels is often encountered in biological systems such as flow of blood through network of branched arteries and veins. In biomedical application, the design of artificial valves requires knowledge of distribution of blood cells in different branches. In the present work, we have investigated the shear induced migration of neutrally buoyant suspensions in symmetric bifurcation channels using the Diffusive flux model (Phillips *et al.* 1992). We have studied the effect of particle concentration, angle of bifurcation, flow rate on velocity, concentration profile and wall shear stresses. The suspension flow profiles showed considerable differences over the Newtonian fluid profile of same viscosity as that of suspension. The velocity and concentration profiles in the daughter branches were observed to be asymmetric. Degree of asymmetry and

bluntness of velocity profile varies with particle concentration and bifurcation angle. Wall shear stress level was found to be the highest near the bifurcation region. We have carried out computational fluid dynamics simulations of suspension flow through symmetric 3D bifurcating channel (T Shape) using the diffusive flux model of shear induced particle migration (Phillips *et al.* 1992). The velocity, concentration and wall shear stresses were studied at various sections in the upstream and downstream sections of the bifurcation. In the diverging flow the symmetric profile in the inlet branch becomes highly asymmetric in the side branches which progressively becomes more symmetric. On the other hand, in case of a converging channel symmetric and peak-valley-peak type of pattern emerges in the downstream of bifurcation whose nature depends on the inlet velocity and concentration. The velocity profile in the inlet branches were fully developed but blunted near the converging section and shifted towards the bottom wall. Particle concentration profile was maximum at the center of channel due to shear induced migration. The locations of merging the two streams in case of the converging flow were also computed. The velocity streams are merging very early but concentration streams takes longer time in the outlet section. This knowledge is required in many applications involving network of branching system to design mixing devices as well as better understanding of system failures in piping networks relevant to industry and physiology.

Keywords: Symmetric bifurcation channel, Shear induced migration, Diffusive flux model, Suspension flow, Numerical simulation.

Table of Contents

भारतीय प्रौद्योगिकी संस्थान गुवाहाटी
Indian Institute of Technology Guwahati

List of Figures

भारतीय प्रौद्योगिकी संस्थान गुवाहाटी
Indian Institute of Technology Guwahati

List of Tables

भारतीय प्रौद्योगिकी संस्थान गुवाहाटी
Indian Institute of Technology Guwahati

Nomenclatures

Symbol	Description	Units
a	Particle radius	m
a_s	Non local factor	dimensionless
b	Constant value	
B	Channel half width	m
E	Rate of strain tensor	1/s
$\mathbf{F}^H$	Hydrodynamic drag force	kg m / s^2
$\mathbf{g}$	Acceleration due to gravity	m/s^2
$\mathbf{j}_\perp$	Migration flux	m/s
k	Boltzmann's constant	kg m^2/s^2 °K
K_c	Diffusion coefficient in concentration	dimensionless constant is taken to be 0.41
K_η	Diffusion coefficient in Viscosity	dimensionless constant is taken to be 0.64
L	Length of the channel	m
N_1	First normal stress difference	kg/m-s^2
N_2	Second normal stress difference	kg/m-s^2
N_b	Flux due to Brownian diffusion	m/s
N_c	Flux due to spatially varying inter-particle interacting frequency	m/s
N_η	Flux due to spatially varying viscosity	m/s
N_t	Total diffusive flux term	m/s
P	Pressure	kg/m-s^2

P_f	Fluid pressure	kg/m-s^2
Pe	Peclet number	dimensionless
Q	Parametric symmetric tensor	kg/m-s^2
Re_p	Reynolds number	dimensionless
S_φ	Source term	1/s
t	Time	s
T	Absolute Temperature	$^\circ$K
U	Bulk suspension velocity	m/s
$U_{\max}$	Maximum centre line velocity of the Newtonian fluid	m/s

Greek Letters

ε	Ratio of particle radius to channel half width	dimensionless
$\boldsymbol{\Sigma}$	Suspension stress tensor	kg/m-s^2
$\boldsymbol{\Sigma}^f$	Fluid stress tensor	kg/m-s^2
$\boldsymbol{\Sigma}^p$	Particle stress tensor	kg/m-s^2
$f(\phi)$	Sedimentation hindrance function	
$[\eta]$	Intrinsic viscosity	kg/m-s
$\eta(\phi)$	Effective viscosity depends on particle volume fraction	kg/m-s
η_N	Particle normal stress viscosity	kg/m-s
η_o	Suspending fluid viscosity	kg/m-s
η_p	Particle shear stress viscosity	kg/m-s
ϕ	Particle volume fraction	dimensionless

ϕ_m	Maximum particle packing volume fraction	dimensionless
ρ	Density of the suspension	kg/m^3
θ	Bifurcation angle	degrees
$\boldsymbol{\tau}$	Stress tensor	kg/m-s^2
$\prod$	Suspension pressure	kg/m-s^2
Γ	Diffusion coefficient	m^2/s
$\dot{\gamma}$	Local shear rate	1/s
$\dot{\gamma}_{nl}$	Non-local shear rate	1/s
$\dot{\gamma}_s$	Mean shear rate	1/s
$\boldsymbol{\nabla}$	Gradient operator	
$\boldsymbol{\nabla}\cdot$	Divergence operator	

भारतीय प्रौद्योगिकी संस्थान गुवाहाटी
Indian Institute of Technology Guwahati

Abbreviations

DFM	Diffusive Flux Model
SBM	Suspension Balance Model
SIMPLE	Semi Implicit Pressure Linked Equations
CFD	Computational Fluid Dynamics
OpenFOAM	Open Field Operation and Manipulation
NMR	Nuclear Magnetic Resonance Imaging Technique
RBCs	Red blood cells
LDA	Laser- Doppler Anemometry

भारतीय प्रौद्योगिकी संस्थान गुवाहाटी
Indian Institute of Technology Guwahati

CHAPTER-1

Introduction and Literature Review

भारतीय प्रौद्योगिकी संस्थान गुवाहाटी
Indian Institute of Technology Guwahati

1. Introduction and Literature Review

1.1. Suspensions

Dispersions of one phase in another are frequently observed in biological and industrial products like blood, paint, food, and slurry transport and in nature as fog, clouds, and rivers. In general, the dispersions comprise of various combinations of the gas, liquid and solid phase and their classification is shown in Table 1.1.

Table 1.1: Dispersion classifications.

		Dispersed Phase		
		Gas	Liquid	**Solid**
Continuous Phase	Gas	-	Vapors	Aero-sol, smoke
	Liquid	Foams	Emulsions	**Suspensions**
	Solid	Solid foams	-	Alloys, Polymers

In this thesis, we will be dealing with dispersion systems of type "suspensions" more specifically. Suspension is a multiphase system in which one phase dispersed (solid particles) in other continuum (liquid) phase. A few examples of suspensions are presented in Figure 1.1 which is found in our day today life and in nature. Depending upon size and shape of the particles, the suspensions are further classified into different categories as shown in Figure 1.2. The nature of inter-particle interactions are influenced by the particle size. Particles smaller than 1 nm are assumed to behave like homogeneous solutions. A suspension of particles is termed colloidal if the size of the particles lies between 1 nm and $1\,\mu m$. Suspensions with

particle sizes greater than $1\,\mu m$ is the subject of our study. In such cases colloidal and Brownian forces are not important.

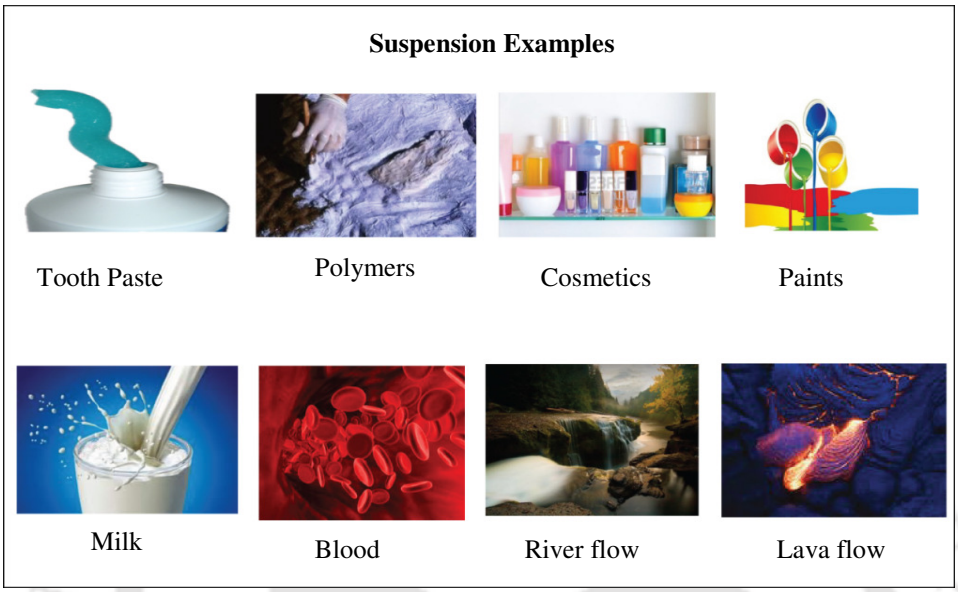

Figure 1.1. Examples of suspensions

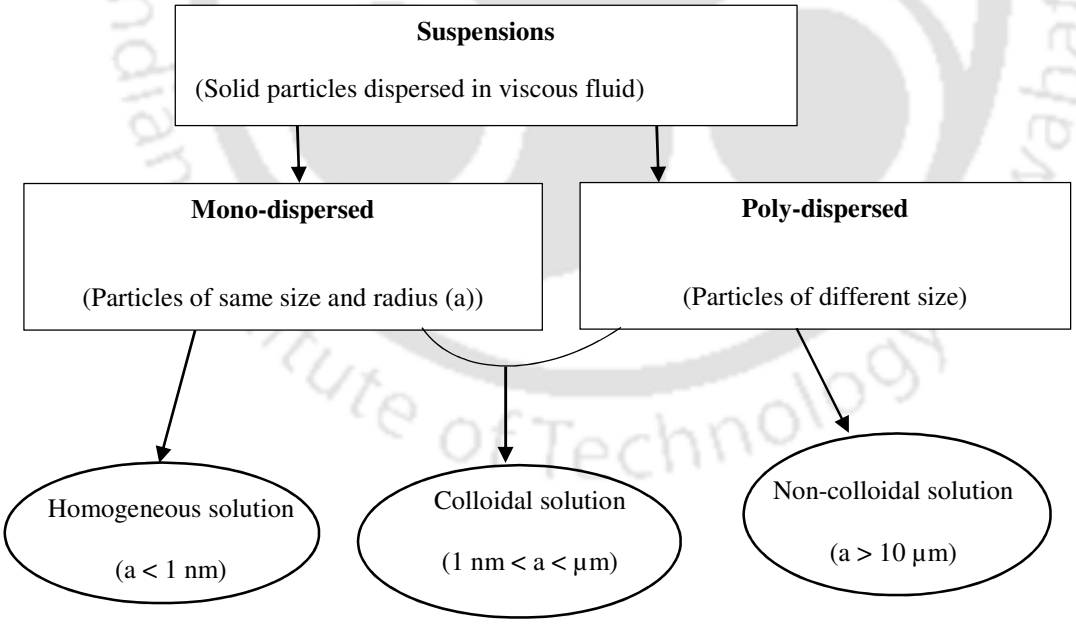

Figure 1.2. Classification of suspensions

Particle shape is also important because it determines the interaction between the particles and the suspending fluid. Though various shapes of particles are encountered in practical applications, our study is limited to spherical particles suspended in Newtonian fluid. Such type of suspensions are of great importance in industry, medicine and research. In industry, suspensions are frequently handled during the manufacture of processed food (juices, sauces etc.), pharmaceuticals, cosmetics, paints etc. In the petroleum industry, suspensions are encountered in various operations such as drilling, well simulation, fracturing and enhanced oil recovery (Schramm, 1996). In pharmaceutical industries improving the stability of drug suspension is a common problem. Suspensions are critical in biomedical engineering, since the most important biological fluid of all, blood, is clearly a mixture of liquid blood plasma and red and white blood cells. Bio chips (gene control chip, neural cells, DNA chip and protein chips) are modern devices that also handle suspension flow in micro channels. Knowledge of suspension flow behavior is also of great importance in improving the efficiency of operations. In many flow procedures the low efficiency is due to the fact that flow and stress properties of the materials involved are not known and thus cannot be controlled in order to optimize the efficiency and safety of the processes (Knowlton *et al.* 1994). The flow behavior of these suspensions is often complex and their rheological properties are often very different from those of the suspending fluid. The complexity arises due to particle-particle and particle-fluid interactions in the suspension. To successfully process the suspensions in engineering applications, it is necessary to understand the fluid dynamics of suspensions and be able to predict suspension flows as a function of flow conditions. For this reason, a great deal of attention from both practical and the fundamental points of view has been generated in recent years.

The suspensions of interest in this work are inertialess, neutrally buoyant, mono dispersed, non-Brownian and non-colloidal spheres suspended in a Newtonian fluid. Neutral buoyancy means that the densities of the particles and fluid are equal and thus settling of the particles due to gravity does not occur. Suspensions are called concentrated when average solid volume fraction is typically greater than 3%. Concentrated suspensions are also the type most frequently encountered in industry and biology. Our work is limited to low Reynolds number transport of concentrated suspension of non-colloidal and non-Brownian particles. Brownian interactions arise from thermal fluctuations, and colloidal forces from intermolecular attraction. At the same time, the particles are small enough so that inertial effects may be neglected and this assumption requires that the Reynolds number based on particle size is very low.

1.2. Forces on particles

Solid-liquid two phase suspension flow is complex as compared to the Newtonian fluid flow. To understand the rheology of solid-liquid suspension we need to know all the forces acting on solids as well as on fluid. We classify forces (which are significant in a two-phase particulate suspension) into two categories: non-hydrodynamic forces and hydrodynamic forces.

1.2.1. Non-hydrodynamic Forces

These forces are present at all times and include Brownian motion, inter particle interactions and external field effects such as gravity or imposed electrical and magnetic fields. Brownian motion results from the random thermal fluctuations of the particles and is significant when

the particle length scale is less than $1\,\mu m$. Inter particle interactions include short-range forces such as hard-sphere repulsion or van der Waals forces. The influence of gravity is significant if the densities of the two phases do not match and electric/magnetic fields are important, if the particulate phase carries a charge or has significant polarization (Russel *et al.* 1989).

1.2.2. Hydrodynamic forces

These forces present themselves only in an imposed flow field and include particle inertia and viscous interactions between the particulate phase transmitted through the fluid. In this study, in order to understand the dynamics of the suspensions we have made some simplifications to flow equations. It is assumed that the flow is laminar and the fluid motion is slow enough to neglect the inertia forces in comparison to viscous forces. The dimensionless number which determines the relative importance of inertial and viscous effects is the Reynolds number based on particle size.

$$\mathrm{Re}_p = \frac{\dot{\gamma}\rho_p a^2}{\eta_o} \qquad (1.1)$$

In the above equation, ρ_p is the density of the particle, a is the particle radius, $\dot{\gamma}$ is the shear rate of the flow field, and η_o is the viscosity of the suspending fluid. For $\mathrm{Re}_p << 1$, viscous forces dominate over the inertial forces and the flow is said to be in the creeping flow regime. The relative importance of Brownian motion is characterized by Peclet number which is defined as:

$$Pe = \frac{\dot{\gamma}a^2}{D_o} \qquad (1.2)$$

In the above equation $D_o = \frac{kT}{6\pi\eta_o a}$ is the Brownian diffusion coefficient for an isolated particle. For the kind of suspension we are studying, Peclet Number is greater than 1 (Pe >> 1). In this study we have considered non-colloidal suspensions, where the dispersed particles are much greater than colloidal size and thermal fluctuations and Brownian motion are also negligible. Such suspensions are industrially important and their study can furnish considerable insight into the behavior of more complex systems.

There have been many studies to explain and predict the rheological behavior of suspensions such as viscosity and normal stresses. Viscosity is one of most important rheological property to be studied and it is discussed in next section.

1.3. Viscosity

The evaluation of rheological properties of suspension are essential for various applications. Viscosity is one of the most important rheological property from practical point of interest. Viscosity of a suspension depends on the structural organization and interaction of constituents within the suspensions. Viscosity of suspension increases with the increase in solid volume fraction. There has been significant effort in the literature to characterize the viscosity of different types of suspension, both from theoretical point of view and from experimental focusing on dilute, semi dilute and concentrated systems. Assuming the absence of interactions between the suspended particles in a dilute suspension of spherical particles in Newtonian fluid, Einstein (1906) predicted the bulk viscosity of the dilute suspension. He showed that the effective suspension viscosity linearly increases with the spheres volume fraction and derived the following formula:

$$\eta = \eta_o(1+2.5\phi) \qquad (1.3)$$

Equation (1.3) is valid for $\phi << 1$. In the above equation, η is the effective viscosity of the suspension η_o is the viscosity of the suspending fluid and ϕ is particle volume fraction.

For more concentrated suspensions it is necessary to consider corrections to the viscosity that are of higher order in the volume fraction. When the flow field around a sphere is influenced by the presence of neighboring spheres, the hydrodynamic interactions cannot be neglected and they could be treated as a contribution to η that is proportional to ϕ^2 for two bodies, to ϕ^3 for three bodies and so on. Batchelor and Green (1972a, 1972b) expressed bulk suspension viscosity in terms of higher order of particle volume fractions as follows.

$$\eta = \eta_o(1+a\phi+b\phi^2) \qquad (1.4)$$

In the above equation, the parameters are defined as $a = 2.5$ and second order coefficient $b = 7.6$ and it becomes equal to 6.2 when Brownian motion is considered (Batchelor, 1977). Ball and Richmond (1982) assumed that in a concentrated suspension the effect of all the particles is additive and proposed the following correlation:

$$\eta = \eta_o(1-C)^{-\frac{5}{2}\phi_m} \qquad (1.5)$$

Here, C accounts for the so-called "crowding" effect. Ball and Richmond's expression is effectively identical to that of Krieger and Dougherty (1959) whose theory also states that, in the general case, the $\frac{5}{2}$ factor should be replaced by the intrinsic viscosity. The value of $\frac{5}{2}$ is the intrinsic viscosity for an ideal dilute suspension of spherical particles. To simplify a little, from now onwards, we will be denoting,

$$\eta_s = \frac{\eta}{\eta_o} \tag{1.6}$$

as the normalized viscosity (relative viscosity), where η is the effective suspension viscosity. Many rheologists measured and modeled the experimental data via various phenomenological equations. In almost all of these models the maximum possible packing fraction of particles ϕ_{m} is taken into account in the expression of effective suspension viscosity.

A variety of empirical equations have considered dependence of effective viscosity (η_s) on particle concentration(ϕ). Some of these equations have been proposed by Maron and Pierce (1956), Krieger and Dougherty (1959), Kriger,(1972), Leighton and Acrivos (1986) and Morris and Boulay (1999) to determine the dependence of effective viscosity on particle volume concentration. We have shown only a few of these and one can chose the equation which best represents the system. The maximum particle volume fraction is one of the important parameter in these equations. According to the Dorr *et al.* (2013), the majority of the models are derived either analytically or by the fitting experimental data. Evidently each of the approaches has its limitations. Krieger and Dougherty (1959) formula is one of the most used one. Maron and Piece (1956) model is valid for low concentrations and all other models are applicable to wide range of concentrations (ϕ to ϕ_m). In this work we have considered the correlation proposed by Krieger (1972) which is found to work well for suspension of mono-dispersed non-colloidal particles. The absolute value for the maximum packing fraction (ϕ_m) depends on the particle shape and particle size distribution. In the Kreiger model, we have used $\phi_m = 0.68$. However, ϕ_m could be considered an adjustable parameter. The models mentioned above are given below as follows.

Maron and Pierce (1956): $$\eta_s = \left(1 - \frac{\phi}{\phi_m}\right)^{-2} \quad (1.7)$$

Krieger and Dougherty (1959): $$\eta_s = \left(1 - \frac{\phi}{\phi_m}\right)^{-2.5\phi_m} \quad (1.8)$$

Leighton and Acrivos (1986): $$\eta_s = \left(1 + \frac{1.5\phi}{1 - \frac{\phi}{\phi_m}}\right)^{2} \quad (1.9)$$

Morris and Boulay (1999): $$\eta_s = 1 + 2.5\varphi\left(1 - \frac{\phi}{\phi_m}\right)^{-1} + 0.1\left(\frac{\phi}{\phi_m}\right)^{2}\left(1 - \frac{\phi}{\phi_m}\right)^{-2} \quad (1.10)$$

Zarraga *et al*. (2000): $$\eta_s = \frac{e^{-2.34\phi}}{\left(1 - \frac{\phi}{\phi_m}\right)^{3}} \quad (1.11)$$

Krieger (1972) has given the following empirical correlation for suspension viscosity that could be fit for concentrated suspensions:

$$\eta(\phi) = \eta_o\left(1 - \frac{\phi}{\phi_m}\right)^{-1.82} \quad (1.12)$$

Zarraga *et al.* (2000) measured ϕ_m experimentally by using fluid displacement method and found it to be 0.62. The value of ϕ_m is highly sensitive especially when the particle concentration approaches the level close to it ($\phi \sim \phi_m$). It implies that there is no longer sufficient fluid to lubricate the relative motion of particles and the viscosity rises to infinity. In the present study, the maximum packing fraction is set to the value of 0.68 in computations which is reasonable only for rigid mono-dispersed spherical particles and this was also considered by Phillips *et al*. (1992) in their simulation of circular Couette flow. If one were to

predict effective viscosity with good precision then the value of ϕ_m must be close to the realistic value suitable for that particular type of suspension. ϕ_m has also been determined by numerical simulations of random close-packing of monodisperse spheres. Rintoul and Torquato (1996) obtained a value of $\phi_m \approx 0.62.$ and Kitano *et al.* (1981) found that $\phi_m \approx 0.68.$ Experiments of *Chong et al.* (1971) gave the value of maximum packing fractions as 0.605 whereas it was between 0.55 - 0.71 in the experiments of Shapiro *et al.* (1992).

1.4. Shear induced migration

The flowing concentrated suspensions even at low Reynolds number exhibit many interesting phenomena such as shear induced migration, aggregation, sedimentation etc. These phenomena which arise from particle-particle and fluid-particle interactions depends on various factors such as the concentration and density of the particles, viscosity of the suspending fluid and applied shear rate. In this work, we focus on shear induced migration phenomena which have attracted wide attention in recent years due to its technological and industrial applications.

Shear induced migration is defined as a phenomenon in which initially well mixed non-colloidal, neutrally buoyant particles in a viscous Newtonian fluid when subjected to in-homogeneous shear flow, becomes non-uniform due to flux of particles migrating from regions of high to low shear rate and from regions of high particle concentration to low. This phenomenon arises from the particle-particle and particle-fluid interactions (Gadala-Maria and Acrivos, 1980; Leighton and Acrivos, 1987).

For better understanding of this migration, we have explained this by illustration in the figure given below. Consider two close rigid solid spherical particles present in suspension.

These two solid particles are moving freely along the streamlines which are separated by a distance d1 as shown in the Figure 1.3a.

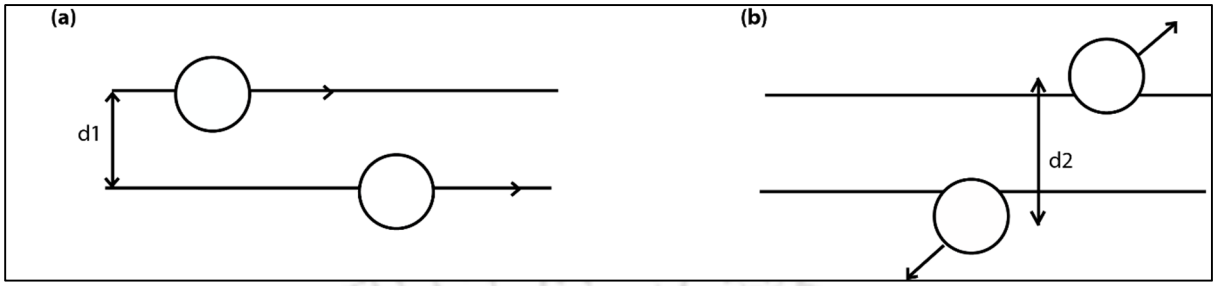

Figure 1.3. Interaction of two solid spheres in a simple shear flow (a) before interaction (b) after interaction. *[From Leighton and Acrivos, 1987b, J. Fluid Mech.* ***181****, 415 Copyright 1987 by the Cambridge University Press]*

In laminar flow the fluid layers moves one over the other with different velocities, and the particles in those layers also move with different velocities. The particle moving with greater velocity interacts with the particle moving with lower velocity. If the interaction is reversible, the particles should return to their original position at the end of collision. After return to the original position the same original distance (d1) has to remain between them. But the particles never return to their original streamlines after their encounter and are separated by distance (d2) different from the original. Hence, this indicates an irreversible interaction taking place, displacing the particles away from their original stream lines. The reason for this irreversible interaction may be due to surface roughness of the particles, Brownian motion of particles and multi body inter-particle interactions. If the separating distance between the particles moved is measured in the order of particle radius (say *a*), then the relative velocity between the particles is $\dot{\gamma}a$. Here, $\dot{\gamma}$ is local shear rate and a is particle radius. Thus, the shear

induced particle diffusivity is proportional to $\dot{\gamma}a^2$. If there is a large gradient in the shear rate across a particle, then the particle experiences more irreversible interactions. Similarly, if there is a small gradient in the shear rate across a particle, then the particle experiences less irreversible interactions. Hence, more migration from the regions of high shear rate compared to the regions of low shear rate occurs. This increases the concentration of particles at regions of low shear rate which leads to gradients in particle concentration.

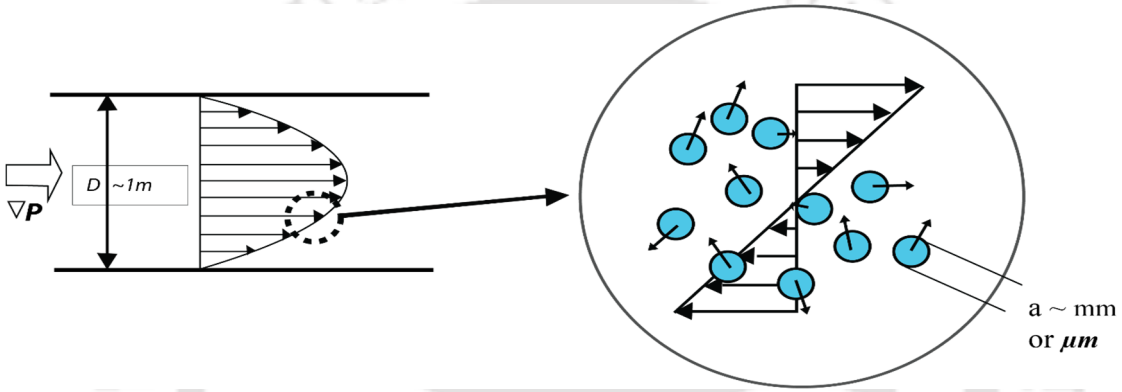

Pipe flow of suspension Micro-structure

Figure 1.4. The macroscopic flow behavior of a suspension will depend on the dynamics at the micro structural level (From Deshpande *et al.* 2010)

However, this gradient in particle concentration results in migration of particles from high concentration to low concentration. This entire phenomenon associated with the shear flow of suspensions is known as shear induced migration and is described in detail by Leighton and Acrivos (1987a). The most practical application is a tube flow where the particles get concentrated in the center due to shear-induced migration. As a result the parabolic velocity profile becomes blunted (Figure1.4).

Particle migration involving flows of concentrated suspensions can be found in many industrial processes which involve uniform distribution of particles in the materials. For

example, the manufacture of plastics, pharmaceuticals and ceramics depends on the consistency of the dispersions to produce a quality product, however, due to lack of current understanding of suspension dynamics, consistency is mostly attained by trial and error processes. A better understanding of particle migration would have an impact on processing of concrete, ceramics and solid propellants. A brief literature survey on this topic is given in the sections 1.4.1 and 1.4.2.

1.4.1. Shear induced migration through general geometries

As mentioned in the previous sections, many researchers have conducted investigations on viscosity of the suspension. Much of the experimental and analytical work has been performed in Couette devices in order to determine the self-diffusion and the corresponding diffusion coefficient which can be used to model flow. The list of publications is extensive and it is impossible to review all these publications in this chapter. Only a brief survey that covers studies of shear induced migration and migration in bifurcation channels is presented here. As mentioned before, Einstein (1906) gave the formula for effective viscosity in very dilute suspension and his formula was considered as the foundation of many studies later on. For long time it was a commonly accepted view that suspensions should behave as Newtonian fluids for all values of the particle concentration up to the maximum flowing fraction. Many years after the work of Einstein, Batchelor and Green (1972b) derived the rigorous extension of Einstein's formula to order of ϕ^2 for suspensions of mono-disperse solid spheres. Eckstein *et al*. (1977) developed a scaling argument for the diffusion coefficient by reducing the dimensionless arguments governing particle-particle interactions. They determined that self-diffusion coefficient was proportional to square of the particle radius and the local shear rate.

The coefficient was found to be nearly linear with concentration up to 20% and constant beyond that. In the range $0.2 < \phi < 0.5$, the trend of self-diffusion coefficient was not clear because of experimental scatter and inaccuracies, and this lead to the conclusion that for $\phi > 0.2$, the self-diffusion coefficient is independent of particle volume fraction. While measuring the viscosity of concentrated suspensions of neutrally buoyant spheres in Newtonian fluids using the Couette viscometer, Gadala-Maria and Acrivos (1980) observed that the effective viscosity of concentrated suspension decreased slowly with prolonged shear until it reached equilibrium value. They could not find a reasonable explanation for this phenomenon. Leighton and Acrivos (1987) repeated the experiments done by Gadala-Maria and Acrivos, and suggested that the apparent decrease in viscosity results from the migration of particles out of the sample being sheared in the gap between the bob and the cup of the Couette device and into the reservoir containing the stagnant part of the suspension. They proposed a mechanism which explained the existence of particle migration in the direction normal to the shearing direction and also predicted the rate of migration. They proposed that the mechanism of particle migration is basically particle diffusion in response to gradients in shear rate and in particle concentration acting through irreversible interactions between particles. As explained earlier the gradients in shear rate and concentration directly affect the frequency and dynamics of collisions between particles. Many studies investigated shear induced particle migration using experimental and theoretical analysis after the work of Leighton and Acrivos (1987). There have been several experimental evidences to support the phenomenon of shear induced particle migration exhibited by concentrated suspensions. All of these experiments were performed in simple flow geometries on model suspensions of non-colloidal, mono-disperse spheres suspended in viscous Newtonian liquids. The shearing flow geometries discussed below

include pressure- driven flow in a circular pipe, pressure-driven flow in a rectangular channel, narrow-gap annular Couette flow, and wide-gap annular Couette flow.

The first quantitative experiments involving pressure-driven flow of concentrated suspensions through tubes at low Reynolds number were performed by Karnis *et al.* (1966) using hand–analysed cinematography and their results are presented in Figure 1.5.

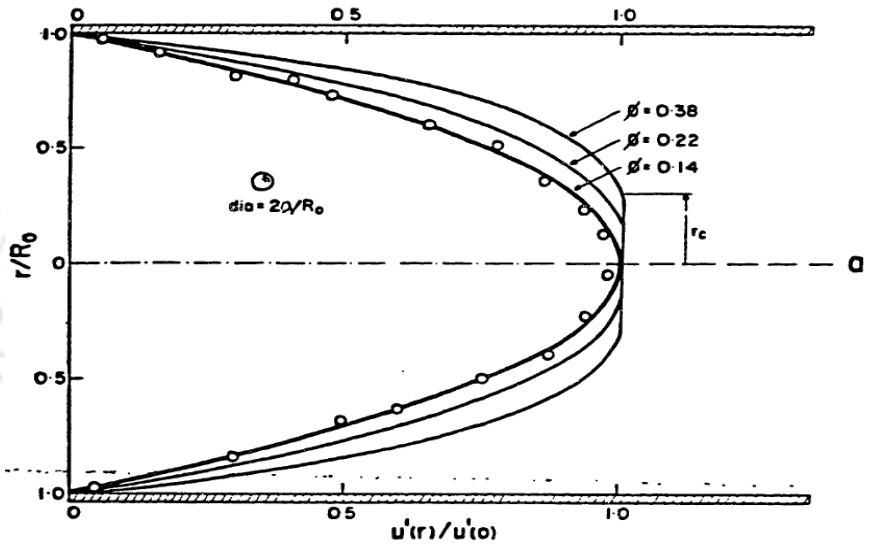

Figure 1.5. Dimensionless steady-state mean suspension velocity profiles measured by Karnis *et al.* (1966) for three values of particle concentration. The velocity profiles shown become increasingly blunted with increasing particle concentration. The flow parameters were: the tube radius R_O=0.4 cm, the ratio of tube radius to particle radius Ro/*a* = 36, and the volumetric flow rate Q=0.0356 cm^3/s. The solid lines are the best fit through the experimental points. The ϕ =0.14 (open circles) curve is parabolic, and accordingly indicates the velocity profile for a Newtonian fluid in this geometry [From Karnis *et al.* 1966, J. Colloid Interface Sci. **22**, 531 Copyright 1966 by the ELSEVIER].

These velocity profiles suggest that particles had drifted into a non-uniform configuration in response to inhomogeneous shear rate or velocity gradient in the flow. Specifically particles moved away from the tube wall where local shear rate was high to regions near the tube center where the local shear rate was low. However, in their experiments, they did not observe any particle migration. They suspected that this blunted velocity profiles are due to wall effects. Later Leighton and Acrivos (1987b) provided evidence supporting the idea of particle migration and mechanism for shear induced migration was proposed. Ultra sound–Doppler anemometry was used by Kowalewski (1980) to measure the velocity profile for concentrated suspensions in tube flows. It was found that the blunting of velocity profiles depends upon the particle concentration and particle size.

Although the ultrasonic experimental method is very useful it cannot distinguish between particle and fluid velocities. The measured velocity profile is presumably a mass or volume averaged value. Clearly no particle concentration data is possible via this technique. To give good information about particle concentration profiles, Sinton and Chow (1991) used Nuclear Magnetic Resonance (NMR) imaging to study the solid-fluid suspension flow in the tube, since it could distinguish between the fluid and solid phases, even in optically opaque suspensions. NMR also provides simultaneous velocity profiles. They found that the velocity profile of suspension was different from the parabolic velocity distribution. The velocity distribution appeared to be blunted with slower than expected velocities towards the center of the pipe for the 42% and 50% volume fraction suspension, while the velocity distribution of suspension of 22% volume fraction exhibited excellent agreement with the parabolic shape. This blunted velocity profile was consistent with the prediction of Leighton & Acrivos (1987).

Like Karnis *et al*. (1966), Sinton and Chow (1991) also did not find any measurable non-uniformity in particle concentration.

Altobelli *et al*. (1991) measured velocity and concentration profiles of suspensions of spheres flowing in a horizontal pipe using magnetic resonance imaging. They observed that velocity profiles of the suspension ($\phi = 0.39$) were blunt and shifted slightly upward. With change in concentration or velocity, both the fluid velocity and concentration profiles become more axisymmetric. Later, Hampton *et al.* (1997), measured the velocity and concentration profiles of particles for pressure-driven flow in circular pipes by NMR imaging and their results are presented in Figure 1.6. In their experiments they observed the non-uniform concentration profiles and simultaneous blunted velocity profiles, for bulk particle volume fractions ranging from 0.1 to 0.50 and also compared with existing shear induced migration models. Figure 1.6 indicates the images taken from their experiment with a/R = 0.0256 (where a is particle radius and R is radius of the tube) which exhibits sharper peaks at lower particle concentration and this sharpness in peaks decreases with the increase in particle concentration. While most of experimental studies on shear-induced migration used the NMR imaging technique, Koh *et al*. (1994) used laser Doppler anemometry (LDA) to study the pressure-driven flow in a rectangular channel. To avoid the problem of optical turbidity, the refractive indexes of the solid and liquid phases were closely matched. This method was chosen such that by counting the number of Doppler signals in a period of time, the local volume fraction was also measured. These measurements showed the existence of blunted velocity profiles that were independent of suspension flow rate but bluntness increases with increase in particle concentration. The maximum particle concentration was observed near the center.

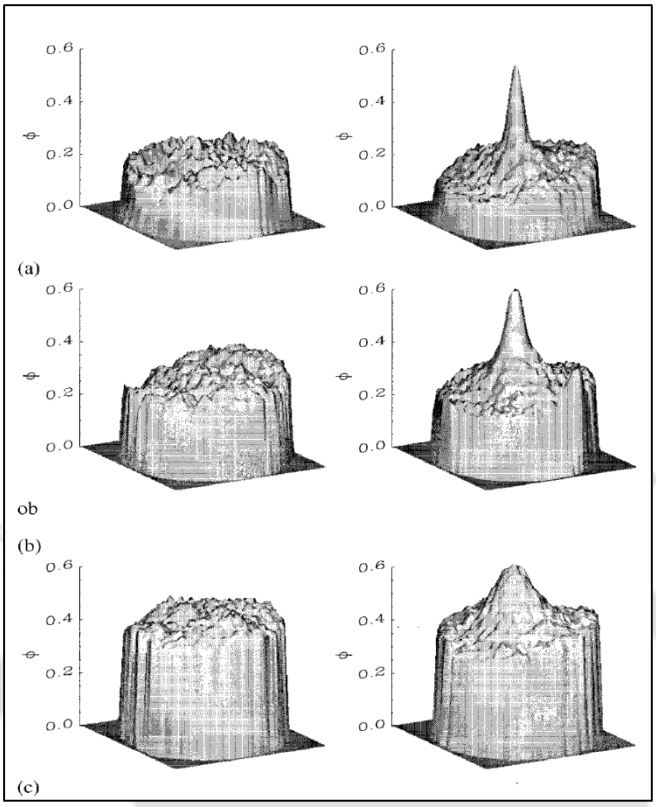

Figure 1.6. NMR images recorded by Hampton *et al*. (1997) of the particle volume fraction (ϕ) profile for pressure-driven suspension flow in a circular pipe. On the left are the initial φ profiles and on the right are the fully developed ϕ profiles. The particle radius to pipe radius ratio (*a*/R) was 0.0256. The bulk particle volume fraction was: (a) 0.20, (b) 0.30, and (c) 0.45 [From Hampton *et al*. (1997), J. Rheol. **41**, 621 Copyright 1997 by the AIP Publishing LLC].

Averbakh *et al*. (1997) also employed Laser-Doppler anemometry to measure velocity profiles in a rectangular duct to detect velocity fluctuations in the viscous flow of the concentrated suspension induced by the particle presence. Lyon and Leal (1998) used modified Laser-Doppler velocimetry (LDV) method to measure fully developed particle velocity and concentration profiles, as well as the mean square amplitudes of velocity fluctuations, for concentrated suspension flowing through rectangular channel and confirmed that velocity

profiles are blunted; the bluntness increases with increase in particle concentration (Figure 1.7). They have performed experiments with suspensions up to particle concentrations of 50% and also compared the profiles with the predictions of diffusive flux and suspension balance models. Shear induced migration is also studied extensively in curvilinear and eccentric flows. Abbott *et al*. (1991) used NMR imaging to observe the evolution of radial concentration and velocity profiles of initially well mixed concentrated suspensions of spheres in viscous Newtonian liquids undergoing flow between rotating concentric cylinders (wide gap, annular Couette flow) and their results are depicted in Figure 1.8.

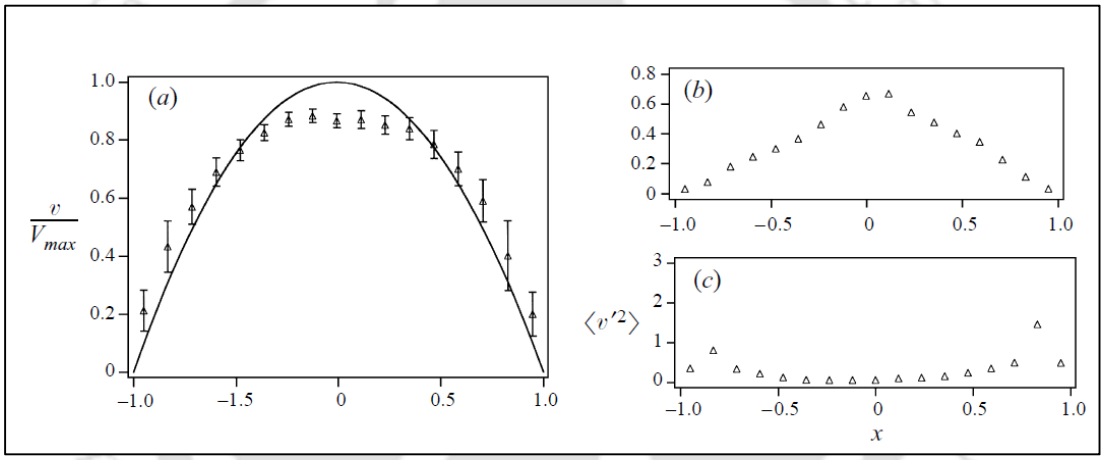

Figure 1.7. Mean velocity (a), particle volume fraction (b), and time averaged velocity fluctuation (flow direction) (c) profiles measured by Lyon and Leal (1998) with Laser Doppler velocimetry for a suspension with average particle volume fraction(ϕ)= 0.4, and the channel half width to particle radius ratio (B/*a*)=11. In (a), the mean velocity profile of suspension is compared with the mean velocity profile of a Newtonian fluid at the same flow rate [From Lyon and Leal, 1998, J. Fluid Mech. **363**, 25 Copyright 1998 by the Cambridge University Press].

In Couette flow, particles migrate from the high shear-rate region near the inner rotating cylinder to the low shear rate region at the outer wall (Figure 1.8a and c). They also reported that the particle fraction near the outer cylinder at steady state reached a value near 0.6, close to 0.63, the maximum random packing fraction for mono-disperse spheres. Abbott *et al*. (1991) also measured the suspension velocity profile and found that the flow in the densely packed region near the outer, stationery cylinder is almost stagnant. Near the center, the particle concentration decreased by at least 30% (Figure 1.8b).

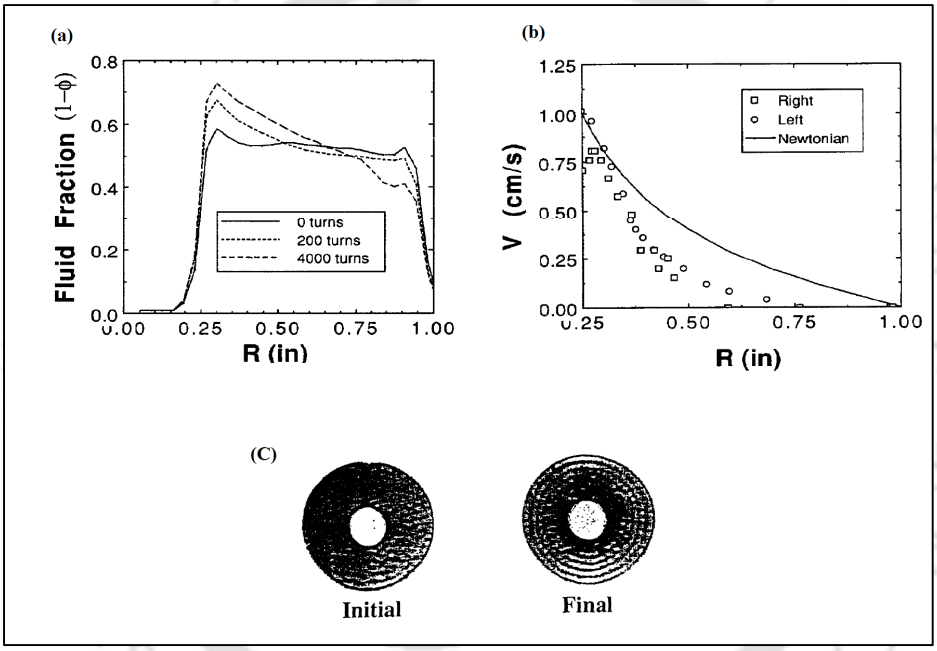

Figure 1.8. Shear induced migration in cylindrical Couette flow by Abbott *et al.* (1991). (a) The radial concentration profile determined from the average value of the signal intensity as a function of radial position. (b) Steady state velocity profile compared with that for a Newtonian fluid. (c) NMR images of a cross section of a suspension of 50% polydisperse spheres flowing between concentric cylinders [From Abbott *et al.* 1991, J. Rheol. **35**, 773 Copyright 1991 by the AIP Publishing LLC].

Chow *et al*. (1994) performed NMR experiments to measure the evolution of suspension concentration profiles in Couette and parallel-plate geometries. In their study, neutrally buoyant suspensions of nearly mono-disperse, non-Brownian spherical particles at a volume fraction of 0.5 in a Newtonian fluid were used. For Couette flow, the experimental results were in good agreement with Leighton-Acrivos (1987). However, they found that there was no significant migration of particles across the entire domain of the parallel plate geometries but some decrease in the apparent viscosity was observed. Chapman (1990) conducted experiments on suspension flow in cone-plate geometry where an outward migration of particles was observed. Chow *et al*. (1995) observed that the particles were found to migrate radially outward, away from the apex of the cone in the cone-and-plate geometry.

Phan-Thien *et al*. (1995) observed the particle migration in a concentrated suspension undergoing flow between rotating eccentric cylinders by conducting experiments and numerical simulations. They used the NMR imaging technique to measure the time evolution of concentration and velocity. They also compared the numerical results with the experimental data and found that there was acceptable agreement. Subia *et al*. (1998) used NMR technique to determine the particle concentration profiles of initially well-mixed suspensions as they separate when subjected to slow flow between counter-rotating eccentric cylinders and in piston-driven flow in a pipe. They have observed good qualitative and quantitative agreement of the numerical predictions with the experimental measurements.

Most of the above mentioned studies have focused extensively on unidirectional and steady flow in simple one and two dimensional geometries such as cylindrical Couette cell parallel plate geometry, cone plate geometry, rectangular channels and the circular pipes. While flow in complex geometries such as bifurcations are not adequately addressed despite

the fact that most of the industrial processes involve flows of suspension through 3D geometries. Flow of particles through constrictions and diversion are also of fundamental importance (Chen, 2013). In the next section we describe the migration in bifurcation channels and previous works done so far in the literature.

1.4.2. Shear induced migration through bifurcation geometries

Transport of suspension through bifurcation channels (where a channel or pipe divides into multiple branches) is often encountered in biological systems such as laminar flow of blood through branched arteries and veins, micro vascular physiology (Pries *et al*., 1989). Bifurcation channels are also used in micro devices for particle separation or mixing (Roberts and Olbricht, 2006). The shear-induced migration phenomenon through bifurcation channels could be important in many of the above applications. For example in the biomedical application the design of artificial valves would require proper understanding of the distribution of the particles in bifurcation channels. Aarts *et al.* (1988) proposed a method known as "plasma *skimming*" which is used to separate red blood cells from whole blood by flowing blood through a network of well-designed bifurcations.

Chien *et al*. (1985) and Yen and Fung (1978) have studied plasma skimming with flexible disks. The plasma skimming technique can be used as an alternative where conventional techniques are ineffective (Jaggi *et al*. 2007; Leonard *et al*. 2004; Faive *et al*. 2006). Pries *et al*. (1989), Krogh (1921), Yan *et al*. (1991), Enden and Popel (1994) observed that the distribution of red blood cells into branches of bifurcation (Y and T type bifurcation) differs from the distribution of bulk flow.

Many studies have shown the shear thinning behavior of blood in Y shaped bifurcation channels numerically and experimentally for low Reynolds number flows. Balan and Balan (2010) and Kanaris (2010) suggested that non-Newtonian fluid shows a flattened axial velocity profile due to its shear thinning behavior. In addition, the red blood cell motions in various bifurcation geometries (like Y and T shape channels) has been the area of research in the recent past with a variety of particles, including rigid spheres (Lagoela *et al*. 2009) and flexible cells (Barber *et al*. 2008). They observed that RBCs significantly deviated from streamlines at bifurcation because of cell migration and obstruction effects. Wang and Xing, (2010) studied the motion of erythrocyte (Red blood cell) suspensions numerically through axisymmetric, pressure driven channels. They observed that the profile of the capillary flow was markedly blunted in comparison to the parabolic profiles of pure plasma flow.

Li *et al*. (2012) investigated the motion of red blood cells (RBCs) in a Y shaped bifurcating micro fluidic channels using dissipative particle dynamics of healthy and unhealthy blood at low Reynolds number and their results predicted that RBC flux in bifurcation channel depends on the deformability of RBCs and the feed hematocrit level of blood. Ishikawa *et al*. (2011) have investigated experimentally the behavior of RBC cells and adhesion of cancer cells in symmetric bifurcations and confluences at low Reynolds number. They revealed that there is a strong asymmetry in the trajectories of RBC cells and cancer cells at the bifurcation and confluences, although the trajectories of tracer particles in pure water were almost symmetric. Subsequent to this Leble *et al*. (2011) have investigated experimentally the red blood cell motions in a micro channel with a diverging and converging bifurcation. They observed asymmetry in velocity profiles of RBC's.

Fridjonsson *et al*. (2011) studied the dynamics and flow partitioning of colloidal particles in the Y shape bifurcation channel formed with circular segments experimentally and numerically. They observed that Newtonian fluids exhibited parabolic profile whereas, Power law fluids exhibited blunted profiles. Gijsen *et al*. (1999) investigated the influence of non-Newtonian properties of blood on the velocity distribution in carotid bifurcation experimentally and numerically. They found that the axial velocity profile of the non-Newtonian fluid was blunted. The non-Newtonian fluid had low velocity gradients at divider wall, and high velocity gradients at non-divider wall. Anastasiou *et al*. (2012) studied the Newtonian and non-Newtonian properties of pulsatile blood flow in micro channels using micro particle image velocimetry. They measured velocity distribution and wall shear stress during the flow of blood. In a recent review article, Kumar and Graham (2012) have discussed the margination of leukocytes, RBCs and platelets and presented a modified shear induced migration model for the segregation behavior in binary suspension of rigid and deformable particles.

Audet and Olbricht (1987) observed that in small vessels, circular particles having the diameters comparable to the vessel diameter could experience significant drift across background fluid streamlines. Ditchfield and Olbricht (1996) performed flow experiments (at low Reynolds number) with suspension of spherical particles through symmetric Y shaped and non-symmetric T- shaped bifurcations. They have observed that the hydrodynamic interactions between the particles have a strong influence on the flux of the particles through bifurcation. For a small value of the particle volume fraction these interactions could be very important. Roberts and Olbricht (2003) analyzed the motion of freely suspended particles in low Reynolds number flows. Their study was mainly focused on Y–shape, T–shape and Oblique bifurcation

channels formed by circular tubes for a range of particle volume fractions up to 0.06. The inference from the results was that there was a difference in the partitioning of the particles between the bifurcation and those of the suspending fluid. From the above inference they suggested a method to design a practical micro fluidic device which has multiple bifurcations to separate particles. Roberts and Olbricht (2006) considered Y-shaped and oblique bifurcations with branches of square or rectangular cross-section for their experimental study. Their observations were similar to that of Roberts and Olbricht (2003) but found that the magnitude of difference depends on the aspect ratio of the cross-section of the channel and also on the bifurcation geometry. They reported greater volumetric flow rate for the particles entering the downstream branch.

Schmid-Schonbein *et al*. (1980), Perkkio and Keskinen (1983) and Barber *et al*. (2008) have proposed mathematical models to understand the flow and particle partitioning and computed the cell distribution at bifurcations. Most of these studies dealt with dilute concentrations and situations where the size of the particles was almost comparable with the channel width. The flow physics of concentrated suspensions of small particles relative to channel width is less studied numerically and experimentally despite their wide application. Xi and Shapley (2008) have performed NMR experiments on flow of concentrated suspensions through asymmetric T-junction bifurcation channel of rectangular cross-section. They observed that the particles are almost equally partitioned in downstream branches even though the flow partitioning is unequal.

Later, Ahmed and Singh (2011) performed numerical simulations based on the diffusive flux model and obtained good agreement with the experimental work of Xi and Shapley (2008). Recently, Reddy and Singh (2014) have carried out numerical simulations of suspension flow

through two dimensional oblique bifurcating channels and reported that flow partitioning and particle partitioning do not seem to be the same because of redistribution of particles in the daughter branches.

In a significant work, Zrehen and Ramachandran (2013) observed the existence of secondary currents in pressure driven flow of concentrated suspension of non-colloidal particles at low Reynolds number passing through a conduit of square cross section. The secondary currents in 3D channel with non-axisymmetric cross-section may influence the particle distribution. Only few studies have focused on suspension flow in complex geometries such as contraction-expansion flows (Iwamiya *et al*. 1994; Altobelli *et al*., 1997; Rao *et al*. 2007; Miller and Morris, 2006; Moraczewski and Shapley, 2006). The above mentioned studies has motivated us to perform detailed studies on the distribution of particles and its relation to the velocity profile considering utilization of this knowledge in several industrial and biological processes where particle migration is an important issue.

To the best of our knowledge there are no experimental and simulation studies on flow of concentrated suspensions in symmetric three dimensional Y and T shape bifurcation channels that are common in microfluidic devices. In this work, we have studied the flow of concentrated suspension of rigid mono dispersed particles in viscous liquid flowing through symmetric bifurcation channel via Computational Fluid Dynamics (CFD) simulations. The CFD simulations based on continuum models such as diffusive flux and suspension balance have advantage over the computationally intensive particle tracking simulations as they can be generalized for complex geometries. In chapter 2, we discussed in detail about models used to study the shear induced migration in bifurcation channels and implementation of model used in this study.

1.5. Objectives

The overall objective of the current study is to study the suspension flow behavior in symmetric Y and T shaped channels. To achieve the overall objective we have performed the following simulations.

1. To study the effect of bifurcation angle, particle concentration and flow rate near the bifurcation on the particle migration of concentrated suspension in two-dimensional symmetric Y shaped bifurcation channel.
2. To study the shear-induced particle migration of concentrated suspension in three dimensional Y shaped bifurcation channel.
3. To study the particle migration of dense suspension through diverging and converging flow in a T shape bifurcation channel.

1.6. Organization of the thesis

The thesis consists of six chapters. The introduction and motivation for the work, including literature review is presented in chapter 1. In chapter 2, we describe continuum models which describe the shear induced migration and their numerical implementation. Chapter 3 describes the shear induced migration of concentrated suspension through two dimensional Y-shaped bifurcation channels. We have validated the simulation results with experimental results available for straight channel. Chapter 4 investigates the shear induced particle migration in three dimensional bifurcation channels. Chapter 5 further investigates the flow of dense suspension in diverging and converging (T-shaped) bifurcation channel. Chapter 6 describes the conclusion of our work and future work that may be carried out in this direction.

भारतीय प्रौद्योगिकी संस्थान गुवाहाटी
Indian Institute of Technology Guwahati

CHAPTER-2

Shear Induced Migration Models

भारतीय प्रौद्योगिकी संस्थान गुवाहाटी
Indian Institute of Technology Guwahati

2. Shear Induced Migration Models

The main interest of this chapter is to present brief survey on the continuum models used to capture the shear induced migration phenomena in complex geometries. The implementations of Diffusive flux model in OpenFOAM and followed by validation of numerical results are also discussed.

2.1. Introduction

Several experimental observations of shear induced migration phenomena in various geometries have motivated a number of theoretical studies to understand this behavior. There are also a number of numerical simulation studies based on continuum based models as well as particle level simulation. Particle tracking simulations, such as Stokesian Dynamics (Brady and Bossis, 1985; Brady and Bossis, 1988; Brady, 1993; Nott and Brady, 1994) and boundary element methods (Ingber, 1990; Phan-Thien and Kim, 1994), have been used to understand the microstructure and rheology of concentrated suspensions. However, these simulations are limited to only few thousand particles due to large computational power and memory requirements. The continuum models allow simulation of realistic problems which are macroscopic in nature and which typically contain a large number of suspended particles. These kinds of problems are of considerable practical interest.

From the continuum point of view, basically there exist two major continuum models which successfully explain the flow physics of the shear induced particle migration in concentrated suspensions. The first model, named as Diffusive Flux Model (DFM) was

developed by Phillips *et al.* (1992) based on the scaling arguments proposed by Leighton and Acrivos (1987b) who argued that the spatially varying inter-particle interaction frequency and effective viscosity are responsible for the particle migration and diffusion. This model is highly successful in prediction of the particle migration in rectangular channel flow (Koh *et al*. 1994; Lyon and Leal, 1998) pressure driven pipe flow (Hampton *et al*. 1997) and in wide gap Couette geometry (Abbott *et al*. 1991). But, the original model has limitations in cone & plate and parallel plate torsional geometries. In the cone and plate geometry, the diffusive flux model predicts no migration of the particles, while inward migration of the particles in the parallel plate geometries. The experimental observations by Chapman (1990) and Chow *et al.* (1994, 1995) were different from the predictions of the diffusive flux model.

Krishnan *et al.* (1996) rectified the setbacks of the diffusive flux model of Phillips *et al*. (1992) by proposing modifications which include the effects of curvature to correct the discrepancies in parallel plate and cone & plate geometries. This led to the effective use of diffusive flux model for the curved geometries. Zhang and Acrivos (1994) extended Phillips model to study the viscous resuspension of heavy particles in fully developed laminar flows in horizontal pipe. They employed Galerkin finite element method to solve the governing equations. Fang and Phan-Thien (1995) conducted their study on the numerical modeling of particle migration in the concentrated suspension by finite volume method. They studied migration in one -dimension and two -dimension flows with arbitrary geometry and boundary conditions. Phan-Thien *et al*. (1995) used the diffusive flux model to find the particle migration in eccentric flows. They employed explicit pseudo-transient finite volume method to solve the governing equations and obtained good agreement with experiment results.

Phan-Thien and Fang (1996) tested the diffusive flux model in channel and pulsatile flows and they employed unstructured finite volume method. Subia *et al.* (1998) also used diffusive flux model based on Galerkin finite element method to study shear induced particle migration in non-homogeneous shear flows of suspensions for two dimensional and three dimensional (axisymmetric) flows. Chen (2013) employed a boundary element method to successfully investigate the migration of one or two particles along the symmetric axis perpendicular to the circular disk.

The second model, named as Suspension Balance Model (SBM) was proposed by Nott and Brady (1994). It is based on the conservation of mass and momentum equations over the bulk suspension (fluid + particle phases) and over particle phase only. The particle velocity fluctuations are introduced with a non-local description of suspension temperature. Morris and Boulay (1999) illustrated the importance of anisotropy and normal stress difference effects in Suspension balance model for predictions of migration in curvilinear flows. Fang and Phan-Thien (1999) proposed a modification in the suspension balance model that can fit in convection-diffusion equation for unstructured finite volume implementation. They compared the velocity and concentration profiles with available experimental results for channel flow. They found that the model predictions of concentration agree well with experimental data, at high bulk concentrations. Fang *et al*. (2002) performed simulations using finite element and finite difference methods for steady and transient states in different flow geometries like Couette flow, pressure driven pipe flow, channel flow and eccentric journal bearing flow. The results obtained are in good agreement with experimental data for consistent sets of empirical constants. Miller and Morris (2006) proposed non-local shear stress term in the suspension

balance model which depends on the particle radius, characteristic length of geometry and maximum velocity in a pressure driven flow. They also introduced the concept of non-local shear rate which is added to the local shear rate to get rid of the unphysical cusp in concentration profile at the center of the channel. They also extended the suspension balance model for general geometries. Kauzlaric *et al*. (2011) overcame this problem by incorporating the effective deformation rate tensor in the diffusive flux model which considers the collisions between the particles at the center of the channel where local shear rate is zero.

Vollebregt *et al*. (2010) demonstrated that the driving force for the particle migration can be expressed in terms of non-equilibrium osmotic pressure and chemical potential and various shear induced migration models can be generalized as a mixture model. This way they have applied the shear induced migration models to the membrane filtration and further extended it to the separation of bi-dispersed suspensions. Both the diffusive flux and suspension balance model over predict the wall concentration. Vollebregt *et al*. (2012) in the mixture model proposed the adjustment of the maximum packing close to the wall, which corrects the depletion of particles near the wall. Recently, van Dinther *et al*. (2013) have probed the role of shear induced diffusion phenomena in the fractionation of droplets based on their size. The suspension balance model was extended by Dbouk *et al.* (2013) to two–dimensional flows through frame–invariant formulations to account for local kinematics of the suspension including buoyancy effects and applied to the resuspension and mixing of mono dispersed suspension in a horizontal Couette cell. Both the diffusive flux and suspension balance models have been used extensively to study the unidirectional and steady flow in simple one and two dimensional geometries. Shapley *et al*. (2004) have evaluated the performance of diffusive flux

and suspension balance model by comparing the simulation results with experimental data obtained from NMR imaging. The diffusive flux model is relatively simple as it couples generalized Newtonian stress/strain relationship with shear-induced migration of particles and effective viscosity depends on the local volume fraction of particles. The modified version of suspension balance model (Morris and Boulay 1999) considers non-Newtonian rheology of concentrated suspensions (particularly normal stress differences) to incorporate the anisotropy in stresses. Though, the stress tensor is still symmetric for suspension, it is not isotropic unlike Newtonian fluids. We have chosen Diffusive flux model as several past studies have confirmed that for rectilinear channel flow, predictions of diffusive flux model and suspension balance model are similar. In bifurcation channel the region where the flow encounters curvature is much smaller compared to the straight section. Since the net migration depends on the total strain, the curvature induced flux is not expected to be important. In a previous study on migration in asymmetric T- junction bifurcation channel (Ahmed and Singh, 2011) the predictions from diffusive flux model were found to be in good agreement with the experiments of Xi and Shapley (2008).Thus, for simplicity of implementation, and economy of computations we have chosen diffusive flux model in our present study which considers symmetric stress tensor. The mass, momentum and particle conservation equations of the diffusive flux model were solved using the finite volume method (FVM). We utilize the finite volume method (FVM), as it proves advantageous due to conservative nature of its construction which enforces mass and momentum conservation over each computational element or control volume (CV) by balancing fluxes between one control volume and its neighbors. The finite volume method is also relatively easy to implement and allows more

flexibility in the numerical setup than the finite element method. In this work, we have used the OpenFOAM environment which uses the Finite Volume Method (FVM) to solve the system of Partial Differential Equations (PDEs). "The OpenFOAM (Open Field Operation and Manipulation) CFD Toolbox is a free, open source CFD code produced by the "OpenCFD Ltd." OpenFOAM can solve systems of partial differential equations ascribed on any 3D unstructured mesh of polyhedral cells. The fluid flow solver uses implicit, pressure-velocity coupling and iterative solution framework.

The governing equations and method of solution are explained in following sections. In section 2.2, we describe briefly the different models that represent the migration that originates from the hydrodynamic particle diffusion in the suspension flow. In next section we describe the implementation of DFM in OpenFOAM.

2.2. Diffusion models

2.2.1. Original Diffusive Flux Model [Phillips *et al.* 1992]

In this model, the constitutive description for the suspension is divided into two parts. First, an expression for the stress tensor is written for suspension and modeled as a Newtonian fluid with viscosity that depends on the local volume fraction of the solids. Second, the distribution of solids is obtained from the solution of the diffusion equation that describes the motion of the particles in a flow field.

2.2.1.1. The stress tensor

The stress tensor for Newtonian fluid is expressed as,

$$\boldsymbol{\tau} = 2\eta(\phi)\mathbf{E} \qquad (2.1)$$

In the above equation, $\mathbf{E}$ denotes the rate of strain tensor which is expressed as,

$$\mathbf{E} = \frac{1}{2}\left[\nabla\mathbf{U} + (\nabla\mathbf{U})^T\right] \tag{2.2}$$

2.2.1.2. Continuity and Momentum equations

The material (i.e. suspension) under flow is considered to be a continuum medium that obeys laws of conservation of mass and momentum (Navier 1823, Stokes 1845).

Continuity equation

The mass conservation of material under flow (suspension) is expressed through the continuity equation as follows,

$$\frac{\partial\rho}{\partial t} + \nabla\bullet(\rho\mathbf{U}) = 0 \tag{2.3}$$

Where, ρ is the density of the suspension, t is time and $\mathbf{U}$ velocity of the suspension.

Momentum equation

The momentum of equation is given by:

$$\frac{\partial\rho\mathbf{U}}{\partial t} + \rho\mathbf{U}\bullet\nabla\mathbf{U} = \nabla\bullet\Sigma + \rho\mathbf{g} \tag{2.4}$$

Here, Σ is bulk stress tensor and $\rho\mathbf{g}$ are the gravitational body forces. The bulk stress tensor can be expressed as $\Sigma = -p\mathbf{I} + \boldsymbol{\tau}$. p is pressure, τ is viscous stress tensor and I is isotropic unit tensor. In this work we consider steady state, incompressible and laminar flow at very low Reynolds Number (Re << 1) without external forces which makes the unsteady

$\left(\rho = const \;\&\; \frac{D\rho}{Dt} = 0\right)$ and the inertial term vanish and the above equations (2.3 and 2.4) simplifies to:

$$\nabla \bullet \mathbf{U} = 0 \tag{2.5}$$

and, $$-\nabla p + \nabla \bullet \boldsymbol{\tau} = 0 \tag{2.6}$$

2.2.1.3. Particle conservation equation

The steady state mass conservation for particles is represented as:

$$\nabla \bullet \mathbf{U}\phi = -\nabla \bullet \mathbf{N}_t \tag{2.7}$$

where, $\mathbf{N}_t$ denotes the particle flux that accounts for different migration mechanisms such as sedimentation, Brownian motion, shear induced migrations. Equation (2.7) is solved together with equations (2.5) & (2.6) to track the evolution of particle concentration ϕ and flow field U. In our study, we have considered the neutrally buoyant and non-colloidal suspensions so that sedimentation and Brownian motion are negligible, which leads to the term N_t in Equation (2.7) equal to sum of fluxes resulting from spatially varying inter-particle interaction frequency $\left(\mathbf{N}_c\right)$ and spatially varying viscosity $\left(\mathbf{N}_\eta\right)$. These particle fluxes that result from gradients of viscosity and collision rate are explained in the following sections.

Flux due to spatially varying interaction frequency

Figure 2.1 shows a schematic diagram of irreversible two body collisions. Figure 2.1a shows that a collision (close interaction) can occur when two particles in adjacent shearing surfaces move past one another. Such collision can cause a particle to be irreversibly moved from its original stream line. A particle experiences a higher frequency of collisions from one direction

than from opposing direction and will migrate normal to the shearing surface in the direction of lower collision frequency. When there is a velocity gradient in shear flow, irreversible two body collisions can occur due to spatially varying frequency of interactions. The number of collisions experienced by a test particle will scale as $\dot{\gamma}\phi$, where, $\dot{\gamma}$ is the magnitude of the local shear rate. The variation in the collision frequency over a distance of *O (a)* is then given by $a\nabla(\dot{\gamma}\phi)$.

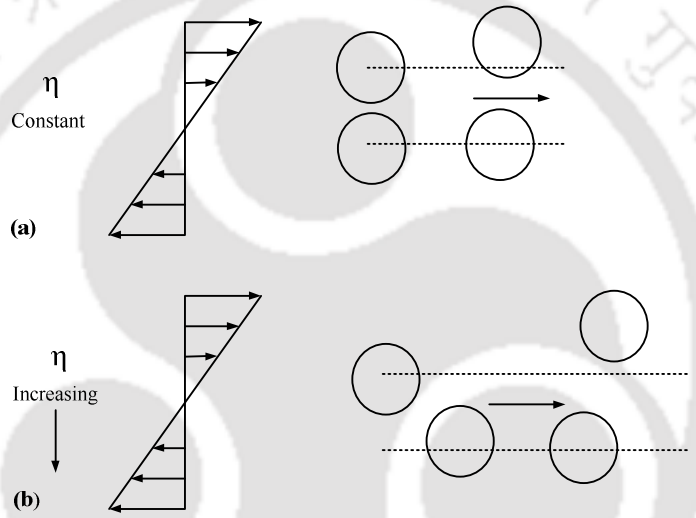

Figure 2.1. Schematic diagrams of irreversible two-body collisions with (a) constant viscosity and (b) spatially varying viscosity (Phillips *et al*. 1992).

Leighton and Acrivos (1987) assumed that the particle migration velocity is linearly proportional to the variation in the collision frequency and that each of these two-body interactions gives rise to a displacement of *O* (*a*) leads to an expression for the flux $\boldsymbol{N}_c$ given as,

$$\boldsymbol{N}_c = -K_c a^2 \phi \nabla(\phi \dot{\gamma}) = -K_c a^2 (\phi^2 \nabla \dot{\gamma} + \phi \dot{\gamma} \nabla \phi) \qquad (2.8)$$

Where, K_c is a proportionality constant of order unity that can be determined from experimental data. In our study, we have chosen $K_c = 0.4$.

The first term on the right side of equation (2.8) implies that even if there is no gradient in the particle volume fraction, migration will result if the particles on one side of a test particle are moving past it more rapidly than on the other side. Because this variation gives a higher number of inter particle interactions on the side with higher $\dot{\gamma}$. Therefore, a high shear rate or high concentration of particles results in a larger frequency of collisions. The second term on right side of Equation (2.8) states that a gradient in particle volume fraction will cause a spatial variation in the frequency of interactions. The flux due to the variation in shear rate and that due to a concentration gradient generally oppose one another.

Flux due to Spatially Varying Viscosity

The spatially varying viscosity $\eta(\phi)$ caused by the existence of gradients in particle concentration as shown in Figure 2.1b can also affect the interaction between two particles. A gradient in viscosity results in the resistance to motion on one side of the particle to be the higher than on the other side. This results in particle being displaced in the direction of decreasing viscosity as shown in Figure 2.1b. The magnitude of this displacement was given quantitatively by Leighton and Acrivos (1987b). They assumed the magnitude of this displacement was proportional to $\left(a/\eta\right)\nabla\eta$, multiplied by the particle radius. For small gradient in concentration, the variation in viscosity is linear in the concentration gradient. The

above expression, multiplied by the rate of interactions $\dot{\gamma}\phi$, gives the corresponding drift velocity. Finally, multiplying by ϕ and using equation (1.12) to express the gradient of viscosity in terms of $\nabla\phi$ gives the flux.

$$\mathbf{N}_\eta = -K_\eta a^2 \dot{\gamma}\phi^2 \frac{\nabla\eta}{\eta} = -K_\eta \dot{\gamma}\phi^2 \left(\frac{a^2}{\eta}\right)\frac{d\eta}{d\phi}\nabla\phi \qquad (2.9)$$

The fact that the expression (2.9) is independent of the magnitude of the viscosity η is consistent with the experimental finding by Abbott *et al*. (1991) that shear induced particle migration rates are independent of the viscosity of the suspending fluid.

In the above equations, a is the particle radius, ϕ is the bulk particle volume fraction and $\dot{\gamma}$ is the local shear rate given as:

$$\dot{\gamma} = \sqrt{2\mathbf{E}:\mathbf{E}} \qquad (2.10)$$

The total flux of particles responsible for migration, implemented in equation (2.7) can be given in the form of:

$$\mathbf{N}_t = \mathbf{N}_c + \mathbf{N}_\eta \qquad (2.11)$$

Two parameters K_c and K_η, presented in above equations (2.8) and (2.9) are proportionality constants and are parameters determined from fitting simulation data to experimental results. These parameters represent different material properties, particle shape, size distribution and surface roughness, as they play an important role in irreversible particle collisions; they are of the order of unity and should be independent of particle size and volume fraction (Phillips *et al*.1992).

Phillips *et al.* (1992) found from a comparison with their experimental results that a ratio of $\frac{K_c}{K_\eta} = 0.66$ provided best fit to the experimental data under a number of flow geometries. The model parameters are taken as $\boldsymbol{K_c = 0.41}$ and $\boldsymbol{K_\eta = 0.62}$ in accordance with the optimal values determined by Phillips *et al*. (1992) based on their comparison of experimental data and numerical results. The applicability of the model parameters in multidimensional shear flows has been supported by the investigations of Zhang and Acrivos (1994) and Fang and Phan-Thien (1995), who have observed reasonable agreement between computed and experimental particle concentration in Couette flow. Leighton and Acrivos (1987a) also proposed similar values for coefficients by comparison with experimental results in their paper. The results are similar to those obtained by Phillips *et al*. (1992). Therefore, we have also used the same parameters that were used by the Phillips *et al.* (1992). Ideally both parameters would be independent of a, ϕ and $\dot{\gamma}$. However, they should also be independent of the flow geometry and particle density. Other researchers (Tetlow *et al*. 1998, Rao *et al*. 2002, Lam *et al*. 2004) have shown that they are completely independent of the particle volume fraction.

2.2.2. Modified Phillips model

Krishnan *et al.* (1996) proposed an additional migration flux originates from the flow curvature. They defined this additional curvature-induced flux as:

$$\boldsymbol{N_r} = K_r \boldsymbol{n} k a^2 \dot{\gamma} \phi \qquad (2.12)$$

Which explains as the flux due to the different curved-streamlines in a shear flow. The term $\boldsymbol{n}$ is the unit normal vector in the radially outward direction in curved streamline shear flow, k is the curvature of the streamline, and K_r is an experimentally fitted parameter that must be re-adjusted with the other two previous parameters K_c and K_η. Finally, the total flux in the modified Phillips model implemented in equation (2.7) would be,

$$\boldsymbol{N}_t = \boldsymbol{N}_c + \boldsymbol{N}_\eta + \boldsymbol{N}_r \tag{2.13}$$

2.2.3. ϕ -Dependent K_c Model

Graham *et al*. (1998) proposed that the parameter K_c as a function of the volume fraction of particles in the modified Phillips model. Their argument was based on the works of Brady and Morris 1997 and Tetlow *et al.* 1998.

2.2.4. Flow-aligned Tensor Model

Fang *et al.* (2002) incorporated the flow aligned tensor model concept into the diffusive flux model and thus modified the two fluxes as the following

$$\boldsymbol{N}_c = -K_c a^2 \boldsymbol{\phi} \boldsymbol{\nabla} (\phi \dot{\gamma} \boldsymbol{Z}) \tag{2.14}$$

$$\boldsymbol{N}_\eta = -K_\eta a^2 \boldsymbol{\phi} (\dot{\gamma} \boldsymbol{\phi} \boldsymbol{Z}) . \boldsymbol{\nabla} \ln \eta \tag{2.15}$$

Where, $\boldsymbol{Z}$ is the flow aligned tensor that can be determined by imposing inhomogeneity in velocity, velocity gradient and vorticity directions.

2.3. Suspension Balance Model (SBM)

It was first proposed by Nott and Brady (1994) and modified later by Morris and Boulay (1999). This model is based on the conservation of mass and momentum for bulk suspension phase as well as particle phase. The particle phase transport equations were derived by averaging the mass and momentum conservation equations over the particle phase. The non-local suspension behavior is explained in terms of particles velocity fluctuations. These fluctuations were obtained from the solution of additional transport equation for suspension temperature.

2.3.1. Governing Equations

The equations were developed by assuming that the particle phase can be approximated as a continuum. An ensemble average, as explained in Drew and Lahey (1993), is taken of the mass and momentum equations over the bulk suspension (fluid and particle phase) and over the particle phase only.

The steady state mass and momentum balance equations for bulk suspension are given as:

$$\nabla \cdot \boldsymbol{U} = 0 \tag{2.16}$$

$$\nabla \cdot \boldsymbol{\Sigma} + \langle \rho \rangle \mathbf{g} = 0 \tag{2.17}$$

where, $\boldsymbol{U}$ is the bulk suspension velocity and $\langle \rho \rangle$ is the average suspension density and $\boldsymbol{\Sigma}$ is the bulk suspension stress, $\langle \boldsymbol{\rho} \rangle \boldsymbol{g}$ is the gravity force. For Neutrally-buoyant particles, the weight is balanced by the buoyancy and hence the net gravity force appearing in equation (2.17) disappears. The particle mass balance is:

$$\frac{\partial \phi}{\partial t} + \nabla \bullet (\boldsymbol{U}^{p} \phi) = 0 \tag{2.18}$$

This may be expressed by virtue of the incompressibility of the bulk flow as,

$$\frac{\partial \phi}{\partial t} + \mathbf{U} \bullet \nabla \phi = -\nabla \bullet \mathbf{j}_{\perp} \tag{2.19}$$

where $\boldsymbol{U}^{p}$ is the local velocity of the particle phase and $\mathbf{j}_{\perp} = \phi(\mathbf{U}^{p} - \mathbf{U})$ is the particle migration flux i.e. the particle flux relative to the bulk motion.

The particle momentum conservation at very small Reynolds number and with no external force is given by:

$$\nabla \bullet \boldsymbol{\Sigma}^{\mathrm{p}} + n \left\langle \mathbf{F}^{\mathrm{H}} \right\rangle_{\mathrm{p}} = 0 \tag{2.20}$$

$\langle \ \rangle p$ is the average on the particle phase, $n = \dfrac{3\phi}{4\pi a^{3}}$ is the number density of particles and

$\mathbf{F}^{\mathrm{H}}$ is the hydrodynamic drag force on a particle given by:

$$\left\langle \mathbf{F}^{H} \right\rangle = -6\pi \eta_{o} a f^{-1}(\phi)(\mathbf{U}^{p} - \mathbf{U}) \tag{2.21}$$

$f^{-1}(\phi)$ is the mean resistance since $f(\phi)$ is the sedimentation hindrance function that represents the mobility of the particle phase

$$f(\phi) = (1 - \phi / \phi_{m})(1 - \phi)^{\alpha - 1} \tag{2.22}$$

The parameter α is given by Richardson and Zaki (1954) and Davis and Acrivos (1985) as $2 \le \alpha \le 4$.

The migration flux in the SBM can be defined as

$$\boldsymbol{N}_{t} = \frac{2a^{2}}{9\eta_{o}} f(\phi) \left[\nabla \bullet \boldsymbol{\Sigma}^{p} \right] \tag{2.23}$$

Using general definition of migration $\mathbf{j}_\perp = \boldsymbol{N}_t$ the final form of migration flux obtained by substituting equation (2.21) into equation (2.20) is

$$\mathbf{j}_\perp = \phi(\mathbf{U}^p - \mathbf{U}) = \frac{2a^2}{9\eta_o} f(\phi)\left[\nabla\bullet\boldsymbol{\Sigma}^p\right] \tag{2.24}$$

The general form of the particle mass conservation equation then becomes,

$$\frac{\partial\phi}{\partial t} + \mathbf{U}\bullet\nabla\phi = -\nabla\bullet\left[\frac{2a^2}{9\eta_o} f(\phi)\left[\nabla\bullet\boldsymbol{\Sigma}^p\right]\right] \tag{2.25}$$

Thus, the knowledge of $\boldsymbol{\Sigma}^p$ and its variation in ϕ allows predicting the particles migration whatever the geometry is.

2.3.2. Suspension stress

In this model, the total stress $\boldsymbol{\Sigma}$ is decomposed into a fluid phase stress $\boldsymbol{\Sigma}^f$ and a particle stress $\boldsymbol{\Sigma}^p$ such that:

$$\boldsymbol{\Sigma} = \boldsymbol{\Sigma}^f + \boldsymbol{\Sigma}^p \tag{2.26}$$

The fluid phase stress $\boldsymbol{\Sigma}^f$ is defined as

$$\boldsymbol{\Sigma}^f = -P_f\mathbf{I} + 2\eta_o\mathbf{E} \tag{2.27}$$

Where, $\mathbf{E} = \frac{1}{2}\left[\nabla\mathbf{U} + (\nabla\mathbf{U})^T\right]$ is the local rate of strain tensor, P_f is the local fluid phase pressure. The constitutive law for the particle stress is that suggested by Morris and Boulay (1999) for shear flows, is given by below equation (2.28) and contains both shear and normal portions.

$$\Sigma^{P} = -\eta_o \eta_N(\phi)\dot{\gamma}\boldsymbol{Q} + 2\eta_o \eta_p(\phi)\mathbf{E} \tag{2.28}$$

$(-\eta_o\eta_N(\phi)\dot{\gamma}\boldsymbol{Q})$ is the particle normal stress diagonal tensor, $(2\eta_o\eta_p(\phi)\mathbf{E})$ is the particle shear stress tensor, $\eta_p(\phi) = (\eta_s(\phi) - 1$ is the shear viscosity of the particle phase non-dimensionlized by the viscosity of the suspension η_o and $\eta_N(\phi)$ is the normal stress viscosity depending on ϕ. In their original paper, Morris and Boulay (1999) proposed the following expression for $\eta_N(\phi)$

$$\eta_N(\phi) = K_N\left(\frac{\phi}{\phi_m}\right)^2\left(1-\frac{\phi}{\phi_m}\right)^{-2} \tag{2.29}$$

Where K_N is a fitting parameter that was set to 0.75 to match the experimental data of Phillips *et al*. (1992).

Shear viscosity can be modeled by using different models including,

Morris and Boulay (1999): $\eta_s(\phi) = 1 + 2.5\phi_m + \dfrac{(\phi/\phi_m)}{(1-\phi/\phi_m)} + \dfrac{K_s(\phi/\phi_m)^2}{(1-\phi/\phi_m)^2}$ (2.30)

Krieger (1972): $\eta_s(\phi) = \left(1-\phi/\phi_m\right)^2$ (2.31)

ϕ_m is the maximum packing particle volume fraction and $K_s = 0.1$

The tensor parameter $\boldsymbol{Q}$ captures the anisotropy of the normal stress with the form

$$\boldsymbol{Q} = \begin{pmatrix} 1 & 0 & 0 \\ 0 & \lambda_2 & 0 \\ 0 & 0 & \lambda_3 \end{pmatrix} \tag{2.32}$$

Where $\lambda_2 \approx 0.8$ and $\lambda_3 \approx 0.3$ provide reasonably good agreement with concentrated suspension rheology (Zarraga *et al.* 2000) and with observed migration in viscometric flows (Phillips *et al*. 1992; Chow *et al.* 1994). The directions of $\boldsymbol{Q}$ correspond to the principal directions of viscometric shear flow with 1, 2 and 3 denoting flow, gradient and vorticity respectively. The anisotropy in the particle stress tensor arises from non-zero normal stress differences in Stokesian suspensions. Several experiments have measured the normal stress differences and particle pressure for concentrated suspensions (Gadala-Maria, 1979, Zarraga *et al*. 2000, Singh and Nott, 2003, Dbouk *et al,* 2013).

The two normal stress differences and the suspension pressure $\prod$ are given in terms of this modeling by

$$N_1 = (\Sigma_{11} - \Sigma_{22}) = (\Sigma_{11}^p - \Sigma_{22}^p) = -\eta_o \eta_N \dot{\gamma}(1-\lambda_2) \qquad (2.33)$$

$$\mathrm{N}_2 = (\Sigma_{22} - \Sigma_{33}) = (\Sigma_{22}^{\mathrm{p}} - \Sigma_{33}^{\mathrm{p}}) = -\eta_{\mathrm{o}} \eta_{\mathrm{N}} \dot{\gamma}(\lambda_3 - \lambda_2) \qquad (2.34)$$

And $$\prod = -\frac{1}{3} tr(\Sigma^p) = -\Sigma_{11}^p \left(\frac{1+\lambda_2+\lambda_3}{3} \right) = \left[\Sigma_{22}^p + \frac{1}{3}(\alpha_1 - \alpha_2) \right] \qquad (2.35)$$

In the above equation: $tr(\Sigma^p) = (\Sigma_{11}^p + \Sigma_{22}^p + \Sigma_{33}^p)$. The combinations of the above definitions for both, the particle phase and fluid phase stress yields finally to bulk suspension stress in the suspension balance model of the form.

$$\boldsymbol{\Sigma} = \boldsymbol{\Sigma}^f + \boldsymbol{\Sigma}^p = -P\mathbf{I} - \eta_o \eta_N(\phi)\, \dot{\gamma} \boldsymbol{Q} + 2\eta_o \eta_p(\phi)\mathbf{E} \qquad (2.36)$$

2.4. Numerical implementation of DFM in OpenFOAM

2.4.1. Model Governing Equations

The system of equations to be solved in DFM was explained in the section (2.2). To implement these equations in OpenFOAM, the governing equations should be in the form of general scalar transport equation. The particle conservation equation has to be solved along with momentum and continuity equations. The steady state continuity and momentum equations for the suspension are given as:

$$\nabla \bullet \rho \boldsymbol{U} = 0 \tag{2.37}$$

$$\nabla \bullet (\rho \boldsymbol{U}\boldsymbol{U}) = -\nabla P + \nabla \bullet \boldsymbol{\tau} \tag{2.38}$$

To solve the particle conservation equation with continuity and momentum equations in OpenFOAM, the particle equation is rearranged as:

$$\nabla \bullet \boldsymbol{U}\phi = \nabla \bullet \left(\Gamma \nabla \phi\right) + S_{\phi} \tag{2.39}$$

Where, Γ is the diffusion coefficient and S_{ϕ} is the source term. These terms are given as:

$$\Gamma = K_c a^2 \phi \dot{\gamma} + K_{\eta} a^2 \dot{\gamma} \phi^2 \frac{1}{\eta_o} \frac{d\eta}{d\phi} \tag{2.40}$$

$$S_{\phi} = \nabla \bullet K_c a^2 \phi^2 \nabla \dot{\gamma} \tag{2.41}$$

The Diffusive Flux Model was encounters difficulties in the regions where the local shear rate approaches to zero. For example in the pressure driven flows the shear rate at the channel center is zero. Since the shear-induced diffusivity is linearly proportional to the local shear rate, at the center the model predicts maximum particle volume fraction which is not

observed in the experiments. This leads to numerical instability and convergence problem as $\phi \to \phi_m$. To overcome this difficulty a small non-local shear rate ($\dot{\gamma}_{nl}$) proposed by Miller and Morris (2006) which is function of particle size and width of the channel is added to the local shear rate $\dot{\gamma}$. The non-local shear rate $\dot{\gamma}_{nl}$ is given by:

$$\dot{\gamma}_{nl} = a_s(\varepsilon)\dot{\gamma}_s \tag{2.42}$$

In the above equation, $\dot{\gamma}_s = \frac{U_{max}}{B}$ where $U_{\max}$ is the centre line velocity and the parameter $a_s(\varepsilon)$ is chosen as $a_s(\varepsilon) = \varepsilon^2$. The parameter $\varepsilon = \frac{a}{B}$ is the ratio of particle diameter to the channel width.

The governing partial differential equations for this transport problem are non-linear (in velocity and concentration). The momentum equation is non-linear in velocity since the effective viscosity of the mixture is a function of both concentration and the shear rate (velocity gradient). The scalar particle transport equation is non-linear in concentration. This is shown explicitly in the terms containing ϕ, ϕ^2 and the gradient of the concentration $\nabla\phi$ as well as the terms containing effective viscosity (η) which is also a function of local solids concentration. The system of Eqns. (2.37-2.39) are implemented by modifying existing "simple Foam" solver in library of the OpenFOAM to a new solver which represents Diffusive Flux Model (DFM). The SIMPLE scheme was employed for the pressure–velocity coupling to satisfy both continuity and momentum equations (Patankar 1981). Rhie-Chow interpolation was used to overcome checker boarding in velocity and pressure resulting from the use of

collocated grid. The flow chart for complete algorithm to solve the governing equations of suspension flow is presented in Appendix A and Diffusive Flux Model implementation in OpenFOAM is given in Appendix B. The solver settings and schemes used in the simulations are shown in Appendix C. The following gives the brief description of the code implementation procedure inside the simpleFoam solver.

```
int main(int argc, char *argv[])
{
    #include "setRootCase.H"
    #include "createTime.H"
    #include "createMesh.H"
    #include "createFields.H"
    #include "initContinuityErrs.H"
    simpleControl simple(mesh);
// * * * * * * * * * * * * * * * * * * * * * * * * * * * * * * * * * * * * //
Info<< "\nStarting time loop\n" << endl;
while (simple.loop())
{
    Info<< "Time = " << runTime.timeName() << nl << endl;
    Calculate parameters like: Γ , γ̇ , η(φ) etc.
    // --- Pressure-velocity SIMPLE corrector
    {
        Solve steady state momentum equation ∇•(ρUU) = −∇p + ∇•τ
```

Correct velocity-pressure to satisfy continuity equation $\nabla \bullet \rho \boldsymbol{U} = 0$

}

Solve particle conservation equation at each and every time step

$$\nabla \bullet \boldsymbol{U}\phi = \nabla \bullet \left(\Gamma \nabla \phi\right) + S_{\phi}$$

runTime.write();

}

Info<< "End\n" << endl;

return 0;

}

2.5. Boundary conditions

The boundary conditions for the suspension flow through channel are:

1. At the inlet, the uniform inlet velocity $\boldsymbol{U}$ and the uniform particle concentration ϕ is applied.
2. At the outlet, fully developed flow condition has been applied. (i.e. surface normal gradients are zero: $\boldsymbol{n} \bullet \nabla \phi = 0$; $\boldsymbol{n} \bullet \nabla \boldsymbol{U} = 0$, where $\boldsymbol{n}$ is the surface normal vector).
3. At the walls, no slip boundary condition for the velocity field and no flux boundary condition for the concentration have been applied. This leads to the following expression for the surface normal gradient.

$$\boldsymbol{n} \bullet \nabla \phi = -\frac{K_c \phi (\boldsymbol{n} \bullet \nabla \dot{\gamma})}{\dot{\gamma}\left(K_c + \phi \frac{K_\eta}{\eta} \frac{d\eta}{d\phi}\right)} \qquad (2.43)$$

The derivation of the above equation is given in appendix D. The validation of the model implementation in OpenFOAM is presented and discussed in the following section.

2.5.1. Validation

The success of any numerical simulation depends on how close it resembles the analytical solution, as well as experimental observations. Our numerical simulations for the pressure – driven flow of a suspension in a 2D rectangular channel are compared with the analytical solution of Phillips *et al.* (1992). The numerical simulation data are also compared with the experiments conducted by Lyon and Leal (1998) who measured the concentration profile and velocity profiles by using LDV method. The computational geometry of 2D straight channel for validation is shown in Figure 2.2a. The length and width of the channel, fluid properties and particle size were same as considered in the experiments of Lyon and Leal (1998). The ratio of channel half width to particle radius (B/*a*) was 18 for this case. Velocity and other simulation parameters that were considered in the simulations are presented in Table 2.1.

To validate the simulations for bifurcation channel we have considered the experimental work by Leble *et al*. (2011). We would like to mention that Leble *et al*. (2011) considered flow of dilute concentration (14%) in a Y-shaped channel which has confluence of converging and diverging branches and measured velocity profiles at various locations close to bifurcation. In our simulation we have considered only the diverging section of the channel and the computational geometry is shown in Figure. 2.2b. The locations at which we have compared the velocity profiles with the data of Leble *et al*. (2011) are also marked. The Y shape bifurcation geometry consists of one inlet and two outlets. The width and length of the inlet

section were 86 µm and 4 cm respectively. The width and length of the daughter channels were 86 µm and 2119 µm respectively. To check the grid independent solution we carried out simulations on four different grids. Grid A consists of 80000 cells (8000 cells in flow direction and 10 cells in axial direction), Grid B consists of 188000 cells (9400 cells in flow direction and 20 in gradient direction), Grid C consists of288000 cells (9600 cells in flow direction and 30 in gradient direction) and Grid D consists of 392000 cells (8000 cells in flow direction and 40 in gradient direction).

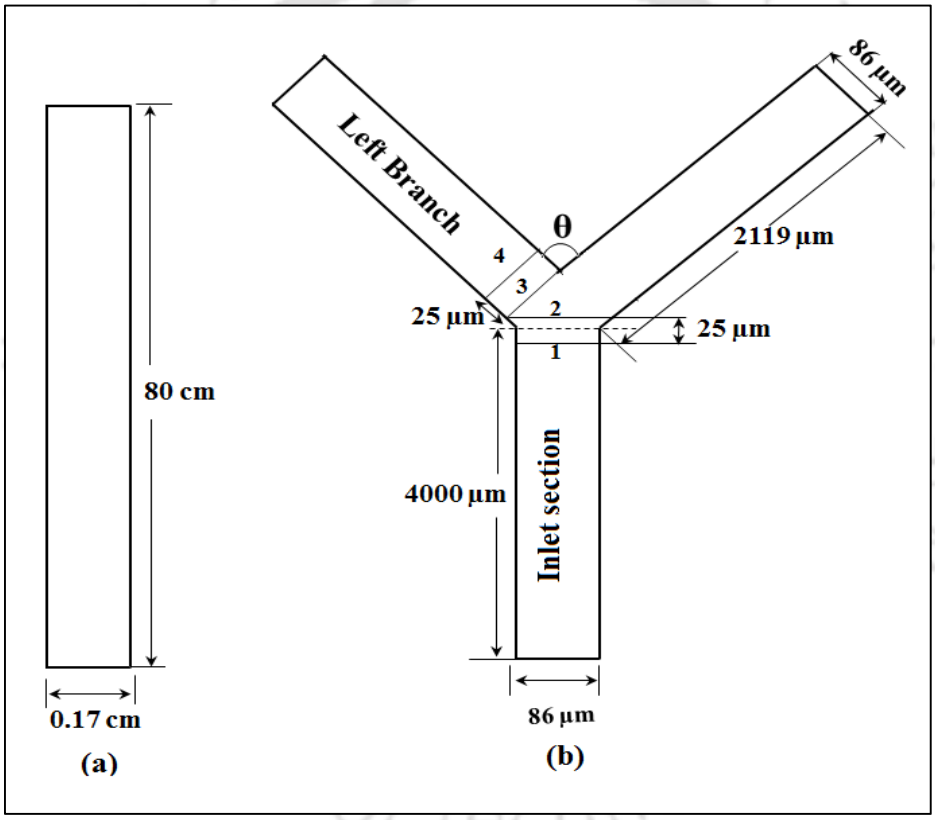

Figure 2.2. Schematic diagram of the geometries considered for the validation (a) rectangular channel used in experimental work of Lyon and Leal (1998) (b) Y shaped geometry used in experimental work of Leble *et al.* (2011).

Table 2.1: Simulation parameters considered for validation.

S.No.	Flow parameter	Symbol (Unit)	Validation Cases	
			Lyon and Leal (1998)	Leble et al.(2011)
1	Bifurcation angle	θ(degree)	-	60°
2	Suspending fluid viscosity	η_o(kg/m-s)	0.48	4.5×10^{-3}
3	Density of suspending fluid	ρ (kg/m^3)	1190	1002
4	Particle volume fraction	ϕ	0.3	0.14
5	Suspension inlet velocity	$\boldsymbol{U}$ (m/s)	3.7×10^{-3}	4.1×10^{-4}
6	Particle radius	a (m)	4.7×10^{-5}	4×10^{-6}
7	Channel half width	B(m)	8.5×10^{-4}	8×10^{-5}
8	Ratio of channel half width to particle radius	B/a	18	20

The length required for the fully developed flow was calculated by using the correlation proposed by Nott and Brady (1994) and is given below,

$$\left[\frac{L}{B}\right]_{ss} \approx \frac{1}{12d(\phi)}\left[\frac{B}{a}\right]^2 \tag{2.44}$$

Where, L is the length required for steady state, B is the half width of the channel and the function $d(\phi)$ accounts for the effect of particle concentration on shear-induced coefficient of diffusion.

$$d(\phi) = \frac{1}{3}\phi^2\left(1+\frac{1}{2}e^{8.8\phi}\right) \tag{2.45}$$

Figure 2.3a shows the comparative plots of the velocity and concentration profiles in a straight channel for bulk particle concentration (ϕ) of 30%. The axial velocity is normalized by the center line velocity ($\boldsymbol{U}_{\max}$) of fully developed flow of Newtonian fluid having the same effective viscosity and flow properties as that of suspension. The relative position in the span wise direction (y) is normalized by the half width of the channel (B). The velocity profiles are also compared with the fully developed parabolic profile of Newtonian fluid. It is observed that for the suspension flow velocity profile is blunted due to particle migration whereas Newtonian fluid shows parabolic profile. The velocity profiles obtained from our simulations are in good agreement with the analytical solution as well as experimental data. The velocity profiles from our simulations for Grids C (288000 cells) and Grid D (392000 cells) are nearly same indicating the grid independent solution.

Figure 2.3b shows the corresponding concentration profiles. Because of shear-induced migration, particles migrate from the region of high shear rate (wall) to the region of low shear rate (center). Thus, the particle concentration at the center line is higher compared to the concentration at the walls. We would like to mention that our numerical simulations were performed with a small but finite non-local shear rate contribution that were absent in the analytical solution. We have calculated the non-local term ($\dot{\gamma}_{nl}$) by using equation (2.42) proposed by Miller and Morris (2006) and it is found that the value of non-local term is 0.026 s^{-1}. As the non-local shear rate is much smaller compared to the local shear rate except at the center (where shear rate is zero), the choice of this parameter influences the results only at the center. The concentration profiles from our simulations are in good agreement with the analytical solution of Phillips *et al*. (1992) except at the center. The results are in qualitative

agreement with the experimental data of Lyon and Leal (1998). Both the analytical solution and our numerical solution show disagreement with the experimental data at the walls. Most of the experiments on shear induced migration have reported difficulty in collecting the data near the wall. There is also the lack of knowledge of proper boundary conditions at the wall. It is well known that in concentrated suspension flow the depletion of particles in a thin region near the wall causes apparent wall slip velocity, whereas in our simulations no slip boundary condition was considered at the walls of the channel.

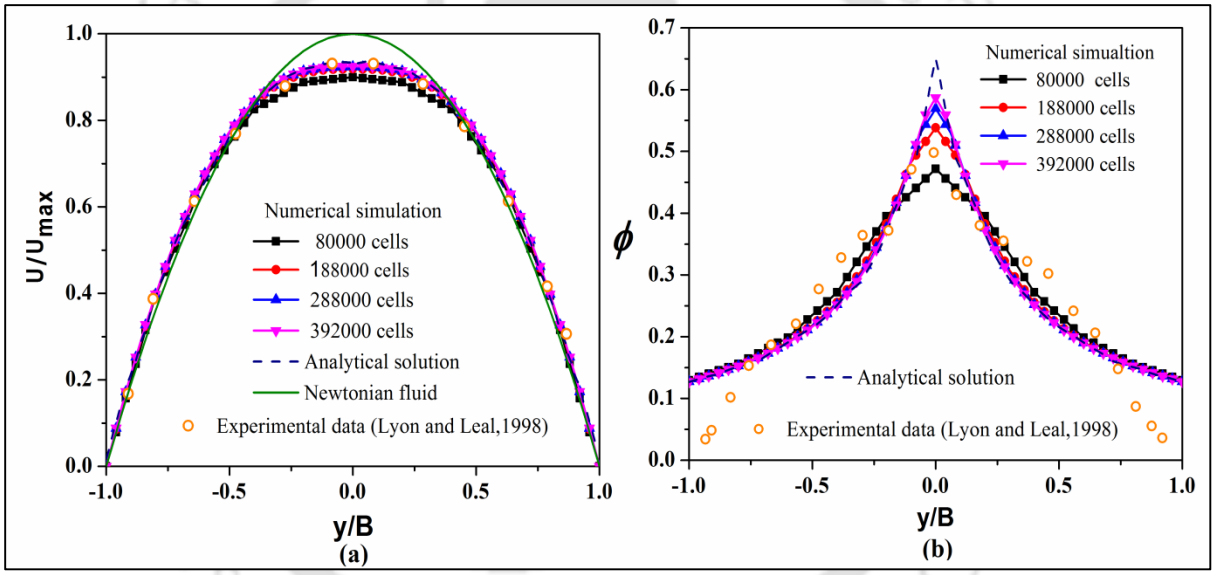

Figure 2.3. Comparison of the velocity profile (a) particle concentration profile (b) obtained from our simulation with the experimental data of Lyon and Leal (1998) and the analytical solution of Phillips *et al.* (1992) for the fully developed profile. The average particle concentration (ϕ) was 30%. The ratio of half channel width to particle radius (B/*a*) was 18.

There is no proper characterization of wall slip in concentrated suspensions. Miller and Morris (2006) have noted that proper choice of K_c and K_η in diffusion equation and providing appropriate wall boundary condition for particle concentration and wall slip velocity would reduce this conflict.

To quantify the difference between our results and those of analytical solution and experimental data we have shown the relative values on 45° line. Figure 2.4a shows the velocity data plot where as Figure 2.4b shows the concentration data. It can be observed that the agreement is good for the velocity but not so good for the concentration. The relative error in prediction of velocity profile was 2.5% and that of concentration profile was 3% when compared with the analytical solution.

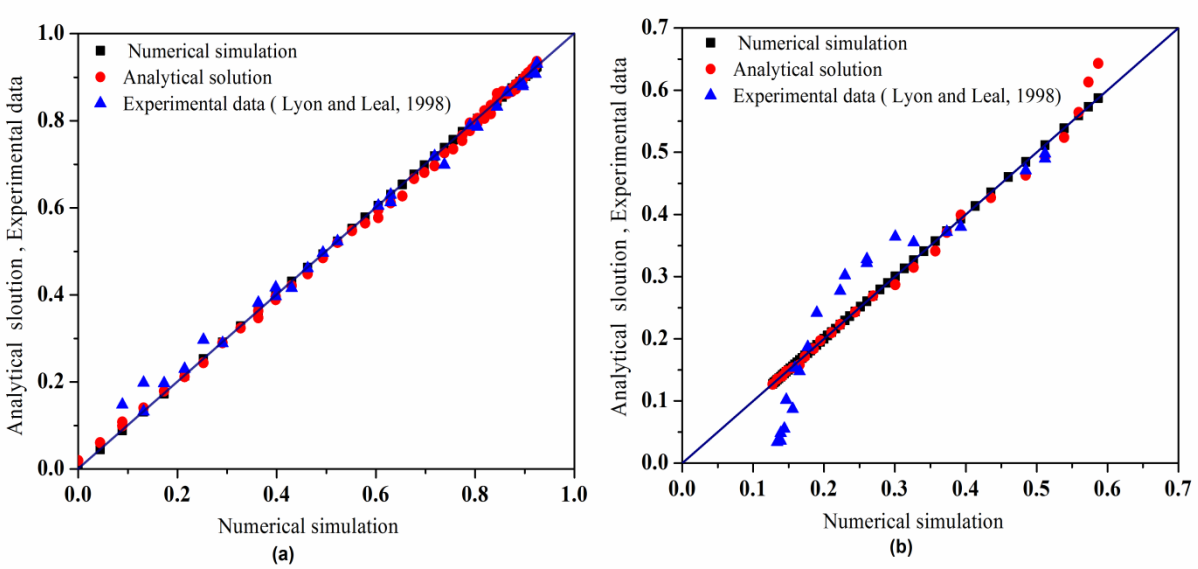

Figure 2.4. A Plot of error in simulation data on 45° degree line relative to the analytical solution of Phillips *et al*. (1992) and experimental data of Lyon and Leal, (1998): (a) velocity profile (b) concentration profile

However, the relative error in prediction of concentration profile was 9% when compared with the experimental data of Lyon and Leal (1998). We have also compared the results from simulation with the available experimental data of Leble *et al*. (2011) in the Y shape bifurcation channel. They have studied the velocity profile of dilute concentration (14%) of 8 μm human RBC cells suspended in a Newtonian fluid, Dextran 40. We have considered the same geometry and material properties that were examined in the experiments of Leble *et al*. (2011) to validate our simulation. The simulations were carried out for 14% bulk particle concentration. The velocity profiles obtained from our simulations are compared with the experimental values of Leble *et al*. (2011) at four different locations. Location 1 in the inlet section is 12.5 μm before the bifurcation and location 2 is 12.5 μm ahead of the bifurcation. Location 3 is at the beginning of left branch and location 4 in the left branch is 25 μm downstream.

We have also tested grid independence of numerical simulations by considering simulations on two different grids. Grid A consists of 90450 cells and Grid B consists of 192450 cells. The profiles of axial velocity (normalized with the maximum velocity) at two locations 1 and 2 (shown in Figure 2.2b) of the inlet branch are shown in the Figures 2.5a and 2.5b respectively. We observe symmetric but blunted velocity profile at location 1 in the inlet branch. The profile from our simulation is in good agreement with the experimental data of Leble *et al*. (2011). The profiles for two different grids are also same indicating the grid independent solution. Ahead of bifurcation (location 2) we observe peak–valley–peak pattern of velocity profile (Figure 2.5b) which is caused by the flow bifurcation into daughter

branches. The peak-valley-peak pattern is more prominent in the experiments compared to the simulations.

Figure 2.5c shows the comparison of velocity profiles at location 3 of the left branch. It can be observed that the profile is not symmetric and the peak is shifted towards the outer wall. At location 4 which is further downstream in the side branch, the profile is comparatively symmetric and nearly parabolic (Figure 2.5d). At these locations also the simulation velocity profiles are in good qualitative agreement with the experimental data. We observe that measurements which are closer to the walls match well and those which are away from the walls do not match well. The main reason for higher uncertainties and discrepancies between simulation and measurements is that irregular illumination caused by different camera positions during the experiments. The uncertainty of the RBC velocities is higher because of non-uniformity of laser illumination and movements in z direction (out of focus plane) due to interaction with neighboring cells. This cause RBCs lose brightness and thus decreased accuracy. Hence velocities obtained for RBCs are more scattered in experiments compared to simulation. We would like to mention that Leble *et al*. (2011) have not reported particle concentration profiles. Therefore, we are unable to show the experimental results but we have included our numerical simulation results for concentration in the Figure 2.5 with blue (Grid A) and green (Grid B) lines. The concentration profiles for suspension at various locations in inlet and daughter branches are shown in Figure 2.5. At locations 1 and 2 in inlet sections fully developed concentration profiles is observed due to shear induced migration of particles and at locations 3 and 4 in daughter branch, maximum concentration is at inner walls. To the best of our knowledge there are no experimental data available for shear induced migration of

concentrated suspension in Y-shaped bifurcation channels. Our simulations of concentrated suspension flow in Y-shaped channels are discussed in the next chapter.

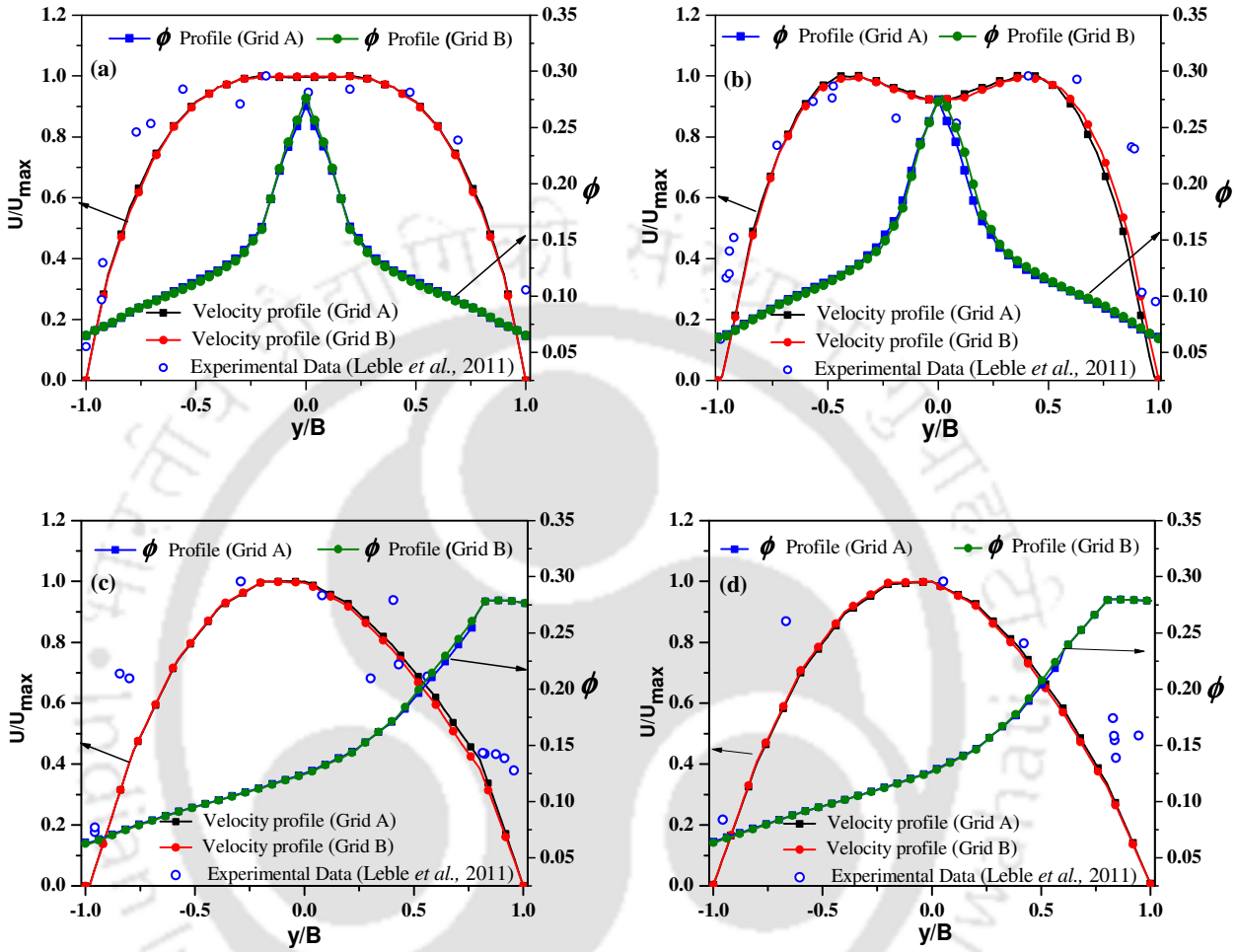

Figure 2.5. A comparative plot of velocity profiles obtained from our simulation with experimental data of Leble *et al*. (2011) and concentration profiles for various locations in the inlet branch (a) at location 1 and (b) at location 2. In the left branch: (c) location 3, (d) location 4.

भारतीय प्रौद्योगिकी संस्थान गुवाहाटी
Indian Institute of Technology Guwahati

CHAPTER-3

Shear Induced Migration of Concentrated Suspension through Y-Shaped 2D Bifurcation Channels

भारतीय प्रौद्योगिकी संस्थान गुवाहाटी
Indian Institute of Technology Guwahati

3. Shear Induced Migration of Concentrated Suspension through Y-Shaped 2D Bifurcation Channels

3.1. Introduction

The flow of concentrated suspensions such as toothpaste, blood, paint, slurry, composites etc. has great importance in manufacturing and processing industries. Handling the transport of concentrated slurries in many process industries still remains a challenging task (Vlasak and Chara, 2011). Whenever these homogeneous suspensions are sheared the corresponding particle migration behavior can be seen in the form of inhomogeneous distribution of particles. Therefore, the study of in-homogeneity of particles distribution in such flows is essential to understand their behavior in various industrial processes. The phenomenon of shear induced migration has attracted the attention of researchers due to its wide applications in processing of solid- rocket propellants, ceramics and reinforced polymer composites, food processing etc. Shear-induced particle migration has also been studied experimentally in various geometries such as rectangular channels (Koh *et al*. 1994; Lyon and Leal, 1998) and circular conduit flows (Hampton *et al*. 1997). Subsequent to these experimental studies two continuum models (diffusive flux model and suspension balance model) were presented to capture the phenomenon of migration. Both the diffusive flux and suspension balance models have been used extensively to study the unidirectional and steady flow in simple one and two dimensional geometries, while flow in complex geometries such as bifurcations are not adequately studied despite the fact that most of the industrial processes involve flows of suspension through bifurcation geometries. Most of the previous work on suspension flow in bifurcation channels have been limited to dilute concentration of particles whose size is comparable to the channel

dimensions (B/a < 4). In contrast, bifurcation flows of small particles compared to channel width (B/a > 20) and at high particle concentration have received less attention. Besides this there is hardly any study to understand the effect of geometry and flow parameters on velocity and concentration profiles in bifurcation channels. In this work, we have considered suspension of neutrally buoyant and rigid mono dispersed particles in viscous liquid, whose material properties are known precisely. These particles are sufficiently large so that Brownian motion is unimportant. The particles are much smaller than the width of the channel and the flow is in low Reynolds number regime. The original diffusive flux model of Phillips *et al*. (1992) was used to model the shear induced migration and its implementation was discussed in the previous chapter.

3.2. Problem Description

After the validation of our simulation method with the experimental data of Lyon and Leal (1998) and Leble *et al*. (2011) we have performed simulation for concentrated suspensions in symmetric Y-shaped bifurcation channel. Our objective was to study the effect of bifurcation angle, bulk concentration and flow rate on velocity and concentration profiles. The computational geometry of the bifurcation channel is shown in Figure 3.1. It consists of an inlet and two outlets. The inlet and downstream branch lengths (required for reaching fully developed profile) are calculated by using the equation 2.44. The length and width of the inlet section were 80 cm and 0.3 cm respectively. The length and width of the daughter channels are same as that of inlet section. The B/a ratio in the present simulations are 35 whereas, Lyon and Leal conducted experiments on straight channel with this ratio ranging from 11 to 24 and observed that steady state velocity and concentration profiles were nearly independent of B/a. In many flow devices and biological flow systems we encounter B/a ratio in this range.

In Figure 3.1, we have also marked the locations at which the velocity and concentration profile in the channel were studied. The flow parameters that were chosen to carry out numerical simulations are listed in Table 3.1.

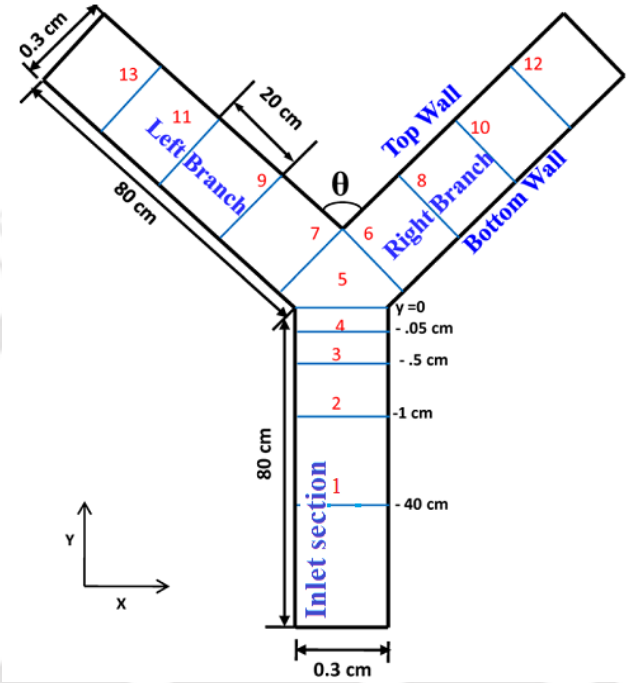

Figure 3.1. Schematic diagram of Y shaped geometry used in our numerical simulations.

Table 3.1. Simulation parameters considered for simulation.

Sl. No.	Flow parameter	Symbol (Unit)	Present Simulation
1	Bifurcation angle	θ (degree)	60°,90° and 120°
2	Suspending fluid viscosity	η_o (kg/m-s)	0.48
3	Density of suspending fluid	ρ (kg/m^3)	1190
4	Particle volume fraction	ϕ	0.3, 0.4 and 0.5
5	Suspension inlet velocity	U (m/s)	0.045 and 0.0045
6	Particle radius	a (m)	4.3×10^{-5}
7	Channel half width	B (m)	15×10^{-4}
8	Ratio of channel half width to particle radius	B/a	35

3.3. Results and Discussion

3.3.1 Velocity field

The effect of suspended particles on the velocity fields can be studied by comparing the suspension velocity with that of Newtonian fluid having the same effective viscosity and other simulation parameters. Figure 3.2 shows the contour planes of velocity magnitude for Newtonian fluid and suspension of 40% particle volume concentration for various bifurcation angles ($\theta = 60^{\circ}, 90^{\circ}$ and 120°).

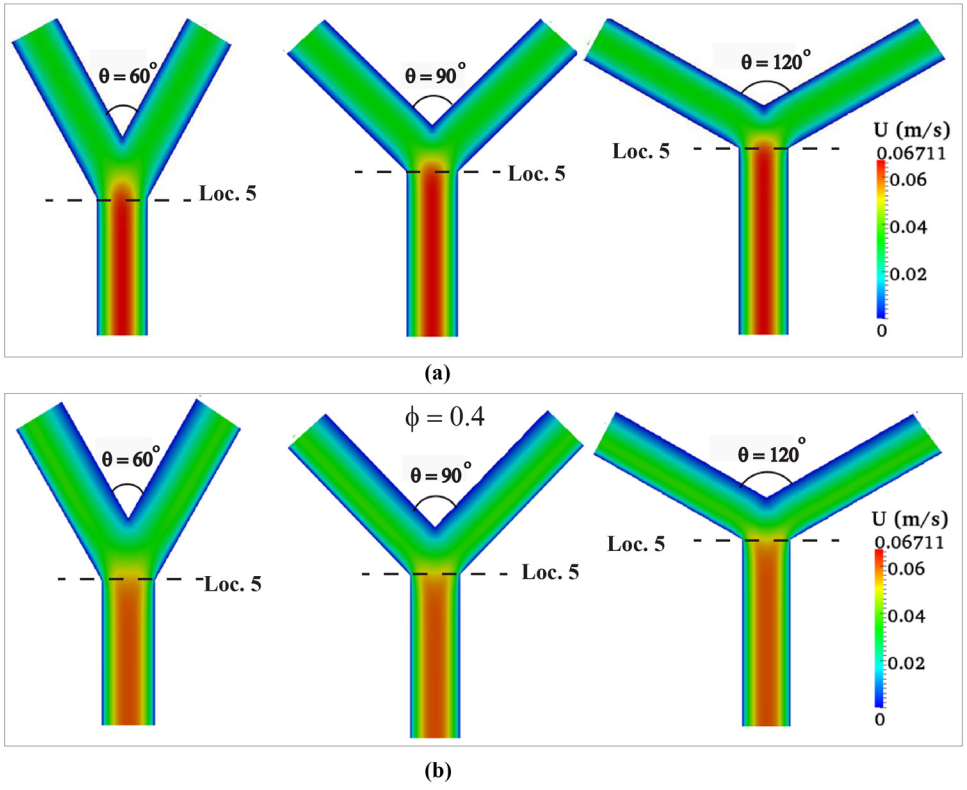

Figure 3.2. Velocity contours planes for various bifurcation angles ($\theta = 60^{\circ}, 90^{\circ}$ and 120°) for (a) Newtonian fluid and (b) suspension flow. The average particle concentration (ϕ) was 40% and the inlet velocity was 0.045 m/s. For clarity of contours only a section of channel is shown here.

We would like to mention that for clarity of contours the full channel is not shown but only a section around the bifurcation is presented in Figure 3.2. Figure 3.2a, shows the velocity contour (colored by the velocity magnitude) for Newtonian fluid. The corresponding velocity contours for the suspension flow are shown in Figure 3.2b. A clear observation of the contours shows the marked difference between the two. A fully developed parabolic velocity profile for Newtonian fluid persists up to the beginning of bifurcation (location 5) where it divides into left and right branches. For the suspension flow the effect of flow partitioning is realized as soon as the flow enters the bifurcation section. The deceleration of the suspension flow starts much before the bifurcation which can be attributed to the presence of particles in the fluid. In case of suspension flow we also observe blunted velocity profile in the inlet channel. The migration of particles causes non-uniform distribution of particles which leads to blunted velocity profile (Koh *et al.* 1994; Lyon and Leal, 1998).

Another important difference is observed in the downstream branches (left and right branch). In the case of Newtonian fluid the contours are symmetric whereas, the profiles for suspension are asymmetric in the downstream branches. The inner wall regions have smaller velocity compared to the outer wall regions. The stream lines for suspension of 40% concentration for various bifurcation angles ($\theta = 60^{\circ}$, $90^{\circ}$and 120°) are shown in Figure 3.3.It is observed that dividing stream line is exactly located at the center of inlet section but in the downstream branches the streamline are denser near the outer walls. Figure 3.4a shows the velocity profiles at various locations in the inlet section for Newtonian fluid for a channel with $\theta = 60^{\circ}$. It is observed that the fully developed parabolic profiles persist up to location 3 (0.5 cm before the bifurcation) in the inlet section and it is observed that the profiles for location 1, 2 and 3 are identical. At location 4, the velocity profile is symmetric but slightly blunted.

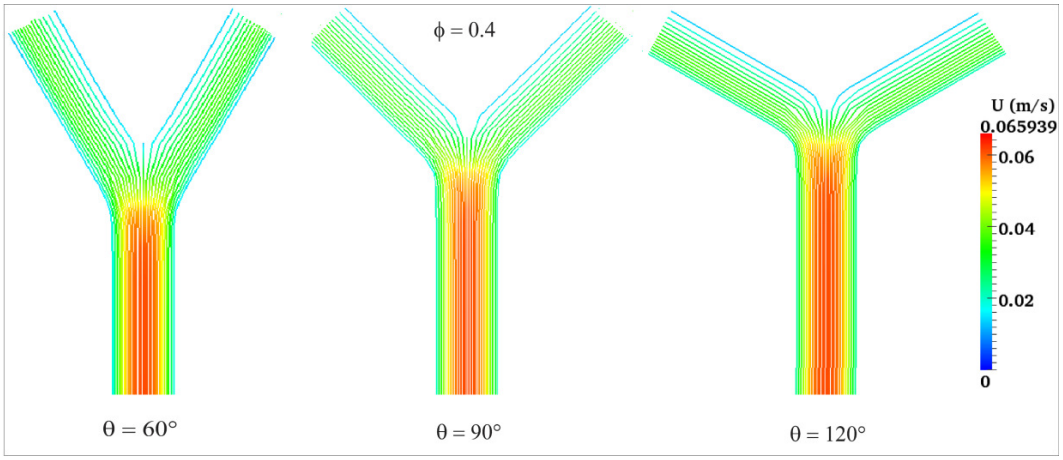

Figure 3.3. Stream lines of suspension flow in bifurcation channel for various bifurcation angles (θ = 60°, 90°and 120°).The average particle concentration (ϕ) was 40% and the inlet velocity was 0.045 m/s. For clarity of contours only a section of channel is shown here.

This effect is more pronounced at the bifurcation section (location 5) but overall the profiles remain symmetric and nearly parabolic. The velocity profiles at the same locations for suspension of 40% concentration for the bifurcation angle of $\theta = 60^{\circ}$ are shown in the Figure 3.4b. We observe that the velocity profiles are blunted for all the locations (in comparison to the Newtonian profiles) and the degree of bluntness increases as we move further downstream in the inlet section. The velocity profiles are nearly the same at location 1, 2 and 3 but the degree of bluntness is more at locations 4 and 5.The velocity profiles for Newtonian fluid and 40% suspension in the left branch is shown in Figure 3.4c and the corresponding profiles in the right branch are shown in Figure 3.4d. It can be observed that at the beginning of daughter branches (location 7 in the left branch and 6 in the right branch) the profiles for suspension flow are more skewed towards outer walls. As we move further downstream the profiles become more blunted and gradually shift towards the center. In contrast the velocity profile for the Newtonian fluid remains symmetric. The asymmetry of velocity profile for suspension

flow results from the shear induced migration. As expected the velocity profiles in the right branch (Figure 3.4d) are the mirror image of the left branch (Figure 3.4c) for the symmetric Y-shaped bifurcation channel. Therefore, in the subsequent analysis we have shown the velocity and concentration profiles of the left branch only.

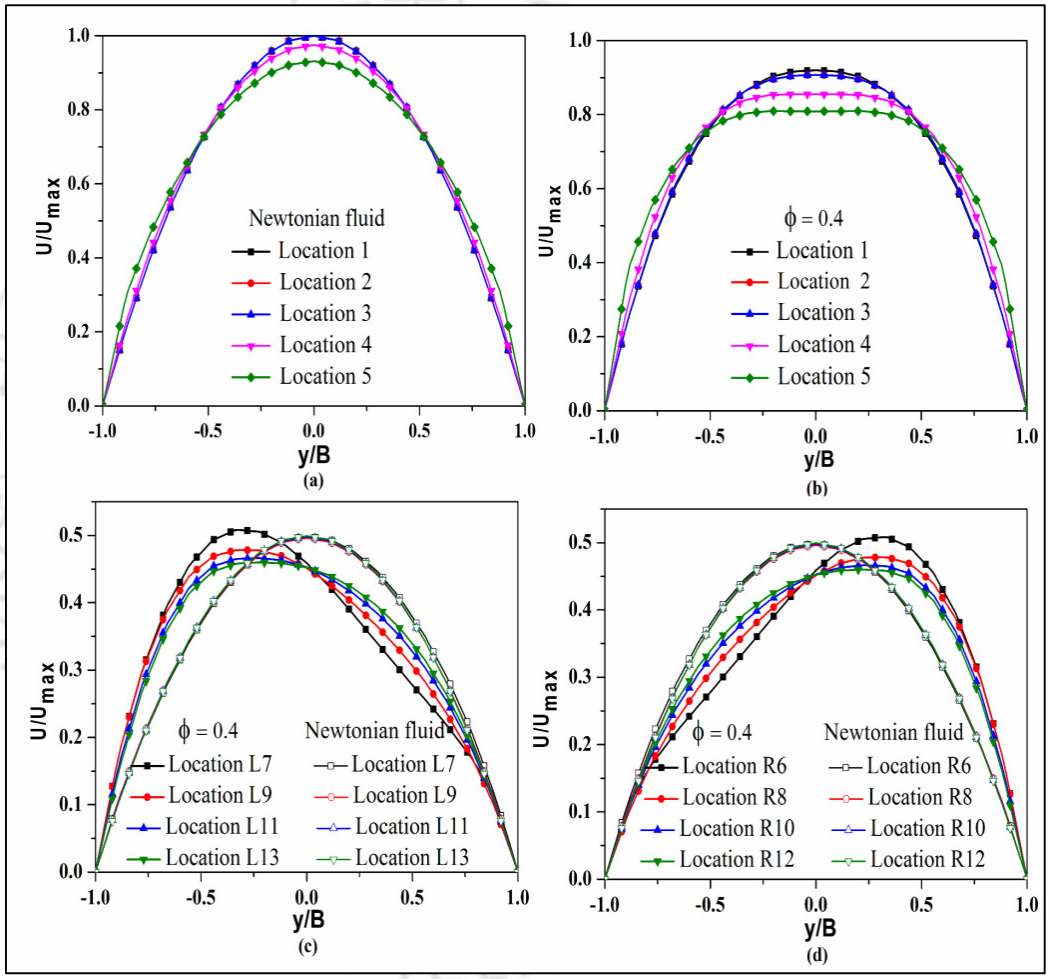

Figure 3.4. Comparative plots of velocity profiles at various locations in the inlet section: (a) Newtonian fluid (b) Suspension. Velocity profiles in the left branch (c) and in the right branch (d). The average particle concentration was (ϕ) 40% and the bifurcation angle of $\theta = 60^{\circ}$ and inlet velocity was 0.045 m/s.

To study the effect of bifurcation angle on the velocity profile at the bifurcation section (location 5 in the inlet section) we have carried out simulations for three bifurcation angles keeping the particle concentration same (40%). The comparative profiles for suspension and Newtonian fluid are shown in the Figure 3.5a. We have noticed that there is hardly any effect of bifurcation angle on the velocity profile for Newtonian fluid. On the other hand, the profiles for suspension flow are blunted and the degree of bluntness increases with the bifurcation angle. For $\theta = 60^{\circ}$ the velocity profile is flat in the center but for $\theta = 90^{\circ}$ and 120° 120° a clear peak-valley-peak pattern is observed. The velocity profiles at location 7 of the left branch are shown in the Figure 3.5b. It was observed that the profiles are asymmetric and skewed towards the bottom (outer wall). When the flow divides into the daughter channels, there is a shift in the velocity peak towards the bottom (outer) wall. For larger bifurcation angle the peak is relatively closer to the bottom (outer) wall. The velocity profile for Newtonian fluid of same viscosity as that of 40% suspension shows less asymmetry and for 60° case the profile is almost symmetric.

Figures 3.5c and 3.5d shows the effect of bulk concentration on the velocity profile in inlet section (location 5) and left branch (location 7) respectively. The velocity profiles in the inlet section at the location 5 are blunted for suspension and the degree of bluntness increases with the bulk particle concentration. In the case of 40% and 50% bulk concentration the peak-valley-peak pattern of profile is clearly observed. As mentioned above, the blunted velocity profile results from the non-uniform distribution of particles in the channel. The inlet of the channel was assigned uniform velocity of 0.045 m/s. Because of shear induced particle migration the particles move towards the center of the channel which increases the local concentration there and the suspension moves like a plug flow in that region. As a result the

velocity profile becomes blunted. At the bifurcation section the flow divides into left and right branches. Owing to no-slip boundary conditions at the wall the velocities are zero at the wall but the undulation in velocity profile shows that there is clear effect of bifurcation. The particle concentration and bifurcation angle has significant influence on the flow pattern as seen by peak-valley-peak pattern at location 5.

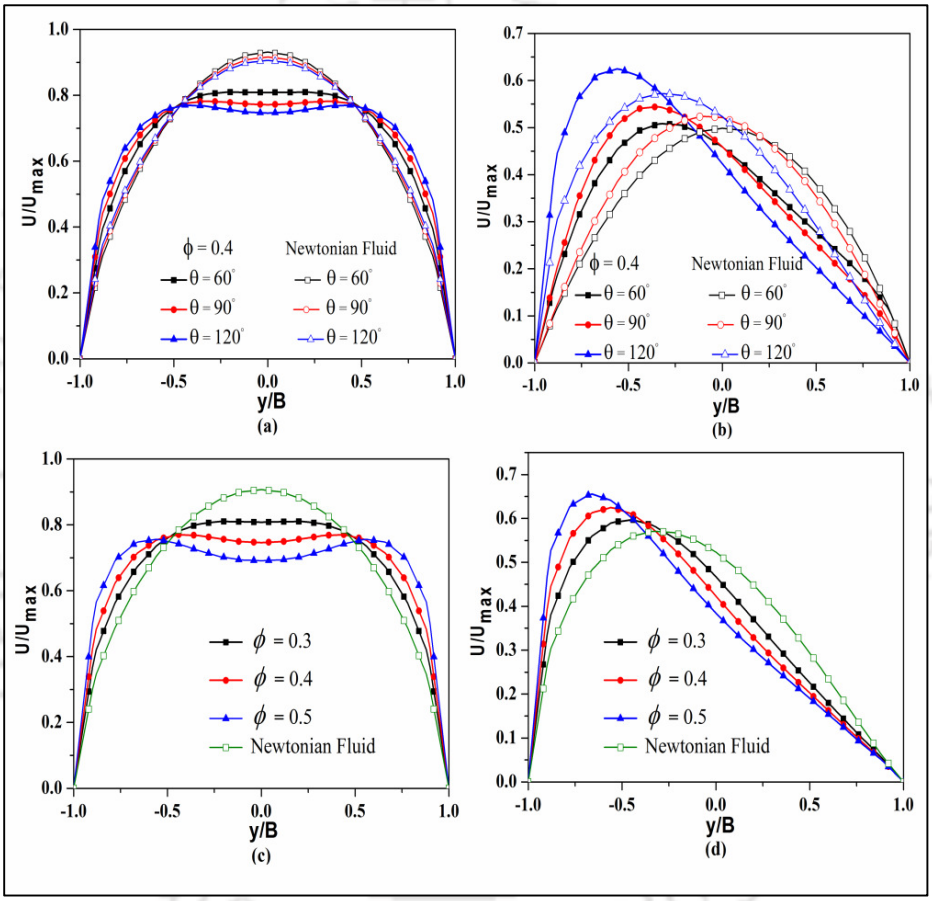

Figure 3.5. A comparison of velocity profiles for Newtonian fluid and suspension for various bifurcation angles (θ): (a) at bifurcation section (location 5) in the inlet section and (b) at location 7 in the left branch. The average particle concentration (ϕ) was 40%. Velocity profiles for various bulk particle concentrations: (c) Location 5 (d) Location 7. The bifurcation angle (θ) was 120° and the inlet velocity was 0.045 m/s.

Ditchfield and Olbricht (1996) have observed that hydrodynamic interactions among particles influence the particle motions and distribution of particles between the downstream branches. These interactions become increasingly important with the increase in particle concentration which affects the velocity profiles. As expected, the velocity profile in the left branch (location 7) is asymmetric and the peak moves closer to the outer wall for higher concentration (Figure 3.5d). The profile of Newtonian fluid is also asymmetric in the left branch with the shift of peak towards the bottom (outer) wall.

3.3.2 Concentration field

Figure 3.6a shows the particle concentration contour maps for various bifurcation angles of the channel for suspension of 40% particle volume concentration.

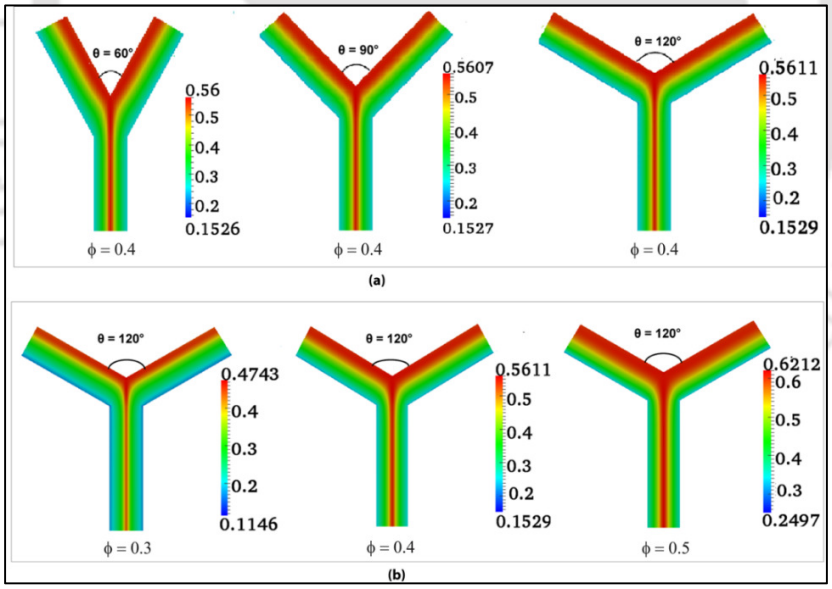

Figure 3.6. Particle concentration contour maps for suspension flow in bifurcation channel. (a) Effect of bifurcation angle (θ) at fixed average particle concentration (ϕ = 40%), (b) Effect of bulk particle concentration at fixed bifurcation angle ($\theta = 120^{\circ}$). The inlet velocity was 0.045 m/s.

For clarity we have not shown the full section of the channel and only the region near the bifurcation are shown. The fully developed concentration profile in the inlet section persists up to the bifurcation point (location 5) and is similar for all the bifurcation angles. The center region of the inlet channel shows the concentration of particles meets the junction of left and right branches of inner walls. In daughter branches the particle concentration is higher near the top (inner) walls where the velocity was lower compared to the bottom (outer) walls. Again because of shear induced migration, the particles migrate toward the center of the channel. It is also observed that bifurcation angle has less effect on the particle concentration field. Figure 3.6b shows the effect of bulk particle concentration on the contours of particle concentrations. The angle of bifurcation was the same ($\theta=120^{\circ}$) in all the three cases. The fully developed concentration profile in the inlet section persists up to the bifurcation. As the bulk concentration increases the degree of particle migration increases.

In the Figure 3.7a we have plotted the concentration profiles for suspension of 40% particle volume concentration at various locations in the inlet section for the channel of 60° bifurcation angle. For comparison we have also plotted the profiles at location 5 for $\theta = 90^{\circ}$ and 120°. At the entrance of the channel the particle concentration was uniform and equal to the bulk concentration. At location 1 we observe that significant migration has already taken place but at this location the concentration profile is not fully developed. At further downstream locations (2 - 5) the concentration profiles are nearly the same indicating fully developed flow. The inlet section exhibits spatial in-homogeneity in the particle concentration. The particle volume fraction at the center was observed to be 0.575 and this value was 0.249 at the wall. Unlike the velocity profile there is no change in concentration profile at the location 5 when compared to that at location 3 and location 4. We have observed similar trends for

channels with other bifurcation angles. This suggests that the bifurcation does not affect the concentration profile in the inlet section. However, the profiles in the daughter branches are greatly affected as can be observed in Figure 3.7b. At the entrance of left branch (location 7) we observe high concentration near the top wall and low concentration near the bottom wall. If we analyze the velocity profiles in the left branch (Figure 3.4a) it can be observed that the region of high concentration corresponds to the region of low shear rate and vice versa.

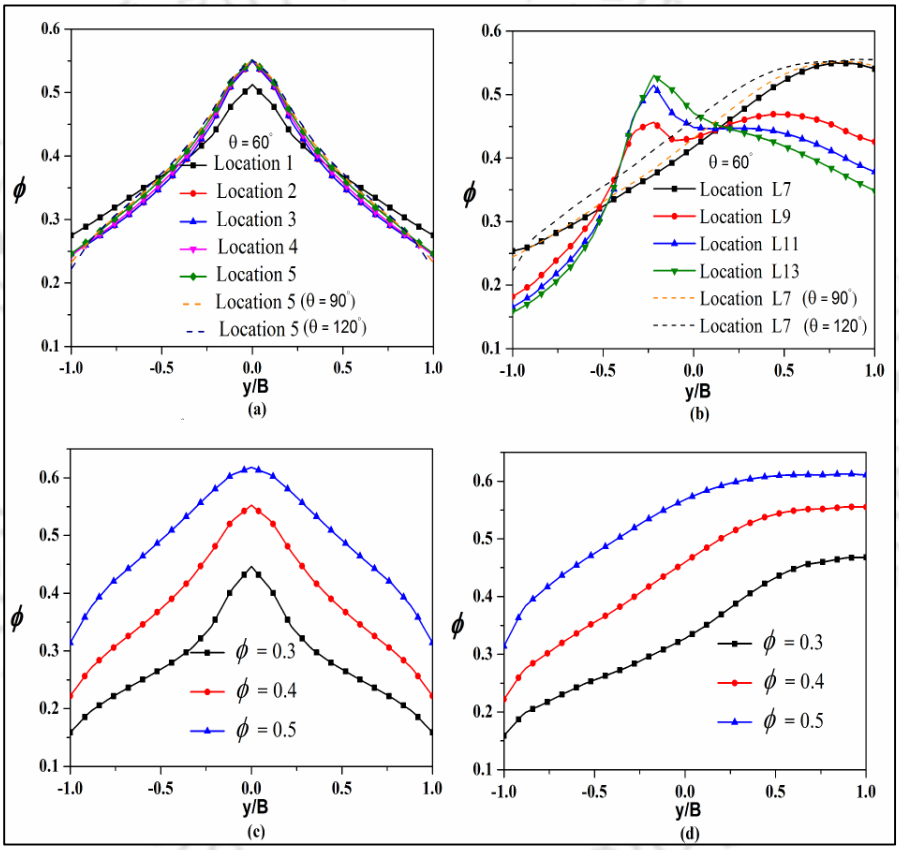

Figure 3.7. Comparison of the concentration profiles for suspension flow at various locations in the inlet branch (a) left branch (b). The bifurcation angle was 60°, the average particle concentration (ϕ) was 40% and the inlet velocity was 0.045 m/s. The effect of bulk particle concentration on the velocity at location 5 in the inlet branch (c) and at location 7 in the left branch (d). The bifurcation angle (θ) was $120^{\circ}$and the inlet velocity was 0.045 m/s.

This causes gradient in particle concentration. The imbalance in the particle diffusive flux due to gradient in shear rate and that of gradient in particle concentration will cause the particles to move to locations where these two fluxes balance. Therefore, we observe gradual shift of concentration profile towards the center of the channel as we move downstream locations of the left branch. The concentration profiles at location 7 are blunted and the degree of bluntness increases with the bifurcation angle.

We have plotted the concentration profiles for suspension of various particle concentrations in the inlet channel at location 5 in the Figure 3.7c and for location 7 in the left branch in the Figure 3.7d. In the case of 30% particle concentration, cusp (inverted V-shape) in the concentration profile is observed. This cusp in concentration profile becomes blunt with increase in particle concentration. It is interesting to note that the difference in the maximum and minimum concentration is nearly the same (0.3) for all the three cases. Figure 3.7d shows the concentration profiles at location 7 of the left branch for three different bulk particle concentrations. The bifurcation angle was 120° in all the three cases. As was the case with the effect of angle on concentration profile, the degree of bluntness also increases with the bulk particle concentration. The profile for 50% bulk concentration is more plug like when compared with 30% suspension.

In Figure 3.8 we have plotted the centerline concentration along the length of the channel to quantify the shear induced migration. As we move in the flow direction along the inlet section of the channel the particle concentration at the center of the channel increases. On the other hand the centerline concentration in the side branch first decreases and then increases. The reason for this trend is due to curvature of streamlines in the bifurcation region. Ahead of location 5 the streamlines are curved towards the daughter branches. This causes the shift of

maximum concentration away from the junction of inner walls. As we move further downstream the gradient in shear rate causes the particles to migrate again towards the center of the channel. However, we notice that the profile at the outlet of the side branch is not fully developed. This is due to the fact that the profile at the entrance of the side branch was asymmetric and therefore, it would take much longer length of the side branch to observe symmetric and fully developed concentration profile. An important consequence of asymmetry of particle concentration in the side branches is variation of wall shear stress. It is well known that wall shear stress has effects on human blood cells and is related to a disease called atherosclerosis. In this disease the plaques develop mainly in the regions of the curvature, bifurcation and branching of the blood vessels. Abnormally high shear stress in arteries increases the risk of thrombosis.

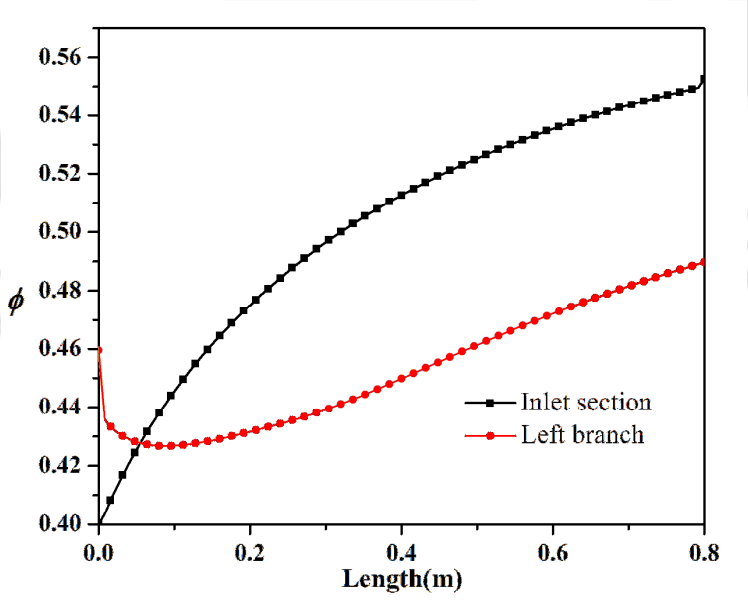

Figure 3.8. Plot of centerline particle concentration along the length of the channel. The bulk particle concentration was 40% and the inlet velocity was 0.045 m/s.

The effect of bifurcation angle on wall shear stress along the channel walls are shown in Figure 3.9. The maximum wall shear stress is observed near the junction of the top (inner) walls of the channel. As the bifurcation angle increases the wall shear stress at the junction decreases. At any given location the top (inner) wall has higher stress value compared to that of the outer wall. As we move downstream in the side branch the wall shear stress decreases.

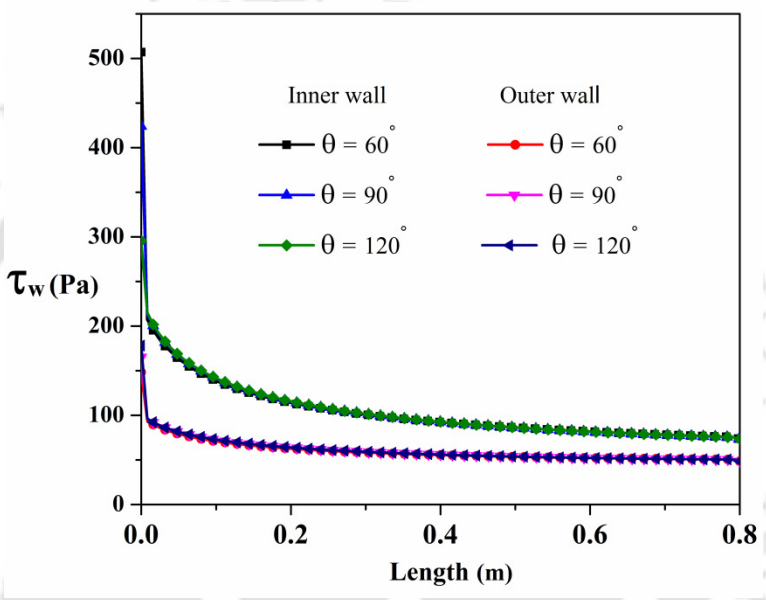

Figure 3.9. Plot of wall shear stress at inner wall and outer wall of the side branch against the length along the flow direction. The other simulation parameters were the same as in Fig. 3.8.

3.3.3 Effect of particle size and flow rate

The effect of particle size on velocity and concentration profiles was studied by carrying out simulation in the bifurcation channel with three different sizes of particles. The bulk concentration (40%) and inlet velocity (U=0.045 m/s) was fixed in these simulations. Figure 3.10a shows velocity profiles and Figure 3.10b shows corresponding concentration profiles at location 5 of the inlet section. We do not observe significant change in the velocity profile with increase in the particle size. But the concentration profile for 200 µm and 250 µm particles is

significantly changed when compared with smaller sizes (75 µm and 86 µm). The migration is relatively more pronounced for larger particle size. In our simulations we have considered the neutrally buoyant particles and the Reynolds number was very small. Therefore, particle inertia is irrelevant here. The fully developed migration profile should be independent of the particle size. However, for smaller sized particles the length required to reach fully developed flow is more than bigger size particles.

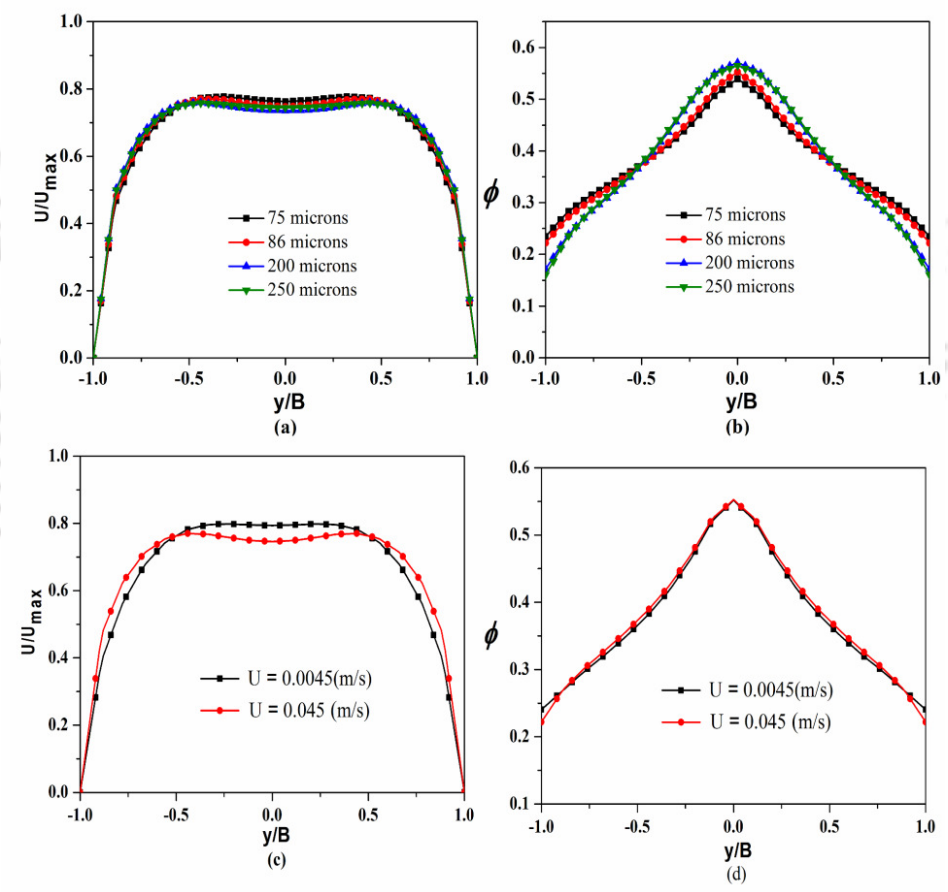

Figure 3.10. Plot of velocity profiles (a) and concentration profiles (b) at location 5 for various particle sizes. The inlet velocity was fixed at 0.045 m/s. Plot of velocity profiles (c) and concentration profiles (d) for two different inlet velocities. The bifurcation angle was 120^0 and the bulk particle concentration was 40% in all the cases.

We observed that the velocity profile in daughter branches is fully developed and independent of particle size but concentration profile does indicate that the fully developed profile was not reached for smaller particles. Though, the length of the branches were more than the predicted length by Nott & Brady (1994), it is to be mentioned that their formula was based on the assumption of uniform distribution of particles at the entrance of the channel. Whereas, in our case the concentration profile at the entrance of the daughter branches are not uniform.

The effect of flow rate on velocity and particle volume fraction profiles was studied by carrying out simulation for two different inlet velocities (U = 0.045 and 0.0045 m/s) which differ by an order of magnitude. Figure 3.10c shows the velocity profiles and Figure 3.10d concentration profiles at location 5. We observe that despite the velocities differing by an order of magnitude there is only a small change in the velocity profile. The peak-valley-peak pattern is clear for higher inlet velocity. There was no significant effect of inlet velocity on the concentration profile. Similar trend was also noticed at other downstream locations and for all bifurcation angles. This suggests that the effect of inertia was much smaller in our studies.

3.4 Conclusion

- Numerical simulations of concentrated suspension flow were carried out in 2D bifurcation channels of Y-shape were conducted.
- The diffusive flux model of Phillips *et al*. (1992) was implemented in OpenFOAM CFD solver to study the shear induced migration in bifurcation channels.
- Results from the simulations were compared with the experimental data of Lyon and Leal (1998) for straight channel and Leble *et al*. (2011) for Y-shaped bifurcation channel.

- The effect of parameters like flow rate, bifurcation angle, particle size and volume fractions of particles on velocity and concentration profiles in the inlet section and side branch of the channels were studied.
- Near the bifurcation peak-valley-peak patterns in velocity profile was observed for channels with larger angles of bifurcation and higher bulk particle concentrations.
- The velocity and concentration profiles were symmetric in the inlet section but asymmetric in the side branches.
- There is small influence of particle size on velocity profile but significant effect was observed on the concentration profiles.
- The wall shear stresses are larger at the top (inner) walls when compared to the outer (bottom) walls of the side branches.

CHAPTER-4

Shear-Induced Particle Migration in 3D Y-Shape Bifurcation Channel

भारतीय प्रौद्योगिकी संस्थान गुवाहाटी
Indian Institute of Technology Guwahati

4. Shear-Induced Particle Migration in 3D Y-Shape Bifurcation Channel

4.1. Problem Description

The computational geometry of the 3D bifurcation channel is shown in Figure 4. 1. It consists of an inlet and two outlets with square cross sections. The inlet and daughter branches were of equal width (0.002 m), whereas the lengths of inlet and daughter branches were 0.2 m and 0.1m respectively. The length required for reaching fully developed profile was calculated by using the formula given by Nott and Brady (1994). Other simulation parameters and geometry details are shown in Table 4.1. In Figure 4.1 we have also shown different axes with dashed lines along which the perpendicular planes were taken for analyzing the velocity and concentration contours. In local co-ordinate system, x denotes the lateral direction, y denotes the flow direction and z represents the span wise direction. Velocity and concentration fields in the cross-sectional planes were also analyzed and the locations of these planes are indicated in Figure 4.1. The computational domain of the straight sections of inlet as well as side branches were discretized using structured grids, whereas the prism shaped region at the bifurcation was discretized by unstructured grids. To check for grid independency of simulation we compared the solution on two different grids. Grid A comprised of 201000 cells (10X10X1000 structured cells in the inlet section, 10X10X500 structured cells in each of the straight sections of side branches and 1000 unstructured cells in the bifurcation zone) and Grid B comprised of 394744 cells (14X14X1000 structured cells in the inlet section, 14X14X500 structured cells in each of the straight sections of side branches and 2744 unstructured cells in

the bifurcation zone). The results from the two grids were found to be similar. The results reported in the following sections are for simulations on grid A.

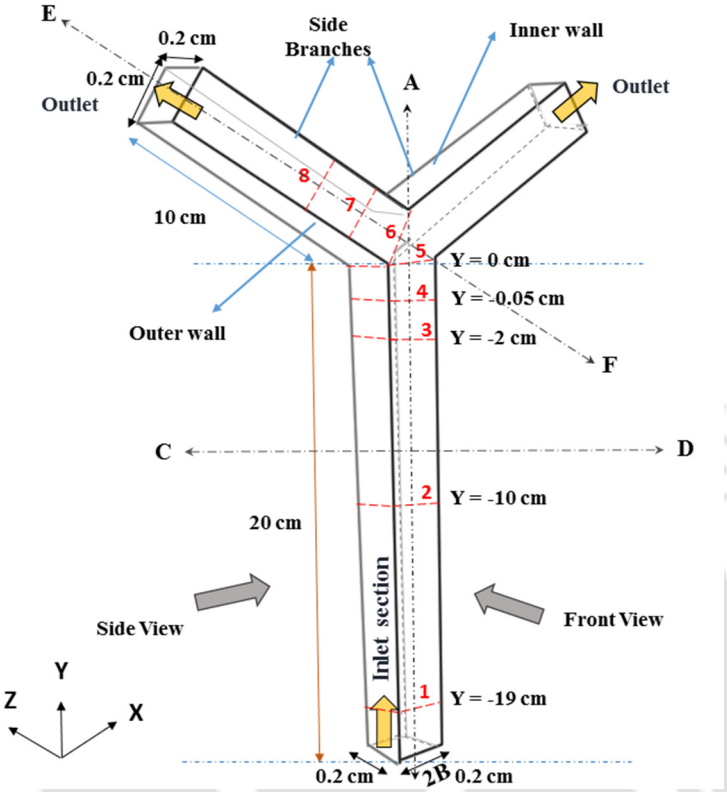

Figure 4.1. Schematic diagram of the computational geometry and locations where velocity and concentration data were analyzed.

Table 4.1. Flow parameters considered for the simulations.

Sl. No.	Flow parameter	Symbol (unit)	Value
1	Bifurcation Angle	θ (Degree)	60,90 and 120°
2	Suspending fluid viscosity	η_o (kg/m.s)	0.48
3	Suspending fluid density	ρ_f (kg/m^3)	1180
4	Particle volume fraction	ϕ	0.3 and 0.4
5	Inlet velocity	U (m/s)	0.045
6	Particle radius	a (m)	45x10^{-6}
7	Channel half width	B (m)	0.001
8	Ratio of channel half width to particle radius	B/a	22.22
9	Particle Reynolds number	N_{Rep}	9.9x10^{-3}
10	Flow Reynolds number	N_{Re}	0.4425

4.2. Straight Vs Bifurcation channels

Figure 4.2 shows the velocity and concentration profiles in lateral direction of inlet section for suspension of 30% and 40% bulk concentrations. These profiles were drawn at different locations in the inlet section and compared with the experimental data of Lyon and Leal (1998). The relative position in the lateral (x) and span wise (z) direction was normalized by the half-width (B) of the channel. It is to be noted that Lyon and Leal (1998) conducted experiments in 3D channel of rectangular cross-section where the depth of the channel was much larger compared to the width. Therefore, in their experiments the migration was measured only in the lateral direction. In order to see the influence of bifurcation on the upstream locations we have also compared the results with simulations performed on square channel without bifurcation (straight channel) whose dimensions were the same as that of inlet section of the bifurcation channel.

The velocity profiles for 30% bulk concentration are shown in Figure 4.2a and that of 40% bulk concentration are shown in Figure 4.2b. It was observed that the profiles in straight as well as bifurcation channel were developed by the end of location 3 as they are nearly same and equal to the profile at the outlet of the straight channel. However, the velocity profiles at location 4 and 5 in the bifurcation channel showed marked difference. The profiles become progressively more blunted as the bifurcation is reached. The corresponding concentration profiles for 30% and 40% suspension are shown in Figures 4.2c and 4.2d respectively. The shear induced migration of particle causes the inhomogeneous concentration profile where the center of the channel shows high concentration and wall region has depleted concentration. There is qualitative agreement with the experimental data of Lyon and Leal (1998) but the agreement is poor near the wall. This can be attributed to the lack of knowledge of proper

boundary conditions at the wall. It is well known that in concentrated suspension flow the depletion of particles in a thin region near the wall causes apparent wall slip velocity, whereas in our simulations no slip boundary condition was considered at the walls of the channel.

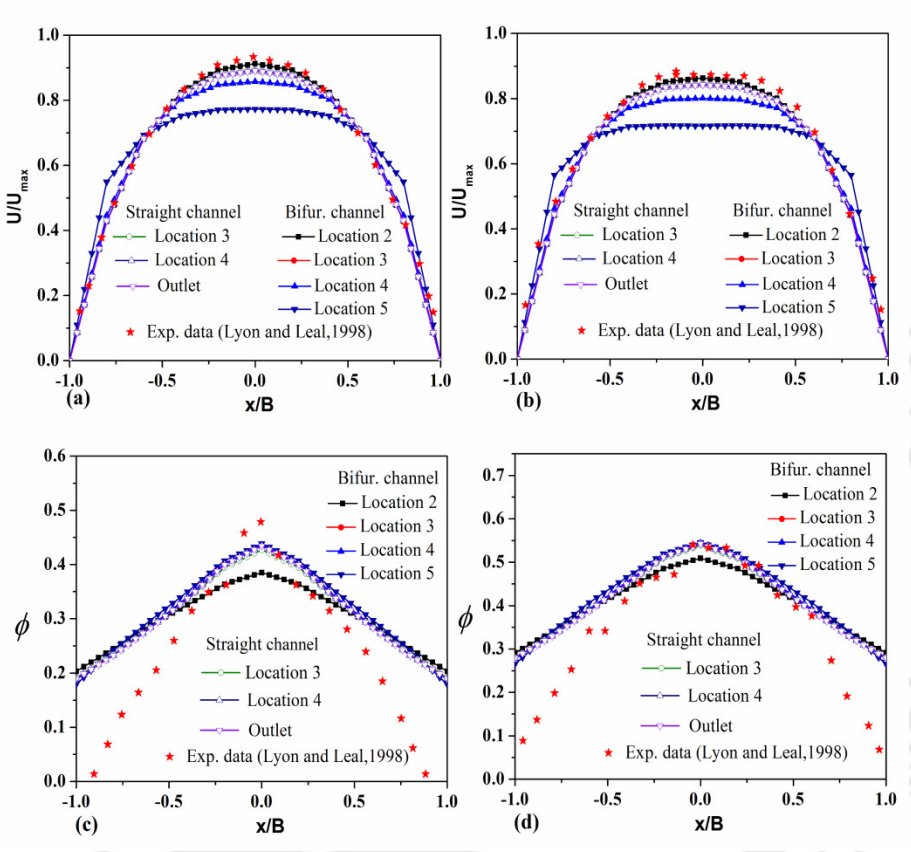

Figure 4.2. Simulation velocity profiles at mid-plane in the lateral direction for 30% bulk concentration (a), 40% bulk concentration (b), and corresponding concentration profiles for 30% concentration (c) and 40% bulk concentration (d), The bifurcation angle (θ) was 120° and the inlet velocity was 0.045 m/s. The profiles in the inlet section of bifurcation channel are compared with the experimental data of Lyon and Leal (1998) and with the simulations of channel without bifurcation.

Another point to be noted is that in the experiments of Lyon and Leal (1998) the depth of the channel was much larger compared to its width, whereas our simulations were for square cross-section where the migration is expected in both lateral and span wise directions. The concentration profile appears to be fully developed by the end of location 3. However, unlike the velocity profile the flow bifurcation has less impact on the concentration profile in the upstream of the bifurcation. This is evident from nearly similar concentration profiles at location 3, 4 and 5. The value of the maximum concentration at the center of the channel increases with the increase in inlet particle concentration.

4.3. Results and Discussion

4.3.1. Velocity field

The impact of particles on the velocity fields are often studied by comparing the suspension velocity with that of Newtonian fluid having the same effective viscosity and other simulation parameters. For this purpose the velocity contour and streamlines (front view) of Newtonian fluid and suspension flow in the mid-plane of the channel are shown in Figure 4.3. For the clarity of view the contours of the full channel are not shown, and only a section around the bifurcation was taken. For the comparison purpose, we have shown the contour planes for Newtonian fluid and suspension of 30% and 40% concentration for channel of bifurcation angle θ = 120°. The viscosity of Newtonian fluid was taken as effective viscosity of 30% suspension. All other simulation parameters were the same. The Newtonian fluid shows nearly parabolic profile across the x-dimension in the inlet channel and this behavior is observed up to the bifurcation (location 5) and after that the flow is divided into daughter branches. In contrast, the suspension flow in the inlet section exhibits blunted velocity profile which is more

apparent near the bifurcation. Another important observation can be made about the maximum centerline velocity which persists little downstream of location 5 for Newtonian fluid, whereas for suspension this location is upstream of location 5. For 40 % suspension the difference is clearly noticeable. This fundamental difference in the velocity field is due to the presence of particles in suspension. Near the bifurcation the particles quickly respond to the change in shear field causing the increase in the bluntness of velocity profile. The increase in the bluntness of velocity profile near the bifurcation in the inlet section is due to curvature of the streamlines towards the left and right daughter branches. The degree of bluntness was found to increase with the increase in bulk particle concentration. The corresponding streamlines are also shown in Figure 4.3. It can be observed that dividing stream line is exactly located at the center of the inlet section of the channel.

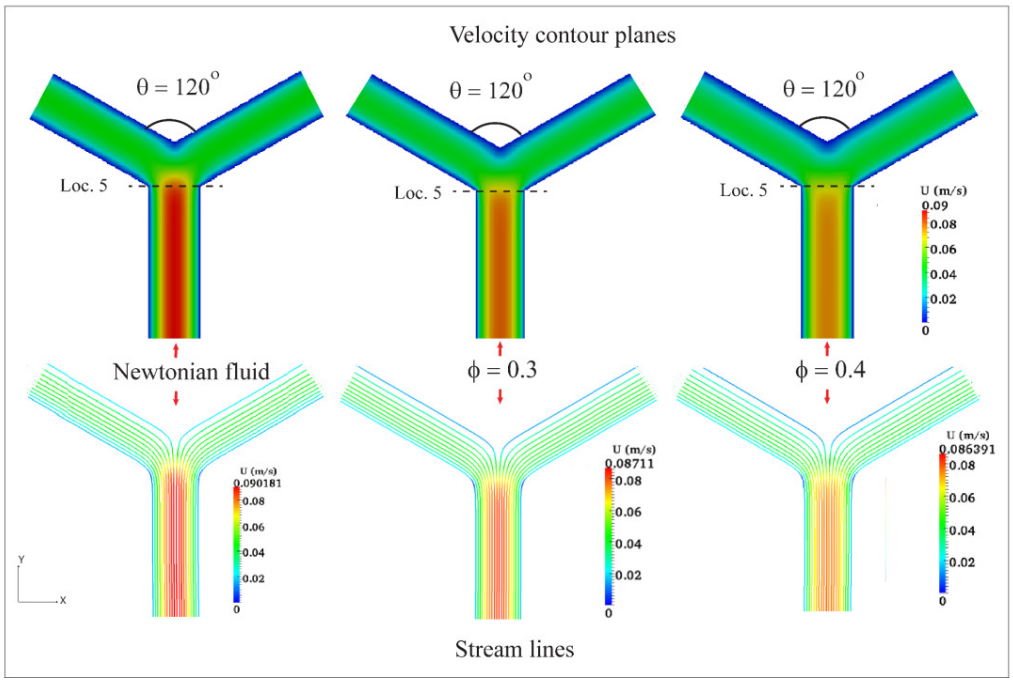

Figure 4.3. Front view of velocity contours planes (first row) and stream lines (second row) from the simulations of Newtonian fluid and suspension of 30% and 40% bulk particle concentration. The bifurcation angle (ϕ) was 120° and the inlet velocity was 0.045 m/s.

This is expected since the channel itself is symmetric and flow is divided equally in the daughter branches. The smearing of velocity profile near the bifurcation can be seen more clearly in these streamline plots.

We have also carried out simulations (not shown here) for fixed bulk concentration but for three different bifurcation angles (60°, 90° and 120°). It was observed that the increase in bifurcation angle does not show any significant effect on bluntness of the velocity profile in the inlet section. The cross-sectional views (x-z plane) of velocity contour at various locations in the inlet section are shown in the Figure 4.4a. These cross-sectional slices were taken at various locations (3, 4 and 5) in the inlet section at planes perpendicular to the flow direction. The bifurcation angle ($\theta = 120^{\circ}$) was same for all the cases shown in this figure. It can be observed that the contours at the three locations are nearly similar for the Newtonian fluid but dissimilar for 30% and 40% suspension. In case of suspension the contour at location 5 is smeared more along the lateral direction. The maximum velocity does not persist up to location 5 as the effect of flow divergence is realized before the bifurcation. Figure 4.4b shows the velocity contour maps in the cross-sectional plane of the side branch. It was observed that at a distance of 1 cm from the center of bifurcation (location 6), which is at the very beginning of the straight section of the side branch, the velocity field is more asymmetric and the peak velocity shifts towards the outer wall. The asymmetry is more pronounced for suspension flow. As we move further downstream locations the velocity field becomes more symmetric and peak velocity shifts towards the center of the channel. For Newtonian fluid the velocity field becomes nearly symmetric at location 7 but in case of suspension flow the shift of velocity peak towards the center is small. At a given location the degree of asymmetry is more for 40% suspension compared to 30%. The length required to become fully developed flow is calculated

from equation (2.44) proposed by Nott and Brady (1994). According to their formula the length of the channel (L) should be 171 times the half width (B) of the channel. In our simulations the length of inlet section was about 17% more than this length. It appears that the velocity fields develop faster than the concentration fields. The entrance length for fully developed flow is much larger for suspension in comparison to Newtonian fluid.

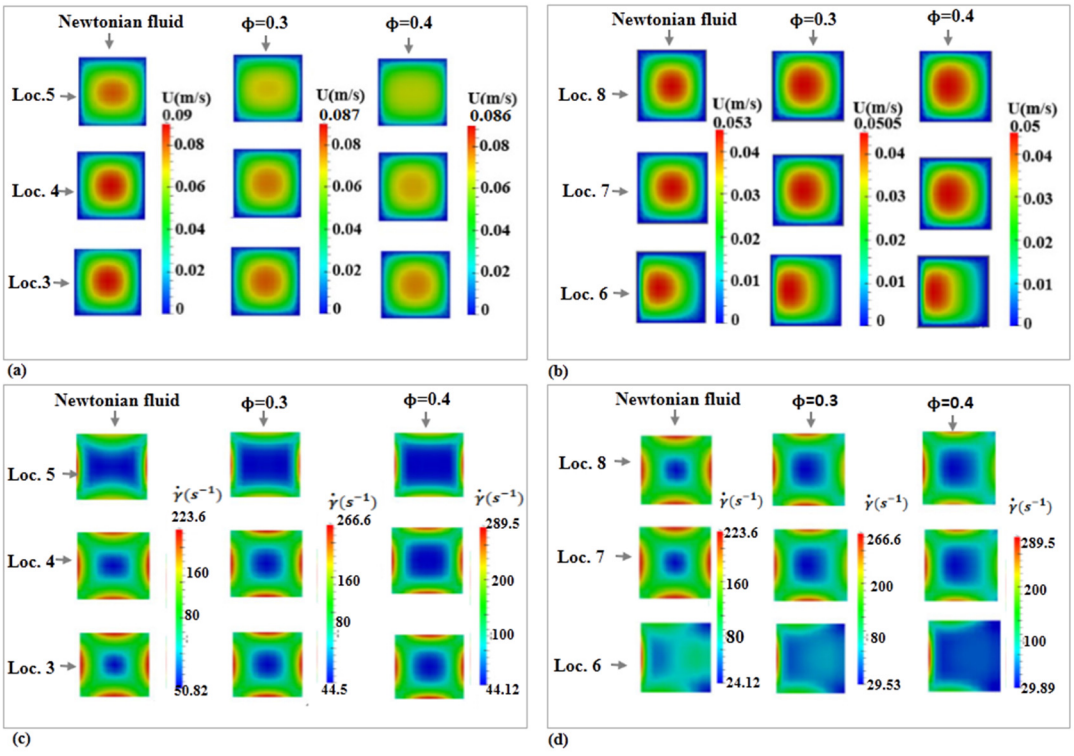

Figure 4.4. The cross-sectional velocity contours (a and b) and shear rate contours (c and d) for Newtonian fluid and suspension flow at various locations in the inlet and side branch. The simulation parameters were the same as in Figure 4.3.

The corresponding shear rate contour planes in the inlet and side branch are shown in Figures 4.4c and 4.4d respectively. In the inlet section the high shear rate is observed near the wall and low in the core of the channel. The corner regions of the channel wall have relatively higher shear rate compared to the middle regions. The shear rate gradients are highest at location 5. At the location 6 of the side branch the high shear rate regions are shifted towards

the outer (left) wall but gradually becomes more symmetric as we move to downstream locations. We would also like to mention that in our simulations based on the diffusive flux model the bulk stress of suspension was isotropic and did not consider normal stress differences. As expected we did not observe any secondary currents and the fluid motion in the plane perpendicular to the flow direction was found to be absent. It would be interesting to follow the modeling approach of Zrehen and Ramachandran (2013) while solving the momentum equation in diffusive flux model to see the effects of secondary currents on shear induced migration.

Figure 4.5 shows the comparison of velocity profiles for Newtonian fluid with 30% and 40% suspension in the inlet and side branch. Figure 4.5a shows the profile of inlet section in lateral direction whereas Figure 4.5b shows the corresponding profiles in the span wise direction. The bifurcation angle was 120° in all the cases. It can be observed that up to location 3 the shape of the profile is same in both lateral and span wise directions. However, at the locations 4 and 5, the bluntness in velocity profile is more in the lateral direction in comparison to the span wise direction. The velocity profiles in the lateral and span wise directions of the side branch are shown in the Figures 4.5c and 4.5d respectively. The location 6 is at the very beginning of the side branch and is 0.01m away from the center of the bifurcation. The other two locations (7 and 8) are 0.025 m and 0.05m apart from location 6. It can be noted from the Figure 4.5c that at location 6 the profiles for both Newtonian fluid and suspension are asymmetric and skewed towards the outer wall. However, the skewness for suspension is more compared to that of Newtonian fluid. The asymmetry of the profile results from the non-uniform distribution of particles which is discussed in detail in the next section. As we move further downstream the profiles shift towards the center of the channel causing it to appear

more symmetric. However, at the same locations in the span-wise direction the profiles are symmetric though blunted (Figure 4.5d). The effect of bifurcation angle on velocity profiles at location 5 of the inlet section for 40% suspension in lateral and span-wise directions are shown in Figures 4.6a and 4.6b respectively. For comparison we have also included the profile of Newtonian fluid for $\theta = 120^{\circ}$.

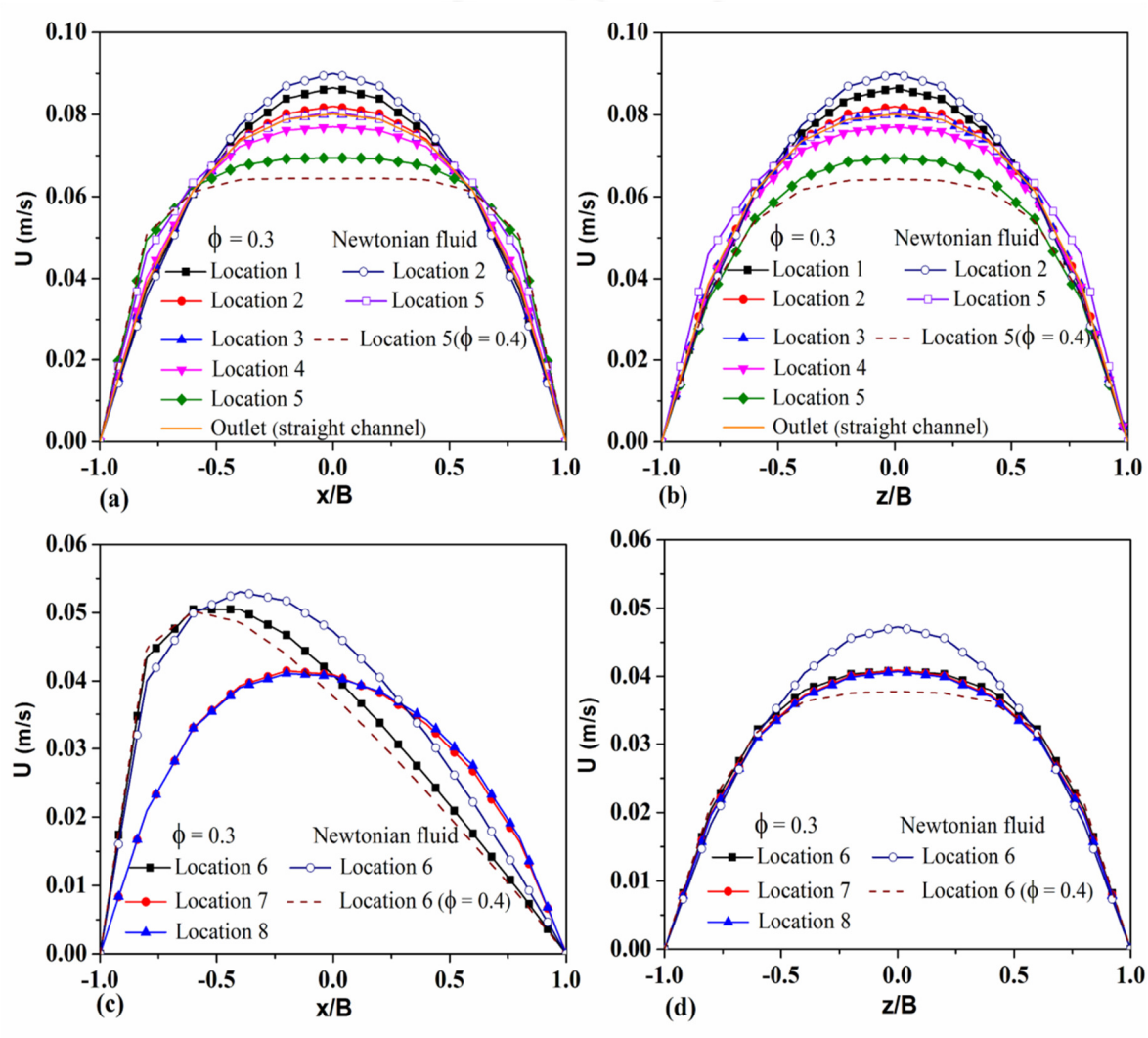

Figure 4.5. Comparison of the velocity profiles for Newtonian fluid and suspensions (30% and 40% particle concentration) at various locations of the inlet section in the lateral direction (a) and span wise direction (b). The velocity profiles of side branch in lateral direction (c) and span wise direction (d). The simulation parameters were same as in Figure 4.3.

It can be clearly noticed that the degree of bluntness of profile increases with the increase in bifurcation angle and the profiles in lateral direction are more blunted in comparison with the span-wise direction. The corresponding profiles at location 6 of the side branch in lateral and span wise directions are shown in Figures 4.6c and 4.6d, respectively.

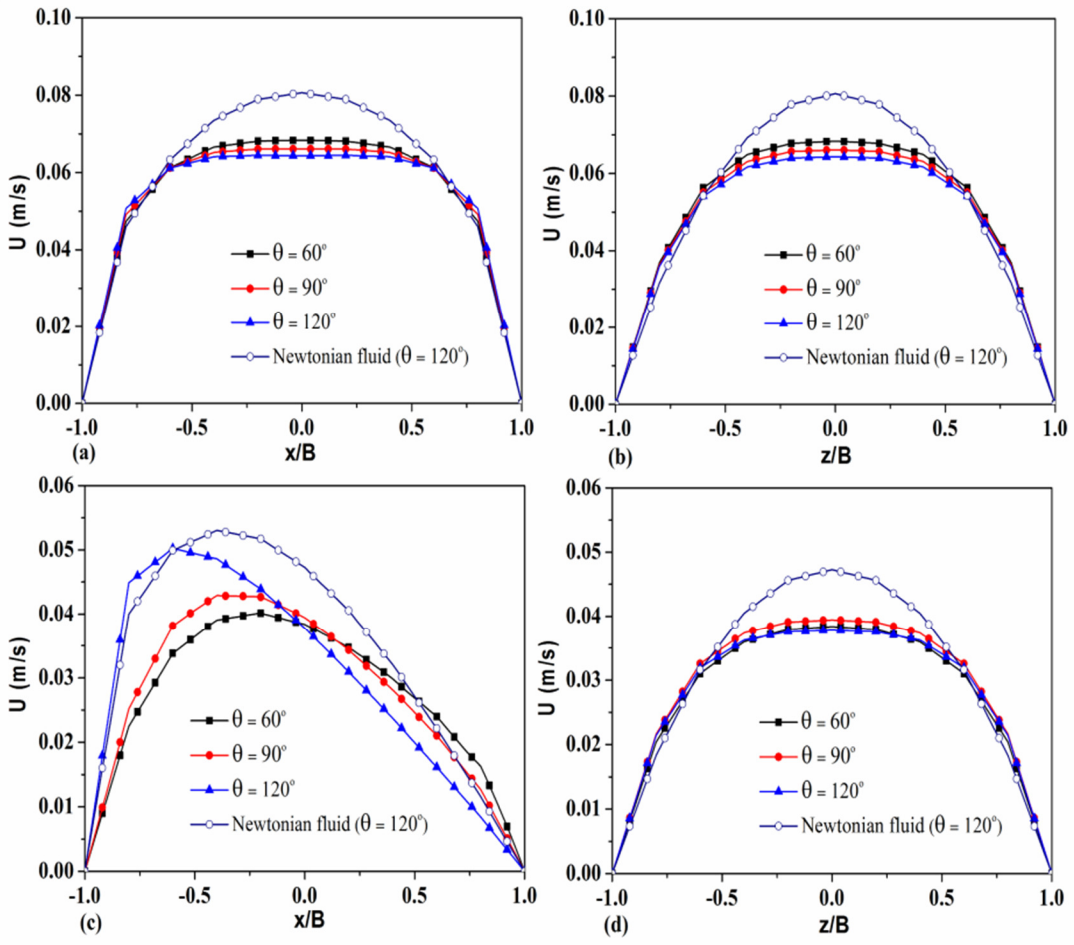

Figure 4.6. Effect of bifurcation angle on velocity profile at location 5 of the inlet section for 40% suspension in the lateral direction (a) and span wise direction (b). Effect of bifurcation angle on velocity profile at location 6 of the side branch in the lateral direction (c) and span wise direction (d). For comparison purpose the profiles at the same locations from the simulation of Newtonian fluid of effective viscosity of 40% suspension corresponding to the bifurcation angle of 120° is also shown. The inlet velocity was 0.045 m/s.

We observe that with the increase in the bifurcation angle the velocity peak shifts towards the outer wall. On the contrary, the profiles in the span wise direction are symmetric. We can also see that there is much less influence of bifurcation angle on the velocity profiles of side branch in the span wise direction. Similar trends were also observed for the suspension of 30% bulk concentration.

4.3.2. Concentration field

The concentration contour maps in the mid-plane (front view) for 30% and 40% suspension are shown in Figure 4.7a. For the clarity of view we have shown only a small section around the bifurcation. In the inlet section the shear induced migration causes the particles to move towards the center of the channel. The central core of the inlet channel which has high concentration of particles meets the junction of left and right branches of inner walls. This makes the particle concentration in the side branches to be more near the inner walls. However, even in the side branch the shear rate at the wall is higher compared to the center (please see Figure 4.4d) and this gradient again drives flux of particles towards the center in the daughter branches. As a result the concentration peak gradually shifts towards the left side (outer wall). We also observe that the peak value of concentration for 40% suspension is higher than that of 30% suspension.

Figure 4.7b shows the cross-sectional view of concentration maps in the inlet section for suspension of 30% and 40% bulk particle concentrations. These slices were taken at planes perpendicular to the flow direction at the locations 1, 4 and 5 of the inlet section. It was observed that as we move downstream in the inlet section the concentration inhomogeneities gradually develop due to particle migration. The depletion of particles in the corner region is less compared to the middle portions near the channel walls. This is because of the fact that

the shear rate gradient is smaller in the corner region (see the Figure 4.4c). Figure 4.7c shows cross-sectional concentration contour maps in the side branch. It was observed that at location 6, the concentration field is asymmetrically distributed and as we move further downstream locations in side branch the particles migrate towards the center of the channel.

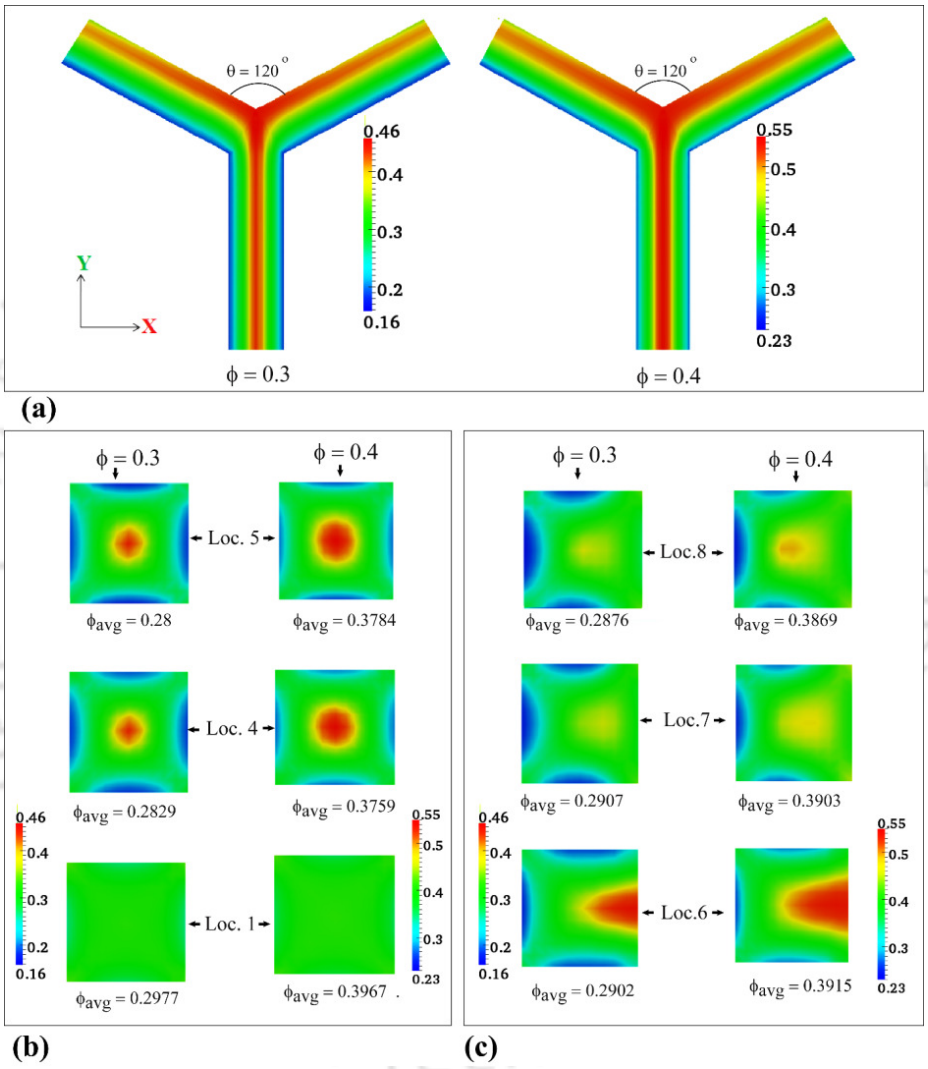

Figure 4.7. Front view of the particle concentration contour maps for suspension of 30% and 40% particle concentration (a), cross-sectional view at various locations of inlet section (b) and cross-sectional view at various locations of side branch (c). The cross-sectional area weighted average concentrations at different locations are also indicated below the maps. All other simulation parameters were the same as in Figure 4.3.

The region close to the top and bottom walls as well as outer wall (except the corners) is devoid of particles as represented by dark blue region. The region close to the inner wall has highest particle concentration since the shear rate is lowest there (see Figure 5.4d). As one moves further downstream the peak value of concentration shifts towards the center of the channel due to the shear induced migration of particles. The migration of particles is faster for 40% suspension compared to 30% suspension which is evident from bright spot at the center of location 8.

We have also computed the cross-sectional area averaged concentration at various locations in the inlet and side branch which are printed below the contour maps. At the entrance of the inlet channel the area weighted average concentration was exactly equal to the bulk concentration. It was noticed that the area-weighted average concentration is not equal to the inlet concentration at downstream locations but the local velocity weighted cross-sectional mean volume fraction was same (and equal to the inlet concentration within 0.1% error) at all the locations. For 30% suspension the area-weighted average concentration decreases as we move from location 1 to location 5 in the inlet section but again increases at location 7 in the side branch. For 40% suspension similar trend was observed except that the average value at location 5 is lower than that at location 4. It is to be noted that for 40 % suspension the peak velocity location was in the upstream of bifurcation, whereas for 30% it was near the bifurcation. These observations are in agreement with the findings of Miller and Morris (2006) that the cross-sectional mean particle volume fraction must decline in a steady state flow as the mixture moves down the axis. This is due to accumulation of solids on the fast moving streamlines, and the need to maintain a constant flux of particles at any axial location. This is consistent with the observation of velocity field in Figure 4.3 where we have seen that for

Newtonian fluid the streamline at the center move faster up to location little ahead of location 5, for 30 % suspension close to location 5 and for 40 % suspension between location 4 and 5.

In order to understand quantitative nature of particle distribution we have shown the concentration profiles in the lateral and span-wise directions of the inlet section in Figures 4. 8a and 4.8b respectively. The corresponding profiles in the side branch are shown in Figures 4. 8c and 4.8d respectively. These profiles were obtained from simulations of bifurcation channel with angle of bifurcation, $\theta = 120^{\circ}$. The concentration profile becomes fully developed at location 4. However, unlike the velocity profile the concentration profile remains unaffected till the beginning of bifurcation section (location 5) and we observe almost identical profile at location 4 and location 5. The concentration profiles of inlet section are similar in both lateral and span wise directions. After the bifurcation the flow divides into left and right branches. We observed that the effect of bifurcation on velocity field is realized little before the bifurcation, whereas the concentration profile at the same location (when compared to the upstream locations) remains somewhat unaffected. The possible reason behind this could be shear induced rearrangement of particles. The stress field ahead of bifurcation is different from that at the locations before the bifurcation. This change in stress field causes shear induced migration, and its effect is such that the particles oppose being carried away by the fluid streamlines.

From the Figure 4.8c it is clear that the maximum concentration at the beginning of the side branch (location 6) is on the inner wall (x/B = +1) which gradually moves toward the center of the channel as we move further downstream locations (location 7 and 8). The lateral profiles are asymmetric but at the same locations the span-wise profiles (Figure 4. 8d) are not only symmetric but do not change much in the downstream locations. In the present

simulations the length of side branch was 0.1 m. We have also performed simulation in which the length of the side branch was doubled (0.20 m) but noticed that even at the outlet locations the asymmetry of the concentration profiles in the lateral direction does persist. This indicates that the estimate of the length required for fully developed flow provided by Nott and Brady (1994) is valid only for the case of uniform and symmetric inlet velocity and concentration. If the inlet velocity or concentration profile is asymmetric then it would take much longer length to reach fully developed flow.

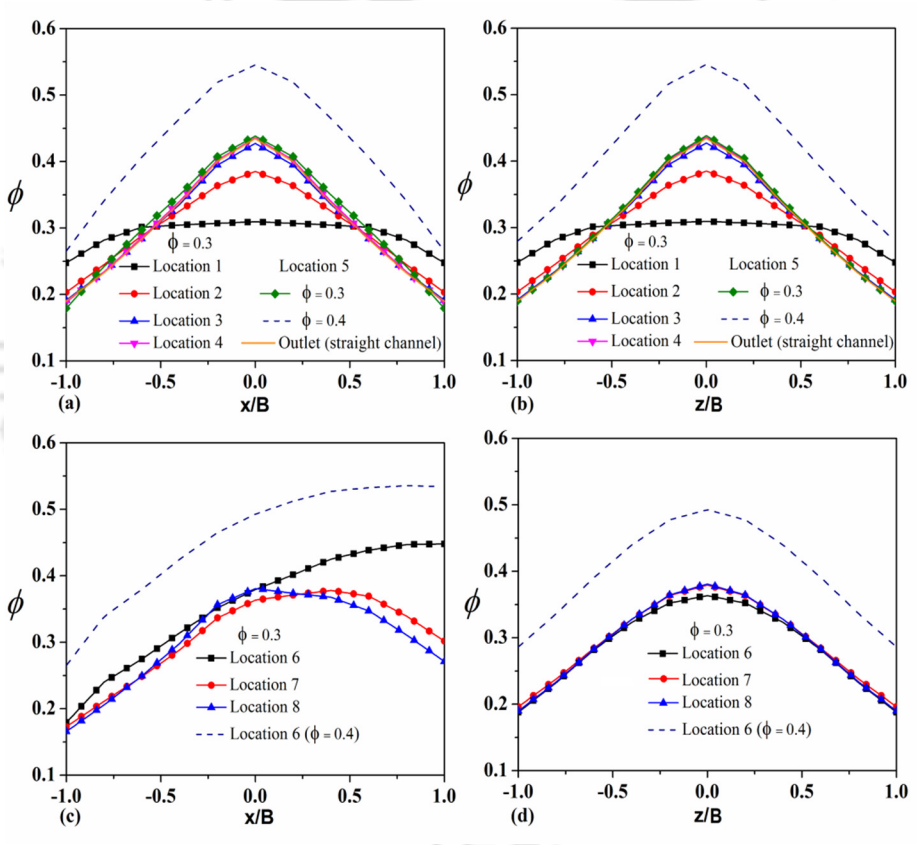

Figure 4.8. Comparison of the concentration profiles for Newtonian fluid and suspensions (30% and 40% particle concentration) at various locations of the inlet section in the lateral direction (a) and span wise direction (b). The concentration profiles at various locations of side branch in lateral direction (c) and span wise direction (d). The simulation parameters were same as in Figure 4.3.

The effect of bifurcation angle on the concentration profiles for bulk particle concentration of 40 % is shown in Figure 4.9. Unlike the velocity profiles at location 5 the concentration profiles in lateral direction shows small dependence on bifurcation angle only near the walls (see Figure 4.9a) and no dependence in the span-wise direction (see Figure 4. 9b). We do see the significant effect of bifurcation angle in the side branch.

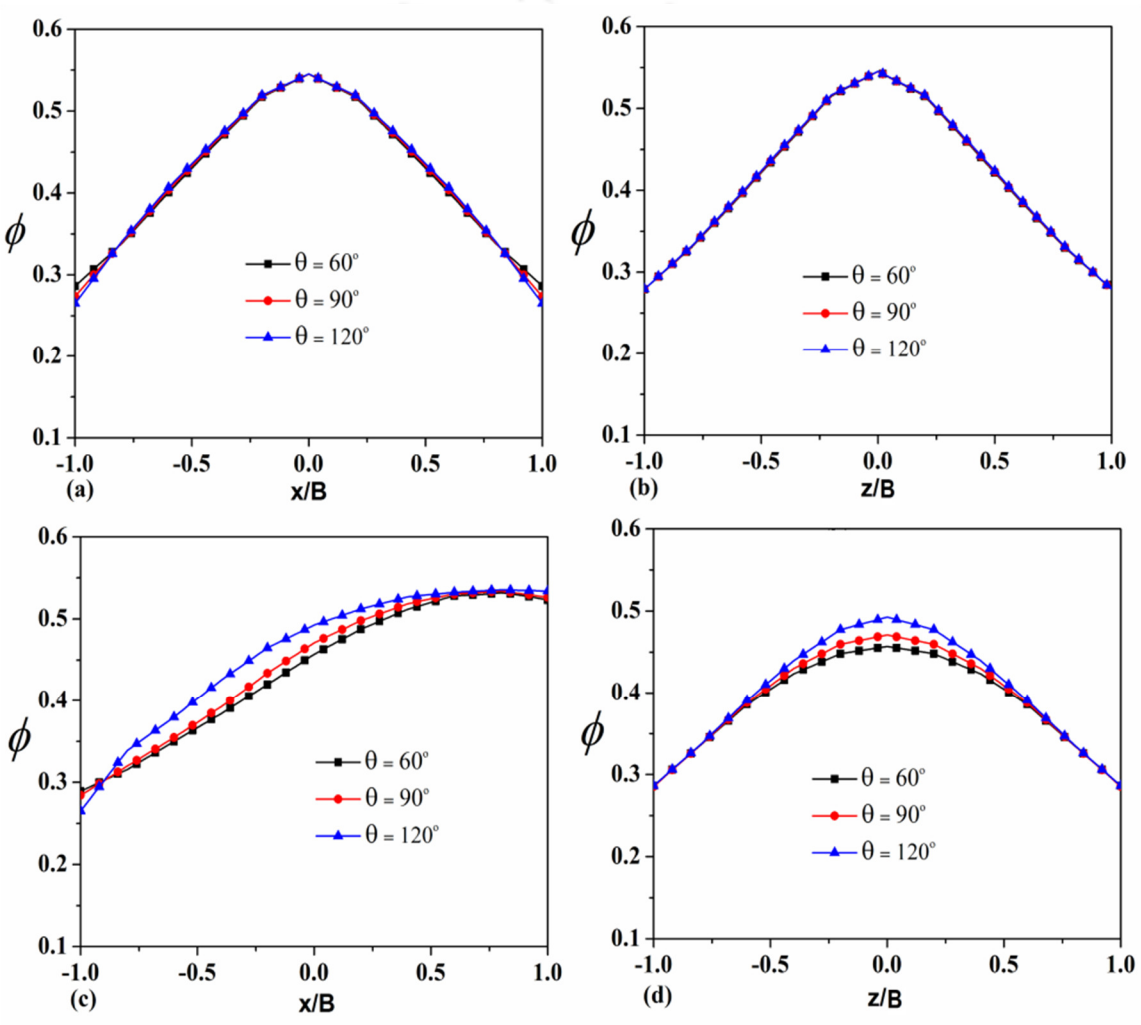

Figure 4.9. Effect of bifurcation angle on concentration profile at location 5 of the inlet section for 40% suspension in the lateral direction (a) and span wise direction (b). Effect of bifurcation angle on concentration profile at location 6 of the side branch in the lateral direction (c) and span wise direction (d). The inlet velocity in all the cases was 0.045 m/s.

The lateral concentration profile of side branch at location 6 (shown in Figure 4.9c) becomes more blunted with increase in bifurcation angle. At the same location the span wise profile in Figure 4. 9d shows that the peak concentration increases with increase in bifurcation angle.

4.3.3. Wall shear stresses

The wall shear stress profiles is another important quantity of interest during the flow of concentrated suspension through a bifurcation channel. It is well known that wall shear stress has profound effects on human blood cells. Shear forces induce physiological signals that modulate vascular and platelet behavior. Abnormally high shear stress in arteries increases the risk of thrombosis. Despite their importance the role of shear induced migration on wall shear stress in bifurcation channels has not received adequate attention in previous works. The wall shear stress can be evaluated from the product of shear rate and effective viscosity at the wall. Since the effective viscosity is function of particle concentration the nature of wall shear stress profile can be understood by observing the velocity profile (Figure 4.5) and concentration profile (Figure 4.8). We have shown the contour map of wall shear stress for the inlet and side branch in Figure. 4.10. In the inlet section the wall shear stress is low at the corner for the full length except near the bifurcation where the high value of shear stress is observed at the corners. This is due to increase in the bluntness of velocity profile between location 4 and 5 that causes high shear rate at the wall. At the junction of inner walls of the side branch both shear rate and concentration are high and hence the wall shear stress level rises (indicated by the bright red spot in the contour map). For low bifurcation angle ($\theta = 60^{\circ}$) the streamline curvature is low and as expected the stress levels at the inner and outer wall are similar but the corner region of inner wall has high stress compared to the middle section. The difference in wall shear stress level between the inner and outer wall is largest for $\theta = 90^{\circ}$.

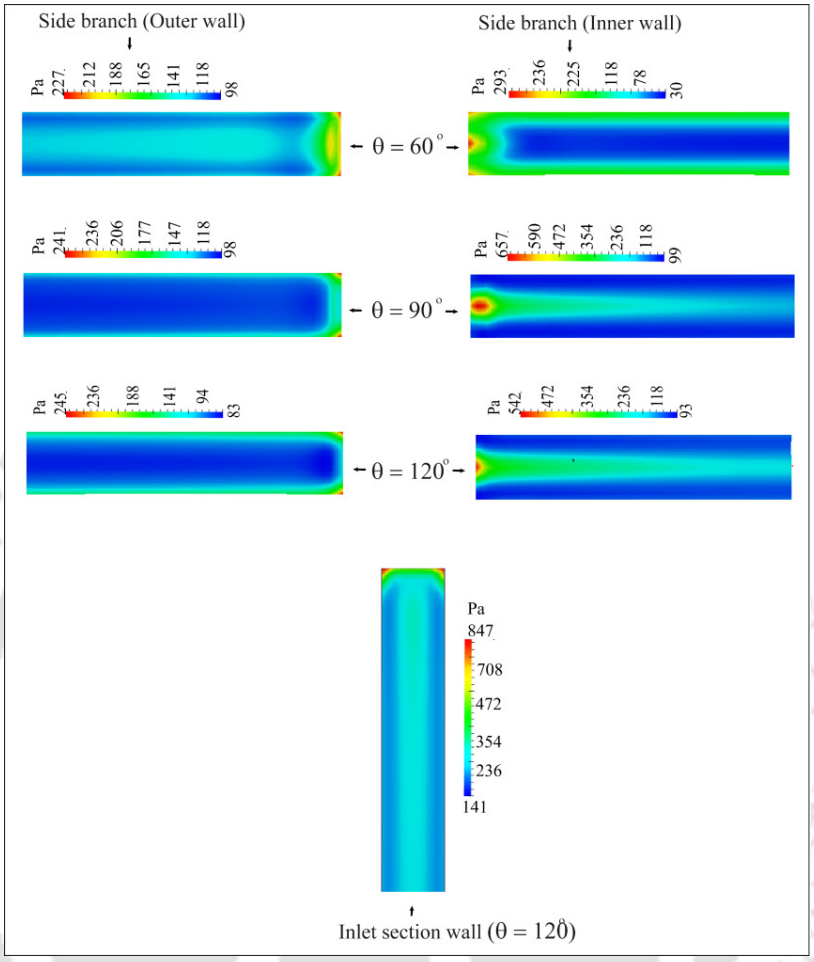

Figure 4.10. Shear stress contours planes for outer and inner walls of side branches for various bifurcation angles. The wall shear stress contour for one of inlet section corresponding to θ= 120° is also shown. The particle concentration in all the cases was 40% and the inlet velocity was 0.045 m/s.

4.4. Conclusion

The Diffusive Flux Model was used to investigate the velocity and particle concentration profile in suspension flow through symmetric 3D bifurcation channel. The mass, momentum and particle conservation equations were solved by the finite volume method (FVM).

Simulations were performed to study the effect of particle concentrations and bifurcation angles on velocity and concentration profiles. The velocity profiles for suspension flow were observed to be different from that of Newtonian fluid of same effective viscosity. At bifurcation the velocity profiles for suspension in lateral and span-wise directions are blunted and degree of bluntness is more apparent with increase in the angle of bifurcation and particle concentration. It was observed that the migration of particles in the downstream branches leads to asymmetric velocity and concentration profiles. The effect of non-uniform concentration distribution including the detailed concentration and velocity profiles in each branch has been well captured by our numerical simulations. The wall shear stress level was observed to be the highest near the bifurcation. In the side branch the difference in wall shear stress level of inner and outer wall was found to be highest for bifurcation angle of 90°.

CHAPTER-5

Shear induced migration in symmetric 3D T-shaped channels

भारतीय प्रौद्योगिकी संस्थान गुवाहाटी
Indian Institute of Technology Guwahati

5. Shear Induced Migration in Symmetric 3D T-Shaped Channels

5.1. Introduction

In a symmetric T- junction the flow splits into two symmetric streams (diverging flow) or two inlet stream joins to form one outlet stream (converging flow). In this chapter, we have studied the migration in three dimensional symmetric T- shaped bifurcation channels for diverging and converging flows. In case 1, there is one inlet and two outlets. Simulations were carried out for three different concentrations of particles, i.e. 30%, 40% and 50%. The inlet velocity was 0.0045 m/s. In case 2 there were two inlets and one outlet (converging flow). Equal particle concentration and velocity (0.0025 m/s) from both the inlets were provided. In the third case (converging flow), the inlet particle concentrations were different but with equal inlet velocity (0.0025 m/s).

5.2. Case 1: Diverging flow

The computational geometry of the three dimensional T shaped bifurcation channel is shown schematically in Figure 5.1. It consists of an inlet and two outlets with square cross section. The inlet and daughter branches were of equal width (0.0018 m) and the channel height was 0.0018 m. The ratio of channel half width to particle radius (B/*a*) was equal to 18.The lengths of inlet and daughter branches were 0.5 m and 0.25 m respectively. The length required for reaching fully developed profile was calculated by using the formula given by Nott and Brady (1994). Other simulation parameters and geometry details are same as in the previous chapter.

In Figure 5.1 we have also shown different axes with dashed lines along which the perpendicular planes were taken for analyzing the velocity and concentration contours.

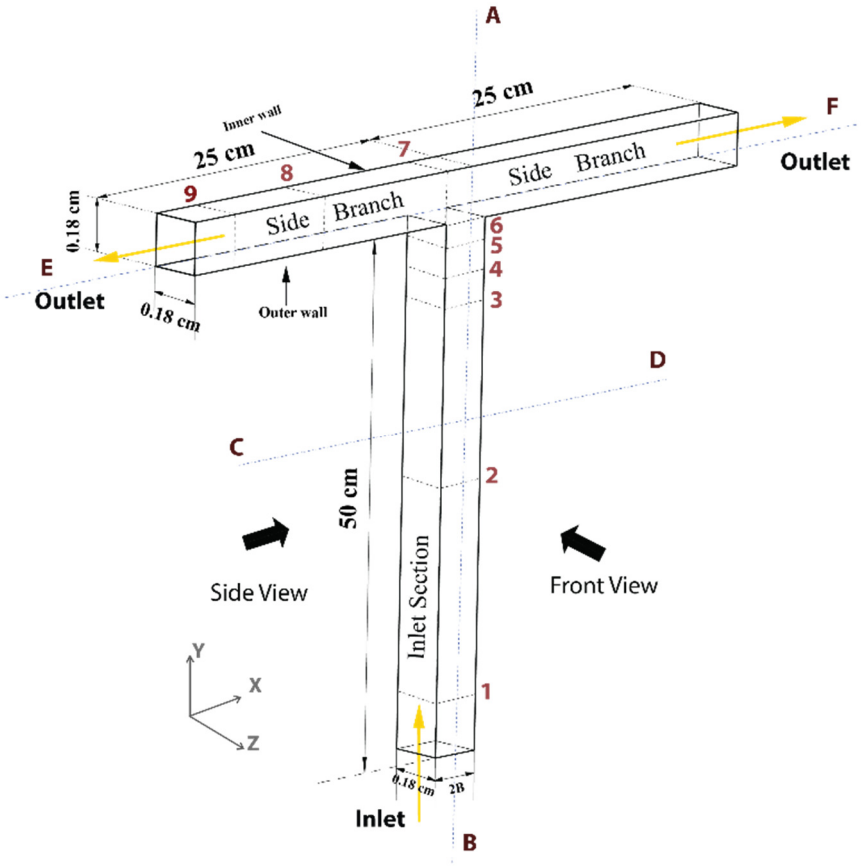

Figure 5.1. Schematic diagram of the computational geometry and locations where velocity and concentration data were analysed.

In local co-ordinate system, x denotes the lateral direction, y denotes the flow direction and z represents the span wise direction. The computational domain of the straight sections of inlet as well as side branches was discretized using structured grids. The Grid comprised of total of 561000 cells (10X2800X10 structured cells in the outlet section, 1400X10X10 structured cells in each of the straight sections of side branches (Inlet section) and 10X10X10 structured cells in the bifurcation zone.

5.2.1. Results and Discussion

5.2.1.1. Velocity field

The impact of particles on the velocity fields are often studied by comparing the suspension velocity with that of Newtonian fluid having the same effective viscosity and other simulation parameters. For this purpose the velocity contour and streamlines (front view) of Newtonian fluid and suspension flow in the mid-plane of the channel are shown in Figure 5.2. For the clarity of view the contours of the full channel are not shown, and only a small section around the bifurcation was taken. For the comparison purpose, we have shown the contour planes for Newtonian fluid and suspension of 40% and 50% concentration. The viscosity of Newtonian fluid was taken as effective viscosity of 40% suspension. All other simulation parameters were the same. It is observed that in the case of Newtonian fluid the parabolic profile in the inlet channel persists up to the bifurcation (location 6) and after that the flow divides into two side branches. However, for the suspension flow we observe blunted velocity profile in the inlet section and the bluntness increases near the bifurcation. Another important observation can be made about the maximum center-line velocity which persists little downstream of location 6 for Newtonian fluid, whereas for suspension this location is upstream of location 6. For 50% suspension the difference is clearly noticeable.

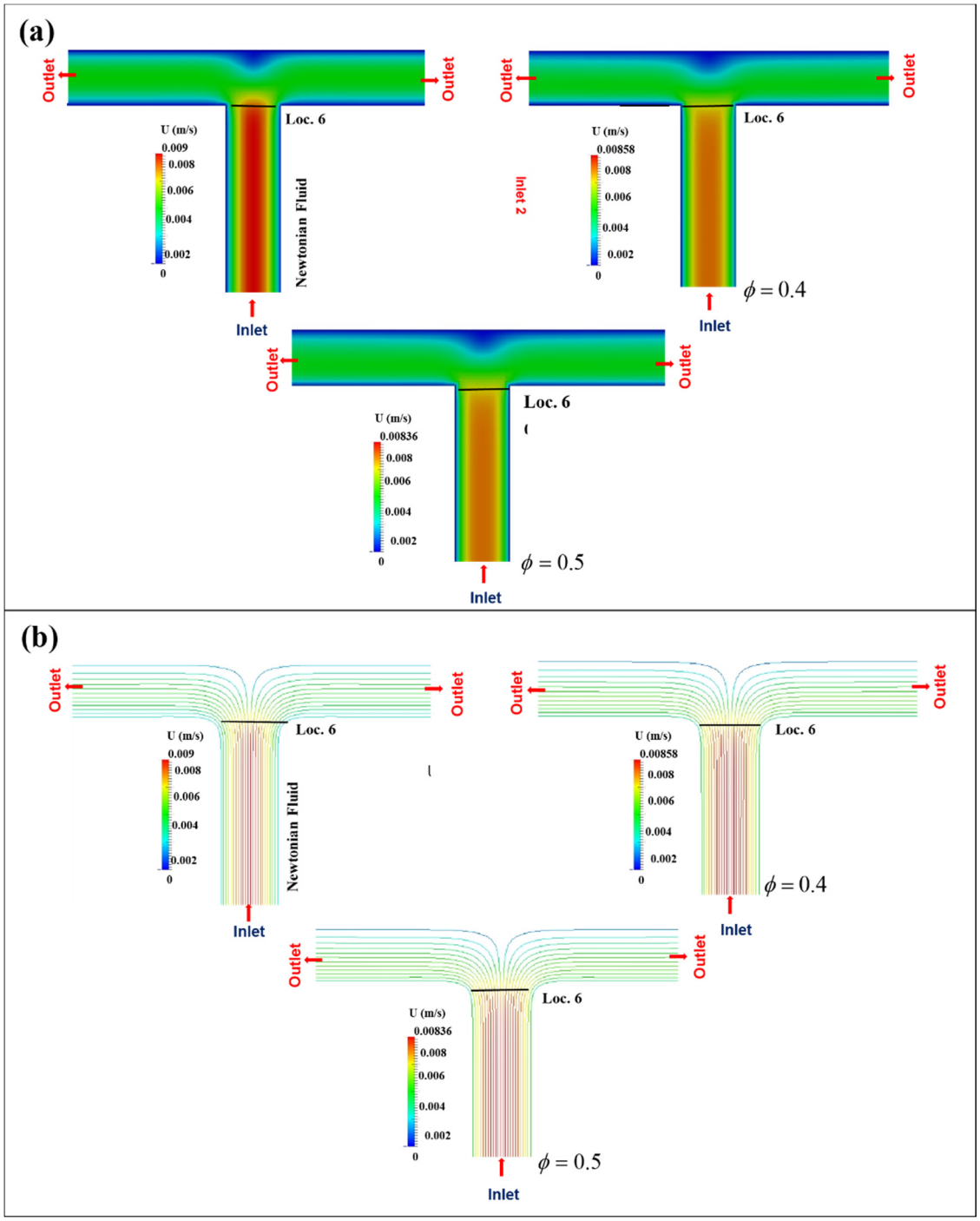

Figure 5.2. The front view of velocity contours planes (first row) and stream lines (second row) for Newtonian fluid and suspension flow (40% and 50% particle concentration) in x-y plane for bifurcation channel. The inlet velocity was 0.0045 m/s.

This fundamental difference in the velocity field is due to the presence of particles in suspension. The increase in the bluntness of velocity profile near the bifurcation in the inlet section is due to curvature of the streamlines towards the left and right daughter branches. The degree of bluntness was found to increase with the increase in bulk particle concentration. The corresponding streamlines are also shown in Figure 5.2b. It can be observed that the dividing stream line is located exactly at the center of the inlet section of the channel. This is expected since the channel itself is symmetric and flow is divided equally in the daughter branches. The smearing of velocity profile near the bifurcation can be seen more clearly in these streamline plots.

Figure 5.3 shows the comparison of velocity profiles of Newtonian fluid with a 30% suspension at various locations in the inlet section for lateral and span-wise direction. For the case of suspension, at location 1 nearly uniform velocity profile is observed. The velocity locations (1,2,3,4,5,6) are taken at the locations -49.98 cm, -25 cm, -1.0cm, -0.5cm, -.05 cm and Y= 0 cm (bifurcation) respectively. As we move further downstream of the channel (locations 2, 3, 4) we observe fully developed blunted velocity profile in both the lateral and span wise directions. However, at the location 5 influence of bifurcation is apparent and at the locations 6, the bluntness in velocity profile is more in the lateral direction in comparison to the span wise direction. Whereas, Newtonian fluid shows nearly parabolic profile at locations 2 and 6 compared to suspension at the same locations in both lateral and span wise directions. We also studied the 40% and 50% suspensions and the results are shown in Figures 5.4 and 5.5. The similar trends of velocity profiles discussed in previously were observed but the bluntness in velocity profile increases with the increase in particle concentration.

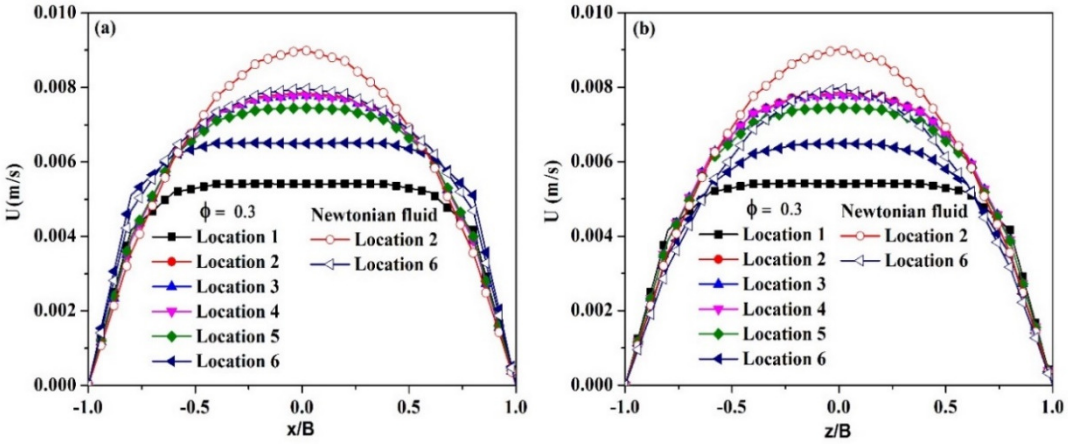

Figure 5.3. Comparison of the velocity profiles for Newtonian fluid and suspension (30% particle concentration) at various locations in inlet section of the symmetric T- shaped bifurcation channel for (a) lateral and (b) span-wise direction. The inlet velocity was 0.0045 m/s.

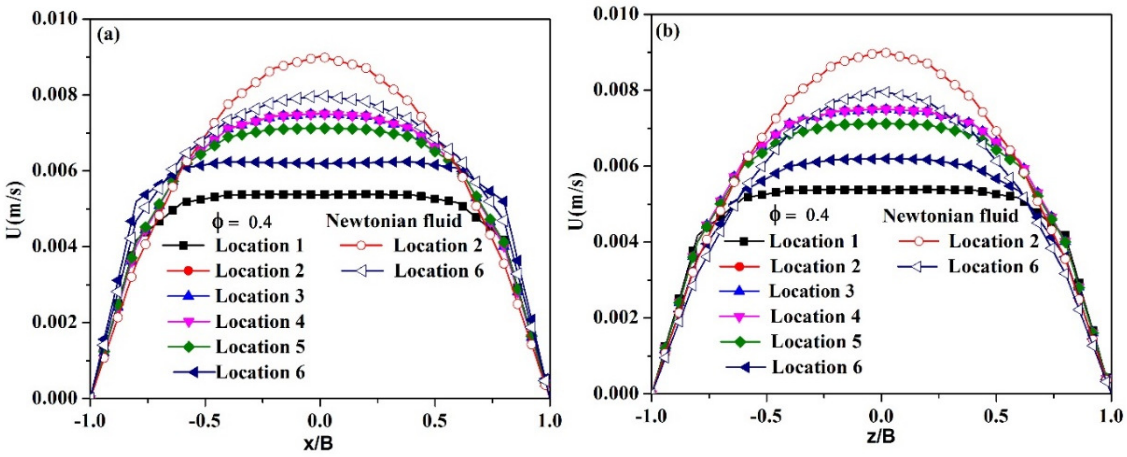

Figure 5.4. Comparison of the velocity profiles for Newtonian fluid and suspension (40% particle concentration) at various locations in inlet section of the symmetric T- shaped bifurcation channel for (a) lateral and (b) span-wise direction. The inlet velocity was 0.0045 m/s.

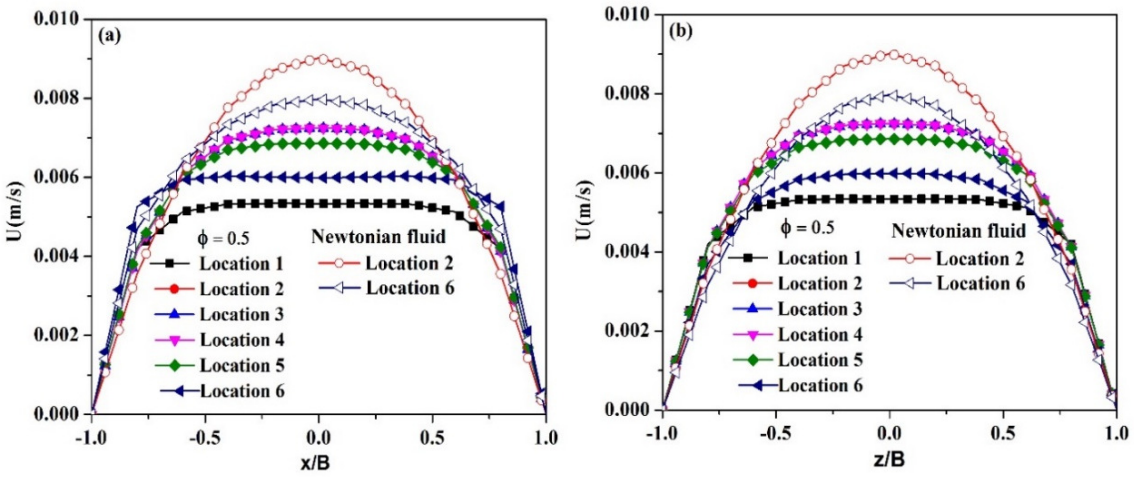

Figure 5.5. Comparison of the velocity profiles for Newtonian fluid and suspension (50% particle concentration) at various locations in inlet section of the symmetric T- shaped bifurcation channel for (a) lateral and (b) span-wise direction. The inlet velocity was 0.0045 m/s.

The cross-sectional views (x-z plane) of velocity contour at various locations in the inlet section for Newtonian fluid and suspension (40% and 50%) are shown in the Figure 5.6a. These cross-sectional slices were taken at various locations (1, 5 and 6) in the inlet section at planes perpendicular to the flow direction. Locations corresponds to -49.98 cm, -.05 cm and Y= 0cm respectively. It can be observed that the contours at the location 1 (entrance of the channel) and location 5 is nearly similar for the Newtonian fluid but when it reaches location 6 (bifurcation point) it spreads in lateral direction. Whereas, in case of suspension (40% and 50%) we observe different behavior compared to the Newtonian fluid. In case of suspension the contour at location 6 is smeared more along the lateral direction. This is more apparent in the case of 50% concentration.

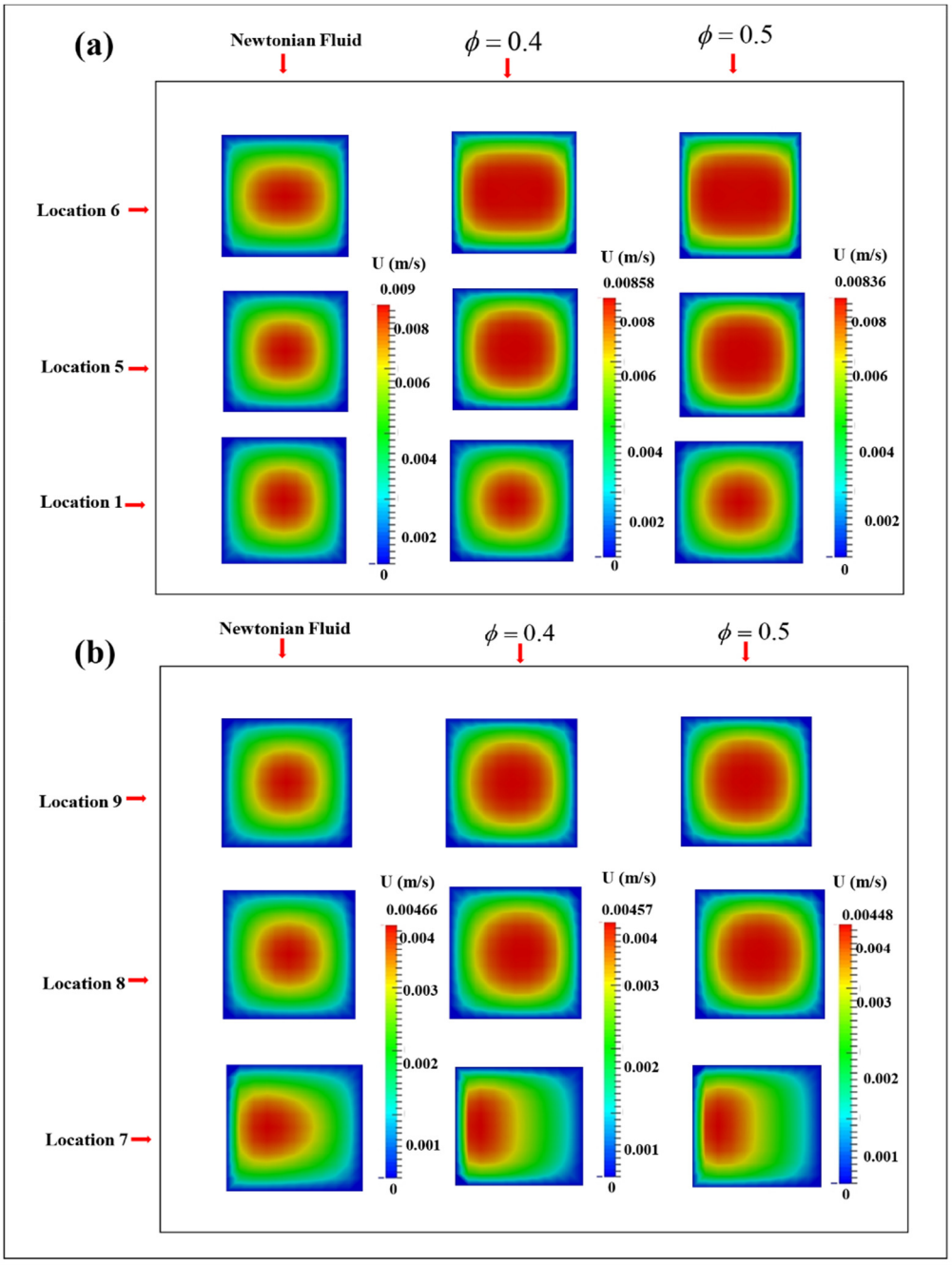

Figure 5.6. The cross sectional velocity contour planes (x-z plane) for Newtonian fluid and suspension flow (40% and 50% concentration) at various locations in the (a) inlet branch and (b) side branch. The inlet velocity was 0.0045 m/s.

Figure 5.6b shows the velocity contour maps in the cross-sectional plane of the side branch. The contour locations (7,8,9) are taken at the locations -.09 cm, -12.5 and 24.98 cm respectively. It was observed that at a distance of 0.09 cm from the center of bifurcation (location 7), which is at the very beginning of the side branch, the velocity field is more asymmetric and the peak velocity shifts towards the outer (bottom) wall. The asymmetry is more pronounced for suspension flow. As we move further downstream locations the velocity field becomes more symmetric and peak velocity shifts towards the centre of the channel. For Newtonian fluid the velocity field becomes nearly symmetric at location 8 but in case of suspension flow the shift of velocity peak towards the center is small. At a given location the degree of asymmetry is more for 50% suspension compared to 40%.

The comparison of velocity profiles of Newtonian fluid and suspension (30%) at various locations in the lateral and span wise directions of the side branch are shown in the Figure 5.7. We have compared the Newtonian fluid velocity and suspension velocity at same locations. The location 7 is at the very beginning of the side branch and is 0.09 cm away from the center of the bifurcation. The other two locations (8 and 9) are 12.5 cm and 24.98 cm apart from center of the bifurcation. It can be noted from the Figure 5.7a that at location 7 the profiles for both Newtonian fluid and suspension are asymmetric and skewed towards the outer (bottom) wall. However, the skewness for suspension is more compared to that of Newtonian fluid. The asymmetry of the profile results from the non-uniform distribution of particles which is discussed in detail in the next section. As we move further downstream the profiles shift towards the center of the channel causing it to appear more symmetric, whereas, Newtonian

fluid shows parabolic profile at locations 8 and 9. However, at the same locations in the span-wise direction the profiles are symmetric though blunted (see Figure 5.7b).

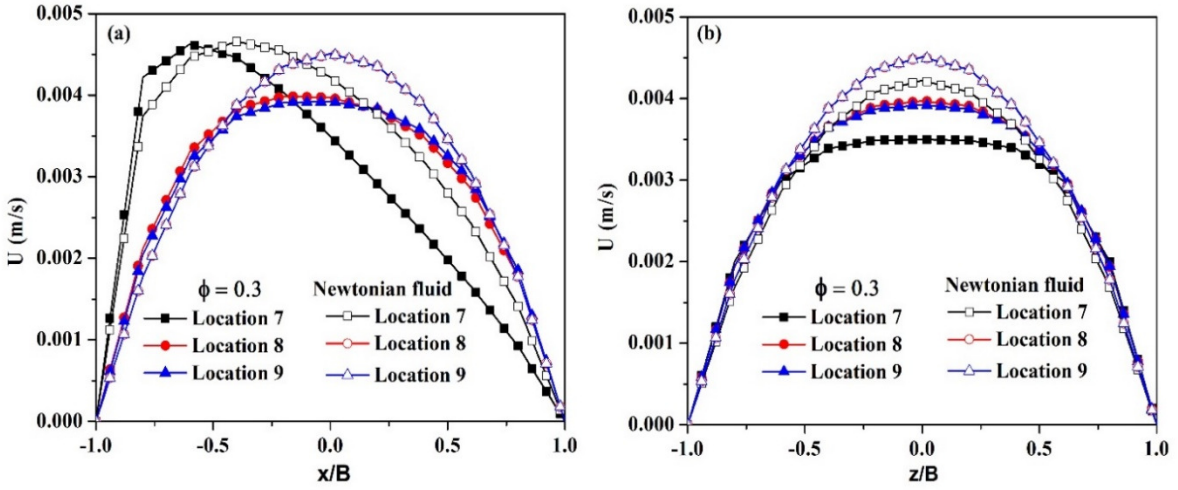

Figure 5.7. Comparison of the velocity profiles for Newtonian fluid and suspension (30% particle concentration) at various locations in the side branch of the symmetric T- shaped bifurcation channel for (a) lateral and (b) span-wise direction. The inlet velocity was 0.0045 m/s.

We also studied velocity profiles for the 40% and 50% particle concentration in lateral and span wise directions and are shown in Figures 5.8 and 5.9 respectively. The similar trends of velocity profiles which were discussed for 30% particle concentration is observed but the shifting of velocity profiles is more towards outer wall in the case of the 50% particle concentration and it can be clearly seen in Figure 5.9a. This skewness increases with the increase in particle concentration.

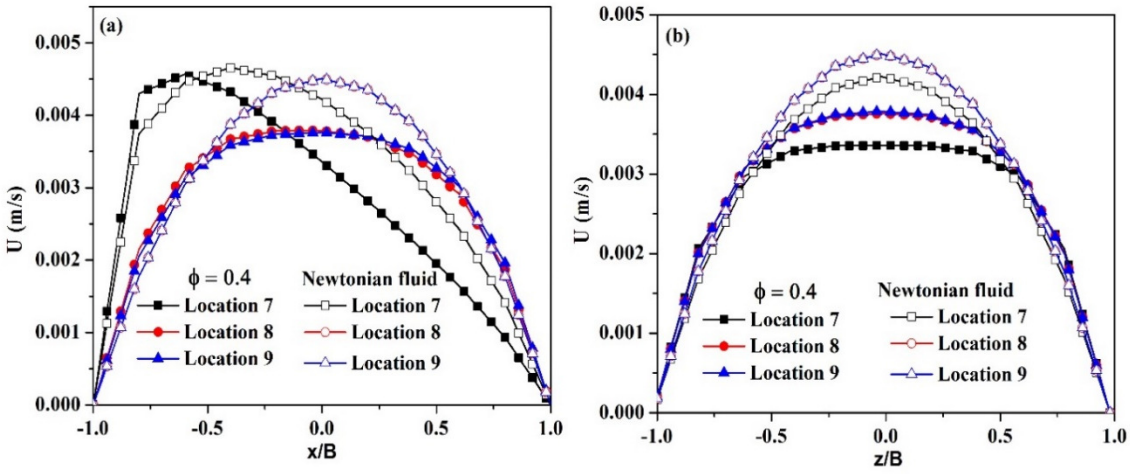

Figure 5.8. Comparison of the velocity profiles for Newtonian fluid and suspension (40% particle concentration) at various locations in the side branch of the symmetric T- shaped bifurcation channel for (a) lateral and (b) span-wise direction. The inlet velocity was 0.0045 m/s.

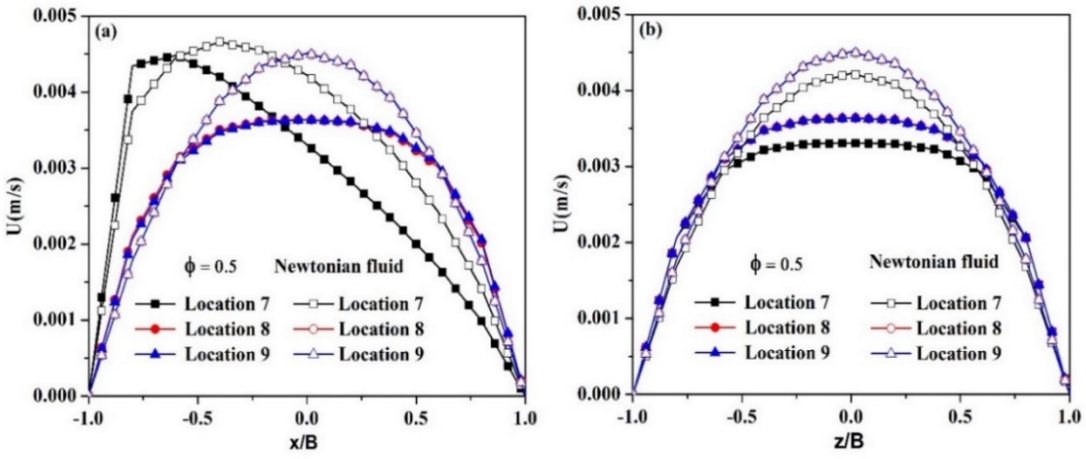

Figure 5.9. Comparison of the velocity profiles for Newtonian fluid and suspension (50% particle concentration) at various locations in the side branch of the symmetric T- shaped bifurcation channel for (a) lateral and (b) span-wise direction. The inlet velocity was 0.0045 m/s.

5.2.1.2. Shear rate field

The front view of shear rate contour maps in x-y plane for Newtonian and suspension of 40% and 50% particle concentrations are shown in Figure 5.10. In the inlet section the high shear rate is observed near the wall and low in the core of the channel. Increase in particle concentration has little influence on shear rate as shown in Figure 5.10. It can be noticed that the daughter branches have low shear rates when compared to inlet section. This is due to the fact that flow coming from the inlet divides into the daughter braches. Since the width of inlet and two daughter branches were the same, it is expected that the average velocity in the daughter branches would be half of that in the inlet branch and so will be the shear rate. The maximum shear rate in the inlet branch for pure fluid, 40% and 50% suspensions were 40.5, 40.6, 41.1 s^{-1} respectively. Whereas, in daughter branches the respective values were 23.4, 29.3, 34.3 s^{-1}.

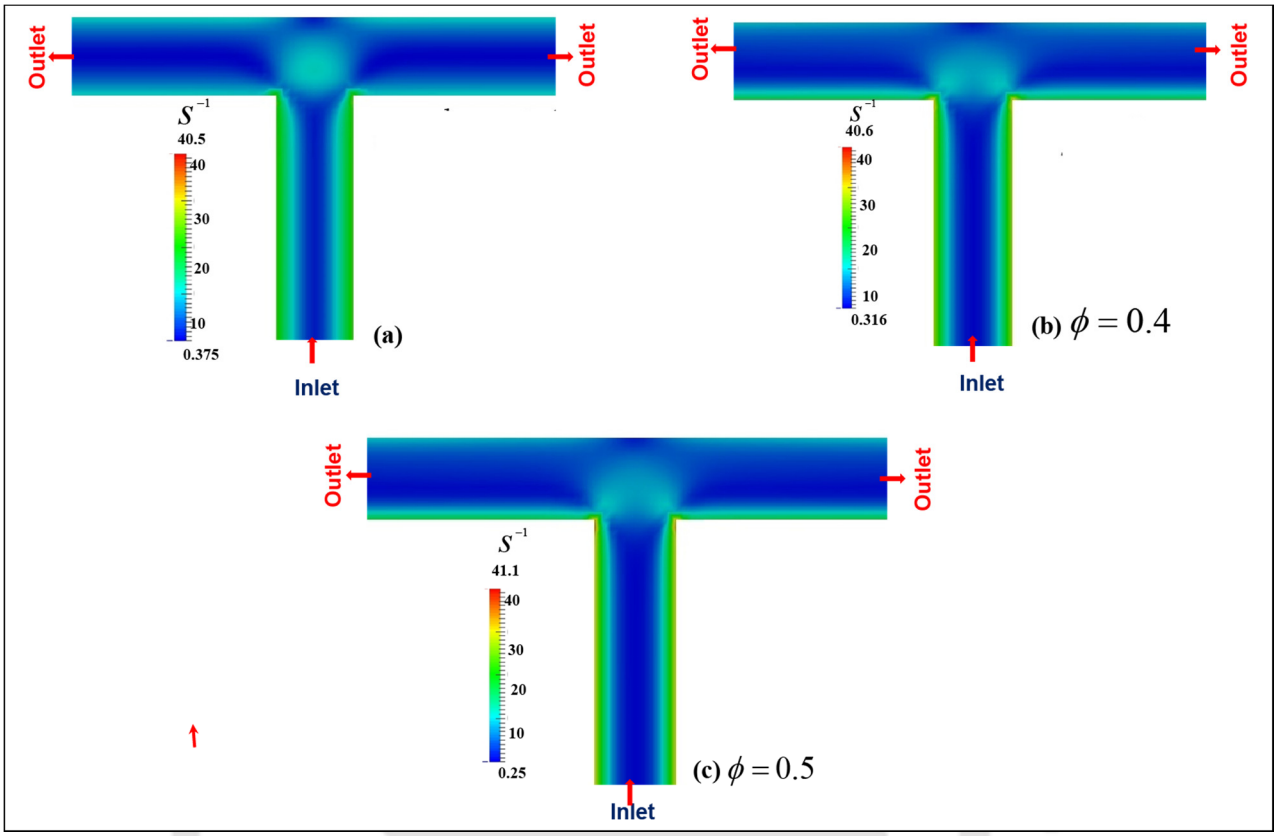

Figure 5.10. The front view shear rate contour planes for Newtonian fluid and suspension flow (40% and 50% concentration) at various locations in the (a) inlet branch and (b) side branch. The inlet velocity was 0.0045 m/s.

The corresponding cross sectional shear rate contour planes (x-z plane) in the inlet and side branch are shown in Figure 5.11. The corner regions of the planes (cross section) have relatively higher shear rate compared to the middle regions. The shear rate gradients are highest at location 6. At the location 7 of the side branch the high shear rate regions are shifted towards the outer (left) wall but gradually becomes more symmetric as we move to downstream locations. We observed that increase in particle concentration influences the shear rate distribution in the channel.

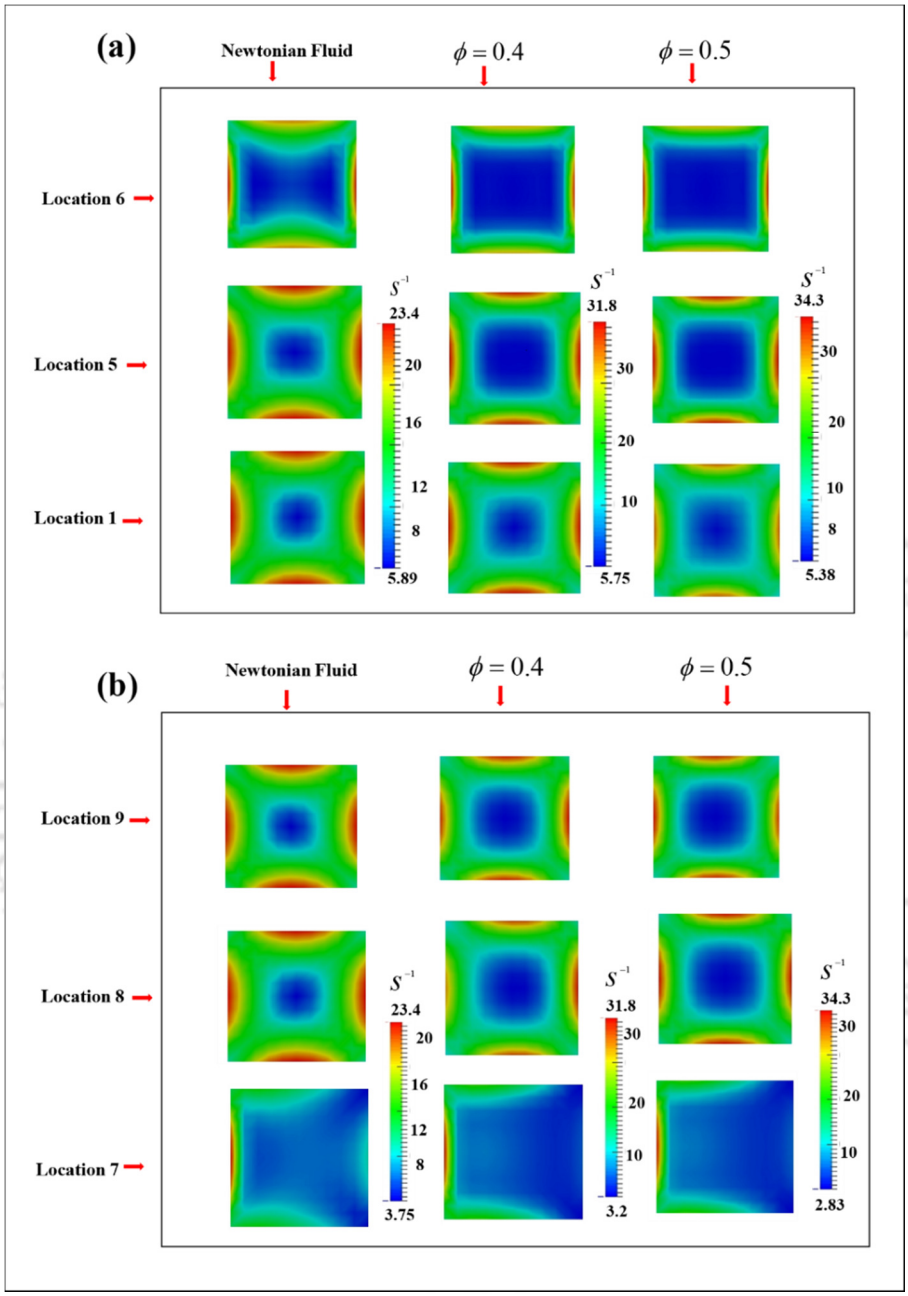

Figure 5.11. The cross sectional shear rate contour planes for Newtonian fluid and suspension flow (40% and 50% concentration) at various locations in the (a) inlet branch and (b) side branch. The inlet velocity was 0.0045 m/s.

5.2.1.3. Concentration field

The concentration and shear stress contour maps in the mid-plane (Z=0) for 30% and 40% suspension are shown in Figure 5.12. For the clarity of view we have shown only a small section around the bifurcation. In the inlet section the shear induced migration causes the particles to move towards the center of the channel. The central core of the inlet channel which has high concentration of particles meets the junction of left and right branches of inner walls. This makes the particle concentration in the side branches to be more near the right walls. However, even in the side branch the shear rate at the wall is more compared to the center (please see Figure 5.11b) and this gradient again drives flux of particles towards the center in the daughter branches. As a result the concentration peak gradually shifts towards the left side (outer wall). We also observe that the peak value of concentration for 50% suspension is higher than that of 40% suspension as shown in Figure 5.12b. Figures 5.12c and 5.12d shows the shear stress maps and it is observed that near the bifurcation (location 6) shear stress is maximum for the case of 50% bulk particle concentration compared to 40% particle concentration. It is due to the fact that shear stress is product of viscosity and shear rate. The middle regions of the inlet section have low shear stress values compared to daughter branches.

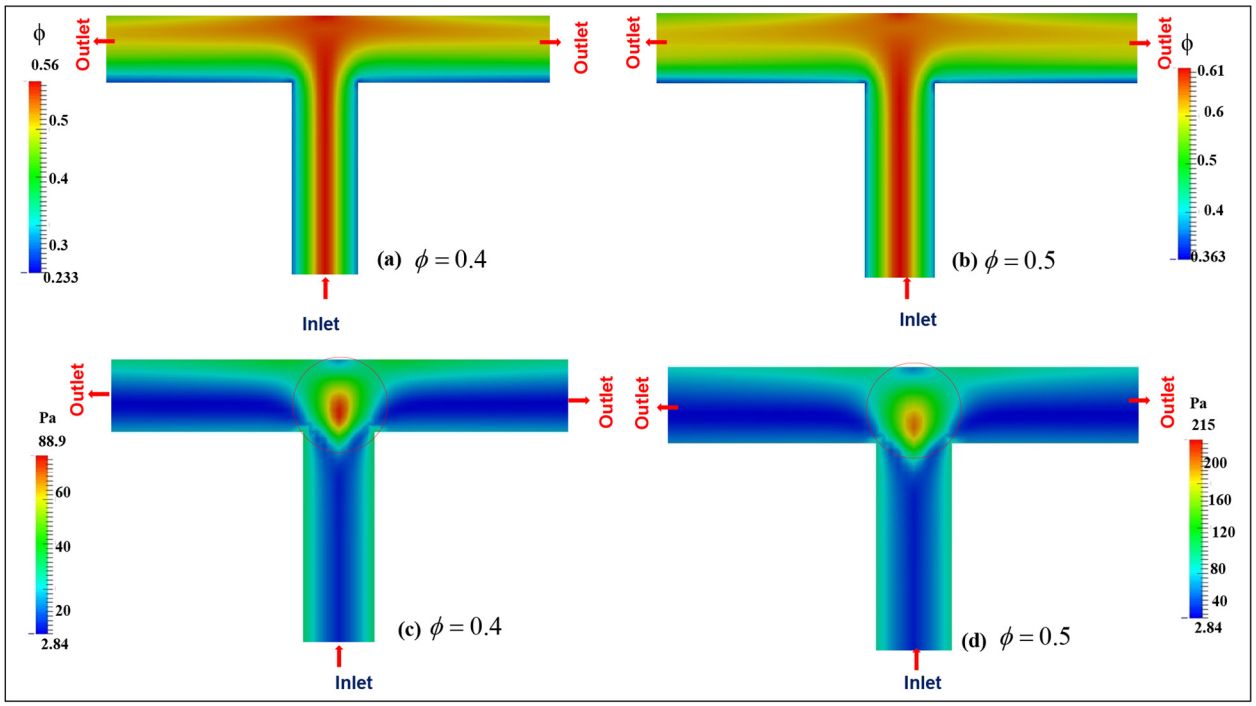

Figure 5.12. Front view particle concentration (a-b) and shear stress (c-d) contour maps in x-y plane at the centerline for suspension of 40% and 50% particle concentration. The inlet velocity was 0.0045 m/s. For clarity of contours only small section of channel near the bifurcation is shown here.

In order to understand quantitative nature of particle distribution we have shown the concentration profiles for 30% particle concentration in the lateral and span-wise directions of the inlet section in Figure 5.13. The concentration profile becomes fully developed at location 5. However, unlike the velocity profile the concentration profile remains unaffected till the beginning of bifurcation section (location 6) and we observe almost identical profile at location 5 and location 6. The concentration profiles of inlet section are similar in both lateral and span wise directions. We observed that the effect of bifurcation on velocity field is realized little before the bifurcation, whereas the concentration profile at the same location (when compared

to the upstream locations) remains somewhat unaffected. The possible reason behind this could be shear induced rearrangement of particles. The stress field ahead of bifurcation is different from that at the locations before the bifurcation. This change in stress field causes shear induced migration, and its effect is such that the particles oppose being carried away by the fluid streamlines. Similar behavior of concentration profiles in lateral and span-wise direction are shown in Figures 5.14 and 5.15 for 40% and 50% particle concentration respectively. We also observed that the lateral concentration profiles for 50% particle concentration were blunted compared to 30% and 40% particle concentrations.

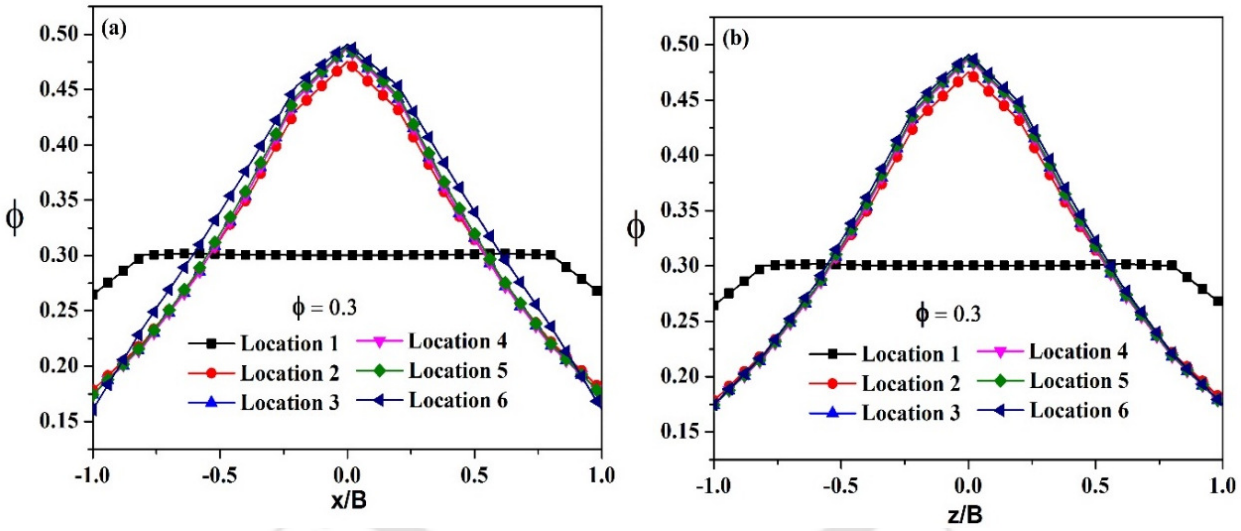

Figure 5.13. Comparison of the concentration profiles for suspension flow (30% particle concentration) at various locations in the inlet section for (a) lateral direction and (b) span-wise direction. The inlet velocity was 0.0045 m/s.

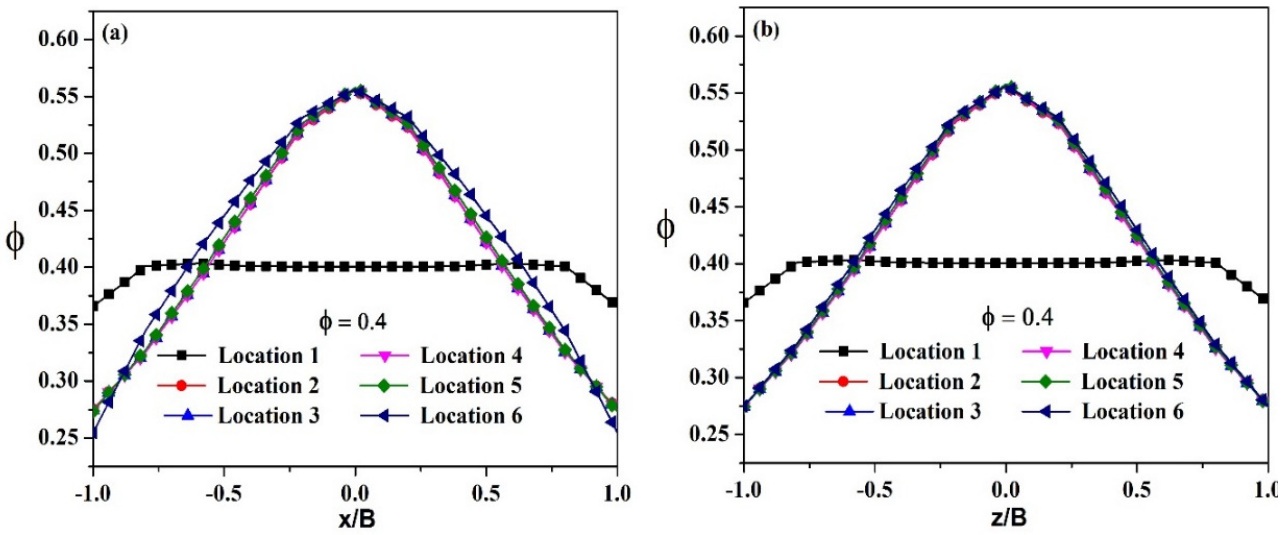

Figure 5.14. Comparison of the concentration profiles for suspension flow (40% particle concentration) at various locations in the inlet section for (a) lateral direction and (b) span-wise direction. The inlet velocity was 0.0045 m/s.

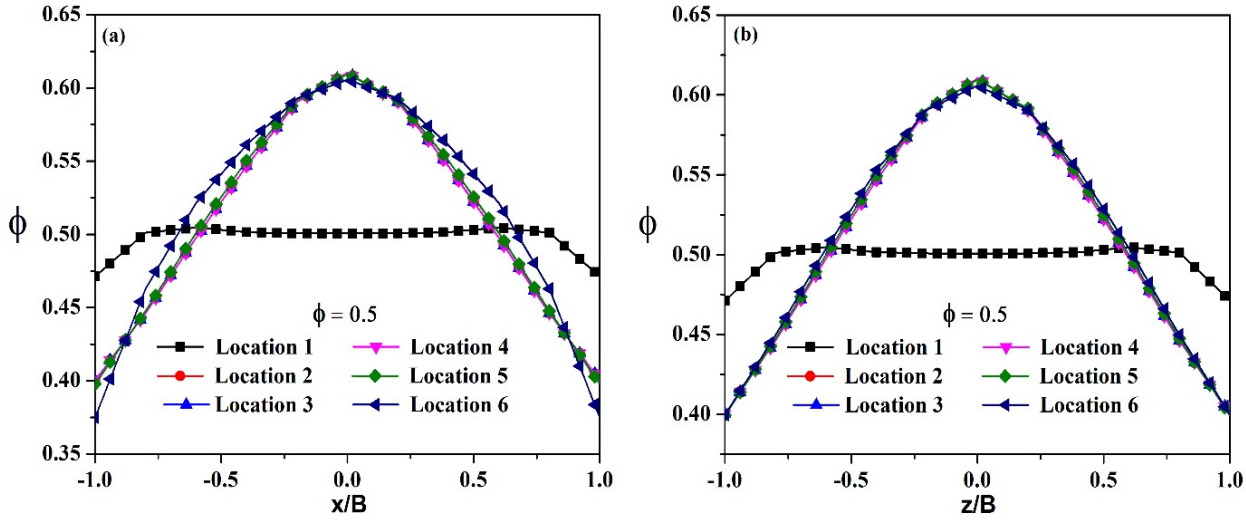

Figure 5.15. Comparison of the concentration profiles for suspension flow (50% particle concentration) at various locations in the inlet section for (a) lateral direction and (b) span-wise direction. The inlet velocity was 0.0045 m/s.

Figure 5.16 shows the cross-sectional view of concentration maps in the inlet section (a) and side branch (b) for suspension of 40% and 50% bulk particle concentrations. These slices were taken at planes perpendicular to the flow direction at the locations 1, 5 and 6 of the inlet section. It was observed that as we move downstream in the inlet section the concentration inhomogeneities gradually develop due to particle migration. The depletion of particles in the corner region is less compared to the middle portions near the channel walls. This is because of the fact that the shear rate gradient is smaller in the corner region (see Figure 5.11a). Figure 5.16b shows cross-sectional concentration contour maps in the side branch. It was observed that at location 7, the concentration field is asymmetrically distributed and as we move further downstream locations in side branch the particles migrate towards the center of the channel. The regions close to the top and bottom walls as well as the outer wall (except the corners) is devoid of particles as represented by dark blue regions. The region close to the inner wall has highest particle concentration since the shear rate is lowest there (see Figure 5.11b). As one moves further downstream the peak value of concentration shifts towards the center of the channel due to the shear induced migration of particles. The migration of particles is faster for 50% suspension compared to 40% suspension which is evident from bright spot at the centre of location 8.

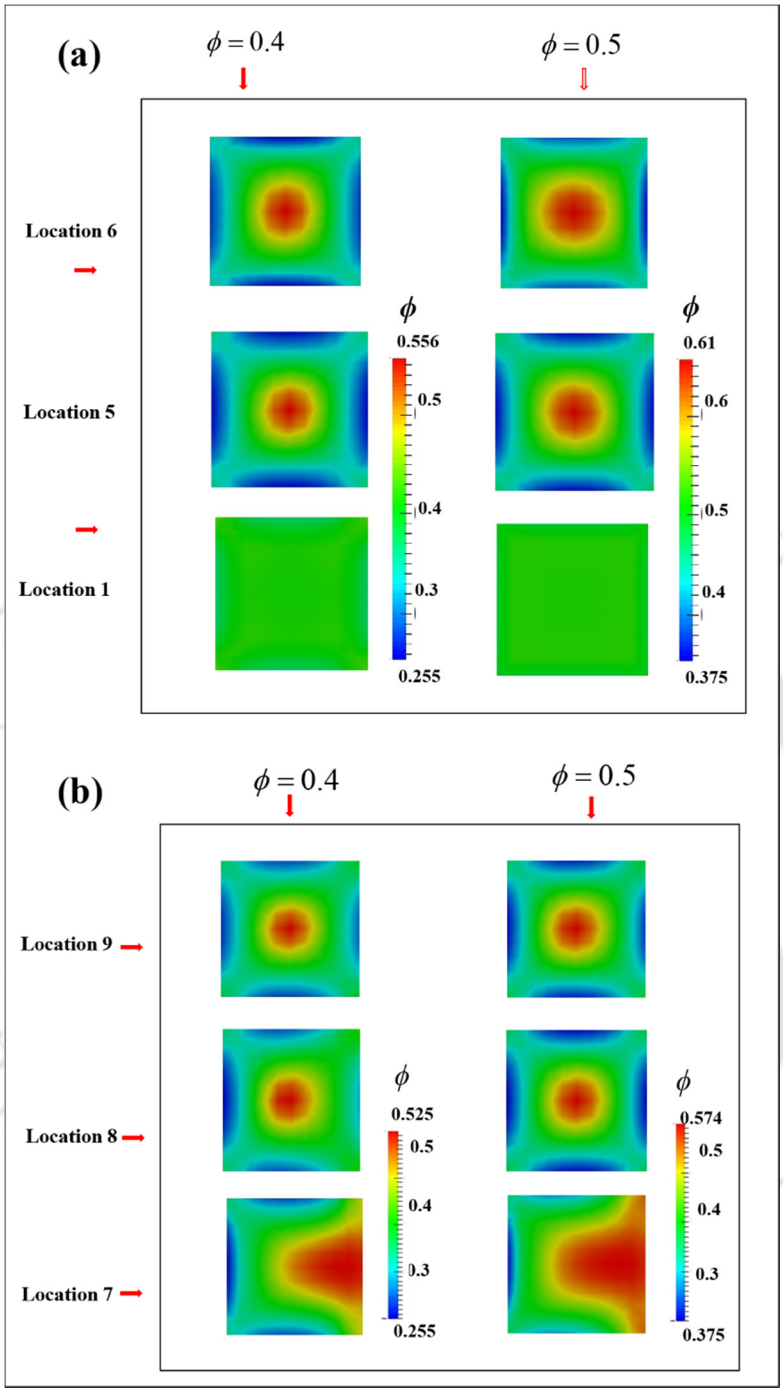

Figure 5.16. Cross- sectional view particle concentration contour maps for suspension of 40% and 50% particle concentration (a) Front view in x-y plane at the centerline (b) in x-z plane for inlet section (c) for side branch. The inlet velocity was 0.0045 m/s.

The corresponding concentration profiles in side branch for 30% particle concentration are shown in Figure 5.17. It is clearly seen from Figure 5.17a that the maximum concentration at the beginning of the side branch (location 7) is on the inner wall (x/B = +1) which gradually moves toward the center of the channel as we move further downstream locations (location 8 and 9). The lateral profiles are asymmetric but at the same locations the span-wise profiles (see Figure 5.17b) are not only symmetric but do not change much in the downstream locations. We have also carried out simulations for 40% and 50% particle concentrations and corresponding concentration profiles are shown in Figures 5.18 and 5.19 respectively. We observed that location of maximum concentration at inner wall increases with increase in particle concentration at location 7.

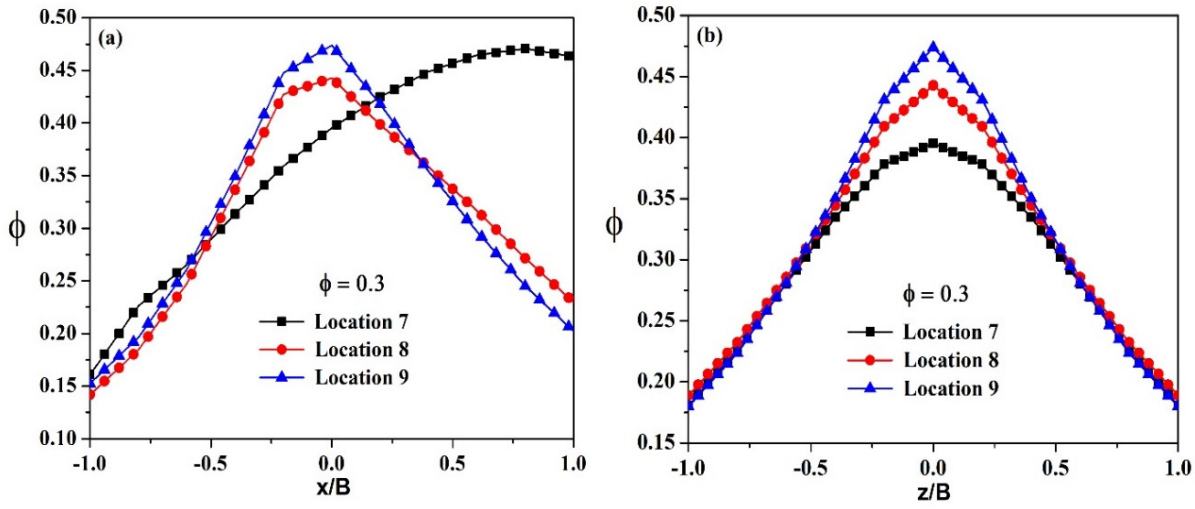

Figure 5.17. Comparison of the concentration profiles for suspension flow (30% particle concentration) at various locations in the side branch for (a) lateral direction and (b) span-wise direction. The angle of bifurcation was ($\theta = 180^{\circ}$) and the inlet velocity was 0.0045 m/s.

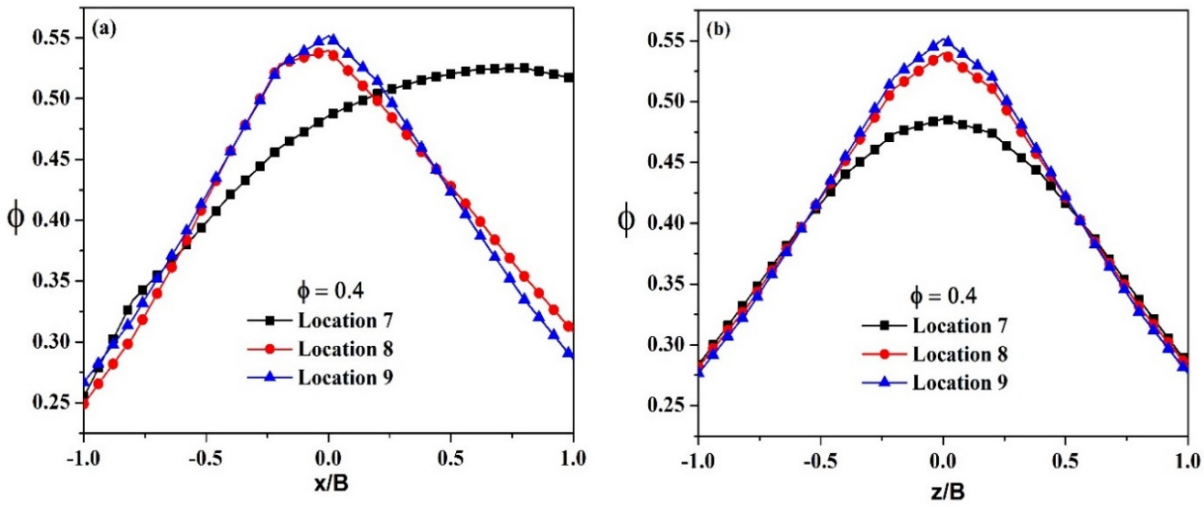

Figure 5.18. Comparison of the concentration profiles for suspension flow (40% particle concentration) at various locations in the side branch for (a) lateral direction and (b) span-wise direction. The inlet velocity was 0.0045 m/s.

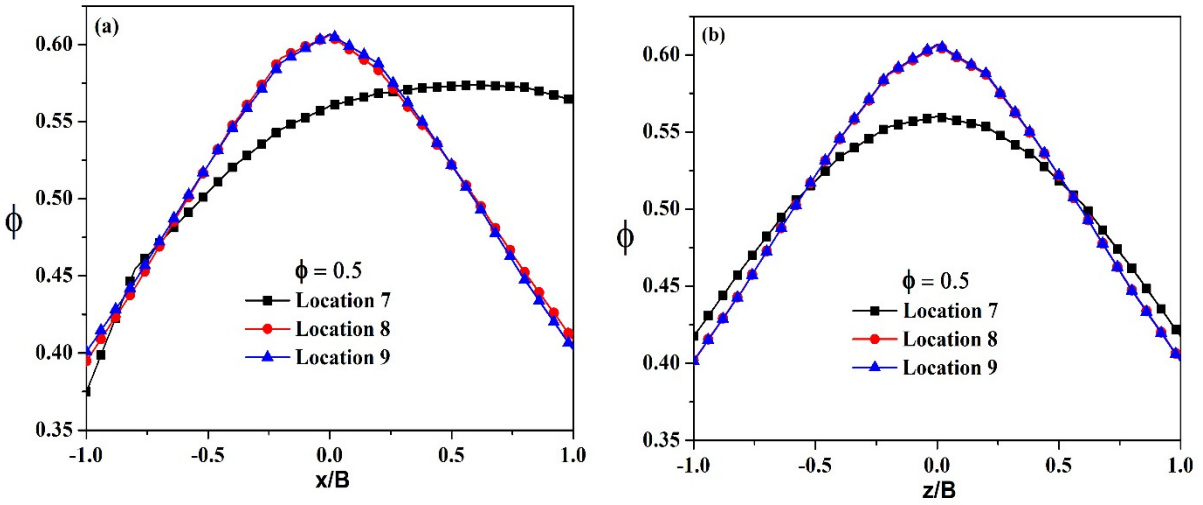

Figure 5.19. Comparison of the concentration profiles for suspension flow (50% particle concentration) at various locations in the side branch for (a) lateral direction and (b) span-wise direction. The inlet velocity was 0.0045 m/s.

5.2.1.4. Wall shear stresses

We have shown the contour map of wall shear stress for the inlet and side branch for 40% and 50% particle concentration in Figure. 5.20. In the inlet section the wall shear stress is low at the corner for the full length except near the bifurcation where the high value of shear stress is observed at the corners. This is due to increase in the bluntness of velocity profile between location 5 and 6 that causes high shear rate at the wall. At the junction of inner walls of the side branch both shear rate and concentration are high and hence the wall shear stress level rises (indicated by the bright red spot in the contour map). We found that wall shear stress at the inner wall is more for 50% particle concentration.

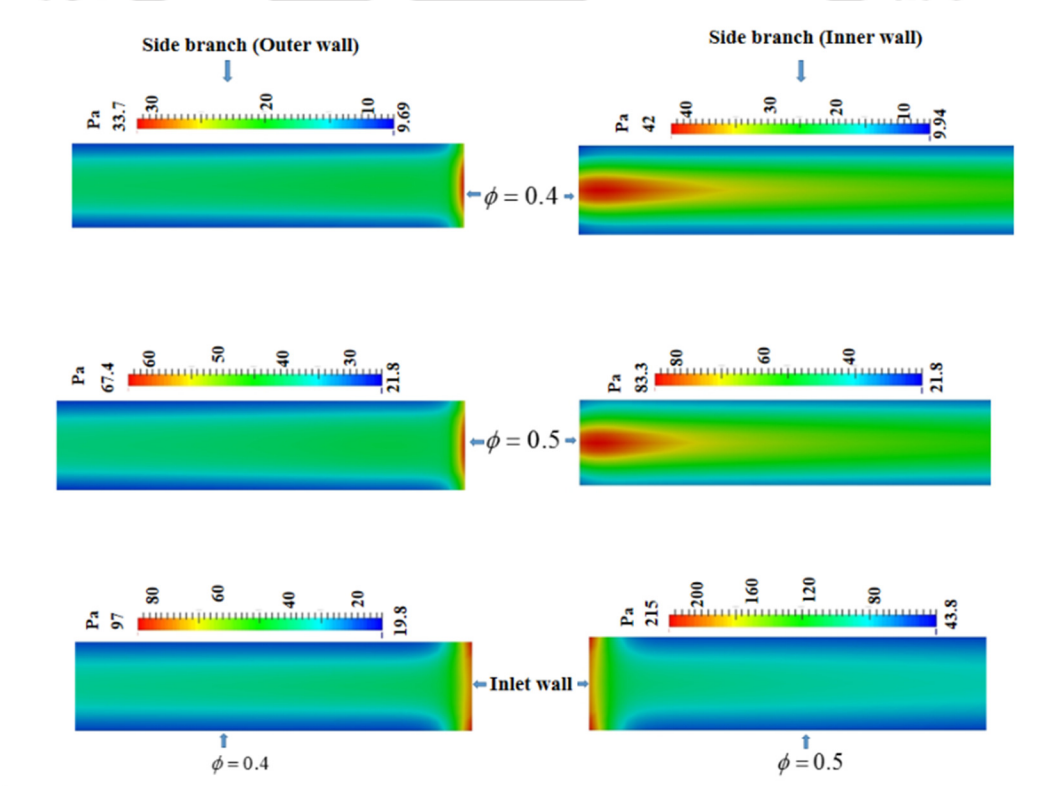

Figure 5.20. Shear stress contours planes for outer and inner walls in side branches for various particle concentrations. The inlet velocity was 0.0045 m/s.

5.3. Case 2: Converging flow with equal inlet concentrations

The computational geometry for this case is shown schematically in Figure 5.21. It consists of two inlets and one outlet with square cross section. The details of the geometry are the same as in the previous case. Flow is provided in each inlet arm with bulk velocity U= 0.0025 m/s. Simulations were carried out for different inlet concentrations of particles. Other simulation parameters and geometry details are shown same as previous case. The same computational grids were used which were mentioned in the previous case.

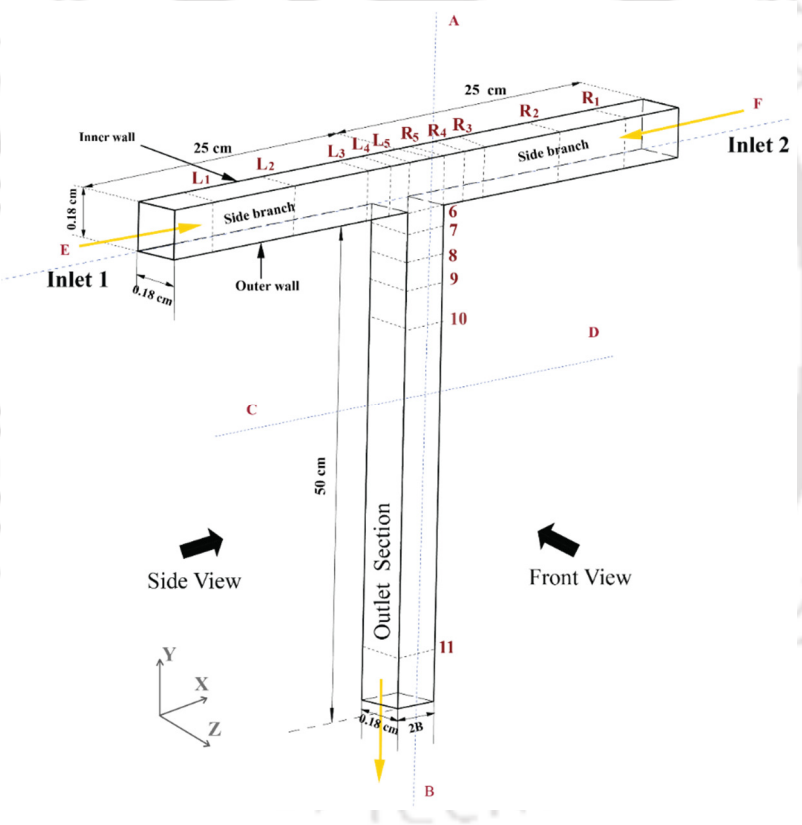

Figure 5.21. Schematic diagram of the computational geometry for converging flow and locations where velocity and concentration data were analyzed.

Since the length of all the branches is same for both converging and diverging channels, we used the same grid. The velocity profiles from the two cases show that the flow field is nearly reversible. Therefore, it is justified to consider the same grid.

5.3.1. Results and Discussion

5.3.1.1. Velocity field

Figure 5.22 illustrates the contours of the velocity field of Newtonian fluid and suspensions flowing through converging T- channel.

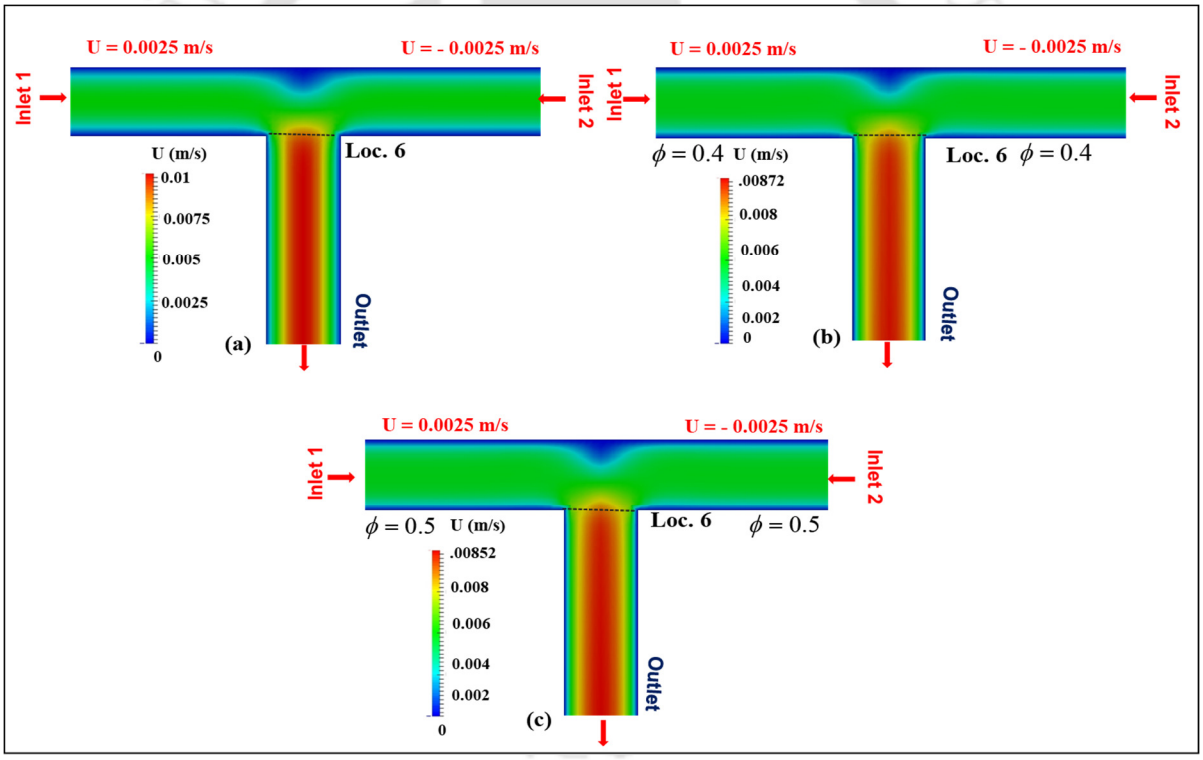

Figure 5.22. The front view of velocity contours planes for Newtonian fluid (a) and suspension of (b) 40% (c) 50% inlet particle concentrations in x-y plane for T- shaped channel. The inlet velocity was 0.0025 m/s given for both the inlets (inlet 1 and inlet 2).

These contour planes were taken at the mid plane (Z=0). We have compared the suspension velocity with that of Newtonian fluid having the effective viscosity equal to that of 40% suspension. The inlet velocity equal to 0.0025 m/s was given through both the inlet 1 and inlet 2. The contour for Newtonian fluid is shown in Figure 5.22a and that of 40% and 50% suspensions are presented in the Figures 5.22b and 5.22c respectively. It is observed that in case of the Newtonian fluid the parabolic profile in the outlet section persists location 6 and an increase in velocity magnitude is observed when compared to the inlet sections (inlet 1 and inlet 2). Whereas, in case of suspension we observe decrease in velocity magnitude in the outlet section after the converging point (location 6) and it is blunted. This effect will be more apparent with an increase in particle concentration which is depicted in Figure 5.22c. The increase in velocity magnitude in outlet section is due to the merging of streams from the inlet1 and inlet 2 which enhances the velocity magnitude in the outlet section. The corresponding streamline plots of Newtonian fluid and suspension are presented in Figure 5.23. It can be observed that maximum velocity is observed at the center of the outlet section of the channel. This is expected since the channel itself is symmetric and flow is divided equally in the daughter branches.

Figure 5.24 shows the cross-sectional view of velocity contour planes of Newtonian fluid and suspension of 40% and 50% particle concentration taken at various locations in the inlet section. The flow direction in these plots can be viewed as normal to the plane of the paper and pointing inside. For the case of Newtonian fluid, it is observed that initially at location 1 nearly uniform velocity of 0.0025 m/s is observed and fully developed flow at locations 2 and 3.

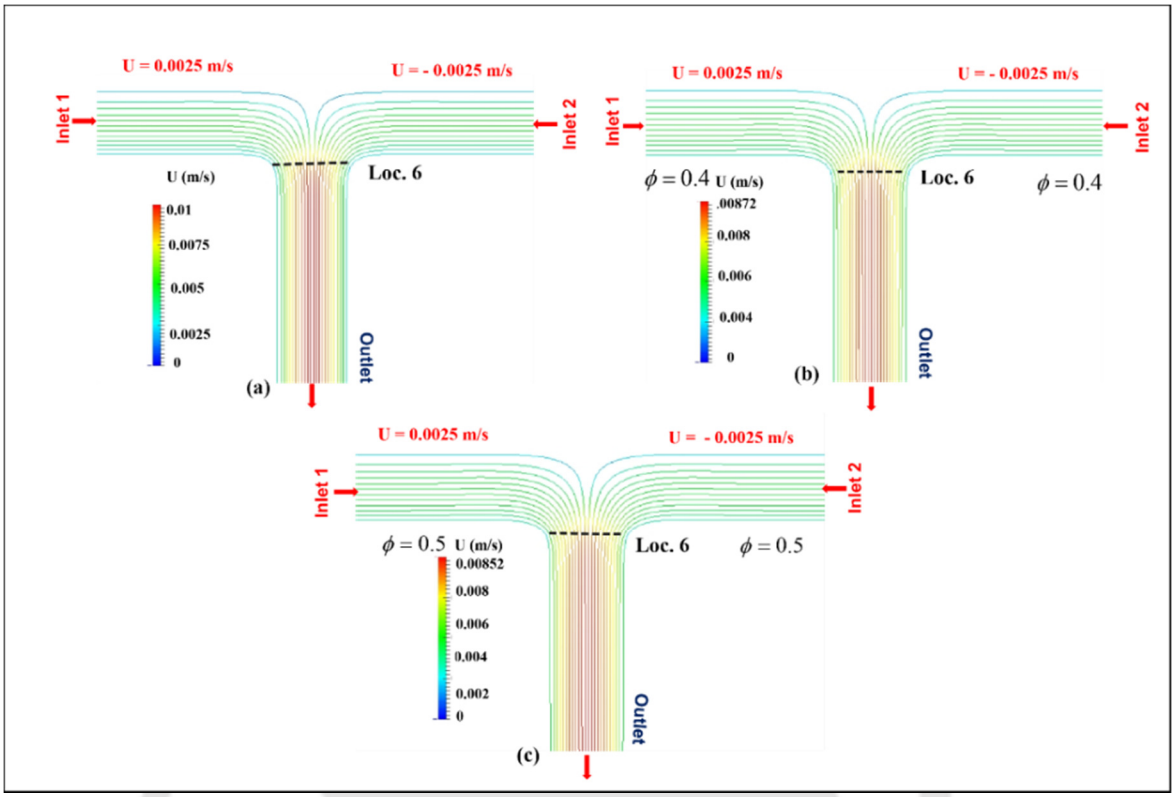

Figure 5.23. The front view of velocity contours planes for Newtonian fluid (a) and suspension of (b) 40% (c) 50% inlet particle concentrations in x-y plane for T- shaped channel. The inlet velocity was 0.0025 m/s given for both the inlets (inlet 1 and inlet 2).

As we move further in downstream of the inlet section, at location 4 the velocity profile tries to move downward as shown in contour at location 4. At location 5, velocity profile shifts more in downward direction. The corresponding velocity contours for 40% and 50% particle concentration are also presented in Figure 5.24. These contours were taken at the same locations where Newtonian fluid contours were studied. We observe that they were following the same trends as the Newtonian fluid but bluntness and decrease in peak velocity magnitude is more apparent in the case of 50% particle concentration when compared to Newtonian fluid.

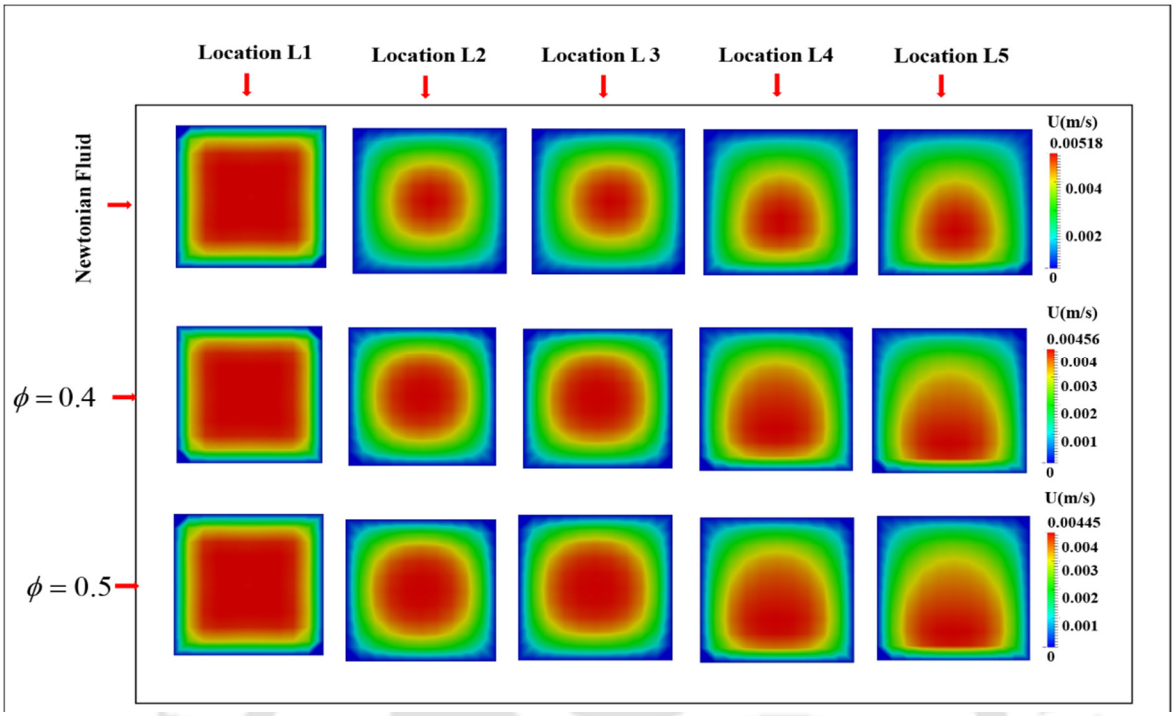

Figure 5.24. The cross sectional velocity contour planes for Newtonian fluid and suspension flow (40% and 50% concentration) at various locations in the x-z plane for inlet branch of converging T- shaped channel. The inlet velocity (0.0025 m/s) was same in both the inlets. The contour (1,2,3,4,5) were taken at the locations -24.98 cm, -12.5 cm, -0.15 cm, -0.1 cm and -0.09 cm respectively.

Figures 5.25 and 5.26 illustrate the trend of velocity profiles of Newtonian fluid and suspensions of 40% and 50% particle concentration in inlet section for lateral and span wise directions. In these graphs Newtonian fluid velocity profiles drawn at locations 2 (middle of the channel), 4 and 5 (these two locations are nearer to the converging point). The profile in lateral direction is nearly parabolic at location 2 but at location 4 the profile shows shifting towards downward direction. At location 5, the profile is more shifted towards the downward direction and increase in velocity magnitude is observed at the same location. Whereas, the

velocity profiles in span-wise direction were parabolic profile at location 2 and little blunted with decrease in velocity magnitude at locations 4 and 5. On the hand suspension velocity profiles shows different behavior. At location 1 (nearer to entrance of inlet 1 section) nearly uniform profile is observed. At locations 2 and 3 the velocity is fully developed but blunted when compared to the Newtonian fluid. At location 4 and location 5 shifting of velocity profile is towards downward direction were observed. The velocity profile of Newtonian fluid and suspension of 50% particle concentration in lateral and span-wise directions were similar as that of 40% particle concentration and results are presented in Figure 5.26. In this graph we also observed that peak velocity magnitude of suspension (50%) has lower values compared to 40% particle concentration.

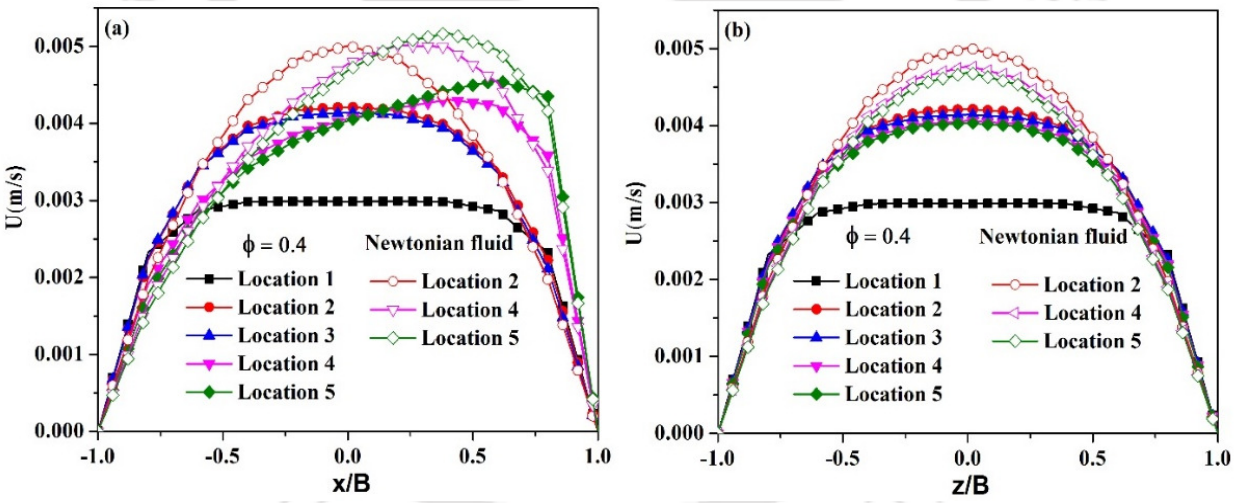

Figure 5.25. Comparison of the velocity profiles for Newtonian fluid and suspension (40% particle concentration) at various locations in the inlet section for T-shaped channel in (a) lateral and (b) span-wise direction. The inlet velocity of 0.0025 m/s was same in both the inlet 1 and inlet 2 and particle concentration was 40%. The velocity locations (1,2,3,4,5) are taken at the locations -24.98 cm, -12.5 cm, -0.15 cm, -0.1 cm and -0.09 cm respectively.

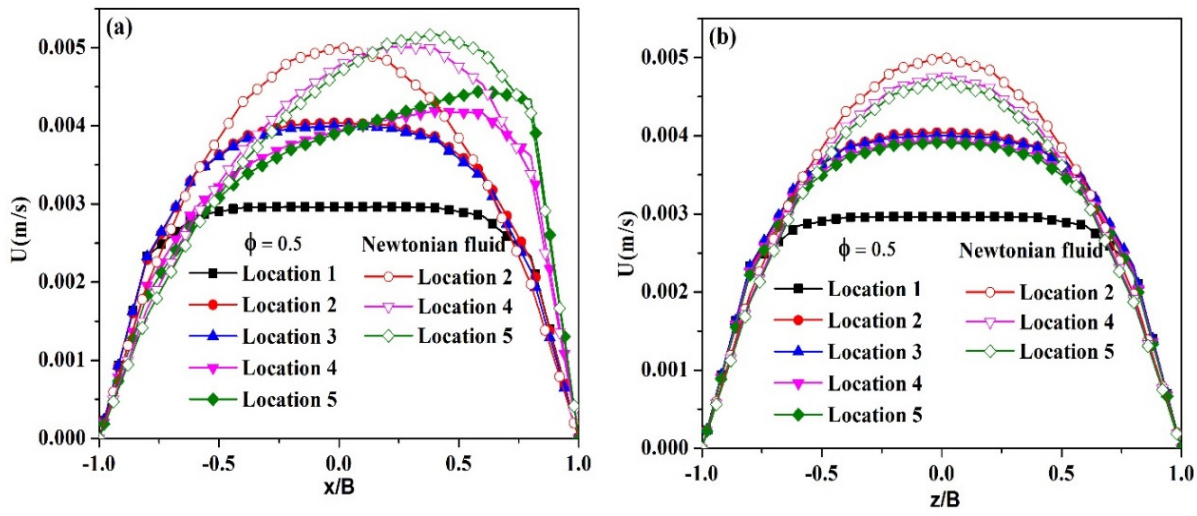

Figure 5.26. Comparison of the velocity profiles for Newtonian fluid and suspension (50% particle concentration) at various locations in the inlet section for T-shaped channel in (a) lateral and (b) span-wise direction. The inlet velocity of 0.0025 m/s was same in both the inlet 1 and inlet 2 and particle concentration was 50%. The velocity locations (1,2,3,4,5) are taken at the locations -24.98 cm, -12.5 cm, -0.15 cm, -0.1 cm and -0.09 cm respectively.

The cross-sectional views (x-z plane) of velocity contour at various locations in the outlet section for Newtonian fluid and suspension (40% and 50%) are shown in the Figure 5. 27. These cross-sectional slices were taken at various locations (6, 7, 8, 9, 10 and 11) in the outlet section at planes perpendicular to the flow direction. First row shows contours of Newtonian fluid and second and third rows the contours of 40% and 50% particle concentrations respectively. It can be observed that the velocity contours of Newtonian fluid at the location 6 (entrance of the outlet section) the contour is smeared and flat in the lateral direction and at this location same velocity magnitudes of two inlet streams are entering into the outlet section due to this the contour at the center is flatter and more stretched. At other

locations of outlet section the profile resembles like fully developed and velocity peak near the center. For the case of suspension we observe different behavior compared to the Newtonian fluid. In case of suspension the contour at location 6 is more smeared and flatter along the lateral direction. This is more apparent in the case of 50% concentration. At further downstream locations in the outlet section velocity contour looks fully developed and similar at all other locations. We also observe that the peak velocity magnitude decreases with the increase in particle concentration.

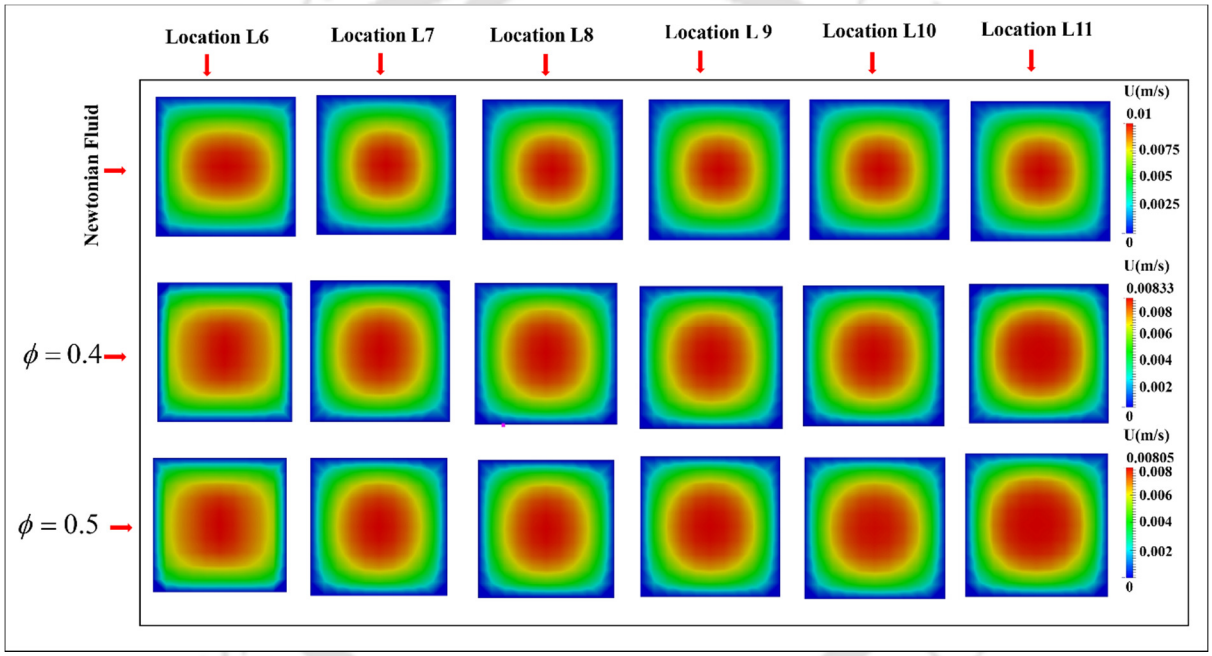

Figure 5.27. The velocity contour planes for Newtonian fluid and suspension flow (40% and 50% concentration) at various locations in the outlet section of T- shaped channel. The inlet velocity of 0.0025 m/s was same in both the inlet 1 and inlet 2. The contour locations (6,7,8,9,10,11) are taken at the locations -0 cm, -0.5 cm, -1 cm, - 1.8 cm -2.5 cm and - 49.98 cm respectively.

The comparison of velocity profiles of Newtonian fluid and suspension (40%) at various locations in the lateral and span wise directions in the outlet section are shown in Figure 5.28 and 5.29. In Figure 5.28 the profiles are drawn up to location 4.5 cm. The Newtonian fluid velocity profile is compared at location 6 only. The profiles for suspension at all the locations which are represented in graphs are blunted and fully developed at all the locations. Profiles in span wise direction are also blunted at all the location except at location 6 (Y=0 cm). The profiles in further down of the outlet section are shown in Figure 5.29. The profile are blunted and fully developed at all the locations but Newtonian fluid profile is parabolic. The similar trends of velocity profiles are observed for 50 % particle concentration and the results are presented in Figures 5.30 and 5.31.

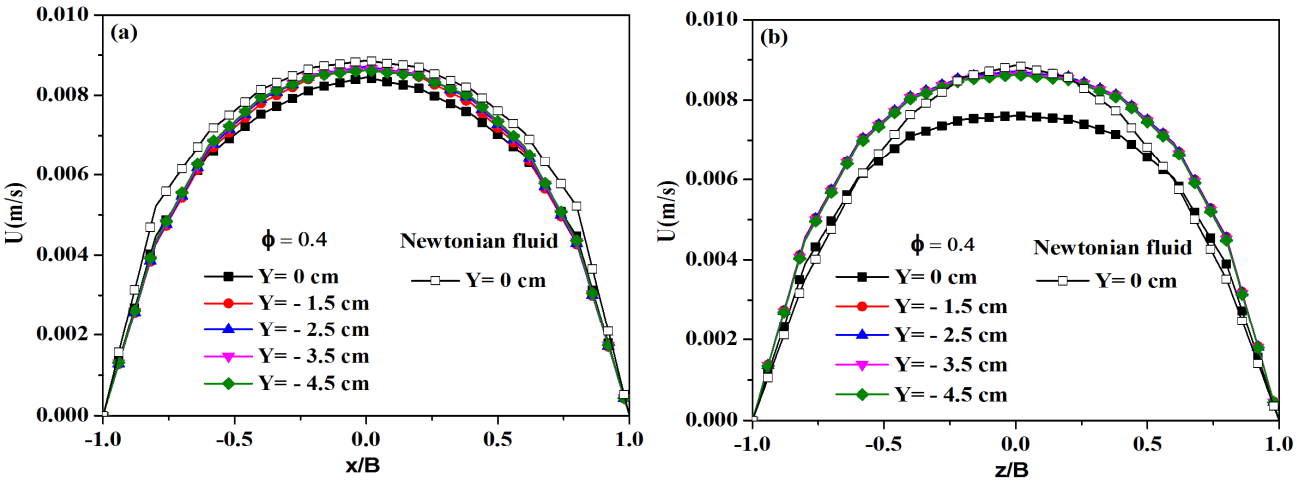

Figure 5.28. Comparison of the velocity profiles for Newtonian fluid and suspension at various locations in the outlet section for T- shaped bifurcation channel in (a) lateral and (b) span-wise direction. The inlet velocity and particle concentration was 0.0025 m/s and 40% respectively.

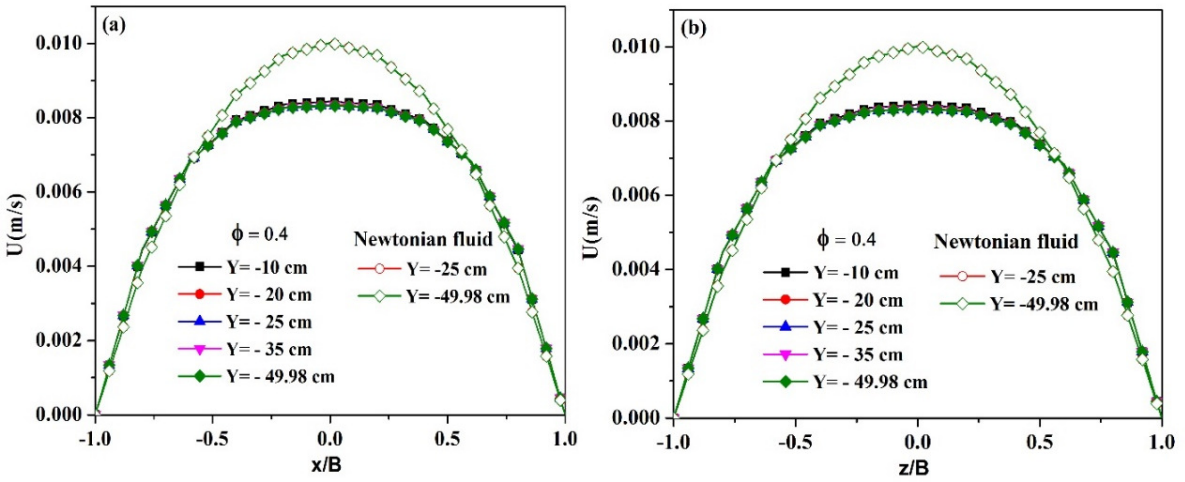

Figure 5.29. Comparison of the velocity profiles for Newtonian fluid and suspension at various locations in the outlet section for T- shaped bifurcation channel in (a) lateral and (b) span-wise direction. See the previous caption.

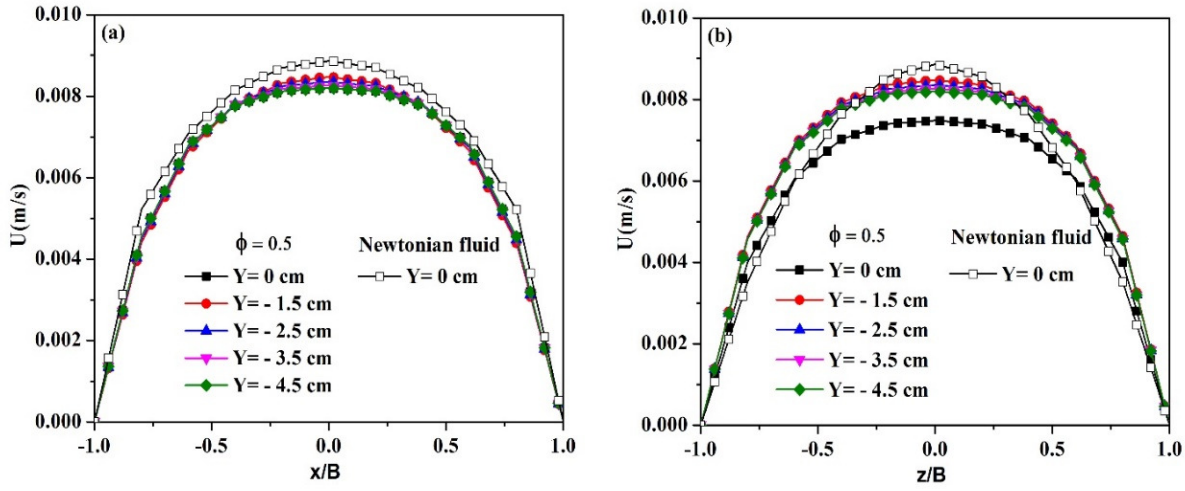

Figure 5.30. Comparison of the velocity profiles for Newtonian fluid and suspension at various locations in the outlet section for T- shaped channel in (a) lateral and (b) span-wise direction. The inlet velocity and particle concentration was 0.0025 m/s and 50% respectively.

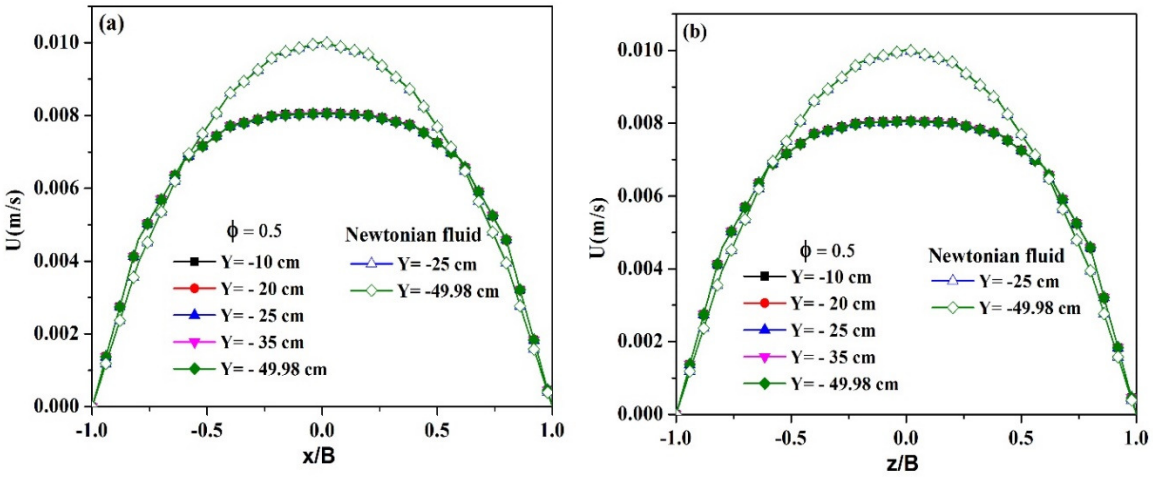

Figure 5.31. Comparison of the velocity profiles for Newtonian fluid and suspension at various locations in the outlet section for T- shaped channel in (a) lateral and (b) span-wise direction. The inlet velocity and particle concentration was 0.0025 m/s and 50% respectively.

5.3.1.2. Shear rate field

The shear rate contour maps in x-y plane for Newtonian and suspension (40% and 50%) are shown in Figure 5.32. For the Newtonian fluid, the outlet section has high shear rate near the wall and low near the converging section (location 6). In case of suspension, increase in particle concentration has little influence on shear rate as shown in Figure 5.32c. The corresponding cross sectional shear rate contour planes (x-z plane) in the inlet section and outlet section are shown in Figures 5.33 and 5.34 respectively. In these contours the flow direction is perpendicular to the plane of paper and pointing inwards. From Figure 5.33 it is observed that for the case of Newtonian fluid at location 1 (the entrance of the inlet section) the shear rate is uniform and low at the center (which is shown with blue colour) and corner regions have high value and as we move to location 2 and 3 the corner regions of the contour planes have

relatively higher shear rate compared to the middle regions. The shear rate gradients are highest at location 5. On the other hand the suspension shows little different behavior and we observe that increase in low shear rate regions (blue spot) and decrease in shear rate at the center of corner regions(upward direction) is more apparent with the increase in particle concentration at locations 2 and 3. At locations 4 and 5 only one side of corner regions (lower) have the high shear rates. This is due to bending of the streamlines towards the outlet section.

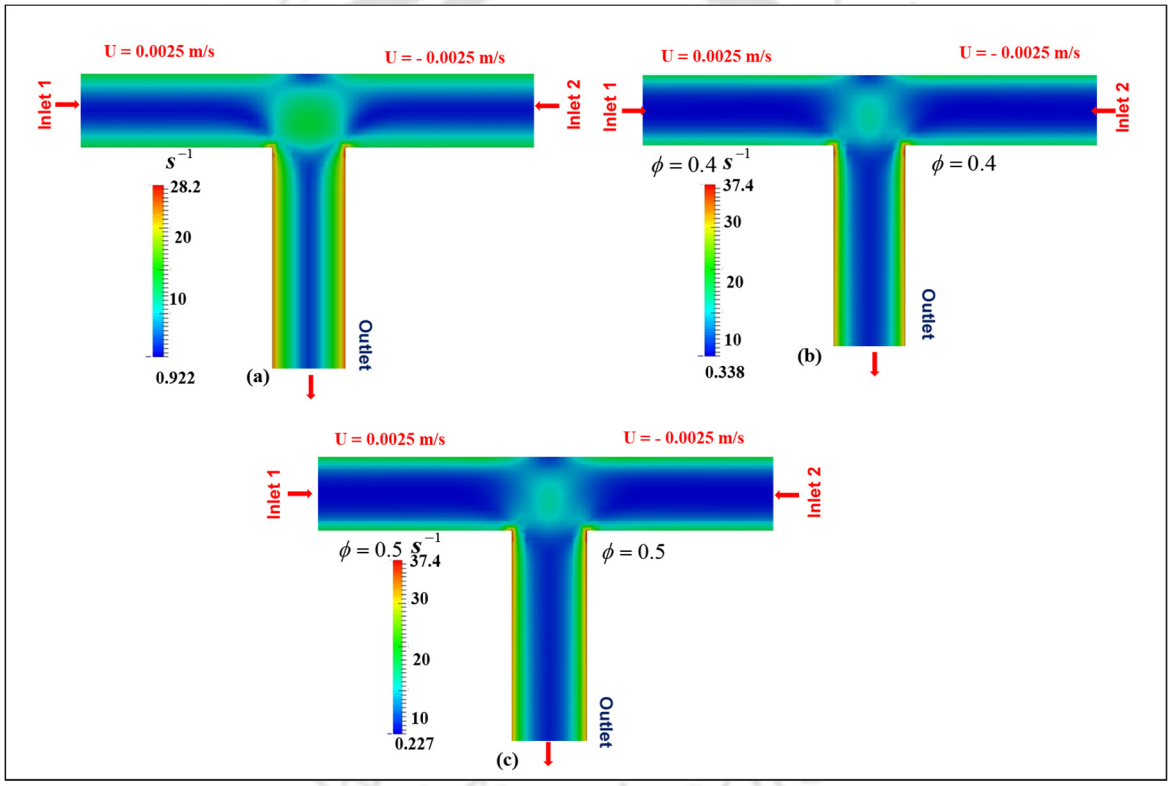

Figure 5.32. The Front view of shear rate contour planes for Newtonian fluid (a) and suspension flow with (b) 40% and (c) 50% particle concentration in a converging T-shaped channel.

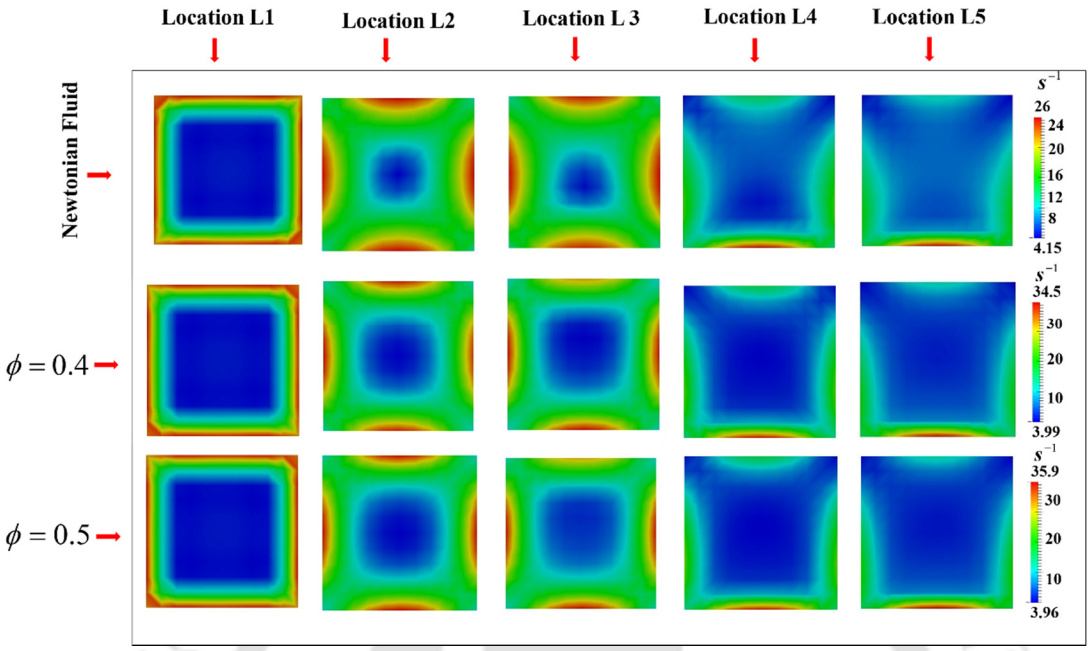

Figure 5.33. The cross-sectional shear rate contour planes for Newtonian fluid and suspension flow (40% and 50% concentration) at various locations in the (a) inlet branch and (b) side branch. The inlet velocity was 0.0025 m/s in both the inlets. The contour locations (1,2,3,4,5) are taken at the locations -24.98 cm, -12.5 cm, -0.15 cm, -0.1 cm and -0.09 cm respectively.

Figure 5.34 shows the shear rate contours at different locations in the outlet section. At the location 6 (beginning of outlet section) the contour is dumbbell shape for the case of Newtonian fluid. This dumbbell shape is due to the fact that fluid from the both inlets tries to squeeze in the outlet section. For the suspension this shape is more flat which increases with particle concentration. This is due to the fact that the two streams of suspension with high concentration of particles at the centre do not mix as easily as the Newtonian fluid. The cross sectional contour planes at other locations are nearly same after location 7 and has low shear rate values at the center.

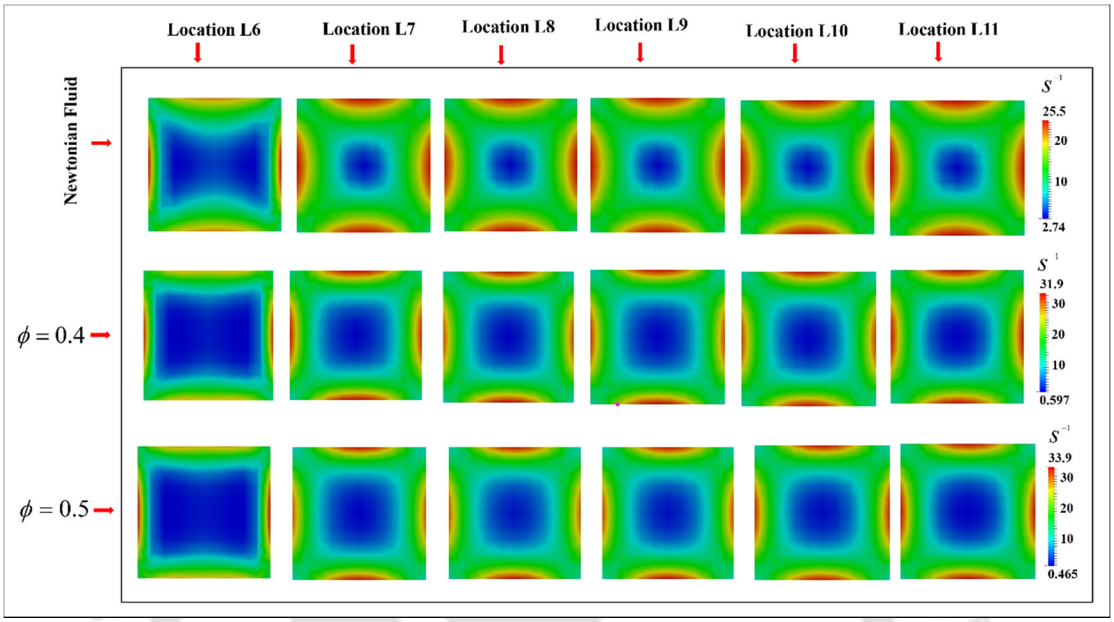

Figure 5.34. The shear rate contour planes for Newtonian fluid and suspension flow (30% and 40% concentration) at various locations in the outlet section of the T- shaped channel. The inlet velocity was 0.0025 m/s in both the inlets. The contour locations (6,7,8,9,10,11) are taken at the locations -0 cm, -0.5 cm, -1 cm, - 1.8 cm -2.5 cm and -49.98 cm respectively.

5.3.1.3. Concentration field

The concentration contour maps in the mid-plane for 40% and 50% suspension are presented in Figure 5.35. For the clarity of view we have shown only a small section around the converging section. We have given the inlet particle concentration 40% and velocity of 0.0025 m/s through inlet 1 and inlet 2. In the inlet sections the shear induced migration causes the particles to move towards the center of the channel. The central core of the inlet channel has high concentration of particles and this central core moves downward in the converging

section. The particles also move in downward direction, thus concentration contours at the location 5 shows bend towards the outlet section. The similar trends was also observed for the particle concentration of 50% shown in the Figure 5.35b. Another interesting observation is that two separated concentration streams are clearly seen in the outlet section which eventually merge.

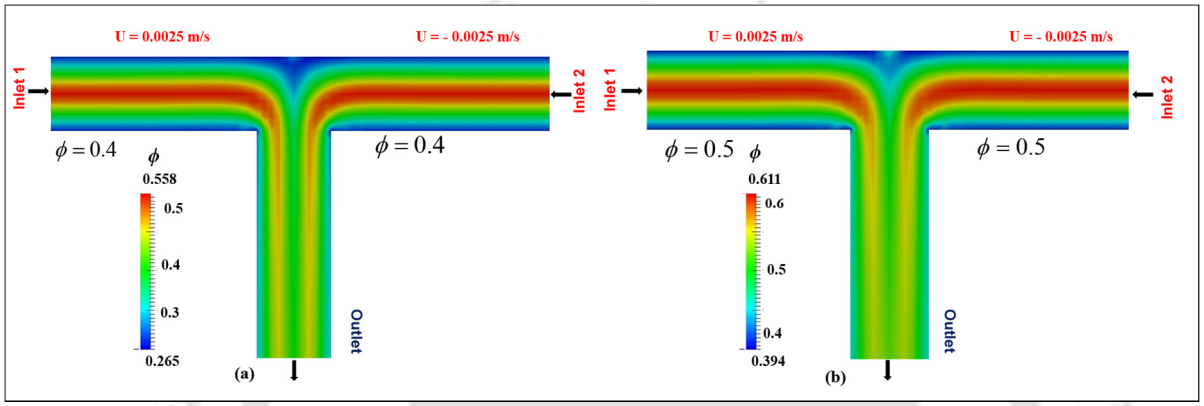

Figure 5.35. Front view of the particle concentration contour maps in x-y plane at the centerline for suspension of (a) 40% and (b) 50% particle concentration. The inlet velocity was 0.0025 m/s in both the inlets sections. For clarity of contours only a section of bifurcation channel is shown here.

Figure 5.36 shows the cross-sectional view of concentration maps (x-z plane) in the inlet section for suspension of 40% and 50% bulk particle concentrations. These slices were taken at planes perpendicular to the flow direction at various locations which are shown with arrow direction on the top of each slices. It was observed that at location 1(staring of inlet-1 section) there is nearly uniform particle concentration and as we move downstream in the inlet section the concentration in-homogeneities gradually develop due to particle migration.

We also observe that the depletion of particles in the corner region is less compared to the middle portions near the channel walls. This is because of the fact that the shear rate gradient is small in the corner region (see Figure 5.33). As we move further downstream of the inlet section asymmetry in concentration contours are seen and we found that at location 5 the concentration contour shift towards the downward direction and this is more intense in the case of particle concentration of 50%. The regions close to the top and bottom walls as well as outer wall (except the corners) is devoid of particles as represented by dark blue regions.

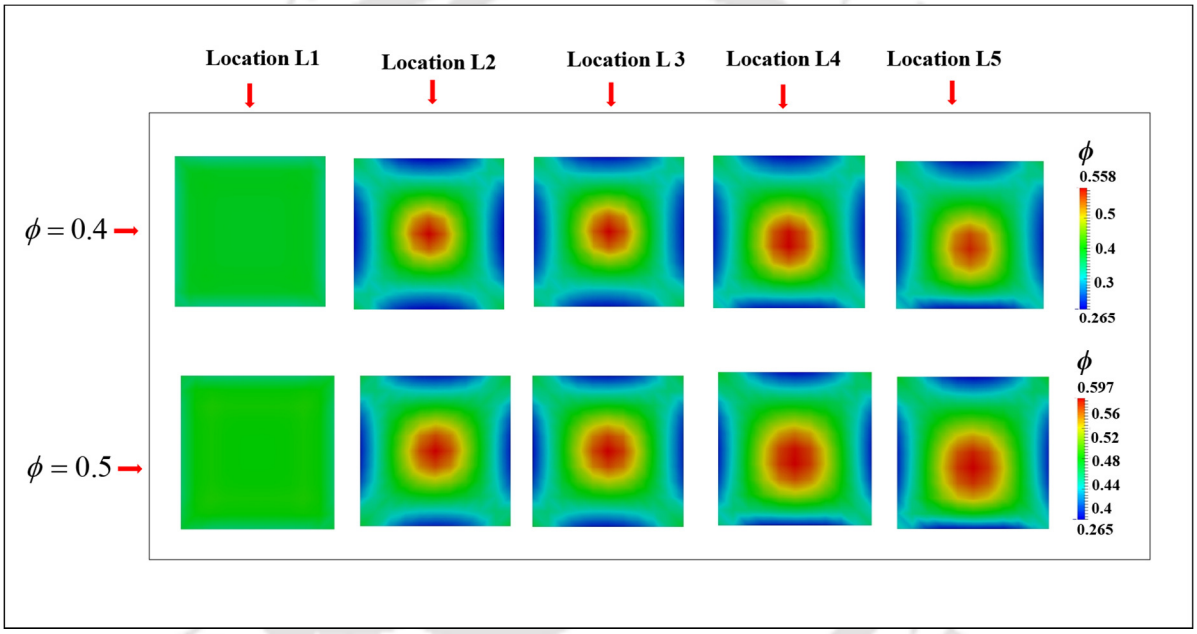

Figure 5.36. Cross- sectional view particle concentration contour maps for suspension of 40% and 50% particle concentration in inlet section of T-shaped channel. The inlet velocity was 0.0025 m/s in both the inlets. The contour locations (1,2,3,4,5) are taken at the locations -24.98 cm, -12.5 cm, -0.15 cm, -0.1 cm and -0.09 cm respectively.

In order to understand quantitative nature of particle distribution we have shown the concentration profiles for 40% particle concentration in the lateral and span-wise directions of the inlet section in Figures 5.37a and 5.37b respectively. The lateral concentration profiles are fully developed at locations 2 and 3. The shape of the fully developed concentration profile looks like inverted V shape. However, unlike the velocity profile the concentration profile remains unaffected till the beginning of converging section (location 6) and we observe almost identical profiles at location 4 and location 5 and shifting towards the downward direction due to the fact that this location is very near to the converging section as shown in Figure 5.37a. The concentration profiles in span wise direction at all the locations are similar and fully developed. The similar behavior of concentration profiles for lateral and span-wise direction is shown for 50% particle concentration in Figure 5.38.

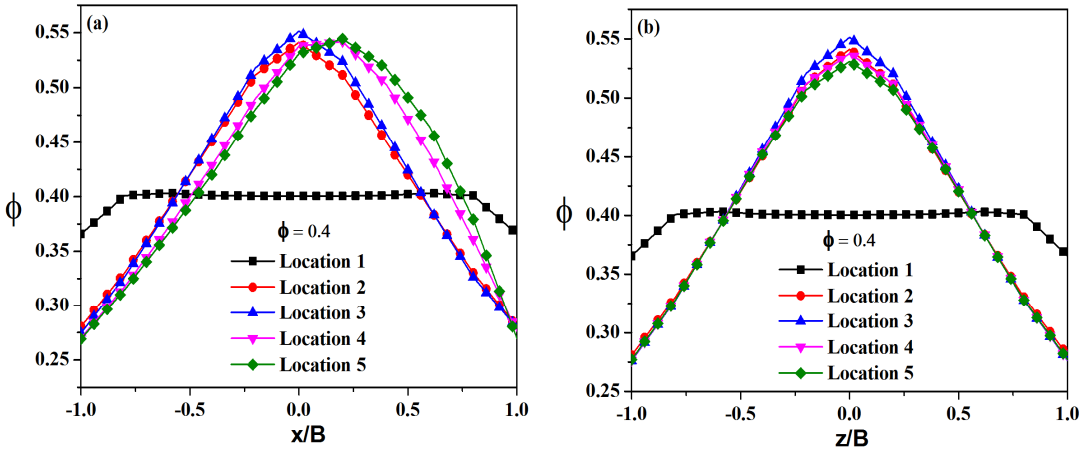

Figure 5.37. Comparison of the concentration profiles of suspension flow (40% particle concentration) at various locations in the inlet section for T-shaped channel in (a) lateral and (b) span-wise direction. The inlet velocity was 0.0025 m/s in both the inlets.

The value of maximum concentration for fully developed is higher for 50% particle concentration when compared to 40% particle concentration.

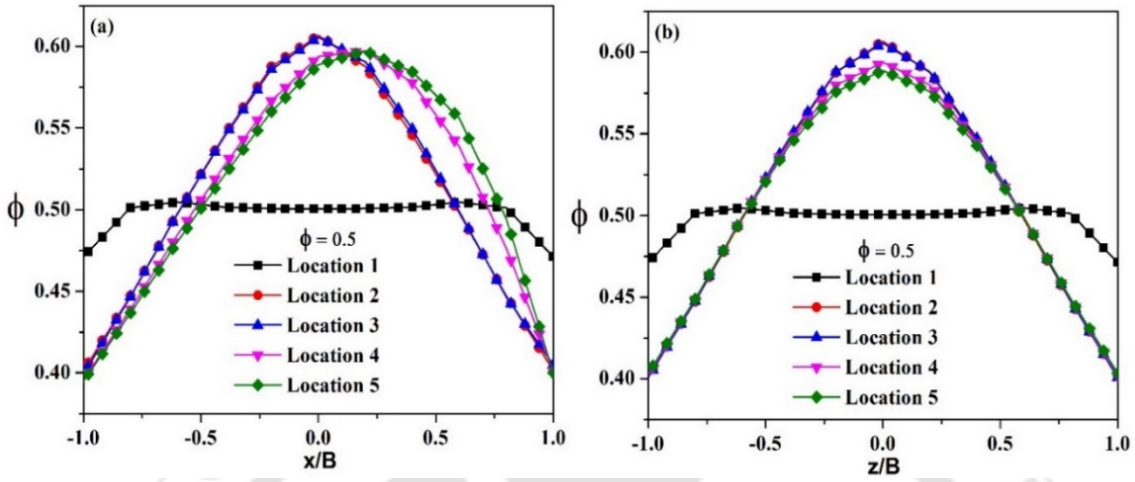

Figure

Figure 5.38. Comparison of the concentration profiles of suspension flow (40% particle concentration) at various locations in the inlet section for T-shaped channel in (a) lateral and (b) span-wise direction. The inlet velocity was 0.0025 m/s in both the inlets.

In Figure 5.39a we have shown the cross sectional concentration contour planes taken at various locations in the outlet section for 40% suspension. In these contours we present how and at what length these two concentration streams meet in the outlet section. The equal inlet velocity and particle concentration was assigned at both the inlets (inlet 1 and inlet 2). It is observed that at location 6 (Y= 0 cm), initially two separated concentration cores appear and as we move downstream in the outlet section the two streams gradually come closer. At location Y= -2.5 cm these two streams of concentration mix completely and get smeared along lateral direction. After the location Y= -2.5 cm particles come to the center and become more concentrated (spherical red spot) and smearing reduces.

As we move down further in the outlet section we observe that the concentration profile is fully developed beyond location 3 (Y= -5cm) and at location 4, all the particles move towards at the center of the channel. The concentration contour maps for the 50% particle concentration are shown in the Figure 5.39b for few locations at which velocity and shear rate contours were taken in the outlet section. At location 8 (Y= -2.5 cm) we found the mixing of two concentration streams and smearing along the lateral direction. Further down, the fully developed profile is observed with peak concentration value at the centre.

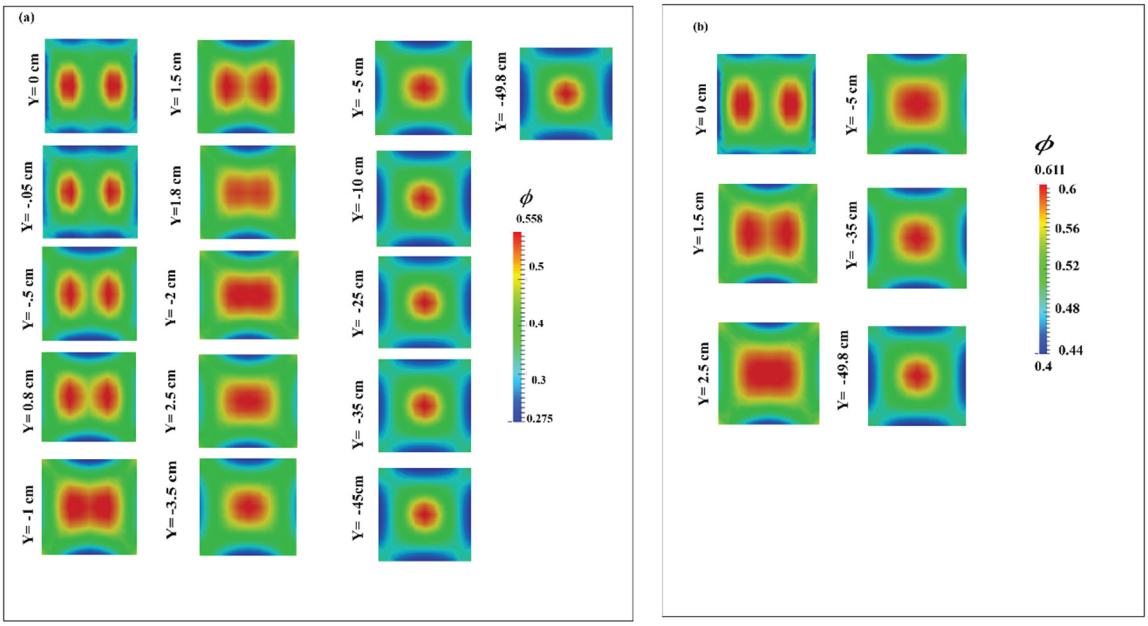

Figure 5.39. The cross- sectional view particle concentration contour maps taken at various locations in outlet section of T– shaped converging channel for suspension flow (a) 40% particle concentration (b) 50% particle concentration.

The corresponding concentration profiles of 40% particle concentration in lateral and span-wise direction are presented in Figure 5.40. The profiles are taken at a difference of 1cm between two successive locations and it is considered up to location Y= -4.5 cm.

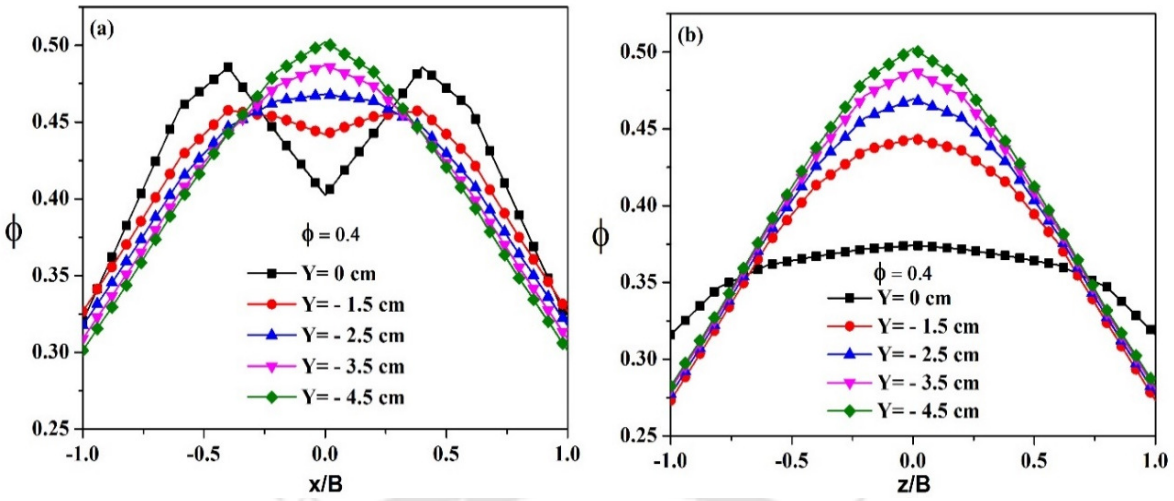

Figure 5.40. Comparison of the concentration profiles of suspension flow (40% particle concentration) at various locations in the outlet section for T-shaped channel in (a) lateral and (b) span-wise direction. The inlet velocity was 0.0025 m/s in both the inlets and particle concentration was 40%.

It is clearly seen from Figure 5.40a that at location 6 (entrance of the outlet section) the peak - valley - peak concentration profile appears and this is due to combining of two streams in the outlet section. As we move downstream locations in the outlet section, the peak- valley-peak pattern in concentration profile gradually decreases and only a single peak in the concentration profile emerges. Another interesting observation is that at location Y= -2.5 cm the two peaks in concentration profile completely merge and then it resembles like a single blunted profile. The profiles in span-wise direction are initially more blunted and gradually develop to inverted V shape profile as we move downstream of the outlet section. We have also shown the profiles in further downstream locations of the outlet section in Figure 5.41. It is observed that the profiles are similar at all locations indicating that flow is fully developed.

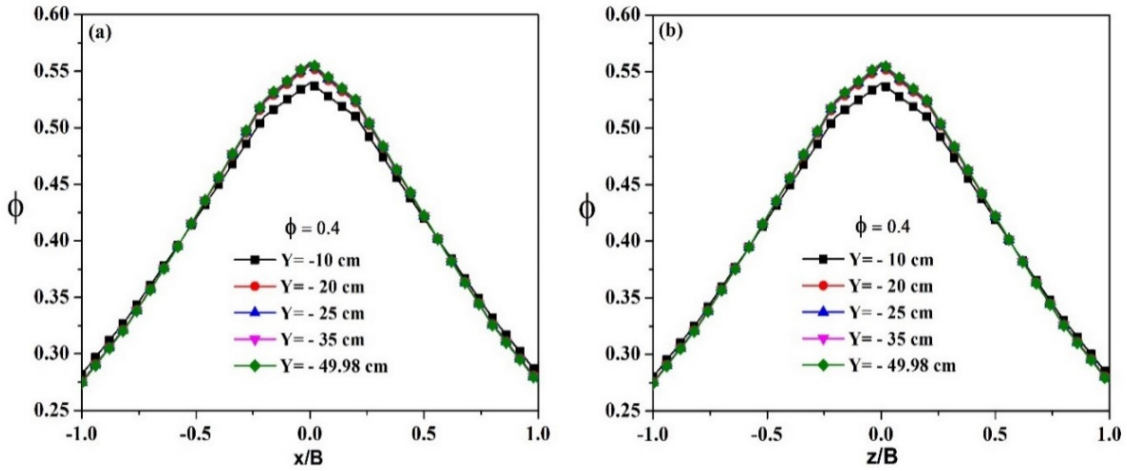

Figure 5.41. Comparison of the concentration profiles of suspension flow (40% particle concentration) at various locations in the outlet section for T-shaped channel in (a) lateral and (b) span-wise direction. The inlet velocity was 0.0025 m/s in both the inlets and particle concentration was 40%.

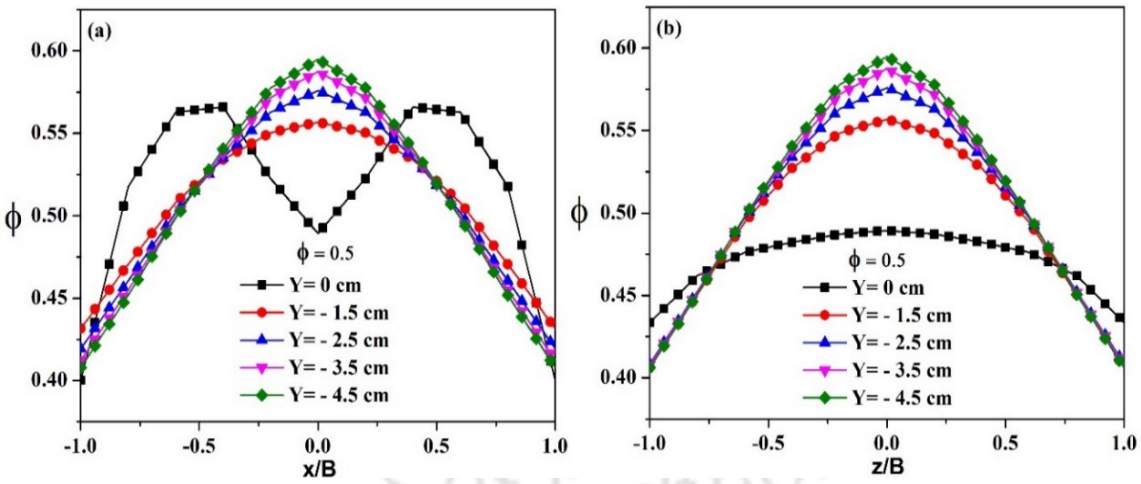

Figure 5.42. Comparison of the concentration profiles of suspension flow (50% particle concentration) at various locations in the inlet section for T-shaped channel in (a) lateral and (b) span-wise direction. The inlet velocity was 0.0025 m/s in both the inlets and particle concentration was 50%.

Similar trend of concentration profiles in lateral and span-wise direction in outlet section are also observed for the case of 50% particle concentration and results are presented in the Figures 5.42 and 5.43 respectively.

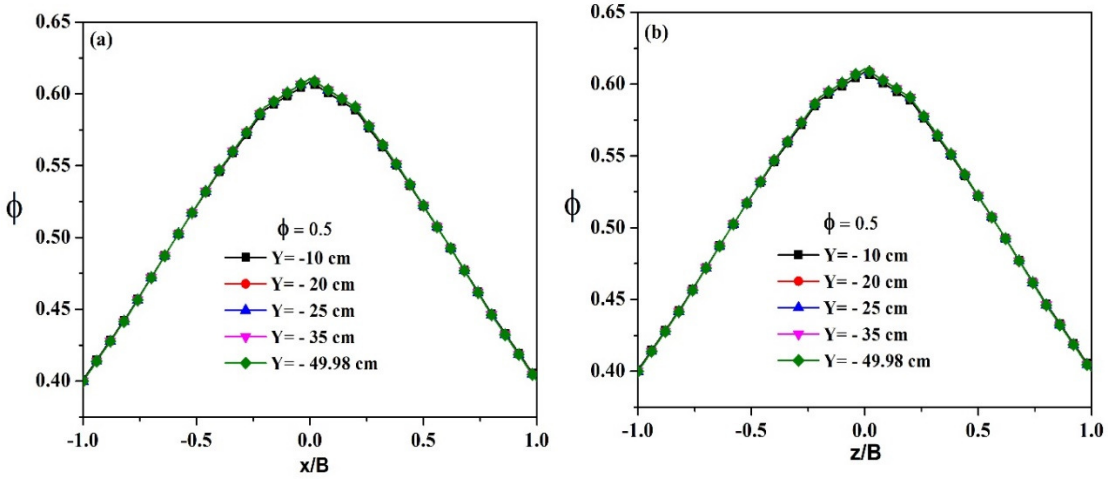

Figure 5.43. Comparison of the concentration profiles of suspension flow (50% particle concentration) at various locations in the outlet section for T-shaped channel in (a) lateral and (b) span-wise direction. The inlet velocity was 0.0025 m/s in both the inlets and particle concentration was 50%.

5.3.1.4. Shear stress field

Figure 5.44 shows the shear stress contour maps in x-y plane for Newtonian fluid and suspension. The profiles for Newtonian fluid and suspension are clearly distinct. For suspension flow two distinct peaks in shear stress values are observed in the converging section. The maximum shear stress value for 50% bulk particle concentration is higher compared to 40% particle concentration and Newtonian fluid. It is due to the fact that shear

stress is product of viscosity and shear rate. In the outlet section the maximum shear stress is observed at the walls.

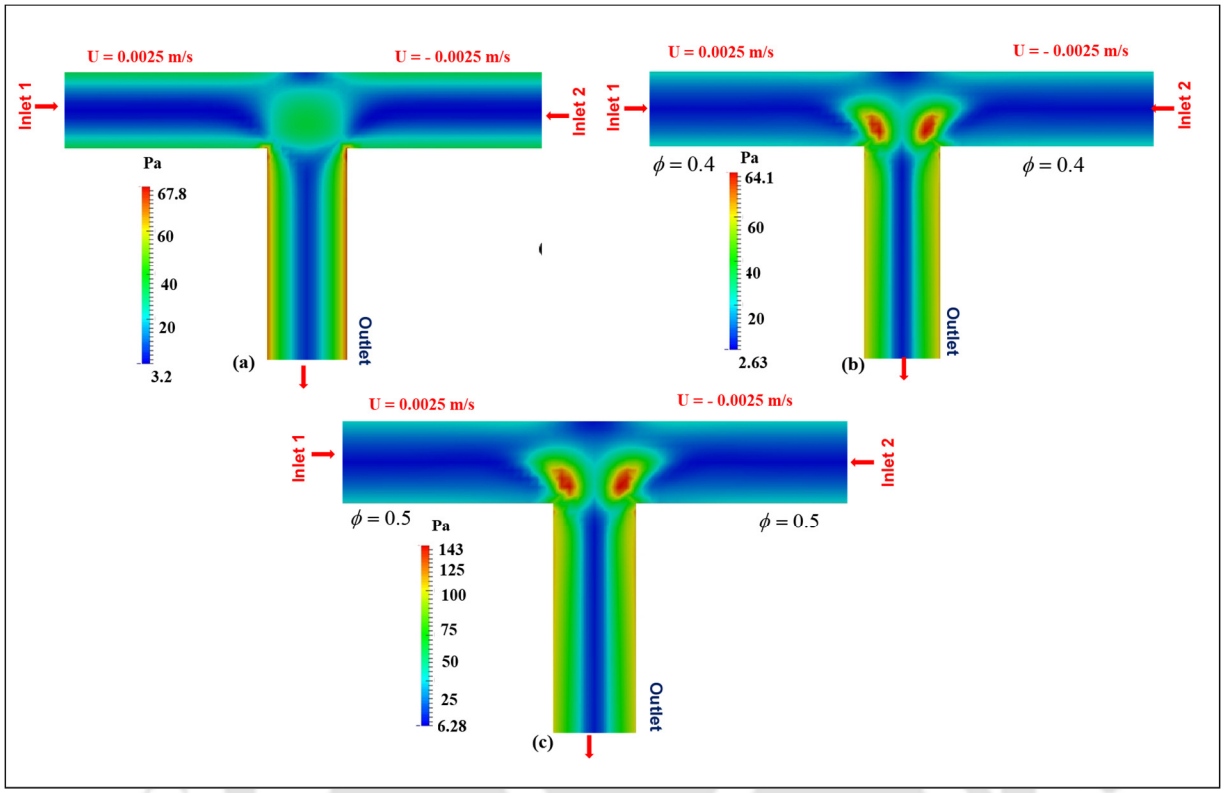

Figure 5.44. The shear stress contour planes for (a) Newtonian fluid, (b) 40 % suspension, and (c) 50% suspension in x-y plane for T-shaped converging channel. The inlet velocity was 0.0025 m/s in both the inlets.

We have shown the contour map of wall shear stress for the inlet and outlet section for 40% particle concentration in Figure 5.45. At the inner wall of the inlet section the wall shear stress is higher compared to the outer wall. This is due to the reason that the inner wall is on the side of outlet section in which the two streams enter. This shifts the high shear rate regions close to the inner wall. In the inlet section the maximum wall shear stress is observed at the corner (entrance of the outlet section). In the outlet section the wall shear stress values are

similar for both the inner and outer wall due to symmetry of the two inlets. However, maximum wall shear stress is observed in the middle. This is due to the fact that the wall shear stress can be evaluated from the product of shear rate at the wall and effective viscosity. Low shear rate but high viscosity can also give rise to large wall shear stresses.

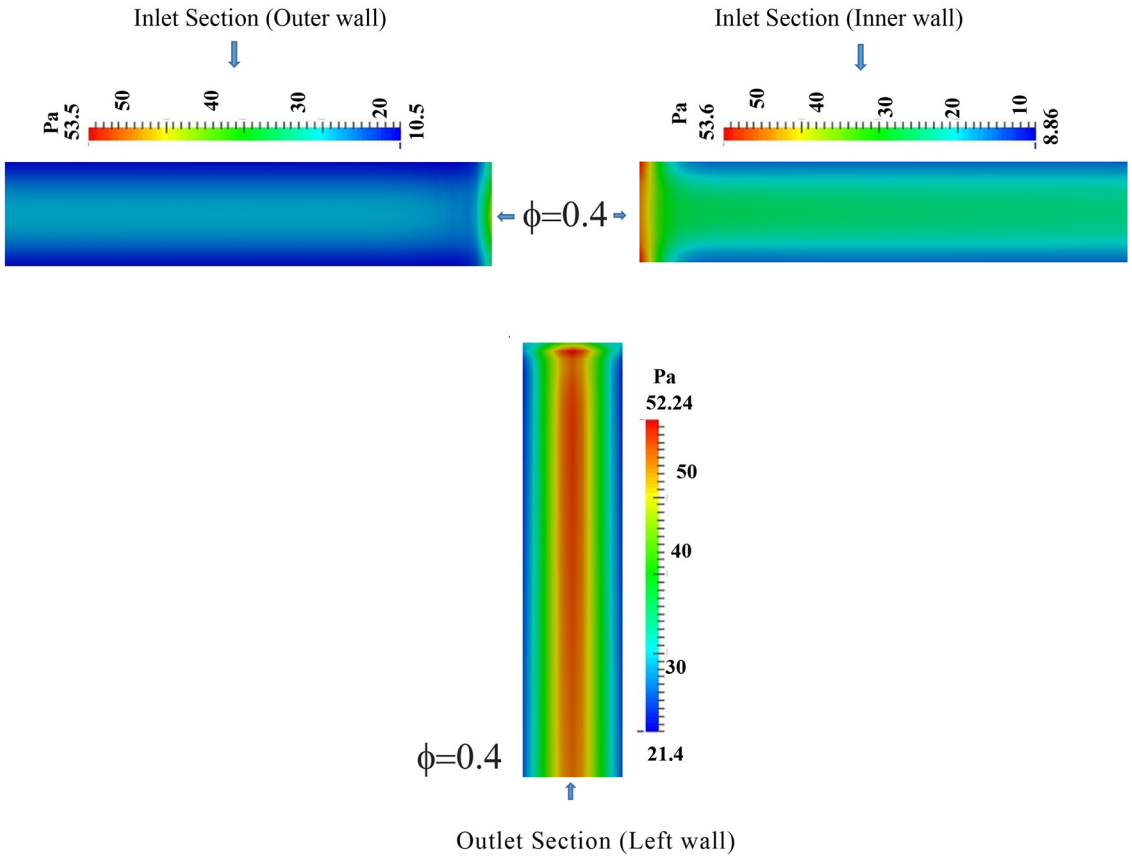

Figure 5.45. Shear stress contours planes for outer and inner walls for converging flow in a T-shaped converging channel. The particle concentration was 40% and the inlet velocity was 0.0025 m/s.

5.4. Case 3: Converging flow with unequal inlet concentration

For this case too we have used the same geometry which was considered in the previous two cases. It consists of two inlets and one outlet with square cross section. The bulk velocity (U = 0.0025m/s) was same for both the inlets but the particle concentration in the two inlets were different.

5.4.1. Results and Discussion

5.4.1.1. Velocity field

Figure 5.46a shows the contour map of suspension velocity and Figure 5.46b shows the stream lines in x-y plane of the T-shaped channel in converging flow. These contour planes were taken at the mid plane (Z = 0). The particle concentration was 30% in inlet-1 and 20% in the inlet-2.

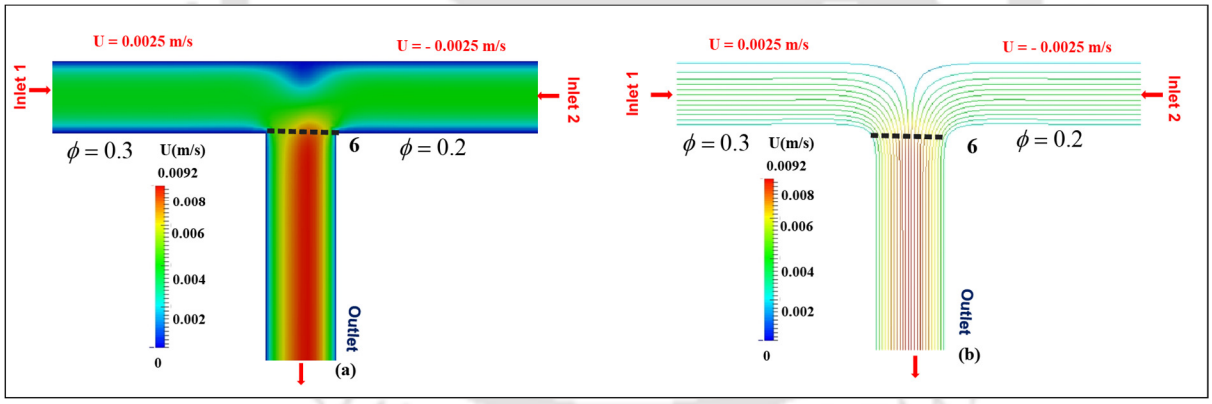

Figure 5.46. The velocity contour planes (a) and streamline plot (b) for suspension flow in x-y plane for T- shaped channel. The inlet velocity and concentration are shown in the figures.

We also observed that the velocity contour at location 6 is shifted towards the inlet having lower concentration. The corresponding streamline plot of suspension flow is presented in Figure 5.46b. Figure 5.47 shows the cross-sectional view of velocity contour planes taken at

various locations in the inlet sections. At location 1, nearly uniform velocity is observed which becomes non-uniform at locations 2 and 3. As we move further in downstream of the inlet-1 section (30% inlet concentration) at locations 4 and 5 the peak velocity is shifted towards the right direction. For the inlet-2 section (20% inlet concentration) the contour slices shows shifting of the peak velocity to the left as the outlet section is approached. After location 5 the two inlet streams curve to enter the outlet section. In these contours the direction of flow can be considered perpendicular to the plane of paper and pointing inwards. The flow in outlet section can be also be visualized in the same manner.

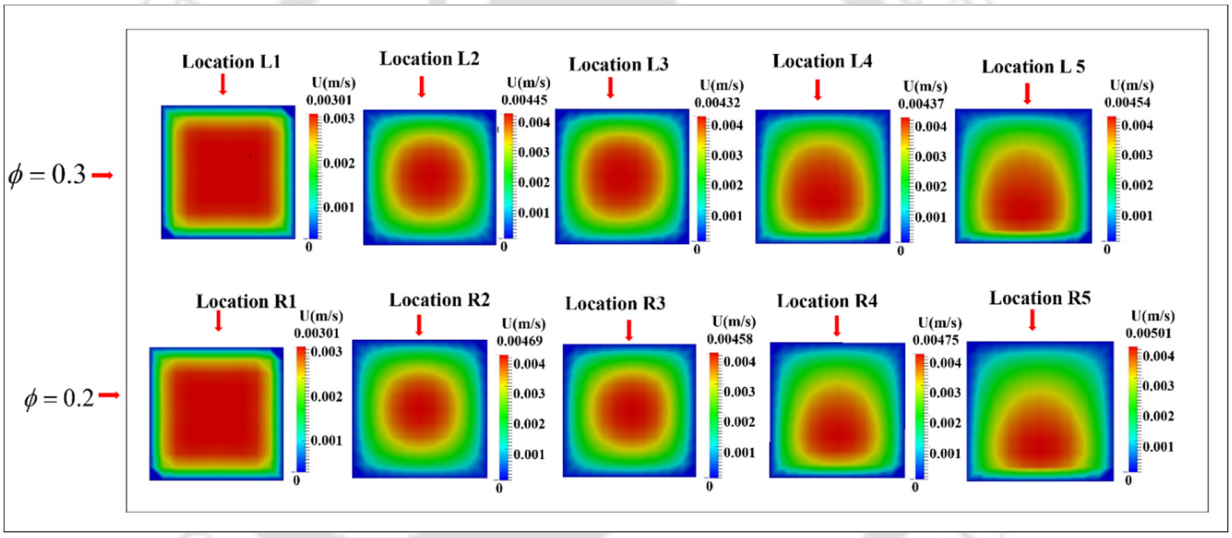

Figure 5.47. The cross sectional velocity contour planes taken at various locations in the x-z plane for inlet sections of T- shaped channel. The inlet velocity was 0.0025 m/s in both the inlets. First row shows contour for 30% particle concentration and second for 20% particle concentration. The contour slices (1,2,3,4,5) are taken at the locations -24.98 cm, -12.5 cm, -0.15 cm, -0.1 cm and -0.09 cm respectively.

Figure 5.48 shows the velocity profiles at various locations for inlet-1 section in lateral and span wise directions. The asymmetry of the lateral velocity profiles at location 4 and 5 can be clearly seen. As expected we do not see any asymmetry in the span wise direction. However, the velocity profiles in both lateral and span wise directions are blunted at all locations due to shear induced migration. The corresponding velocity profiles for the inlet-2 section are shown in Figure 5.49. The profiles are similar to that of inlet-1 section but the peak velocity at locations 4 and 5 are higher in the inlet-2 section.

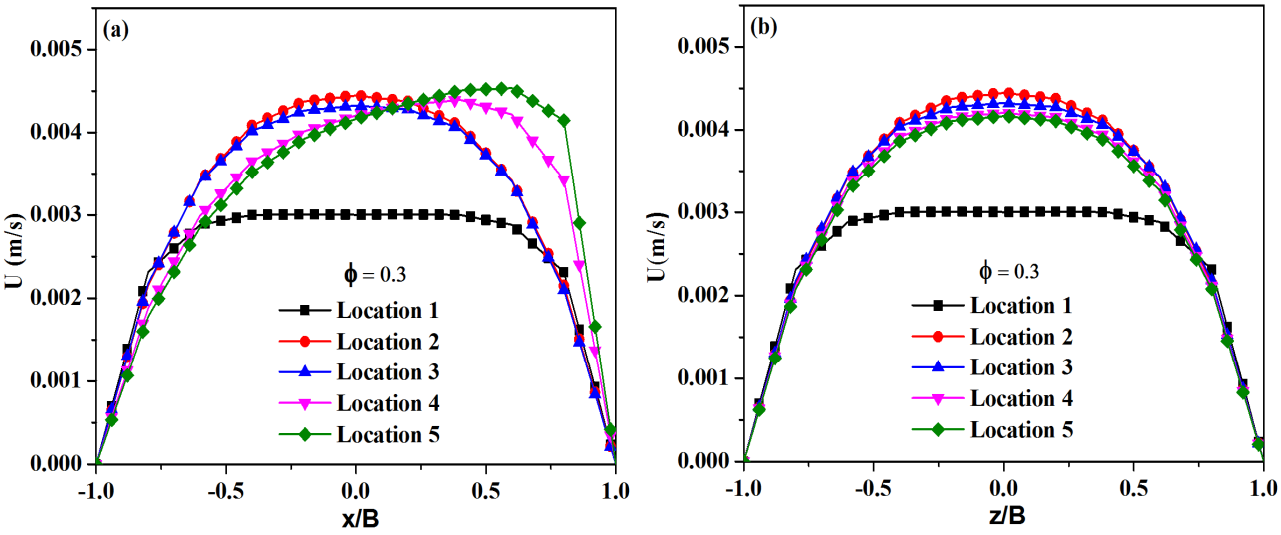

Figure 5.48. The velocity profiles of suspension at various locations in the inlet-1 section (30% particle concentration) in (a) lateral and (b) span-wise directions. The profiles (1,2,3,4,5) are taken at the locations -24.98 cm, -12.5 cm, -0.15 cm, -0.1 cm and -0.09 cm respectively.

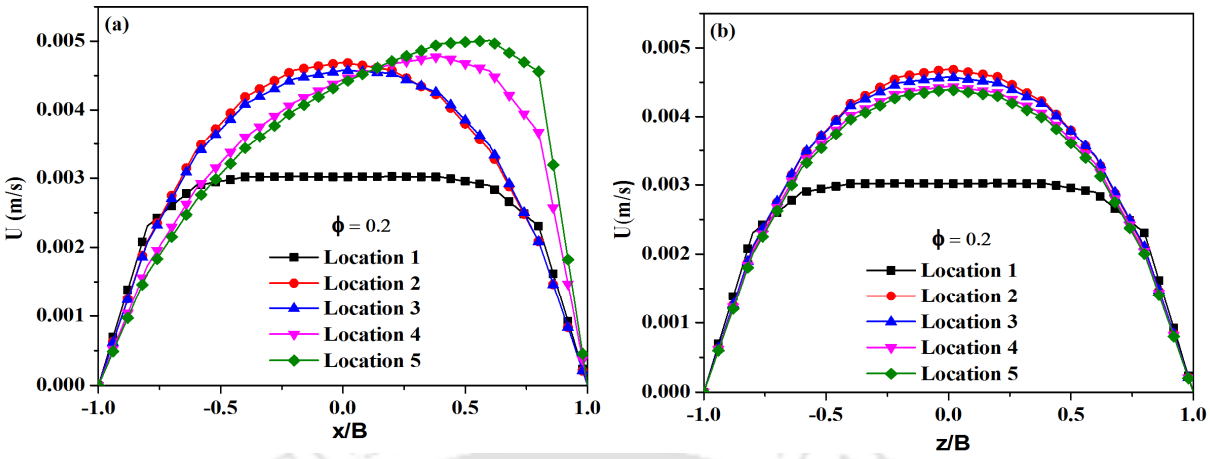

Figure 5.49. The velocity profiles of suspension at various locations in the inlet-2 section (20% particle concentration) in (a) lateral and (b) span-wise directions. The profiles (1,2,3,4,5) are taken at the locations -24.98 cm, -12.5 cm, -0.15 cm, -0.1 cm and -0.09 cm respectively.

The cross-sectional views (x-z plane) of velocity contour at various locations in the outlet section for suspension are shown in Figure 5.50. These cross-sectional slices were taken at planes perpendicular to the flow direction. The locations are given on the left side of each slice in the figure. At location 6 (Y=0 cm), the velocity field is asymmetric and shifted towards the right side. As we move downstream in the outlet section, gradually this asymmetry in velocity disappears. Symmetric and fully developed velocity profile is observed at the location Y = -12 cm. At other locations of outlet section the profile resembles like fully developed and velocity peak is near the center.

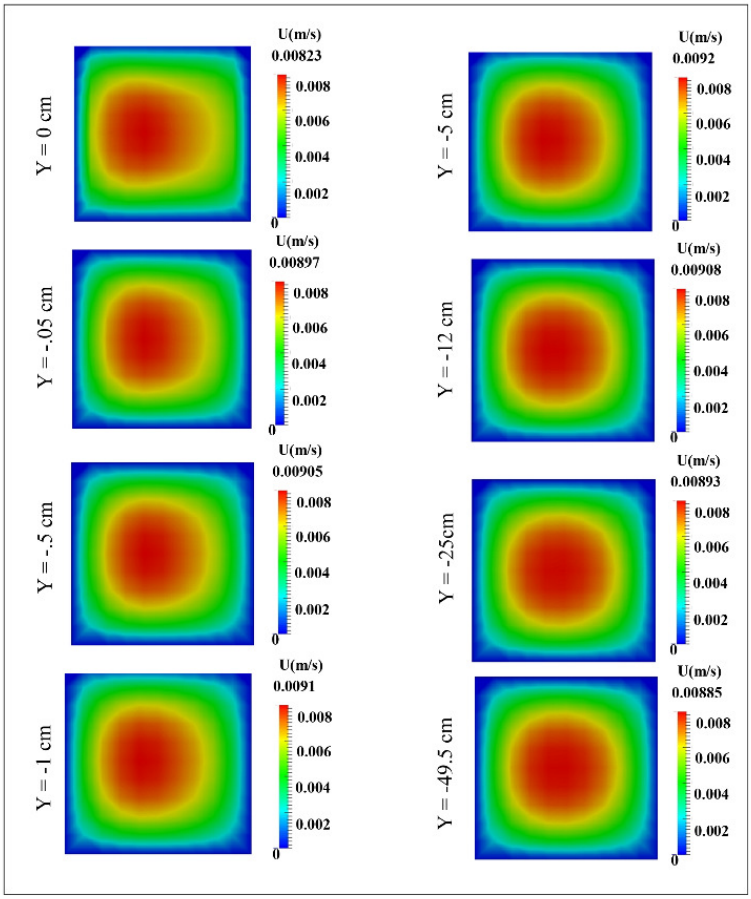

Figure 5.50. The cross sectional view of velocity contour planes taken at various locations in the x-z plane of the outlet section of T- shaped channel. The flow parameters were same as in Figure 5.49.

The velocity profiles of suspension at various locations in the outlet section in the lateral direction is shown in Figure 5.51. The velocity profiles at initial locations are shifted towards the right direction (on the side of low concentration inlet). However further downstream locations the profiles are again symmetric (See Figure 5.51b).

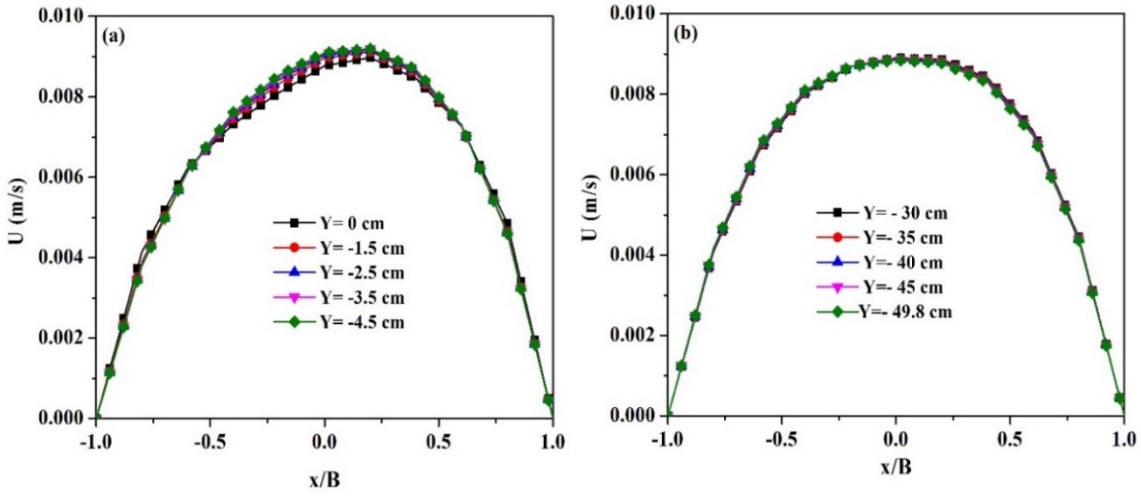

Figure 5.51. The lateral velocity profiles of suspension at various locations in the outlet section of T-shaped channel. The flow parameters were same as in Figure 5.50.

5.4.1.2. Shear rate field

The shear rate and shear stress contour maps in x-y plane of outlet section are shown in Figure 5.52. High shear rate is observed near the right wall of the outlet section but high shear stress in observed on the left side. Peak in the shear stress is clearly observed on the high concentration inlet section near the confluence of the two streams. The corresponding cross sectional shear rate contour planes (x-z plane) in the inlet sections are shown in Figure 5.53. The asymmetry in the shear rate field can be easily observed near the confluence (locations 4 and 5). Again we would like to mention that in the contour maps of Figure 5.53 and 5.54 the flow direction is perpendicular to the plane of paper and pointing inward.

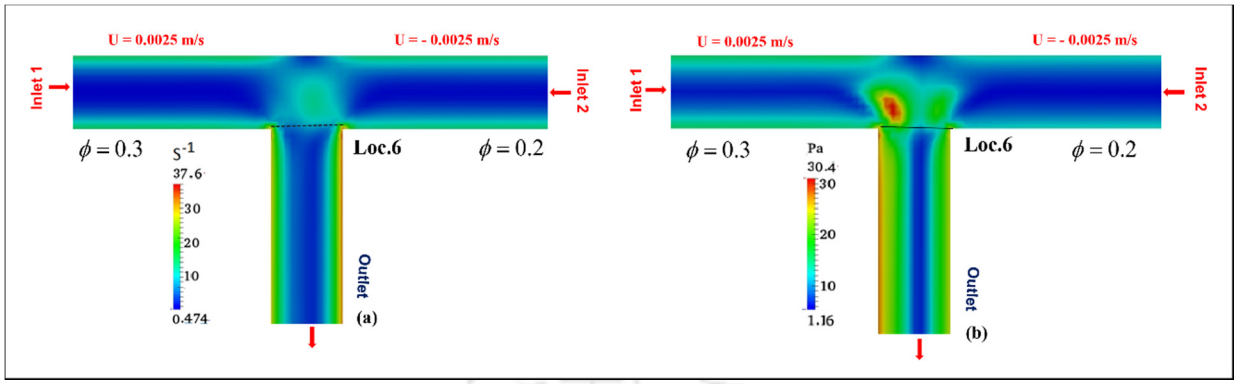

Figure 5.52. The contour planes for shear rate (a) and shear stress (b) in x-y plane of the T-shaped channel in converging flow.

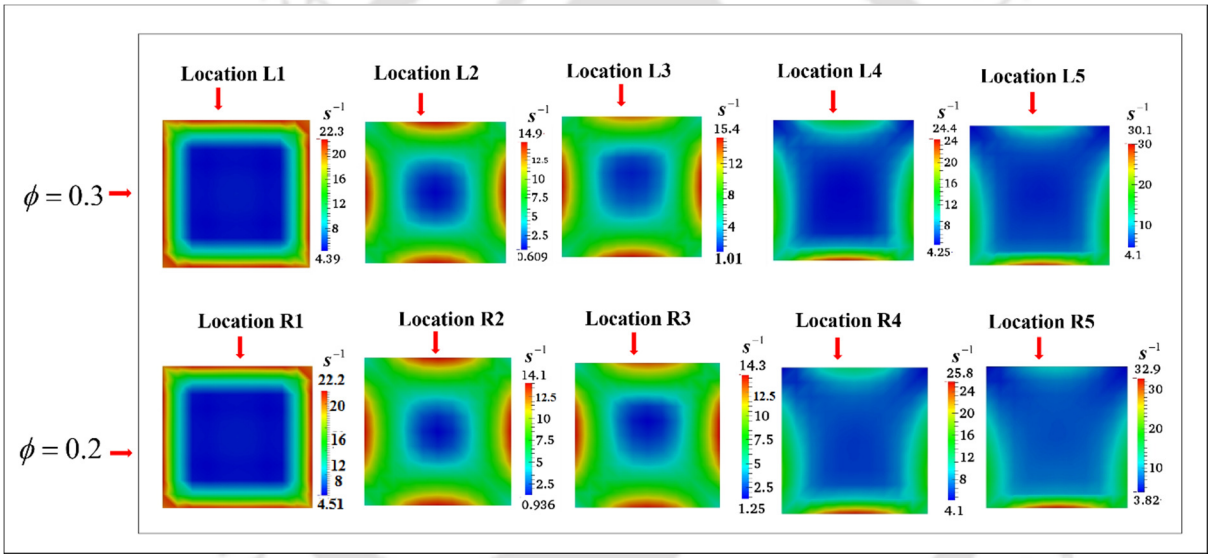

Figure 5.53. The cross sectional contour planes of shear rate field in the inlet sections of the T-shaped channel. The slices (1,2,3,4,5) were taken at the locations -24.98 cm, -12.5 cm, -0.15 cm, -0.1 cm and -0.09 cm respectively.

Figure 5.54 shows the cross sectional shear rate contour planes at different locations in the outlet section. At location 6 (Y=0 cm), which is the beginning of outlet section the contour the shear rate filed is asymmetric but the high values are on the side of outlet section. As we

move further downstream locations it is observed that the shear rate field gradually becomes symmetric with highest values near the middle of wall regions and lowest at the centre.

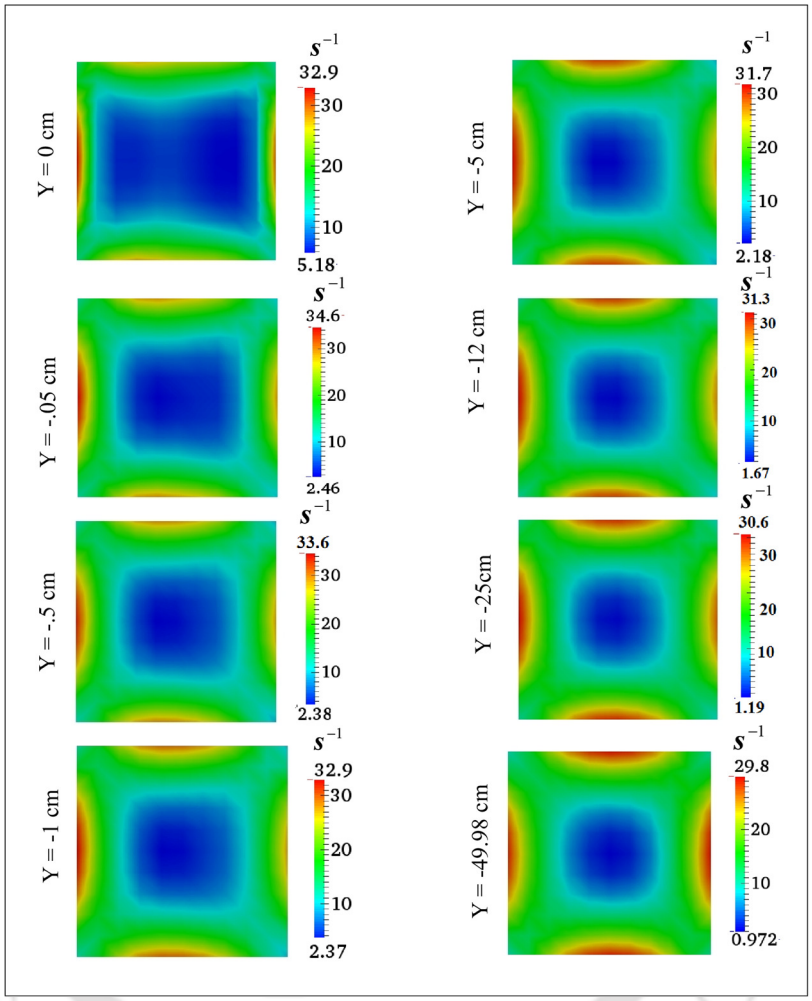

Figure 5.54. The cross sectional contour planes of shear rate field at various locations in the outlet section in converging flow in a T shaped channel.

5.4.1.3. Concentration Field

The front view concentration contour maps in the mid-plane are presented in Figure 5.55. For the clarity of view we have shown only a small section around the converging section. In the inlet sections the shear induced migration causes the particles to move towards the center of the channel. The peak concentration in inlet-1 section (30% inlet concentration) is more compared to the inet-2 section whose inlet had 20% particle concentration. The central core of both the inlets moves downward in the converging section and enters the outlet section at location 6. The high concentration core which originated in inlet-1 persists in the outlet section as well for some distance which gradually merge at downstream locations.

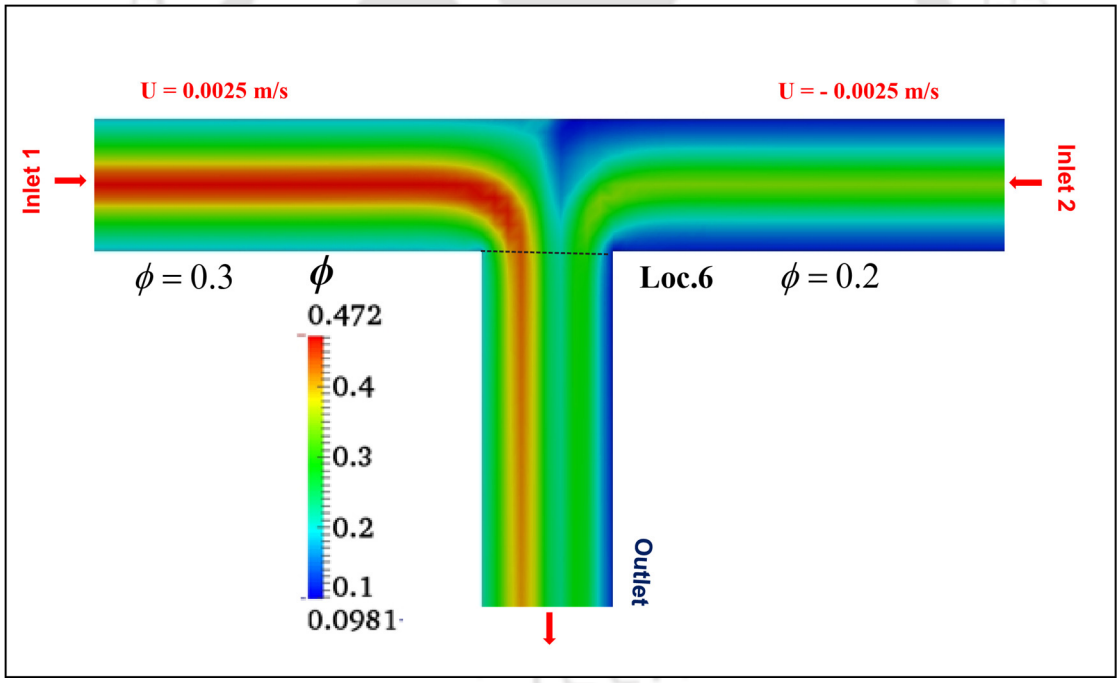

Figure 5.55. Concentration contour map in x-y plane (Z=0) for converging flow in a T-shaped channel with same velocity but different inlet concentrations. For clarity of contours only a small section of bifurcation channel is shown here.

In Figure 5.56 we show the cross-sectional view of concentration maps (x-z plane) in the inlet sections. As expected the nature of these contour maps is very similar to that described in the previous case. In order to understand quantitative nature of particle distribution we have shown the concentration profiles in the inlet section 1 for the lateral and span-wise directions in Figures 5.57 and that of inlet-2 section in Figure 5.58. The nature of these profiles are similar to the one described in the previous case. The cross sectional concentration contours taken at various locations in the outlet section are shown in Figure 5.59. Unlike the case-2 (equal velocity and equal concentration at both the inlets) in this case we observe asymmetric concentration profile at the beginning of the outlet section (location 6). The peak concentration gradually shifts towards the center of the outlet section and the profile becomes more symmetric.

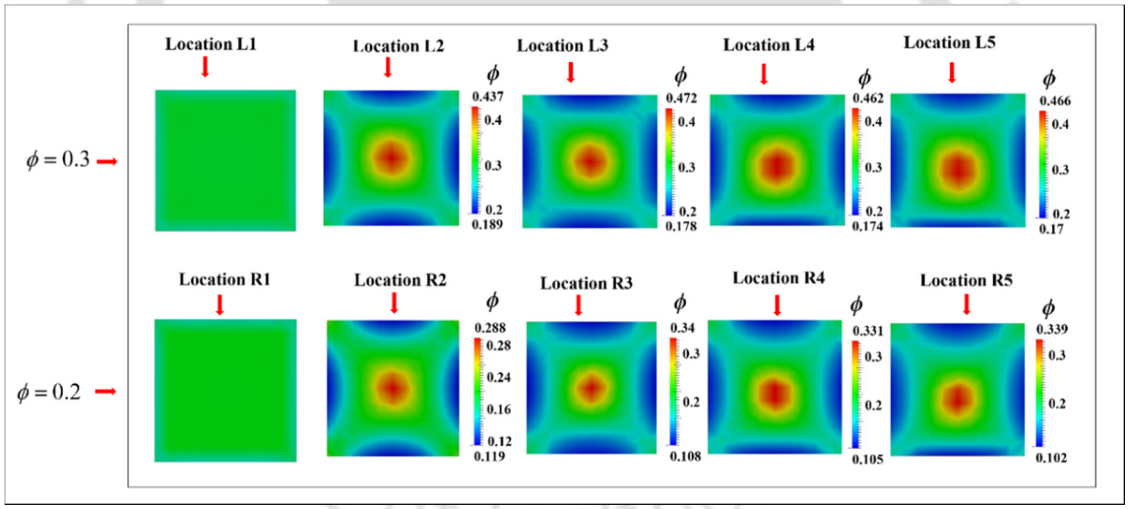

Figure 5.56. Cross- sectional contour maps of particle in the inlet sections of T-shaped channel in converging flow with same velocity but different inlet concentrations. The contour (1,2,3,4,5) were taken at the locations -24.98 cm, -12.5 cm, -0.15 cm, -0.1 cm and -0.09 cm respectively.

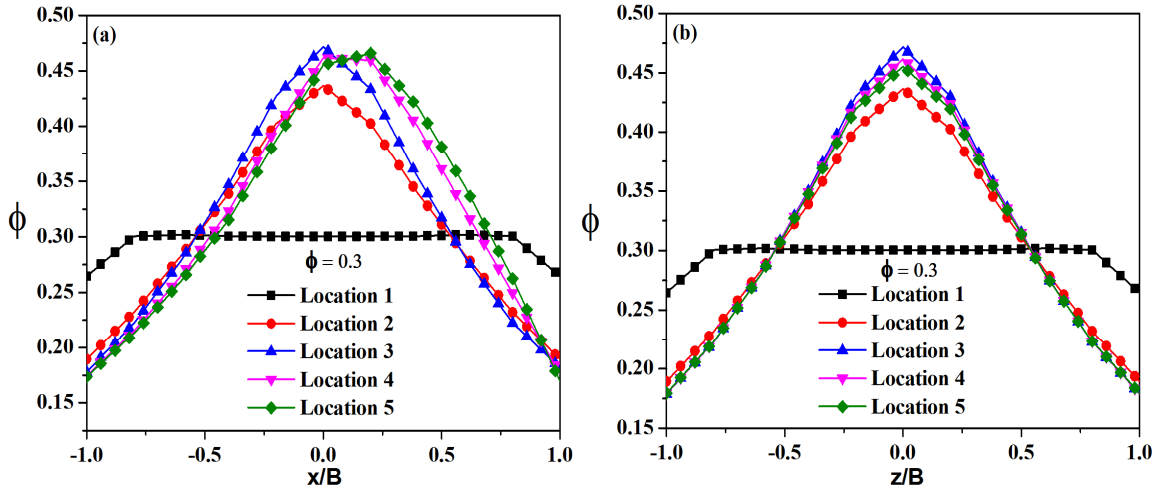

Figure 5.57. Concentration profiles at various locations in the inlet-1 section of converging T-shaped channel flow: (a) lateral direction, and (b) span-wise direction. All other parameters were same as in Figure 5.56.

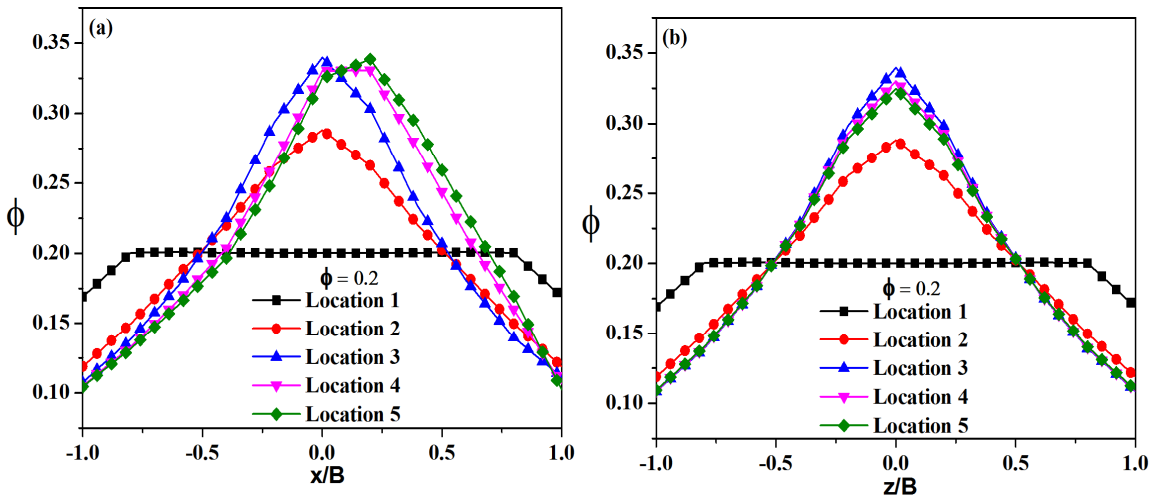

Figure 5.58. Concentration profiles at various locations in the inlet-2 section of converging T-shaped channel flow: (a) lateral direction, and (b) span-wise direction. All other parameters were same as in Figure 5.56.

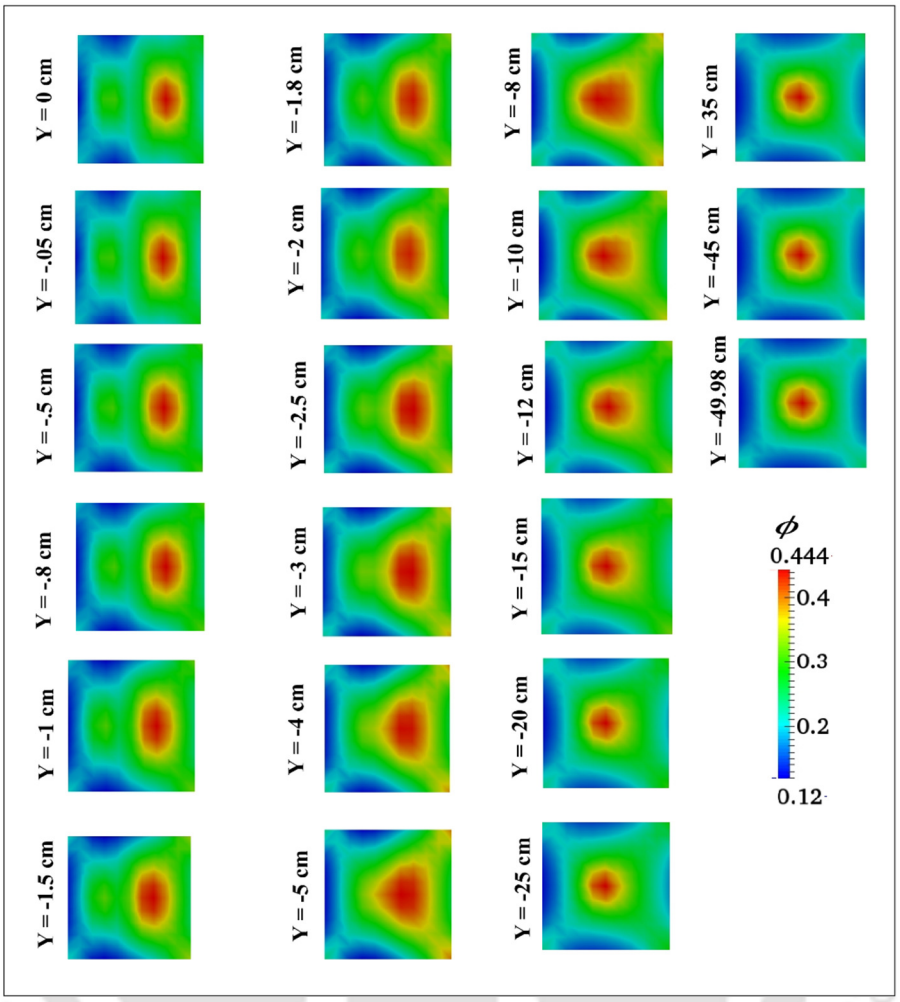

Figure 5.59. Cross- sectional contour maps of particle concentration in the outlet sections of T-shaped channel in converging flow with unequal inlet concentration but equal inlet velocity.

The corresponding concentration profiles at various locations of outlet section in lateral direction are presented in Figure 5.60. At location 6 (entrance of the outlet section) the peak-valley-peak pattern in concentration profile is clearly observed. The left peak corresponding to 30% inlet section shows high value and compared to the right peak which corresponds to 20% inlet section. As we move downstream locations in the outlet section, the peak- valley-peak pattern in concentration profile gradually vanishes and we get concentration profile with

a single peak which is shifted towards the left. The shear induced migration causes further migration of the particles towards the center of the channel and finally leading to symmetric profile that resembles that of a straight channel.

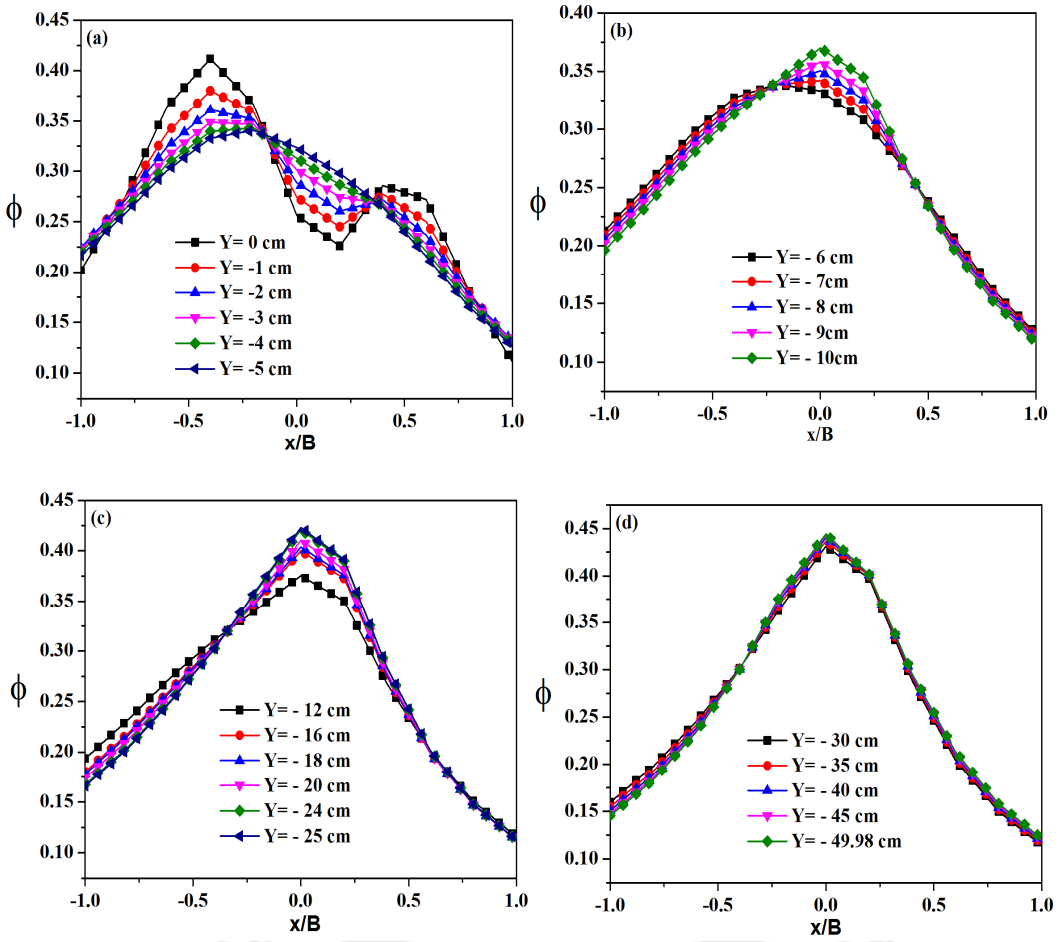

Figure 5.60. Concentration profiles at various locations of the outlet section in T-shaped channel with converging flow having equal inlet velocity (0.0025 m/s) but unequal particle concentration (30% in inlet-1 and 20% in inlet-2).

5.4.1.4. Wall shear stress

The contour map of wall shear stress for the case of unequal inlet particle concentration is shown in Figure 5.61. The wall shear stress is higher on the wall of the inlet which is on the side of the outlet section (bottom wall) and the peak concentration is observed near the corner at the junction of inlet and outlet sections. The wall shear stress values are more for inlet-1 section (30% inlet concentration) compared to the inlet-2 section whose inlet had 20% particle concentration. In the outlet section the wall shear stress values are higher in left wall compared to right wall. However, maximum wall shear stress is observed in the middle. This is due to the fact that in the outlet section the peak concentration is in the centre of the channel.

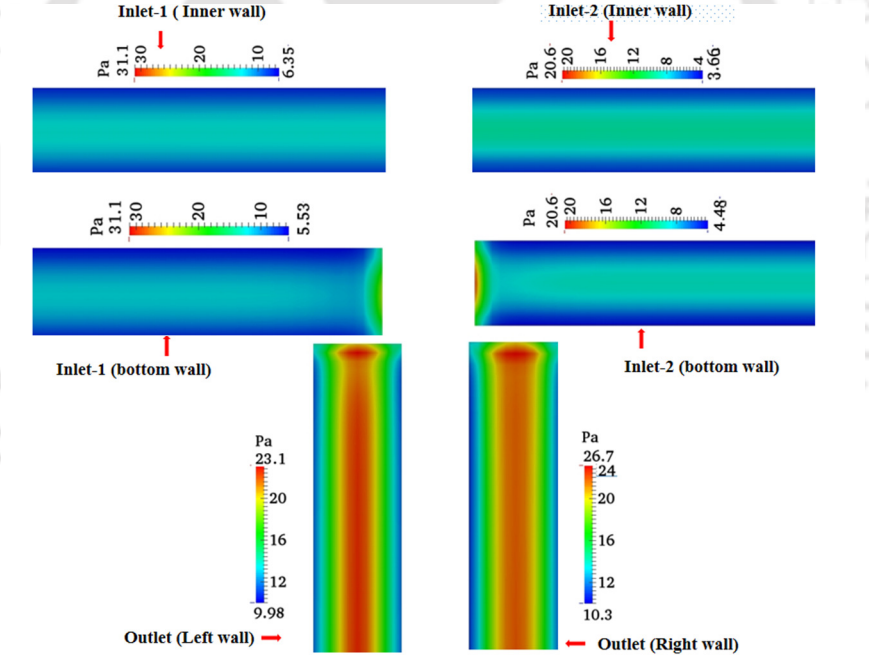

Figure 5.61. Wall shear stress contours planes for outer and inner walls of T-shaped channel in converging flow. The particle concentration was 40% and the inlet velocity was 0.0025 m/s.

5.5. Conclusion

- In case for diverging flow in T shaped bifurcation channel, at bifurcation the velocity profiles for suspension in lateral and span-wise directions are blunted and degree of bluntness is more for suspension of higher particle concentration. In side branches the velocity profiles in lateral direction are more shifted towards outer wall. The concentration profiles in inlet section are blunted and in the side branch the location of maximum concentration is shifted towards the inner wall.
- In converging flow in T-shaped channel, for the case of equal inlet particle concentration and velocity it was observed that the two inlet streams merge in the outlet section. In the beginning of the outlet section the velocity field shows single peak with blunted velocity profile but the concentration peaks corresponding to the fully developed profiles in the inlet section persists for some distance. In the downstream locations both the velocity and concentration profiles undergo significant changes. The velocity profile becomes less blunted. The two peaks in concentration progressively merge to give a single peak. The two distinct peaks in shear stress values are observed in the converging section. The maximum shear stress value for 50% bulk particle concentration is higher compared to 40% particle concentration and Newtonian fluid. The wall shear stress was found to be highest at the corner regions of the junction of inlet and outlet sections.
- Similar trend as mentioned above was also observed in converging flow in T channel, for the case of unequal inlet particle concentration but equal velocity. The increase in velocity magnitude in outlet section is due to the merging of streams from the inlet-1 and inlet-2 which enhances the velocity magnitude in the outlet section. It was also observed

that the shifting of velocity profile near the entrance of the outlet section is towards that inlet section which had lower concentration. However at further downstream locations the profiles are again symmetric. At the entrance of the outlet section asymmetric peak-valley-peak pattern in concentration profile was observed. The left peak corresponding to 30% inlet section showed high value when compared to the right peak which corresponds to 20% inlet section. As we move downstream locations in the outlet section, the peak- valley- peak pattern in concentration profile gradually vanishes and we get concentration profile with a single peak which is shifted towards the side of higher concentration inlet.

भारतीय प्रौद्योगिकी संस्थान गुवाहाटी
Indian Institute of Technology Guwahati

CHAPTER-6

Conclusions and Future direction

भारतीय प्रौद्योगिकी संस्थान गुवाहाटी
Indian Institute of Technology Guwahati

6. Conclusions and Future Direction

6.1. Conclusions

This thesis covers the low Reynolds number flow physics of concentrated suspensions of non-Brownian particles suspended in a Newtonian fluid. The main theme of this thesis is to study the phenomenon of shear-induced migration of particles in bifurcation channels through numerical simulations based on the Diffusive Flux Model. The transport equations were solved in Open source Computational Fluid Dynamics (CFD) package named OpenFOAM. It is based on the Finite Volume Method (FVM) to solve the system of Partial Differential Equations (PDEs). First we have validated the results obtained from simulation of suspension flow in 2D rectangular channel with experimental data of Lyon and Leal (1998) and analytical results of Phillips *et al.* (1992). The results were found to be in good agreement with experimental and analytical solution. For bifurcation geometry, we have validated the numerical results with the experiments of Leble *et al.* (2011). The geometry and flow parameters considered in our simulations were similar to that in the experiments. The experiments of Leble *et al.* (2011) were only for 14% particle concentration and they have provided the measurements of velocity field. The measurements of concentration field were not performed. In this thesis we have investigated shear-induced migration for highly concentrated suspensions (more than 30% particle concentration) which are industrially important. We have studied the shear induced migration of particles of concentrated suspensions through symmetric 2D and 3D bifurcation channels. We have studied the effect of concentration, flow rate, effect of angle on velocity profile and concentration profile near the bifurcation and before the bifurcation. Shear rate and

wall shear stresses were also studied. First we discussed the results of suspension flow in two -dimensional channel and then flow in symmetric 3D Y-shaped geometry followed by results obtained for dense suspension flow in 3D T shaped geometry. Important results from our simulations can be summarized as:

- The velocity profile for the suspension flow showed considerable differences over the Newtonian fluid profile of the same viscosity as that of suspension. This is attributed to the shear induced migration of particles.
- In the Stokes flow regime there is no effect of flow rate on velocity and concentration profile. Near the bifurcation peak-valley-peak patterns in velocity profile were observed for channels with greater angles of bifurcation and higher bulk particle concentrations. The velocity and concentration profiles were symmetric in the inlet section but asymmetric in the side branches. There is small influence of particle size on velocity profile but significant effect was observed on the concentration profiles. The wall shear stresses are larger at the inner walls when compared to the outer walls of the side branches.
- In symmetric three dimensional bifurcation channels, at bifurcation the velocity profiles for suspension in lateral and span-wise directions are blunted and degree of bluntness is more apparent with increase in the angle of bifurcation and particle concentration. It was observed that the migration of particles in the downstream branches leads to asymmetric velocity and concentration profiles. The wall shear stress level was observed to be the highest near the bifurcation. In the side branch the difference in wall shear stress level of inner and outer wall was found to be highest for bifurcation angle of 90^0.

- In case for diverging flow in T shaped bifurcation channel, at bifurcation the velocity profiles for suspension in lateral and span-wise directions are blunted and degree of bluntness is more apparent with increase in the particle concentration. In side branches the velocity profiles in lateral direction are more shifted towards outer wall. The concentration profiles in inlet section are blunted and in the side branch the location of maximum concentration is shifted towards the inner wall.
- In converging flow in T-shaped channel, for the case of equal inlet particle concentration and velocity it was observed that the two inlet streams merge in the outlet section. In the beginning of the outlet section the velocity field shows single peak with blunted velocity profile but the concentration peaks corresponding to the fully developed profiles in the inlet section persists for some distance. In the downstream locations both the velocity and concentration profiles undergo significant changes. The velocity profile becomes less blunted. The two peaks in concentration progressively merge to give a single peak. The two distinct peaks in shear stress values are observed in the converging section. The maximum shear stress value for 50% bulk particle concentration is higher compared to 40% particle concentration and Newtonian fluid. The wall shear stress was found to be highest at the corner regions of the junction of inlet and outlet sections.
- Similar trend as mentioned above was also observed in converging flow in T channel, for the case of unequal inlet particle concentration but equal velocity. The increase in velocity magnitude in outlet section is due to the merging of streams from the inlet-1 and inlet-2 which enhances the velocity magnitude in the outlet section. It was also observed that the shifting of velocity profile near the entrance of the outlet section is towards that inlet

section which had lower concentration. However at further downstream locations the profiles are again symmetric. At the entrance of the outlet section asymmetric peak-valley-peak pattern in concentration profile was observed. The left peak corresponding to 30% inlet section showed high value when compared to the right peak which corresponds to 20% inlet section. As we move downstream locations in the outlet section, the peak-valley- peak pattern in concentration profile gradually vanishes and we get concentration profile with a single peak which is shifted towards the side of higher concentration inlet.

We hope that our study has provided some insight into the flow physics of concentrated suspensions which is required in many applications involving network of branching system to design mixing devices as well as better understanding of system failures in piping networks relevant to industry and physiology. Also, bifurcations are the key element in flow devices for mixing (Wong *et a*l, 2004), heat exchange (Haller *et al,* 2009) and droplet formation (Link *et al*. 2004). Whereas these devices have been studied in great detail for Newtonian fluids, much less is known about the about transport of concentrated suspensions. The flow of non-Newtonian fluids (without particles) in T shaped channels has been much more studied in the literature (Matos and Oliveira 2013; Matos and Oliveira 2014), mainly focused on the investigating the stress and velocity field but the flow of concentrated suspensions through bifurcation channels are less studied.

6.2. Future Direction

In this work we have performed numerical simulations for suspension flow in bifurcation channels by using Diffusive Flux Model. This model gives satisfactory results for rectilinear flows like channel flow but is not suitable for more complicated geometries. With this model we are unable to capture the secondary flows since the rheology of suspension is assumed to be Newtonian with effective viscosity. Suspension Balance Model proposed by Nott and Brady (1994) can overcome the drawback of Diffusive Flux Model since it couples the migration to non-Newtonian rheology of suspension including the normal stress differences. In the future one can use Suspension Balance Model to capture the flow physics in bifurcation consisting of circular or elliptical cross sections. It is a challenging work to perform unsteady simulations in real time but the progress in these directions is underway. The experimental measurement in bifurcation channels is also needed for better understanding of flow physics. In many practical applications the suspending fluid are non-Newtonian with complex rheology. It would be interesting to couple the shear-induced migration models with non-Newtonian rheology such as shear-thinning, shear thickening, time-dependent non-Newtonian fluids. One can also work perform particle level simulations such as Stokesian Dynamics in complex bifurcation geometries and compare results with Diffusive Flux Model and Suspension Balance Models.

भारतीय प्रौद्योगिकी संस्थान गुवाहाटी
Indian Institute of Technology Guwahati

Appendix

भारतीय प्रौद्योगिकी संस्थान गुवाहाटी
Indian Institute of Technology Guwahati

Appendix A

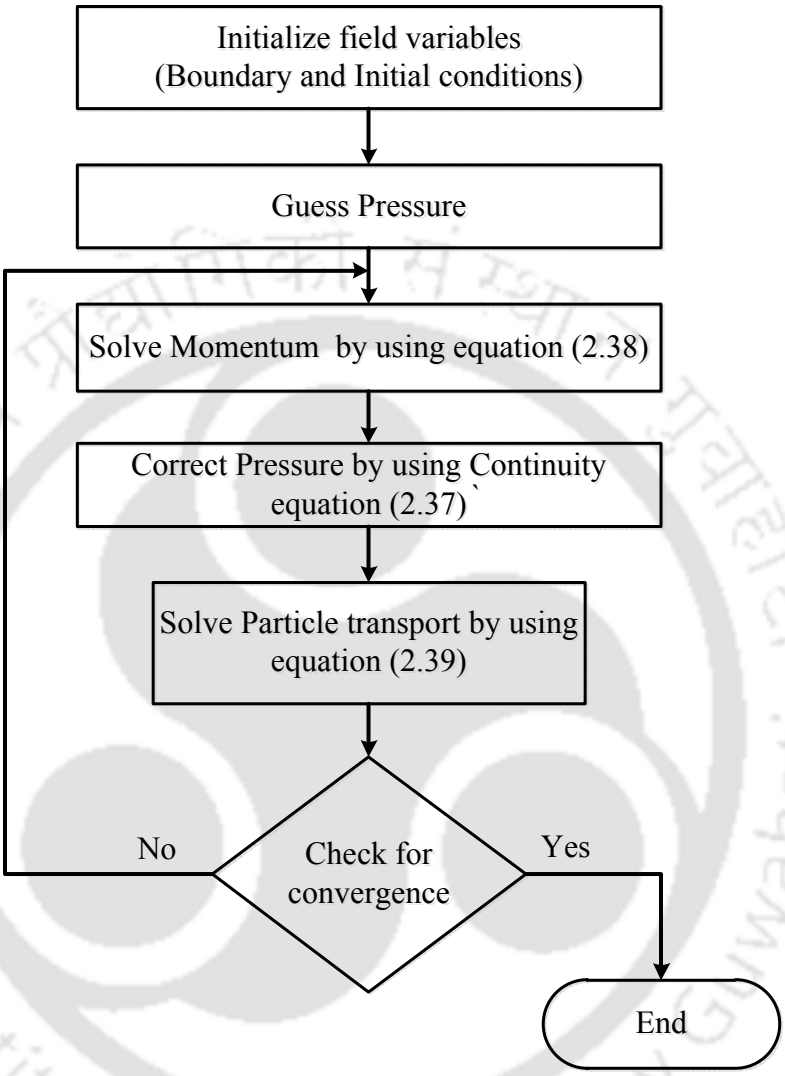

Flow chart for algorithm used in simulation

Appendix B

Implementation of the SIMPLE algorithm in OpenFOAM

The SIMPLE algorithm can be implemented in OpenFOAM as follows (The complete implementation of the algorithm can be seen in the source code of the simpleFoam solver provided with OpenFOAM):

- Store the pressure calculated at the previous iteration, because it is required to apply under-relaxation

  p.storePrevIter();

- Define the equation for U

  tmp<fvVectorMatrix> UEqn
  (
  fvm::div(phi, U)
  - fvm::laplacian(nu*pow(1- ϕ/0.68,-1.82), U)
  );

  Note: tmp< > is used to reduce peak memory.

- Under-relax the equation for U

  UEqn().relax();
  fvOptions.constrain(UEqn());

- Solve the momentum predictor

  solve(UEqn() == -fvc::grad(p));
  fvOptions.correct(U);

- Update the boundary conditions for p

  p.boundaryField().updateCoeffs();

- Calculate the a_p coefficient and calculate U

```
volScalarField rAU(1.0/UEqn().A());
volVectorField HbyA("HbyA", U);
 HbyA = rAU*UEqn().H();
UEqn.clear();
```

- Calculate the flux

```
surfaceScalarField phiHbyA("phiHbyA", fvc::interpolate(HbyA) & mesh.Sf());
fvOptions.makeRelative(phiHbyA);
 adjust Phi(phiHbyA, U, p)
```

- Define and solve the pressure equation and repeat for the prescribed number of non-orthogonal corrector steps

```
fvScalarMatrix pEqn
        (
         fvm::laplacian(rAU, p) == fvc::div(phiHbyA)
         );
 pEqn.setReference(pRefCell, pRefValue);
    pEqn.solve();
```

- Correct the flux

```
phi = phiHbyA - pEqn.flux();
```

- Calculate continuity errors

```
# include "continuityErrs.H"
```

- Under-relax the pressure for the momentum corrector and apply the correction

```
p.relax();
U = HbyA - rAU*fvc::grad(p);
   U.correctBoundaryConditions();
   fvOptions.correct(U);
```

- fvScalarMatrix ϕ Eqn

```
volScalarField mu1=0.62*1.82*pow(a,2)*γ̇*pow(φ,2)*pow(0.68- φ,-1);
volScalarField mu2=0.41*pow(a,2)* γ̇* φ ;
volScalarField mu3=0.41*pow(a,2)* φ * φ;
        solve
            (
            fvm::div(phi, φ)
            - fvm::laplacian(mu1, φ)
            - fvm::laplacian(mu2, φ)
                ==
             fvc::laplacian(mu3, γ̇)
                    );
```

- Check for convergence and repeat from the beginning until convergence criteria are satisfied.
- The value of the initial residual can be obtained when solving the corresponding equation using the initialResidual() method. Two syntax are possible

```
eqnResidual = solve
        (
          UEqn() == -fvc::grad(p)
        ).initialResidual();
```

or, equivalently, for the pressure equation, since it has been already defined,

```
eqnResidual = pEqn.solve().initialResidual();
```

Appendix C

Implementation of the SIMPLE algorithm in OpenFOAM

The different discretization schemes, solvers and relaxation factors used in OpenFOAM solver setting is described in the following sections [OpenFOAM User's Guide].

Discretization schemes:

```
gradSchemes
{
        default         Gauss linear;
}
divSchemes
{
        default         Gauss linear;
}
laplacianSchemes
{
        default         Gauss linear corrected;
}
interpolationSchames
{
        default         linear;
}
snGradSchemes
{
        default         corrected;
}
```

Solvers settings used in OpenFOAM for present simulations

```
Solvers
{
```

```
    p
    {
        solver          PCG;
        preconditioner  DILU;
        tolerance       1e-7;
        relTol          0;
    }

    U
    {
        solver          PBiCG;
        preconditioner  DILU;
        tolerance       1e-7;
        relTol          0;
    }

T ( c ≡ φ ) (concentration of the particles)
    {
        solver          PBiCG;
        preconditioner  DILU;
        tolerance       1e-7;
        relTol          0;
    }
}
SIMPLE
{
        nCorrectors             2;      // minimum 2
        nNonOrthogonalCorrectors 2;
        pRefCell                0;
        pRefValue               0;
}
```

```
relaxationFactors
{
  fields
  {
        p       0.2;
        T       0.9;
  }
  equations
  {
        U       0.7;
  }
}
```

Appendix D

Derivation of Zero Flux Boundary Condition

Flux due to varying interaction frequency is given as,

$$N_c = -K_c a^2(\phi^2 \nabla\dot{\gamma} + \phi \nabla\dot{\gamma}\phi)$$

Flux due to varying viscosity is given as,

$$N_\eta = -K_\eta \dot{\gamma}\phi^2 \left(\frac{a^2}{\eta}\right)\left(\frac{d\eta}{d\phi}\right)(\nabla\phi)$$

Zero flux boundary condition is given as,

$$\eta.\left(N_c + N_\eta\right) = 0$$

$$-K_c a^2\left(\phi^2 \eta.(\nabla\dot{\gamma}) + \phi\dot{\gamma}(\eta.\nabla\phi)\right) - K_\eta \dot{\gamma}\phi^2 \left(\frac{a^2}{\eta}\right)\left(\frac{d\eta}{d\phi}\right)(\nabla\phi) = 0$$

$$(\eta.\nabla\phi)\left[-K_c a^2 \phi\dot{\gamma} - K_\eta \dot{\gamma}\phi^2 \left(\frac{a^2}{\eta}\right)\left(\frac{d\eta}{d\phi}\right)\right] = K_c a^2 \phi^2 \eta.(\nabla\dot{\gamma})$$

$$(\eta.\nabla\phi) = -\frac{K_c \phi(\eta.\nabla\dot{\gamma})}{\dot{\gamma}\left(K_c + \phi\left(\frac{K_\eta}{\eta}\right)\left(\frac{d\eta}{d\phi}\right)\right)}$$

References

भारतीय प्रौद्योगिकी संस्थान गुवाहाटी
Indian Institute of Technology Guwahati

References

Aarts, P.; Vandenbroek, S. A. T.; Prins, G. W.; Kuiken, G. D. C.; Sixma, J. J.; Heethaar, R. M., Blood-platelets are concentrated near the wall and red blood-cells, in the center in flowing blood. *Arteriosclerosis.* **1988,** 8 (6), 819-824.

Abbott, J. R.; Tetlow, N.; Graham, A. L.; Altobelli, S. A.; Fukushima, E.; Mondy, L. A.; Stephens, T. S., Experimental-observations of particle migration in concentrated suspensions - Couette-flow. *Journal of Rheology.* **1991,** 35 (5), 773-795.

Ahmed, G. M. Y.; Singh, A., Numerical simulation of particle migration in asymmetric bifurcation channel. *Journal of Non-Newtonian Fluid Mechanics*. **2011,** 166 (1-2), 42-51.

Altobelli, S. A.; Givler, R. C.; Fukushima, E., Velocity and concentration measurements of suspensions by nuclear-magnetic-resonance imaging. *Journal of Rheology.* **1991,** 35 (5), 721-734.

Anastasiou, A.D.; Spyrogiannia, A.S.; Koskinasb K.C.; Giannogloub, G.D.; Paras S.V., Experimental investigation of the flow of a blood analogue fluid in a replica of a bifurcated small artery. *Journal of Medical Engineering & Physics*. **2012,** 34, 211-218.

Audet, D. M.; Olbricht, W. L., The motion of model cells at capillary bifurcations. *Microvascular. Research.* **1987,** 33(3), 377-396.

Averbakh, A.; Shauly, A.; Nir, A.; Semiat, R., Slow viscous flows of highly concentrated suspensions-part I: laser-Doppler velocimetry in rectangular ducts. *International Journal of Multiphase Flow.* **1997,** 23 (3), 409-424.

Balan, C. M.; Balan, C., μPIV measurement and numerical computation of the velocity profiles in micro channels. *UPB Scientific Bulletin.Series D*. **2010,** 72 (3), ISSN 14544 -2358.

Ball, R.C.; Richmond, P., Dynamics of colloidal dispersions. *Physics and Chemistry of Liquids.* **1980,** 9, 99-116.

Barber, J. O.; Alberding, J. P.; Restrepo, J. M.; Secomb, T. W., Simulated two-dimensional red blood cell motion, deformation, and partitioning in microvessel bifurcations. *Annals of Biomedical Engineering.* **2008,** 36 (10), 1690-1698.

Batchelor, G. K., The effect of Brownian motion on the bulk stress in a suspension of Spherical particles. *Journal of Fluid Mechanics.* **1977,** 83, 97–117.

Batchelor, G. K.; Green, J. T., The hydrodynamic interaction of two small freely-moving spheres in a linear flow field. *Journal of Fluid Mechanics.*1**972a,** 56, 375–400.

Batchelor, G. K.; Green, J. T., Determination of bulk stress in a suspension of spherical-particles to order c^{-2}. *Journal of Fluid Mechanics.* **1972b,** 56*,* 401-427.

Brady, J F., The rheological behaviour of concentrated colloidal dispersions. *Journal of Chemical Physics*. **1993,** 99, 567-581.

Brady, J. F.; Bossis, G., The rheology of concentrated suspensions of spheres in simple shear-flow by numerical-simulation. *Journal of Fluid Mechanics.***1985,** 155, 105-129.

Brady, J. F.; Bossis, G., Stokesian dynamics. *Annual Review of Fluid Mechanics.* **1988,** 20, 111-157.

Chapman, B.K., Shear induced migration phenomena in concentrated suspensions. Ph.D. Thesis, University of Notre Dame. **1990.**

Chen, S.B., Axisymmetric creeping motion of particles towards a circular orifice or disk. *Physics of Fluids .**2013**,* 25, 043106-14.

Chien, S.; Tvetenstrand, C. D.; Epstein, M. A. F.; Schmidschonbein, G. W., Model studies on distribution of blood-cells at microvascular bifurcations. *American Journal of Physiology.* **1985,** 248 (4), H568-H576.

Chong, J. S.; Christiansen, E.B.; Baer. A.D., Rheology of concentrated suspensions. *Journal of Applied Polymer Science.* **1971**, 15, 2007-2021.

Chow, A. W.; Sinton, S. W.; Iwamiya, J. H.; Stephens, T. S., Shear-induced particle migration in couette and parallel-plate viscometers - NMR imaging and stress measurements. *Physics of Fluids.***1994,** 6 (8), 2561-2576.

Chow, A.W., Sinton, S.W., Iwamiya, J. H., Leighton, D. T., Particle migration of non – Brownian, concentrated suspensions in a truncated cone-and–plate. *Society of Rheology Meeting,* Sacramento, CA.**1995.**

Dbouk, T.; Lobry,L. Lemaire.,E.; Moukalled, F., Shear-induced particles migration; predictions from experimental determination of the particle stress tensor. *Journal of Non-Newtonian Fluid Mechanics.* **2013,** 198, 78-95.

Dbouk, T.; Lobry, L.; Lemaire, E., Normal stresses in concentrated non-Brownian suspensions. *Journal of Fluid Mechanics*. **2013**, 715, 239 - 272.

Deshpande. A.P.; Murali Krishanan, J.; Sunil Kumar. P.B., Rheology of Complex Fluids. Springer Publishers. **2010.**

Ditchfield, R.; Olbricht, W. L., Effects of particle concentration on the partitioning of suspensions at small divergent bifurcations. *Journal of Biomechanical Engineering-Transactions of the ASME* .**1996,** 118 (3), 287-294.

Drew D. A.; Lahey, R. T, Analytical modeling of multiphase flow in particulate two-phase flows, edited by M.C. Roco (Butterworth-Heinemann, Boston), **1993**.

Dorr, A.; Sadiki, A.; Mehdizadeh, A**.,** A discrete model for the apparent viscosity of polydisperse suspensions including maximum packing fraction. *Journal of Rheology.* **2013,** 57. 743-765.

Eckstein, E. C.; Bailey, D. G.; Shapiro, A. H., Self-diffusion of particles in shear-flow of a suspension. *Journal of Fluid Mechanics.* **1977,** 79*,* 191-208.

Einstein, A., Eine neue Bestimmung der Moleküldimensionen. *Annalen der Physik.* **1906,** 19, 289-306.

Enden, G.; Popel, A. S., A numerical study of plasma skimming in small vascular bifurcations. *Journal of Biomechanical Engineering-Transactions of the ASME.***1994,** 116 (1), 79-88.

Faivre, M.; Abkarian, M.; Bickraj, K.; Stone, H. A., Geometrical focusing of cells in a microfluidic device: An approach to separate blood plasma. *Biorheology.* **2006,** 43 (2), 147-159.

Fang, Z. W.; Mammoli, A. A.; Brady, J. F.; Ingber, M. S.; Mondy, L. A.; Graham, A. L., Flow-aligned tensor models for suspension flows. *International Journal of Multiphase Flow.* **2002,** 28 (1), 137-166.

Fang, Z. W.; Phan-Thien, N., Numerical-simulation of particle migration in concentrated suspensions by a finite-volume method. *Journal of Non-Newtonian Fluid Mechanics.* **1995,** 58 (1), 67-81.

Fridjonsson, E. O.; Seymour, J. D.; Cokelet, G. R.; Codd, S. L., Dynamic NMR microscopy measurement of the dynamics and flow partitioning of colloidal particles in a bifurcation. *Experiments in Fluids.* **2011,** 50 (5), 1335-1347.

Gadala-Maria, F.; Acrivos, A., Shear-induced structure in a concentrated suspension of solid spheres. *Journal of Rheology.***1980,** 24 (6), 799-814.

Gadala-Maria. F., The Rheology of concentrated suspensions. PhD Thesis, Stanford University, **1979.**

Gijsen, F. J. H.; van de Vosse, F. N.; Janssen, J. D., The influence of the non-Newtonian properties of blood on the flow in large arteries: steady flow in a carotid bifurcation model. *Journal of Biomechanics.***1999,** 32 (6), 601-608.

Graham, A. L.; Altobelli, S. A.; Fukushima, E.; Mondy, L. A.; Stephens, T. S., NMR imaging of shear-induced diffusion and structure in concentrated suspensions undergoing Couette-flow. *Journal of Rheology.***1991,** 35 (1), 191-201.

Haller, D.; Woias. P.; Kockmann, N., Simulation and experimental investigation of pressure loss and heat transfer in micro channel networks containing bends and T- junctions. *International Journal of Heat and Mass Transfer.***2009,** 52(11), 2678-2689.

Hampton, R. E.; Mammoli, A. A.; Graham, A. L.; Tetlow, N.; Altobelli, S. A., Migration of particles undergoing pressure-driven flow in a circular conduit. *Journal of Rheology.* **1997,** 41 (3), 621-640.

Ingber, M. S., Dynamic simulation of the hydrodynamic interaction among immersed particles in Stokes-flow. *International Journal for Numerical Methods in Fluids.* **1990,** 10 (7), 791-809.

Ishikawa, T.; Fujiwara, H.; Matsuki, N.; Yoshimoto, T.; Imai, Y.; Ueno, H.; Yamaguchi, T., Asymmetry of blood flow and cancer cell adhesion in a micro channel with symmetric bifurcation and confluence. *Biomedical Micro devices* .**2011,** 13 (1), 159-167.

Iwamiya, J. H.; Chow, A. W.; Sinton, S. W., NMR flow imaging of Newtonian liquids and a concentrated suspension through an axisymmetric sudden contraction*, Rheologica. Acta***. 1994**, 33, 267-282.

Jaggi, R. D.; Sandoz, R.; Effenhauser, C. S., Microfluidic depletion of red blood cells from whole blood in high-aspect-ratio microchannels. *Microfluidics and Nanofluidics.* **2007,** 3 (1), 47-53.

Kanaris, A. G.; Anastasiou, A. D.; Paras, S. V., Numerical study of pulsatile flow in micro channels, *7th European Congress of Chemical engineering ECCE-7. Prague, Czech Republic*. **2010.**

Karnis, A.; Goldsmith, H. L.; Mason, S. G., The kinetics of flowing dispersions, 1.Concentrated suspensions of rigid particles*, Journal of Colloid Interface Science.* **1966,** 22, 531-553.

Kauzlaric, D.; Greiner, A.; Korvink, J. G., A non-local extension of the Phillips model for shear induced particle migration. *Microsystem Technologies.* **2011,** 17 (2), 265-272.

Kitano, T.; Kataoka, T.; Shirota, T., An empirical-equation of the relative viscosity of polymer melts filled with various inorganic fillers*. Rheologica Acta.* **1981, 20**, 207-209.

Knowlton, T. M.; Carson, J. W.; Klinzing, G. E.; W. Yang., Particle Technology: The importance of storage, transfer, and collection. *Chemical Engineering Progress.* **1994,** 90 (4), 44-54.

Koh, C. J.; Hookham, P.; Leal, L. G., An experimental investigation of concentrated suspension flows in a rectangular channel. *Journal of Fluid Mechanics.***1994,** *266*, 1-32.

Kowalewski, T. A.,Velocity profiles of suspension flowing through a tube. *Archives of Mechanics*. **1980,** 32, 857- 865.

Krieger, I. M., Rheology of monodisperse lattices. *Advances in Colloid and Interface Science.* **1972**, 3, 111-136.

Kriger, I. M.; Dougherty, T. J., A mechanism for non-Newtonian flow in suspensions of rigid spheres. *Transactions of the Society of Rheology- III.* **1959,** 3, 137-152.

Krishnan, G. P.; Beimfohr, S.; Leighton, D. T., Shear-induced radial segregation in bidisperse suspensions. *Journal of Fluid Mechanics.* **1996,** 321, 371-393.

Krogh, A., Studies on the physiology of capillaries: II. The reactions to local stimuli of the blood-vessels in the skin and web of the frog. *The Journal of Physiology.* **1921,** 55 (5-6), 412-

422.

Kumar, A.; Graham, M. D., Margination and segregation in confined flows of blood and other multicomponent suspensions. *Soft Matter.* **2012,** 8 (41), 10536-10548.

Lagoela, M.; Oliveira, B.; Cidre, D.; Fernandes, C.; Balsa, C.; Lima, R.; Dias, R.; Ishikawa, T.; Imai, Y.; Yamaguchi, T., Motions of particles and red blood cells in a bifurcation: comparison between experiments and numerical simulations. *Second ECCOMAS Thematic Conference on Computational Vision and Medical Image Processing*," *Porto, Portugal*. **2009.**

Lam, Y.C.; Chen, X.; Tan, K.W.; Chai. J.C.; Yu, S.C.M., Numerical investigation of particle migration in poiseuille flow of composite system. *Composites Science and Technology.* **2004,** 64, 1001-1010.

Leble, V.; Lima, R.; Dias, R.; Fernandes, C.; Ishikawa, T.; Imai, Y.; Yamaguchi, T., Asymmetry of red blood cell motions in a micro channel with a diverging and converging bifurcation. *Biomicrofluidics.* **2011,** 5, 044120-15.

Leighton, D.; Acrivos, A., Viscous resuspension. *Chemical Engineering Science.* **1986,** 41 (6), 1377-1384.

Leighton, D.; Acrivos, A., Measurement of shear-Induced self-diffusion in concentrated suspensions of spheres. *Journal of Fluid Mechanics.* **1987a,** 177, 109-131.

Leighton, D.; Acrivos, A., The shear-induced migration of particles in concentrated suspensions. *Journal of Fluid Mechanics.***1987b,** 181, 415-439.

Leonard, E. F.; West, A. C.; Shapley, N. C.; Larsen, M. U., Dialysis without membranes: how and why?. *Blood Purification.* **2004,** 22 (1), 92–100.

Li, X. J.; Popel, A. S.; Karniadakis, G. E., Blood-plasma separation in Y-shaped bifurcating microfluidic channels: a dissipative particle dynamics simulation study. *Physical Biology.* **2012,** 9 (2), 026010- 026022.

Link, D. R.; Anna, S.L.; Weitz, D.A.; Stone. H.A., Geometrically mediated breakup of drops in microfluidic devices. *Physical Review Letters*. **2004.** 92(5), 054503-4.

Lyon, M. K.; Leal, L. G., An experimental study of the motion of concentrated suspensions in two-dimensional channel flow. Part 1. Monodisperse systems. *Journal of Fluid Mechanics*

1998, 363, 25-56.

Maron S. H.; Pierce P. E., Application of Ree-Eyring generalized flow theory to suspensions of spherical particles. *Journal of Colloid Science*. **1956,** 11, 80 - 95.

Matos, H. M.; Oliveira, P. J., Steady and unsteady non-Newtonian inelastic flows in a planar t-junction. *International Journal of Heat Fluid Flow*. **2013,** 39, 102-126.

Matos, H. M.; Oliveira, P. J., Steady flows of constant – viscosity viscoelastic fluids in a planar t-junction. *Journal of Non-Newtonian Fluid Mechanics*. **2014,** 213, 15-26.

Miller, R. M.; Morris, J. F., Normal stress-driven migration and axial development in pressure-driven flow of concentrated suspensions. *Journal of Non-Newtonian Fluid Mechanics.* **2006,** 135 (2-3), 149-165.

Miller, R. M.; Singh, J. P.; Morris, J. F., Suspension flow modeling for general geometries. *Chemical Engineering Science.* **2009,** 64 (22), 4597-4610.

Moraczewski, T.; Shapley, N. C., The effect of inlet conditions on concentrated suspension flows in abrupt expansions. *Physics of Fluids. **2006,*** 18, 123-303.

Morris, J. F.; Boulay, F., Curvilinear flows of noncolloidal suspensions: The role of normal stresses. *Journal of Rheology.* **1999,** 43 (5), 1213-1237.

Morris, J. F.; Brady, J. F., Pressure-driven flow of a suspension: Buoyancy effects. *International Journal of Multiphase Flow.* **1998,** 24 (1), 105-130.

Navier, C. L. M. H.; Sur les lois de l'´equilibre et du mouvement des corpes solides´elastique. *Bulletin of Society of Philomath*. **1823,** 75, 177-183.

Nott, P. R.; Brady, J. F., Pressure-driven flow of suspensions - simulation and theory. *Journal of Fluid Mechanic.***1994,** 275, 157-199.

Patankar, S. V., Numerical Heat Transfer and Fluid Flow. Hemisphere, New York, **1981.**

Perkkio, J.; Keskinen, R., Hematocrit reduction in bifurcations due to plasma skimming. *Bulletin of Mathematical Biology.***1983,** 45 (1), 41-50.

Phan-Thien, N., Constitutive equation for concentrated suspensions in Newtonian liquids. *Journal of Rheology.* **1995,** 39 (4), 679-695.

Phan-Thein, N.; Fang, Z., Entrance length and pulsatile flows of a model concentrated suspension. *Jouranl of Rheology*. **1996,** 40, 521-529.

Phan-Thien, N.; Graham, A. L.; Altobelli, S. A.; Abbott, J. R.; Mondy, L. A., Hydrodynamic particle migration in a concentrated suspension undergoing flow between rotating eccentric cylinders. *Industrial & Engineering Chemistry Research.* **1995,** 34 (10), 3187-3194.

Phan-Thien,N.; Kim,S., Microstructure in elastic media: Principles and computational methods, Oxford University Press, New York. **1994.**

Phillips, R. J.; Armstrong, R. C.; Brown, R. A.; Graham, A. L.; Abbott, J. R., A constitutive equation for concentrated suspensions that accounts for shear-induced particle migration. *Physics of Fluids.***1992,** 4 (1), 30-40.

Phung, T. N.; Brady, J. F.; Bossis, G., Stokesian Dynamics simulation of Brownian suspensions. *Journal of Fluid Mechanics.***1996,** 313, 181-207.

Pries, A. R.; Ley, K.; Claassen, M.; Gaehtgens, P., Red-cell distribution at microvascular bifurcations. *Microvascular Research.***1989,** 38 (1), 81-101.

Rao, R. R.; Mondy, L. A.; Altobelli, S. A., Instabilities during batch sedimentation in geometries containing obstacles: A numerical and experimental study. *International Journal for Numerical Methods in Fluids.* **2007,** 55 (8), 723-735.

Rao, R. R.; Mondy, L. A.; Baer, T. A.; Altobelli, S. A.; Stephens, T.S. NMR measurements and simulations of particle migration in non-Newtonian fluids. *Chemical Engineering Communication*. **2002,** 189, 1-22.

Reddy, M. M.; Singh, A., Flow of concentrated suspension through oblique bifurcating channels. *AIChE Journal.* **2014,** 60 (7), 2692-2704.

Rintoul, M. D.; Torquato, S., Computer simulations of dense hard-sphere systems. *Journal of Chemical Physics*. **1996,** 105, 9258–9265.

Roberts, B. W.; Olbricht, W. L., Flow-induced particulate separations. *AIChE Journal.* **2003,** 49 (11), 2842-2849.

Roberts, B. W.; Olbricht, W. L., The distribution of freely suspended particles at microfluidic bifurcations. *AIChE Journal.* **2006,** 52 (1), 199-206.

Russel, W. B.; Saville, D. A.; Schowalter, W. R., Colloidal Dispersions. Cambridge University Press. **1989**.

Schmid-Schonbein, G. W.; Skalak, R.; Usami, S.; Chien, S., Cell distribution in capillary networks. *Microvascular Research.* **1980,** 19 (1), 18-44.

Schramm, L. L., Editor. Suspensions: Fundamentals and Applications in the Petroleum Industry. American Chemical Society, Washington D.C., **1996.**

Shapley, N. C.; Brown, R. A.; Armstrong, R. C., Evaluation of particle migration models based on laser Doppler velocimetry measurements in concentrated suspensions. *Journal of Rheology.* **2004,** 48 (2), 255-279.

Shapiro A.P.; Probstein. R.F., Random packings of spheres and fluidity limits of mono-disperse and bidisperse suspensions. *Physical Review Letters.* **1992,** 68 (9), 1422-1425

Shauly, A.; Averbakh, A.; Nir, A.; Semiat, R., Slow viscous flows of highly concentrated suspensions .2. Particle migration, velocity and concentration profiles in rectangular ducts. *International Journal of Multiphase Flow*.**1997,** 23 (4), 613-629.

Singh, A.; Nott, P. R., Experimental measurements of the normal stresses in sheared Stokesian suspensions. *Journal of Fluid Mechanics*. **2003,** 490, 293 - 320.

Sinton, S. W.; Chow, A. W., NMR flow imaging of fluids and solid suspensions in poiseuille flow. *Journal of Rheology*.**1991,** 35 (5), 735-772.

Stokes, G. G., On the theories of internal friction of fluids in motion. *Transactions of Cambridge Philosophical Society*. **1845,** 8, 287-305.

Subia, S. R.; Ingber, M. S.; Mondy, L. A.; Altobelli, S. A.; Graham, A. L., Modelling of concentrated suspensions using a continuum constitutive equation. *Journal of Fluid Mechanics.* **1998,** 373, 193-219.

Tetlow, N.; Graham, A. L.; Ingber, M. S.; Subia, S. R.; Mondy, L. A.; Altobelli, S. A., Particle migration in a couette apparatus: Experiment and modeling. *Journal of Rheology.* **1998,** 42 (2), 307-327.

van Dinther, A. M. C.; Schroen, C. G. P. H.; Imhof, A.; Vollebregt, H. M.; Boom, R. M., Flow-

induced particle migration in microchannels for improved microfiltration processes. *Microfluidics and Nanofluidics.***2013,** 15 (4), 451-465.

Vlasak, P.; Chara, Z., Effect of Particle Size Distribution and Concentration on Flow Behavior of Dense Slurries. *Particulate Science and Technology.* **2011,** 29 (1), 53-65.

Vollebregt, H. M.; van der Sman, R. G. M.; Boom, R. M., Suspension flow modelling in particle migration and microfiltration. *Soft Matter.* **2010,** 6 (24), 6052-6064.

Vollebregt, H. M.; van der Sman, R. G. M.; Boom, R.M., Model for particle migration in bidisperse suspensions by use of effective temperature. *Faraday Discuss*. **2012,** 158, 89-103.

Wang,T.; Xing, Z., Characterization of Blood Flow in Capillaries by numerical simulation. *Journal of modern physics.* **2010,** 1, 349-356.

Xi, C.; Shapley, N. C., Flows of concentrated suspensions through an asymmetric bifurcation. *Journal of Rheology.* **2008,** 52 (2), 625-647.

.

Yan, Z. Y.; Acrivos, A.; Weinbaum, S., A three-dimensional analysis of plasma skimming at microvascular bifurcations. *Microvascular Research.* **1991,** 42 (1), 17-38.

Yen, R. T.; Fung, Y. C., Effect of velocity distribution on red-cell distribution in capillary blood-vessels. *American Journal of Physiology.* **1978,** 235 (2), H251-H257.

Zarraga, I. E.; Hill, D. A.; Leighton, D. T., The characterization of the total stress of concentrated suspensions of non-colloidal spheres in Newtonian fluids. *Journal of Rheology.***2000,** 44 (2), 185-220.

Zhang, K.; Acrivos, A., Viscous resuspension in fully developed laminar pipe flow. *International Journal of Multiphase Flow.***1994,** 20, 579–591.

Zrehen, A.; Ramachandran, A., Demonstration of secondary currents in the pressure-driven flow of a concentrated suspension through a square conduit. *Physical Review Letters.* **2013,** 110 (1), 018306-018311.

Wong, S.; Ward, M.; Wharton, C., Micro T-mixer as a rapid mixing micromixer. *Sensors and Actuators B: Chemical.* **2004,** 100(3), 359-379.

List of Publications

भारतीय प्रौद्योगिकी संस्थान गुवाहाटी
Indian Institute of Technology Guwahati

List of Publications

International Publications

1. **S. Yadav**, M. Mallikarjuna Reddy and Anugrah Singh (2015). Shear-induced particle migration in three-dimensional bifurcation channel. Int. J. Multiphase Flow, 76, pp. 1-12.

2. **S. Yadav**, M. Mallikarjuna Reddy and Anugrah Singh (2016). Shear Induced Migration of Concentrated Suspension through Y-Shaped Bifurcation Channels. Particulate Science and Technology, 34 (1), 83-95.

3. **S. Yadav**, M. Mallikarjuna Reddy, Ankur Kanaujiya and Anugrah Singh (2015). Numerical simulation of dense suspension flow in symmetric T-shape 3D bifurcation channel. (Manuscript under preparation).

International Conferences

1. **S. Yadav** and Anugrah Singh. Numerical simulation of particle migration in symmetric bifurcation channel. International conference on Applications of Fluid Engineering (CAFE 2012) held at GL Bajaj Institute of Technology and Mangament, Noida, Uttar Pradesh, India on 20 - 22, September, 2012.

2. **S. Yadav**, M. Mallikarjuna Reddy and Anugrah Singh. Numerical simulation of particle migration in symmetric 3D bifurcation channel. International conference on Chemical engineering – Emerging dimensions and challenges Ahead & Indo Japanese Symposium on Separation Technology for green environment (CHEMCON 2014) held at Dr. SSB University

Institute of chemical engineering and technology, Panjab University, Chandigarh, India. On 27 - 30, December, 2014.

3**. S. Yadav,** M. Mallikarjuna Reddy, Ankur Kanaujiya and Anugrah Singh (2015). Numerical simulation of dense suspension flow in symmetric T-shape 3D bifurcation channel. XXVII IUPAP Conference on Computational Physics, held at Department of Physics, IIT Guwahati, on 2 - 5, December, 2015.